



Exciplexes in OLEDs: Principles and promises

Monima Sarma ^{a,*}, Li-Ming Chen ^b, Yi-Sheng Chen ^b, Ken-Tsung Wong ^{b,c,**}

^a Department of Chemistry, KL Deemed to be University (KLEF), Greenfields, Vaddeswaram, Andhra Pradesh 522502, India

^b Department of Chemistry, National Taiwan University, Taipei 10617, Taiwan

^c Institute of Atomic and Molecular Sciences, Academia Sinica, Taipei 10617, Taiwan



ARTICLE INFO

Keywords:

Organic light emitting diode
Thermally activated delayed fluorescence
Exciplex
Intermolecular charge transfer
Electroluminescence
Host material

ABSTRACT

Science has always been full of surprises, and organic light-emitting diodes (OLEDs) are no exception. What exasperates scientists today may entice society tomorrow. The world has witnessed a revolution in display technology in the past two decades. In this period, the displays with bulky and heavy cathode ray tubes were transformed into ultra-slim OLED display panels. Commercialization of any new technology requires a delicate balance between device efficiency and manufacturing cost. OLEDs are still costlier than the popular liquid crystal-based displays (LCDs) because of their higher production cost. However, OLEDs are gradually replacing LCDs. The current OLED-based devices mainly utilize phosphorescent emitters that exhibit some cost and environmental concerns. Therefore, developing OLEDs with only organic components has remained the primary goal in OLED research. The discovery of thermally activated delayed fluorescence (TADF) OLEDs presents a major impetus in this area. Organic TADF molecules can be feasibly realized by manipulating the intramolecular or intermolecular charge transfer between electron-donor and electron-acceptor. The current article discusses the exciplexes formed by intermolecular charge transfer and their versatile applications in OLEDs. In the past OLED research, scientists were often bothered by the red-shifted electroluminescence band along with the desired excitonic emission, which was later identified as the exciplex emission. Exciplexes are virtual emitters that exist only in the electronically excited states. They are formed when electron-rich and -deficient compounds with appropriate frontier molecular orbitals come close enough for orbital participation, one of them being in the excited state. Given the lack of sophisticated characterization technology, exciplex emission was not fully understood back then and was considered a defect in device design. However, some were also inquisitive about the possibilities. The importance of exciplexes in OLEDs was finally recognized in the early 2010s when scientists were elated about the enormous opportunities they could offer. These emitters can be easily generated in a blend of donor and acceptor molecules without the need for complicated syntheses. They also exhibit excellent TADF emission. The researchers were exuberant about the discovery, and a slew of publications have followed the original article published by Adachi and coworkers in 2012. Exciplexes can be applied as emitters and hosts in OLEDs. The efficiency of the relevant devices gradually approaches the phosphorescent OLEDs. In the present article, we have systematically reviewed this success story, reminding the OLED community of the transformation of annoyance into ecstasy, to assist this community in developing high-performing devices based on the data accumulated herewith.

1. Introduction

1.1. Background of the exciplex OLEDs

Since the first practical organic light-emitting diode (OLED) by Tang and Van Slyke at Eastman Kodak (1987), the high-performing OLED device has become the holy grail in the display market [1]. Over the past

two decades, the evolution of technology has witnessed the replacement of the bulky cathode ray tube-based displays with the liquid crystal display (LCD) flat panels followed by the commercialization of the phenomenal OLED displays. Kodak and Sanyo introduced the 2.4-inch active-matrix, full-color OLED display in 1999, which was the first of its kind in the market. The first OLED television (Sony XEL-1) was introduced by Sony in 2007. Since then, a revolution in OLED

* Corresponding author.

** Corresponding author at: Department of Chemistry, National Taiwan University, Taipei 10617, Taiwan.

E-mail addresses: monima.22@gmail.com (M. Sarma), kenwong@ntu.edu.tw (K.-T. Wong).

technology, including LG's super thin 2.57 mm 4 K OLED W8 wallpaper TV, has occurred. Compared with the conventional LCDs, OLED displays have obtained global attention for obvious reasons, such as high contrast ratio, crisp picture, wide viewing angle, high refresh ratio, and possibilities of flexible device fabrication.

The light emission mechanism in OLEDs is electroluminescence (EL), i.e., the emission of photons under electrical excitation [2]. Unlike the conventional LCDs where the colors are produced through light-blocking, OLED pixels are self-emissive. These organic semiconductors produce light through recombination of electrically injected charge carriers (electrons and holes), which form Frenkel-type excitons with high-exciton binding energy (0.5–1.0 eV) in the emissive layer that decay radiatively [2]. The key factors that control the overall device efficiency (external quantum efficiency [EQE], η_{ext}) include internal quantum efficiency (η_{int}), which depends on the photoluminescence quantum yield (PLQY) of the emitter, and light out-coupling efficiency (η_{out}), which relies on the orientation of the emitters to the substrate plane. The excited states in photoluminescence (PL) are formed by the absorption of photons. By contrast, the excited states in EL are created by the recombination of injected charge carriers in the organic emitting materials. The recombination of charges maintains the spin statistics, where singlet and triplet excited states are formed in a 1:3 ratio [3]. The fluorescence emitters employ only the singlet excitons. Thus, the EQE of the earlier OLEDs was seriously limited. Incorporating both the singlet and triplet excitons into the emission channel is the only possibility to boost device performance. This goal was achieved by the discovery of phosphorescent OLEDs (PhOLEDs) [4]. Although the commercially available OLEDs primarily utilize metal-centered, mainly iridium, phosphorescent emitters, some concerns associated with them remain. These concerns include device fabrication costs due to the rarity of natural metal resources and the environmental toxicity of metal. The search for new "all-organic" materials with 100 % exciton harvesting ability culminated in the discovery of pure organic thermally activated delayed fluorescence (TADF) emitters (2011) [5]. These materials have a small singlet-triplet gap (in the order of $k_B T$, where k_B is Boltzmann constant, and T is the temperature in Kelvin) that allows them to upconvert the triplet excitons to the singlet ones utilizing the thermal energy available in the surroundings, followed by the emission of delayed fluorescence. Thus, their fluorescence is characterized by the combination of a fast (prompt; τ , ns) component and a slow (delayed; τ , μ s) component, where the occurrence of the delayed emission is due to reverse intersystem crossing (RISC) from the triplet excitons. This process is known as the TADF, which was first observed in an eosin solution (E-type delayed fluorescence). Considerable progress has been achieved since the first discovery of TADF OLEDs by Adachi and coworkers at Kyushu University, Japan [5]. A tentative timeline of the evolution of OLED devices is shown in Fig. 1.

The delayed fluorescence mechanism enhancing device efficiency entices the researchers because of some crucial facts, such as (a) non-

requirement of organometallic complexes as emitters, (b) conversion of dark triplet excitons into the emissive states at the cost of available thermal energy, (c) lower device fabrication cost for the organic emitters compared with that for the phosphorescent organometallic complexes. RISC is a thermally activated process, and the rate constant for TADF emission is temperature-dependent and expressed by an Arrhenius-type equation as $k_{TADF} = A \exp(-\frac{\Delta E_{ST}}{RT})$, where A is the frequency factor, and R is the gas constant [6]. The immediate outcome of this equation is the requirement of a small singlet-triplet gap (usually <100 meV) for efficient TADF emission. Therefore, an appropriate molecular design that can achieve small ΔE_{ST} along with high PLQY has become the primary goal of OLED researchers. The TADF OLEDs with EQE as high as that of PhOLEDs were soon discovered. A notable example in this context is our report of above 30 % EQE from a TADF OLED employing a simple donor-acceptor molecule as the emitter [7]. We obtained device efficacy that crossed the theoretical limit of approximately 30 % through careful molecular design and proper device optimization. This high efficiency comparable with that of the PhOLEDs is due to superior PLQY of the emitting film in conjunction with the improved light out-coupling due to the horizontal orientation of the emitter molecules [7]. In particular, scientific publications describing TADF OLEDs have increased since the first report by Adachi and coworkers [8].

Although the conventional TADF emitters have remained a popular OLED research topic to date, another type of emitters known as exciplexes, which are excited-state charge-transfer complexes, has gradually gained the pace of the EQE race. Exciplexes are often considered the intermediate in the electron transfer process. Complete electron transfer within the exciplex framework generates charge-separated species, which is essential in organic photovoltaic devices. Alternatively, the electron-hole bound state can undergo photon emission, as required in the OLEDs. Exciplex emission in OLED was observed in 1994, approximately half a decade before discovering PhOLEDs. Researchers at the University of Massachusetts Amherst observed a new emission peak while investigating the EL of the blends of poly(N-vinyl carbazole) [9]. This undesirable emission was attributed to an exciplex formation between the components. Exciplex formation between the hole-transporting layer (HTL) and electron-transporting layer (ETL) or between the emitter and one of the transporting layers had been a serious concern for nearly two decades; the reason is that excitonic emission is usually accompanied by the exciplex emission (red-shifted), which impedes color purity and lowers device efficiency [10,11]. The exciplex formation occurs if the carrier injection barrier in the heterojunction is high regardless of whether the excitonic emission prevailed at the low injection barrier [11]. However, some early attempts to capture the electrogenerated exciplexes by quantum dot nanocrystal (NC) emitters through the Förster mechanism in NC-OLEDs were made to realize device performance and color purity adequately [11]. Exciplex emission was considered a detrimental effect until positive outcomes were finally realized in 2012. These materials possess innate RISC ability

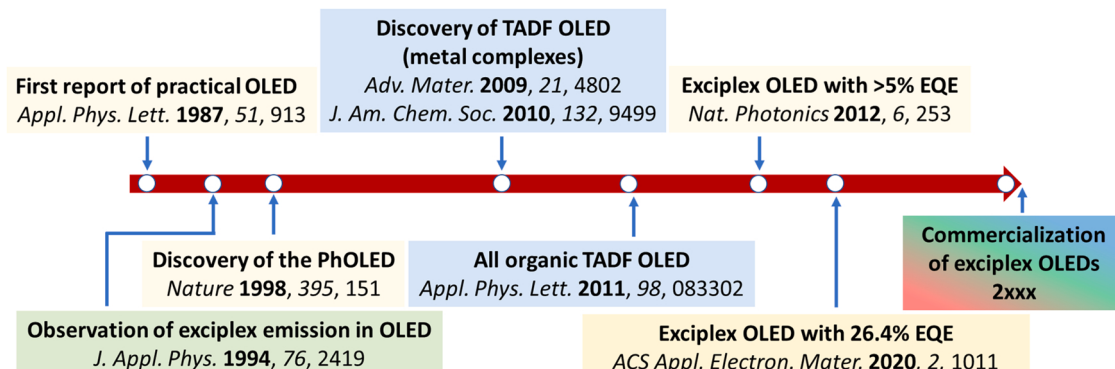


Fig. 1. Timeline of the evolution of OLED devices.

to upconvert the dark triplet excitons to the singlet excited states. Thus, the emission due to exciplex is fluorescence. Similar to TADF materials, exciplexes exhibit a prompt and a delayed component in their emission. In contrast to TADF materials, which usually require tedious synthetic

efforts, exciplexes can be generated in a blend of commercially available donor and acceptor materials. This simple concept, along with the charge transfer character of the exciplexes, led to many anticipations that inspired the scientists for a comprehensive investigation. Adachi

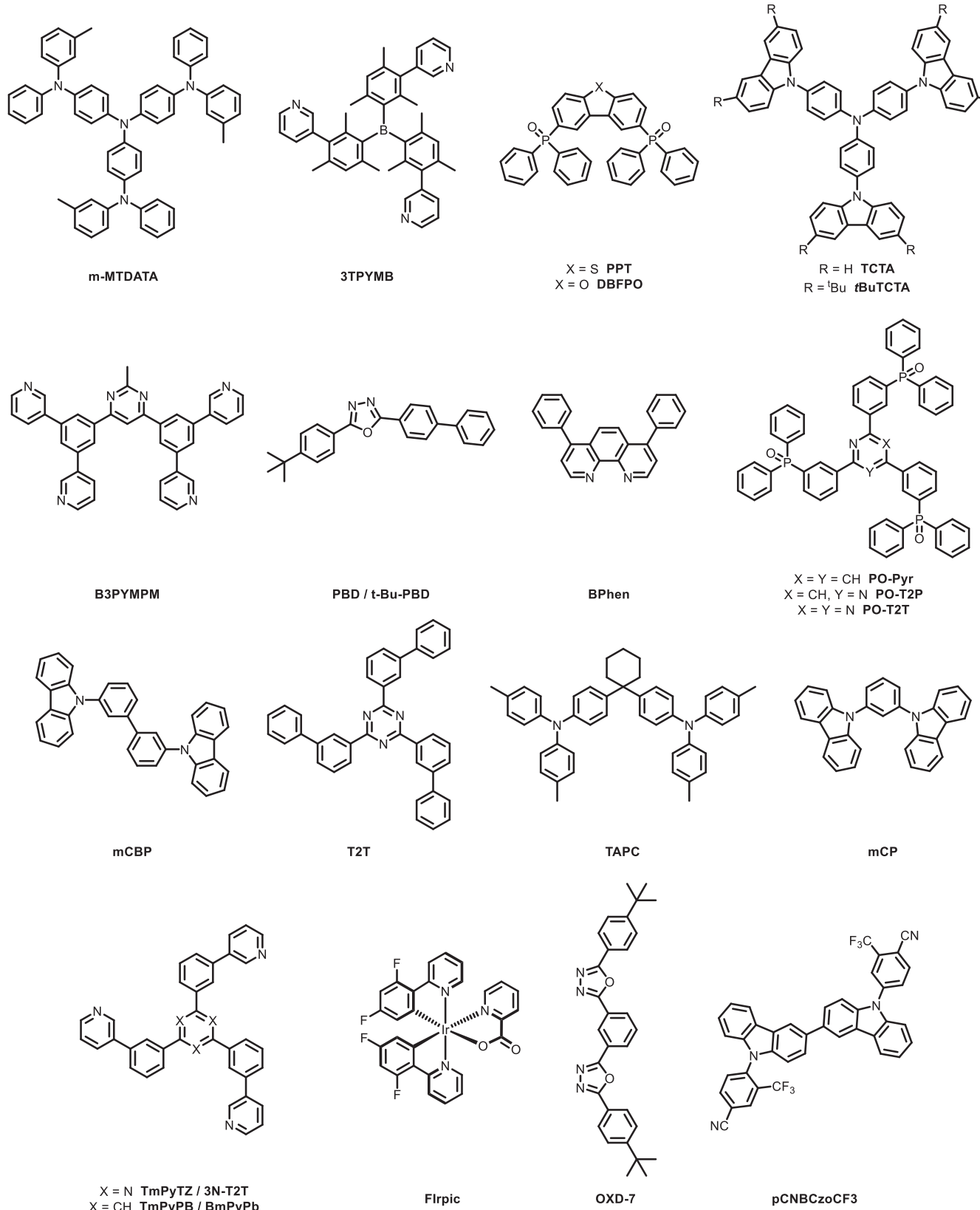


Fig. 2. Molecular structures of some common exciplex-forming donor and acceptor components.

and coworkers (2012) reported 5.4 % EQE from an exciplex OLED based on a 1:1 blend film of 4,4',4''-tris[phenyl(m-tolyl)amino]triphenylamine (m-MTADATA, donor, Fig. 2) and tris(2,4,6-trimethyl-3-(pyridine-3-yl)phenyl)borane (3TPYMB, acceptor, Fig. 2) [12]. The enhanced EQEs of such OLEDs compared with those of the conventional fluorescent OLEDs are clearly due to the operation of the TADF mechanism in the exciplex emission. In the same year, the same research group demonstrated 10 % η_{ext} and 47.0 lm W⁻¹ power efficiency (PE) from an exciplex-based OLED using a blend of m-MTADATA as the electron donor and 2,8-bis(diphenyl-phosphoryl)-dibenzo[b,d]thiophene (PPT, Fig. 2) as the electron-accepting material. [13] In a separate report the following year, the researchers at Seoul National University demonstrated 10 % EQE from an exciplex OLED based on tris(4-carbazoyl-9-ylphenyl)amine (TCTA, donor, Fig. 2) and 4,6-bis(3,5-di(pyridine-3-yl)phenyl)-2-methyl pyrimidine (B3PYMPM, acceptor, Fig. 2) [14]. These inspiring findings are another milestone in OLED research, motivating detailed investigation of exciplex OLEDs. Similar to the goal of any other OLED type, the aim of the exciplex OLEDs is the discovery of high-performing devices by improving η_{int} , efficiency roll-off, power, current efficiencies, and light out-coupling efficiency. A recent research article by Chapran *et al.* demonstrated 20 % EQE from exciplex OLEDs, sustaining the hope of commercialization of this type of device in the future [15]. In 2020, Al Amin *et al.* announced 26.4 % EQE from an exciplex emitter-based OLED [16]. Material scientists have been exploring exciplex OLEDs for a few years now and produced some noteworthy results, which are discussed in the subsequent sections.

In this article, we aim to review the historical progress of exciplex OLEDs comprehensively. The exciplex formation in OLEDs is usually achieved by either mixing donor and acceptor materials in an appropriate ratio or blending donor- or acceptor-type material with a bipolar material. The EQE of exciplex OLEDs depends not only on the PLQY of the emitter but also on many factors, such as appropriate triplet energy of the individual components for successful confinement of the triplet excitons within the exciplex, the charge carrier mobility of the donor and acceptor counterparts, the appropriate energy gap between the frontier molecular orbitals (FMOs), and accumulation of the considerable amount of charge carriers at the donor-acceptor interface. The high device efficiency is due to the cumulative contribution from all the materials used in a device. A systematic insight is also vital for proper material selection. We divided the article into several sections for easy comprehension of the readers. Exciplexes have been explored both as emitters and as hosts in OLEDs. Exciplexes in white light-emitting devices have also been investigated in addition to those in light production of a specific color. The photophysics of exciplexes is slightly different from those of conventional emitters. In addition, a conceptual distinction exists between the photonically and electrically generated exciplexes. Therefore, we begin our discussion with a brief description of the light-emitting properties of the exciplexes. Although hundreds of publications about TADF OLEDs have appeared to date, exciplex OLEDs remain underrated. A review of the progress of the latter would assist the researchers to delve deeply into the topic to produce competitive results.

1.2. Manipulating the singlet-triplet gap (ΔE_{ST})

The ability to harvest all the electrically generated excitons to achieve the theoretical internal quantum efficiency limit ($\eta_{\text{int}}^{\max} = 1$) makes TADF materials immensely popular. The primary criterion to obtain efficient TADF is a small ΔE_{ST} , in the range of k_BT (~30 meV at 298 K). Based on quantum chemical calculations, ΔE_{ST} is roughly twice the electron exchange energy (singlet and triplet excited states), which is expressed by the following equation:

$$\begin{aligned} J &= \iint (\phi)^1 (\phi^*)^1 \frac{e^2}{r_{12}} (\phi^*)^1 (\phi)^1 d\tau_1 d\tau_2 \\ &= \iint \frac{[(\phi)^1 (\phi^*)^1 e] [e (\phi^*)^1 (\phi)^1]}{r_{12}} d\tau_1 d\tau_2, \end{aligned}$$

where ϕ and ϕ^* are the wavefunctions for the ground and excited states, respectively [17]. J is presumably similar to the Coulombic repulsive interaction between two equal charge densities ($\phi\phi^*e$), where a small value of the overlap integral $\langle\phi|\phi^*\rangle$ favors J and ΔE_{ST} . For efficient TADF emission, the materials should have a small J value. This value can be obtained by spatially separating the highest occupied molecular orbital (HOMO) and the lowest unoccupied molecular orbital (LUMO) of the relevant molecules. This process can be achieved by disposing of the donor and acceptor fragments in sterically congested molecular geometry, thereby minimizing the overlap between the FMOs. However, this procedure reduces the oscillator strength of the relevant transitions as they become increasingly space forbidden. Therefore, the radiative decay rate decreases with the minimization of orbital overlap. This challenge of the inherent lowering of photoluminescent quantum yield in such systems is addressed seriously, and many TADF materials with excellent PLQY are reported [8]. Similar to the conventional TADF materials where the steric bulkiness between the donor and acceptor counterparts causes spatial separation of the FMOs, exciplexes exhibit a spatial distribution of the FMOs. The only difference is that the intermolecular nature of the orbital dispersal exists in the case of the latter, whereas the intramolecular nature of the orbital dispersal exists in the former.

1.3. Exciplexes in solution

Exciplexes are intermolecular donor-acceptor charge-transfer complexes generated by the collision between the photoexcited donor or acceptor molecules and dissimilar ground-state molecules (acceptor or donor) in the solution. Therefore, exciplex formation is a diffusion-controlled bimolecular process in solution, and this phenomenon is observed only at the high concentration of the relevant materials when the probability of subsequent encounter is high [18]. The interaction between the components is repulsive in the ground state and attractive in the excited state, as the complex formation occurs selectively after photoexcitation. Therefore, the potential energy surface of the electronically excited state goes through a minimum that represents the exciplex. The concept that the complex formation occurs specifically in the excited state is realized from unchanged ground-state absorption spectra of the physical mixture of donor and acceptor components from the individual components. Exciplexes are often invoked as the intermediates in electron transfer reactions and are formed only when the attraction between the components is considerably high because of the partial charge delocalization from a donor-based orbital (D*/D) to an acceptor-based orbital (A/A*) [18]. The wavefunction of the exciplex is expressed as a linear combination of the ground and excited-state constituents as

$$\Psi(DA)^* = c_1 \Phi(DA) + c_2 \Phi(D^*A) + c_3 \Phi(DA^*) + c_4 \Phi(D^{\delta+}A^{\delta-})^* + c_5 \Phi(D^{\bullet+}A^{\bullet-})^*,$$

where c₁–c₅ are the coefficients of the pertinent components, (D^{δ+}A^{δ-})^{*} is the exciplex situation, and (D^{•+}A^{•-})^{*} represents a complete electron transfer. The contribution from the ground state is negligible; thus, this equation reduces to the following:

$$\Psi(DA)^* \approx c_2 \Phi(D^*A) + c_3 \Phi(DA^*) + c_4 \Phi(D^{\delta+}A^{\delta-})^* + c_5 \Phi(D^{\bullet+}A^{\bullet-})^*$$

If the possibility of the complete electron transfer is temporarily neglected, i.e., c₅ < < 1, then the exciplex can either decay radiatively at a wavelength characteristically longer than the donor or the acceptor or dissociate into its constituents (D^{*} + A / D + A^{*}). At this juncture, the exciplex formation is facilitated by the donors with low ionization

energy (IE) and acceptors with high electron affinity (EA). The fluorescence spectra of exciplexes are usually broad, structureless, and sensitive to the medium, and they depend on the degree of charge transfer in the complexes. Although the concept of exciplexes in EL differs from that in solution, the emission characteristic is similar.

The formation of exciplexes is favored when the two components (usually planar π -conjugated organic molecules) approach each other in a face-to-face orientation. In a solution, the tumbling of the molecules can sometimes hinder attaining a specific intermolecular arrangement. By contrast, locking the molecules in their positions in a solid film can indeed facilitate this intermolecular arrangement. Moreover, the distance between the molecular planes should be small enough for adequate orbital participation. However, developing molecules with specific objectives is one of the advantages of molecular engineering. Thus, planar molecules, where exciplex formation is intentional, can be selected based on the requirements, whereas sterically congested molecules can be designed if exciplex formation is not intended. The microheterogeneity around the emitting species is expected to be less in the solid-state than that in the solution; thus, complex dynamics are observed for the exciplex emission in the blend films of m-MTDATA and 2-(biphenyl-4-yl)-5-(4-tert-butyl phenyl)-1,3,4-oxadiazole (PBD, Fig. 2), where a distribution of excimers with slightly different charge transfer character and emission energy is observed [19]. At times, excimer formation further complicates the scenario that needs careful assessment.

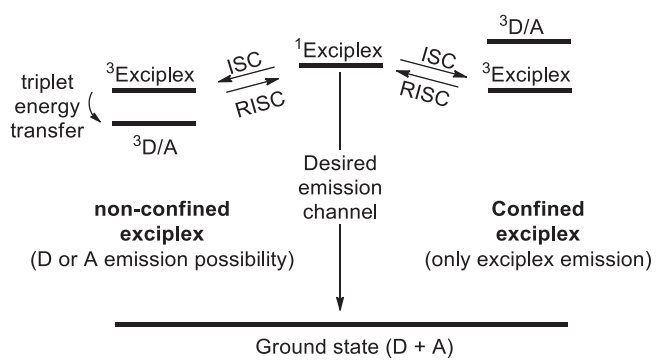
A theoretical distinction exists between exciplex formation ($D^{\delta+}A^{\delta-}$)^{*} and photoinduced electron transfer that generates charge-separated ion pairs ($D^{\bullet+}A^{\bullet-}$)^{*} through the complete transfer of electrons. However, the charge-separated species is approximated as the exciplexes in OLEDs. Thus, we should briefly discuss the electron transfer process before proceeding to the exciplexes in OLEDs. The ion pair formation can be expressed by the following equation:

$$\Delta_{ET}G^0 = F \left(E_{D^{\bullet+}}^0 - E_{A^{\bullet-}}^0 \right) - N_A h \vartheta_{00} - \frac{N_A e^2}{4\pi\epsilon R},$$

where the E^0 's are the standard reduction potential of the donor and acceptor counterparts, F is the Faraday constant (96,485 C mol⁻¹), $\Delta E_0 = h\vartheta_{00}$ is the 0–0 transition energy, e is the charge of an electron (1.6×10^{-19} C), ϵ is the permittivity of the medium, and R is the distance between the two ions [18]. This equation reveals that compared with that in the ground state of the D and A mixture, the probability of charge separation in the excited state is increased because of the decrease of the Gibbs energy upon photoexcitation.

1.4. Electrically generated exciplexes in organic solid films

Exciplex formation occurs at the interface of the layers in OLEDs. The injected electrons and holes in the conventional OLEDs are transported through the various organic layers. They are finally recombined at the emitters, where they undergo exciton formation. These excitons are homo molecular. However, the situation is slightly different in the case of an exciplex OLED. The FMOs of the donor counterpart are at higher energy than that of the acceptor molecules (see Scheme 1). Given that the emitting species is the donor-acceptor blend, the carriers are now inserted into the LUMO of the acceptor (electron) and HOMO of the donor (hole). Therefore, the corresponding exciton, which is formed, is heteromolecular because the bound state is distributed over two molecules. This situation is approximated to an exciplex. The fermions can be transferred in whole numbers only. Thus, the charge transfer state in electrical excitation is the charge-separated species instead. Given the distribution of the contributing orbitals over two different molecular species (donor and acceptor molecules), the scenario is correlated with the spatial separation of FMOs in the conventional TADF molecules. As expected, the exciplex emitters are subjected to realize a tiny singlet-



Scheme 1. Illustration of nonconfined and confined exciplexes.

triplet energy gap, even smaller than that in the conventional TADF emitters, making exciplex emitters promising materials for OLEDs. In addition, the exciplex-based OLEDs are expected to operate at a low driving voltage because of the low injection barrier for exciton formation. The Gibbs energy for the formation of exciplex in the solid state is usually expressed by a modified Rehm-Weller equation: $-\Delta G_{exciplex} = E_{exciton} - E_{exciplex}$, where $E_{exciton}$ is the exciton energy of the constituting molecules ($E_{D^{\bullet+}}$ or $E_{A^{\bullet-}}$), and $E_{exciplex}$ is the exciplex energy. Excitonic energy, which is assumed to be the energy difference between the HOMO of the donor and LUMO of the acceptor, is estimated by electrochemistry. Exciplex energy can be determined from the photoluminescence maxima of the blend. The estimation of the Gibbs energy is crucial because it can guide the selection of appropriate donor and acceptor; the optimal condition for exciplex formation is $-\Delta G_{exciplex} > 0.57$ eV [20].

The triplet energy of the exciplex (${}^3\text{Exciplex}$) may be either higher or lower than its counterparts (${}^3\text{D/A}$). If ${}^3\text{Exciplex} > {}^3\text{D/A}$, then the exciplex triplet energy can be transferred to one of its components through triplet-triplet energy transfer populating the counterpart triplet state. This scenario corresponds to a leakage of the exciplex triplet energy, and the relevant exciplex is nonconfined (Scheme 1) [21]. On the contrary, if ${}^3\text{Exciplex} < {}^3\text{D/A}$, then the appropriate exciplex state is stable, and the exciplex is confined within the emission layer (Scheme 1). This situation is desired in the exciplex OLEDs. Careful assessment of the relevant triplet energies is necessary to obtain high device efficiency. A recent finding by Yan, Ma, and coworkers consolidates this scenario. The researchers studied the magneto-PL (MPL) and magneto-EL (MEL) of two exciplex OLEDs based on m-MTDATA:3TPYMB and m-MTDATA:BPhen (4,7-diphenyl-1,10-phenanthroline, Fig. 2) [22]. The triplet exciplex in the m-MTDATA:3TPYMB blend film is well-confined because the triplet energy of the exciplex is estimated to be lower than that of m-MTDATA and 3TPYMB. However, a possibility of leakage of the exciplex triplet excitons exists because the triplet energy of BPhen is lower than that of the m-MTDATA:BPhen exciplex. Therefore, compared with the device based on the latter exciplex, the device based on the former exciplex yields superior results. Another recent article by Xiong and coworkers demonstrated direct observation of RISC from fully confined triplet exciplexes in an m-MTDATA: 2,4,6-tris[3-(diphenylphosphinyl)phenyl]-1,3,5-triazine (PO-T2T, Fig. 2) blend by MEL studies [22].

The emission characteristics of exciplexes in OLEDs are full of conundrums, such as a red shift of the emission spectra with delay time. Some special cases occur, where the fluorescence of some probe molecules exhibits excitation wavelength dependence when excited at the red edge of their absorption spectra. This phenomenon, known as the red-edge effect, occurs when microheterogeneity exists around the excited molecules in highly viscous media, such as ionic liquids [19,23]. In these media, heterogeneous solvation shells around the excited probe molecules may be possible, thereby causing the existence of various closely emitting species. Probe molecules with slightly different solvation shells are selectively excited upon excitation at the long-wavelength edge of

the absorption spectrum. They also undergo photon emission at close wavelengths, causing the red-edge effect. A similar concept of micro-heterogeneity explains the time dependence of the exciplex emission spectra in OLEDs. Adachi and coworkers observed a few nanometers of red-shifted delayed fluorescence, which was compared with the prompt component in the streak image of a 50 mol% 4,4',4''-tris[3-methyl-phenyl(phenyl)amino]triphenylamine

(m-MTDATA):2-(biphenyl-4-yl)-5-(4-tert-butyl phenyl)-1,3,4-oxadiazole (t-Bu-PBD, Fig. 2) film at 300 K; this scenario was proposed to be due to the variation of the polarization of the host material with time [12]. Another theory refers to the concept of conformational disorder of the exciplex geometries with slightly different charge transfer characters to explain the spectral shift, that is, the high charge transfer congeners emitting at the long wavelengths and vice versa [24]. Another theory was proposed by Baldo and coworkers to explain the time dependence of the exciplex emission spectra based on an FMO distribution of the donor and acceptor counterparts in the blend films [25].

The hitherto discussed exciplexes demonstrate the charge transfer or electron-hole coupling between adjacent molecules. The extent of this coupling and the exciton binding energy is expected to vary with the D-A distance. The radiative decay of such exciplexes corresponds to the transition of an electron from the LUMO of the acceptor molecule to the HOMO of the donor molecule. Scientists are naturally inquisitive to know whether a long-range electron-hole coupling can control the exciton binding energy and size of the exciton. Adachi and coworkers studied the EL of a thin film with D-S-A (donor-spacer-acceptor) structure by employing m-MTDATA (D), 3,3-di(9H-carbazol-9-yl) biphenyl (mCBP, S, Fig. 2) and 2,4,6-tris(biphenyl-3-yl)-1,3,5-triazine (T2T, A, Fig. 2) [26]. The red-shifted and broad exciplex emission is observed in the PL spectra of the D-S-A blend film even up to the spacer thickness of 15 nm, indicating the possibility of long-range electron-hole coupling. The mCBP spacer is chosen because of its high carrier injection barrier, which would lead to the charge carrier accumulation at both interfaces of the spacer that would allow controlling of the long-range coupling through variation of the spacer layer thickness. The EL spectra of the subsequent films exhibit solo exciplex emission up to the spacer thickness of 5 nm; after which, the emission from one of the components becomes prominent. Nevertheless, this investigation uncovered the possibility of a new type of excitonic device. The long-range exciplex formation was also documented by Chen, Su, and coworkers in a simple OLED with device structure indium tin oxide (ITO)/1,1-bis [(di-4-tolylamino)phenyl]cyclohexane (TAPC, D, 85 nm)/1,3-bis (N-carbazolyl)benzene (mCP, S, Fig. 2)/2,4,6-tris(3-(pyridine-3-yl)phenyl)-1,3,5-triazine (TmPyTZ, A, Fig. 2, 85 nm)/lithium fluoride (LiF, 1 nm)/Al (150 nm). [26b] Similar to the report by Adachi and coworkers, the results from the study of Chen, Su, and coworkers indicated that exciplex emission can be observed up to the spacer thickness of 8 nm. The devices with 1–6 nm spacer thickness perform better than those with TAPC-TmPyTZ interfacial exciplex. Mu and coworkers observed exciplex emission from mCP and 1,3,5-tris(3-pyridyl-3-phenyl) benzene (TmPyPB, Fig. 2) with an ultrathin layer of bis[2-(4,6-difluorophenyl)pyridinato-C²,N](picolinato)iridium(III)] FIrpic (Fig. 2) (0.3 nm) inserted between them [26]. Some studies reported an exciplex-forming layer sandwiched between two blue phosphorescent emitting layers (EMLs) to improve the overall device performance [27].

2. Exciplexes as emitters in OLEDs

The research in exciplex OLED begins with the exciplexes employed as emitters. Exciplexes form only between the selective donor and acceptor molecules, not between arbitrary pairs of conjugated organic molecules. The prerequisites of exciplex formation under PL conditions include (a) a substantial change in dipole moment upon photoexcitation and (b) sizeable molecular polarizability. These prerequisites are the key factors for a simple charge transfer. The EL experiment is resource-demanding. Thus, appropriate donor and acceptor components can be

chosen by a simple PL-based litmus test. Exciplex formation under PL condition is also a positive indication of exciplex formation under EL excitation because the molecules already remain in the charge-separated state in the latter.

2.1. Early reports

The past OLED reports suggested that the appearance of the exciplex emission along with the excitonic emission confused scientists. However, some were inquisitive about the possibilities and began exploring the exciplexes in OLEDs. However, their efficiencies were then inadequate. Nevertheless, we decided to include those devices in this section because of their historical importance. Nayak *et al.* aptly demonstrated the exciplex formation between 3,6-diarylcbazole derivatives, namely, 3,6-di-(p-cyanophenyl)-N-hexylcarbazole (CNHC) and 3,6-di-(p-acetyl phenyl)-N-hexylcarbazole (ANHC) (Fig. 3) as the acceptors and the triphenylamine donor N,N'-bis(3-methyl phenyl)-N,N'-diphenyl benzidine (TPD, Fig. 3) and the underlying principles [28]. Although the device outcomes are basic, some crucial revelations are determined, such as the effect of the charge injection barrier on the operation of the exciplex-based OLEDs. In 2003, Kafafi *et al.* [28] demonstrated exciplex formation between N,N'-diphenyl-N,N'-(2-naphthyl)-(1,1'-phenyl)-4,4'-diamine (NPB, Fig. 3) as the donor and two silole derivatives, namely, 2,5-bis(2,2'-bipyridine-6-yl)-1,1-dimethyl-3,4-diphenylsilacyclopentadiene (PyPySPyPy) and 2,5-di(3-biphenyl)-1,1-dimethyl-3,4-diphenylsilacyclopentadiene (PPSPPP) (Fig. 3), as the acceptors. Siloles possess large electron affinities owing to the π^* - σ conjugation between the π^* orbital of butadiene and the σ orbital of the exocyclic Si-C bond in the silole ring. The relatively large difference between HOMO of NPB and LUMO of silole PPSPPP leads to exciplex formation. The (NPB:PPSPPP) exciplex emission is centered at 495 nm with PLQY of up to 62 %. A three-layer device is fabricated with PyPySPyPy and NPB as the electron- and hole-transporting materials, respectively, and PPSPPP as the emissive layer. The pertinent device exhibits an operating voltage of 4.5 V at 100 cd m⁻² and EQE of 3.4 % at 100 A m⁻².

At times, exciplex emission is accidentally observed in devices that produce white light using luminescent metal complexes as emitters. In 2002, Wang *et al.* reported high-performance white EL from a double-layer (DL) device constructed with a luminescent boron complex of the dianion of [(mdppy)BF] (Fig. 3) and NPB. The device displays a considerably broad EL spectrum covering the total wavelength region of the visible light emission, with Commission Internationale de l'Elairage (CIE) coordinates of (0.30, 0.36) [29]. Li *et al.* demonstrated a way to tune the EL color based on exciplex formation. A color-tuning material (CTM), composed of a Gd-complex [Gd(DBM)₃bath] (Fig. 3), is sandwiched between m-MTDATA (Fig. 2) and 2,2',2''-(1,3,5-benzinetriyl)-tris(1-phenyl-1-H-benzimidazole) (TPBI, Fig. 3) layers. The EL colors shift from green to orange with an increase in the CTM thickness. These emissions are observed from two combined exciplexes (formed at the interface between m-MTDATA and Gd complex and between m-MTDATA and TPBI). This result indicated that the Gd complex is a good electron-transporting material; thus, exciplex can be easily generated with m-MTDATA because of its low ionization potentials. Photovoltaic devices and white OLED based on the two exciplexes can also be fabricated, thereby providing roadmaps for developing such materials for future use [29]. Furthermore, exciplex formation between the excited state of TPD and the ground state of a rare earth complex [Eu (DBM)₃bath] (Fig. 3) was also studied by Wang *et al.* The augmentation of red emission from the Eu complex is perceived by modifying the compositional ratio in the mixture and by incorporating the blend in the device structure [29c]. Jenekhe and coworkers demonstrated multicolored exciplex OLEDs based on a quinoline acceptor and various donors with different ionization potentials. The authors investigated exciplex formation in the D:A blend as well as in the donor-acceptor interface. They found that the latter is more effective than the former in tuning the

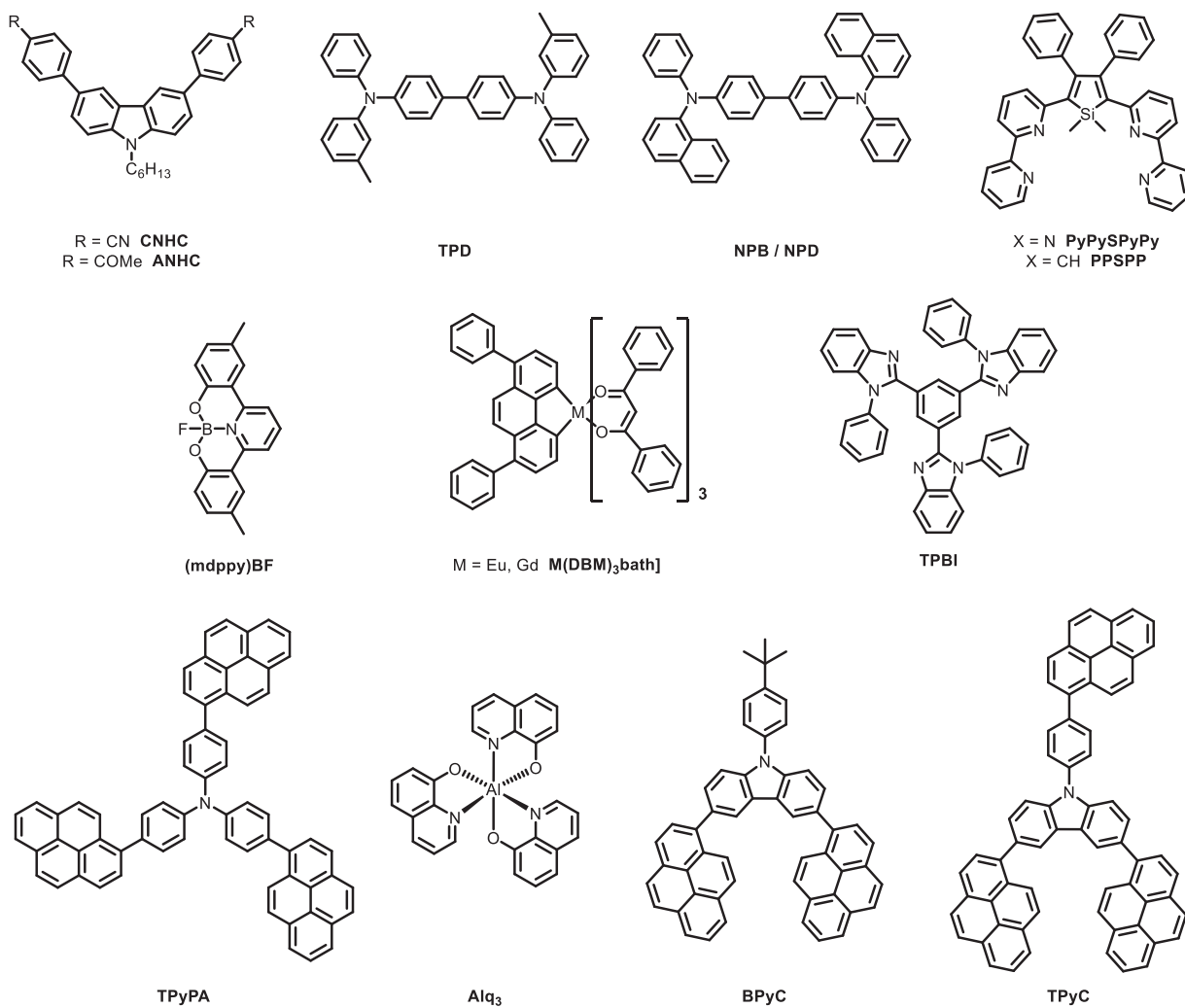


Fig. 3. Molecular structures of donor and acceptor materials employed in the early reports of exciplex OLEDs.

emission color. The exciplex emission competes with the bulk emission depending on the thickness of the acceptor layer in the interface exciplex formation [30]. Lai *et al.* synthesized a trispyrene substituted triphenylamine donor 4,4',4''-trispyrenylphenylamine (TPyPA, Fig. 3) and attempted to conclude based on the influence of acceptor on the interfacial exciplex emission by selecting three acceptor cores, viz, tris (8-hydroxyquinoline) aluminum (Alq_3 , Fig. 3), BPhen (Fig. 2), and TPBI (Fig. 3). The acceptor materials with comparable electron affinities are chosen to mitigate their effect on the emission color. The EL maxima and EQE for the relevant devices are 472 nm (3.93 %), 570 nm (2.83 %), and 516 nm (0.96 %) for BPhen, TPBI, and Alq_3 , respectively. Both the excitonic (472 and 516 nm) and exciplex (570 nm) emissions in these devices are observed because of the unbalanced charge carrier ratio at the interface caused by the difference in the hole and electron mobilities in the carrier transporting materials [31]. Tong, Lee, and coworkers explored exciplex emission in a blend of carbazole–pyrene hybrid as the donor (BPyC and TPyC, Fig. 3) and TPBI as the acceptor; they also fabricated non-doped OLEDs that exhibited EQE of 3.1 % [32]. The device efficiency remains a serious concern in all those historical exciplex OLEDs. Nevertheless, these reports lead to the discovery of a new generation of high-efficiency devices. Tsz-Wai Ng *et al.* investigated the correlation between ground-state energy levels of the donor-acceptor interface and exciplex emission using photoemission studies. They concluded by examining six different exciplex-forming heterojunctions that the charge carrier depletion at the D/A interfaces results in the formation of a charge-transfer state that favors the exciplex formation

[33].

2.2. New generation exciplex OLEDs

In 2012, exciplex-based OLEDs with device efficiencies higher than the fluorescence OLED theoretical limit of 5 % were reported. Adachi and coworkers initially explored the EL of a 1:1 blend film of *m*-MTDATA and *t*-Bu-PBD (Fig. 2) [12]. However, the EQE of the relevant device is as low as 2 %. This result is attributed to the low PLQY of the blended film (~20 %). Replacing *t*-Bu-PBD with another acceptor, 3TPYMB (Fig. 2), enhances the device efficiency primarily because of the high PLQY of the new blend (*m*-MTDATA:3TPYMB) by delayed fluorescence. Therefore, an EQE of 5.4 % for a device with the structure of ITO (110 nm)/*m*-MTDATA (20 nm)/1:1 *m*-MTDATA:3TPYMB (60 nm)/3TPYMB (20 nm)/LiF (0.8 nm)/Al (50 nm) is higher than the EQE of only 2 %, achieved from the *t*-Bu-PBD-containing device [12]. This study indicated that the leakage of the triplet excitons of the exciplex in the blend film, *m*-MTDATA:*t*-Bu-PBD, is responsible for the inferior performance of the device. This investigation revealed that a proper combination of donor and acceptor molecules is essential in confining the triplet excitons within the exciplex to realize high-performance devices. In another publication, the Adachi group demonstrated a 10 % EQE and 47.0 lm W⁻¹ PE from an exciplex-based OLED, utilizing a blend of *m*-MTDATA as the electron donor and PPT (Fig. 2) as the electron-accepting material [13]. The donor: acceptor ratio plays an important role in the overall device efficiency. At a high

donor concentration (70 %), both the PL and EL quantum efficiencies are low because of the triplet energy transfer from the exciplex to the donor. At a low donor concentration, PLQY improves, but the EQE deteriorates because of the nonradiative deactivation of the triplet excitons into the HTL [13]. Since then, various research groups have engaged in understanding the formation and dynamics of exciplexes under electrical excitation. Huang *et al.* documented the evolution of exciplexes (*m*-MTDATA:3TPYMB) using transient PL and EL measurements [34]. At least one recent report demonstrated the intermolecular exciplex formation between two D-A molecules and the subsequent application of the relevant charge transfer system in OLED [35].

In this section, the development of exciplex-based OLEDs, where exciplexes are used as emitters, is reviewed. Exciplex systems have two types: (a) donor-acceptor blends (or interface) and (b) blends consisting of either a donor or an acceptor in conjunction with a donor-acceptor molecule (or interface). Thus, we divided the entire section into two subsections and summarized the pertinent device data in Table 1.

2.2.1. Exciplexes in the donor/acceptor blend or interface as the emitters

If a carefully selected blend of a hole-transporting-type donor material and an electron transporting-type acceptor material is inserted between the HTL and ETL, then exciplex is formed under electrical excitation. The emitter in such OLEDs can be accessed without complex synthetic efforts. The electron-donating groups in the donor materials mainly include carbazoles, triphenyl amines, acridines, and other amino functionalities. By contrast, a wide range of electron-deficient substances, such as azines, oxazoles, arylborons, and aryl phosphine oxides, is used as the acceptor materials. At this point, the mechanistic illustration of exciplex-based TADF systems by Monkman *et al.* is worth mentioning. The time-resolved spectroscopic studies on the three D:A blends, viz, *m*-MTDATA:TPBI, TPD:TPBI, and TPD:OXD-7 (Fig. 2), determined that the TADF is facilitated if the ¹CT and ³LE states are energetically close to one another, whereas triplet-triplet annihilation (TTA) is probable for the systems with large energy gap. The outcome suggests the El-Sayed principle of intersystem crossing; nevertheless, the investigation helps select the exciplex components to obtain considerable TADF and consequently high PLQY [36]. In OLEDs, donor-acceptor (D-A) materials are used as intramolecular TADF emitters and exciplex-forming components to obtain intermolecular TADF emission. This scenario was effectively illustrated by Bunzmann *et al.* in a recent article using 4,4'-(9 H,9'H-[3,3'-bicarbazole]-9,9'-diyl)bis(3-(trifluoromethyl) benzonitrile) (pCNBCzoCF₃, Fig. 2). The electrically generated intermediate triplet states responsible for light emission are delocalized over either one molecule featuring intramolecular TADF or two nearby molecules involved in the exciplex formation based on the techniques EL-detected magnetic resonance and PL-detected magnetic resonance [37].

RISC is one of the major fundamental factors in exciplex OLEDs. The triplet-to-singlet up-conversion requires spin mixing, causing a fluctuation of the magnetic moment. This phenomenon is preferably studied using MEL. Liu *et al.* investigated the MEL of TADF OLEDs comprising normal and deuterated analogs of MCP and B3PYMPM. Proton (I = $\frac{1}{2}$) and deuterium (I = 1) have very different spin characteristics. Thus, the research aimed to provide meaningful information about the isotopic effect on RISC. The subsequent study found no appreciable effect of isotopic substitution on the spin-dependent current and MEL responses of the devices at ambient temperature. By contrast, a dramatic impact is observed at a cryogenic condition, where RISC is thermally forbidden. The relevant research suggested the importance of spin mixing in the triplet exciplexes instead of the hyperfine interactions as the controlling factor for RISC [38]. In another article, Niu *et al.* described the effects of intersystem crossing on spin mixing influenced by hyperfine interaction, spin-orbit coupling (SOC), and Zeeman splitting. Based on MEL, the external magnetic field predominantly influences the radiative exciplex recombination rate. However, it slightly influences the total recombination rate. The report further suggested that MEL is independent of the

RISC spin-mixing mechanism [39].

2.2.1.1. Triazine acceptors. The highly symmetrical triazine core gained much attention as the electron acceptor in exciplex OLEDs. Three potential sites exist for structural modification in triazine where the tris-modified compounds, such as 2,4,6-tris(biphenyl-3-yl)-1,3,5-triazine (T2T, Fig. 2), 2,4,6-tris[3-(diphenylphosphinyl)phenyl]-1,3,5-triazine (PO-T2T, Fig. 2), 2,4,6-tris(3-(2-pyridyl)phenyl)-1,3,5-triazine (3N-T2T, Fig. 2), 2,4,6-tris(2-(1 H-pyrazole-1-yl)phenyl)-1,3,5-triazine (3P-T2T), and 3',3'',3''''-(1,3,5-triazine-2,4,6-triyl)tris(([1,1'-biphenyl]-3-carbonitrile)) (CN-T2T), yield C₃-symmetry structures (Fig. 4). The electronic properties of triazine vary with the substituents. These materials are popular in OLEDs because of their excellent electron-transporting ability. They are also widely used as the acceptors in exciplex OLEDs, and PO-T2T is the most common candidate. Our group developed the phosphine oxide-modified electron transport material PO-T2T, which immediately gained much attention in OLED research, as shown in a large number of related data in Table 1. Another notable discovery is the tri-pyrazolyl substituted derivative 2,4,6-tris(3-(1 H-pyrazole-1-yl)phenyl)-1,3,5-triazine, commonly known as 3P-T2T, which has a LUMO slightly lower than that of PO-T2T. Employing PO-T2T as the acceptor, we attempted tuning the color of the exciplex OLEDs from blue to red by blending the acceptor with different donors, such as mCP, TCTA, TAPC (Fig. 2), NPB (Fig. 3), N,N'-diphenyl-N,N'-di-[4-(N,N-diphenyl-amino)phenyl]benzidine (NPNPB, Fig. 4), and 9,9-di[4-(di-*p*-tolyl)aminophenyl]fluorine (DTAF, Fig. 4), and constructing all exciplex white OLED [40]. The emission color is expected to obey the formula $h\nu_{exciplex} = E_{LUMO}^A - E_{HOMO}^D$, which justifies the utilization of a range of donor materials in this investigation. PO-T2T exhibits excellent thermal stability, no evident glass transition, and high triplet energy (~3.0 eV). As intended, a range of EL maximum is obtained from the exciplex OLEDs with various donor materials: mCP (471 nm, blue), TCTA (552 nm, green), DTAF (572 nm, yellow), TAPC (586 nm, orange), and NPNPB (657 nm, red) [40]. The mCP:PO-T2T-based (blue) device has a unique performance among the series, with η_{ext} , current efficiency (CE), and PE of 8.0 %, 15.5 cd A⁻¹, and 18.4 lm W⁻¹, respectively. However, the performance of the NPNPB:PO-T2T-based (red) device is the poorest (EQE = 0.2 % only), possibly because of the energy gap law. An all-exciplex tandem white OLED is then fabricated for the first time using the blue- and orange-emitting configurations, i.e., mCP:PO-T2T and DTAF:PO-T2T. The relevant white OLED (wOLED) is outstanding at an EQE of 11.6 % with a low turn-on voltage of 4.0 V, a current efficiency of 27.7 cd A⁻¹, and PE of 15.8 lm W⁻¹ [40]. In another report, we demonstrated an interfacial exciplex OLED using a donor of C₃ symmetry (TCTA) with another acceptor molecule (3P-T2T) of the same symmetry, in which three pyrazolyl fragments are attached with the 2,4,6-triphenyl-1,3,5-triazine core [41]. At that time, the exciplex OLEDs using D:A blends as the emitters outperform those employing the D|A interfaces. However, the TCTA|3P-T2T-based interfacial device exhibits interesting performance (7.8 %, 23.6 cd A⁻¹, 26.0 lm W⁻¹), which is attributed to the high carrier mobilities of the components, balance charge transport, and counterbalancing energy levels at the D|A interface. Moreover, the confinement of the triplet excitons of the exciplexes within the interface, due to the high triplet energy of TCTA and 3 P-T2T, may have contributed positively to including the triplet excitons into the emission process through RISC, thereby increasing the PLQY and overall device efficiency. However, brightness and current density are enhanced when the D:A blend is used as the emission layer instead of the interface [41]. Zhang *et al.* demonstrated a blue exciplex system CDBP:PO-T2T with high triplet energy and efficient TADF emission. An OLED based on this exciplex emitter (476 nm) exhibits EQE as large as 13.0 % [42].

Another report by Hung *et al.* described efficiency enhancement by a remote steric effect on the donor molecules. The relevant exciplex systems comprise triphenylamine-fluorene hybrids, DTAF, and DSDTAF as

Table 1

Device data table – exciplexes as the emitters (the values in the parenthesis indicate data at 1000 nit).

Device structure (the exciplex component is underlined)	Φ_{film} (%)	V_{on} (V)	λ_{EL}^{max} (nm)	EQE (%)	CE (cd A ⁻¹)	PE (lm W ⁻¹)	CIE	Ref
Exciplexes in donor-acceptor blend or interface as the emitters								
ITO (10 nm)/-MTDATA (20 nm)/1:1 m-MTADATA:t-Bu-PBD (60 nm)/t-Bu-PBD (20 nm)/LiF (0.8 nm)/Al (50 nm)	20.0	—	540	2.0	—	—	—	[12]
ITO/m-MTADATA (20 nm)/1:1 m-MTADATA:3TPYMB (60 nm)/3TPYMB (20 nm)/LiF (0.8 nm)/Al	26.0	—	540	5.4	—	—	—	[12]
ITO/m-MTADATA (35 nm)/1:1 m-MTADATA:PPT (30 nm)/PPT (35 nm)/LiF (0.8 nm)/Al	28.5	—	510	10.0	—	47.0	—	[13]
ITO/TAPC (30 nm)/TCTA (10 nm)/1:1 TCTA:B3PYMPM (30 nm)/B3PYMPM(40 nm)/LiF (1 nm)/Al (100 nm)	36.0	2.8	495	3.19	—	—	—	[14]
ITO/NPB (10 nm)/TCTA (10 nm)/CzSi (5 nm)/1:1 CzSi:PO-T2T (20 nm)/PO-T2T (50 nm)/LiF (1 nm)/Al (100 nm)	—	3.0	465	6.1	8.9	7.0	0.16, 0.21	[15]
ITO/NPB (10 nm)/TCTA (10 nm)/mCP (5 nm)/1:1 mCP:PO-T2T (20 nm)/PO-T2T (50 nm)/LiF (1 nm)/Al (100 nm)	—	3.0	480	16 (12.9)	27.0	26.4	0.16, 0.28	[15]
ITO/NPB (30 nm)/TCTA (10 nm)/mCPP01 (5 nm)/1:1 mCPP01:PO-T2T (20 nm)/PO-T2T (50 nm)/LiF (1 nm)/Al (100 nm)	—	3.0	480	6.5 (4.5)	9.4	8.0	0.18, 0.29	[15]
ITO/NPB (30 nm)/TSBPA (10 nm)/1:1 TSBPA:POT2T (20 nm)/PO-T2T (50 nm)/LiF (1 nm)/Al (100 nm)	—	2.5	528	20 (18.0)	60.9	71.0	0.33, 0.57	[15]
ITO/NPB (40 nm)/TCBPA (10 nm)/1:1 TCBPA:POT2T (20 nm)/PO-T2T (60 nm)/LiF (1 nm)/Al (100 nm)	—	2.5	542	12.8 (12.0)	43.7	45.8	0.38, 0.56	[15]
ITO/TAPC (20 nm)/NPB (10 nm)/1:1 NPB:PO-T2T (20 nm)/PO-T2T (50 nm)/LiF (1 nm)/Al (100 nm)	—	3.5	585	2.4 (2.1)	5.0	4.8	0.53, 0.47	[15]
ITO/TAPC (40 nm)/TPD (10 nm)/1:1 TPD:PO-T2T (20 nm)/POT2T (50 nm)/LiF (1 nm)/Al (100 nm)	—	3.0	585	1.7 (1.0)	2.4	2.1	0.52, 0.46	[15]
ITO/NPB (30 nm)/DNTPD (10 nm)/1:1 DNTPD:PO-T2T (20 nm)/POT2T (50 nm)/LiF (1 nm)/Al (100 nm)	—	4.0	628	0.15	0.1	0.05	0.60, 0.39	[15]
ITO /HATCN (7.5 nm)/TAPC (35 nm)/BCzPh (10 nm)/CN-T2T (60 nm)/LiF (1 nm)/Al (100 nm)	—	2.5	540	7.7 (6.7)	25.5 (22.5)	32.1	0.36, 0.57	[16]
ITO/HATCN (7.5 nm)/TAPC (35 nm)/BCzPh (10 nm)/1:1 BCzPh:CN-T2T (30 nm; 1:1)/CN-T2T (30 nm)/LiF (1 nm)/Al (100 nm)	—	2.5	529	26.4 (19.3)	61.5 (61.3)	77.3	0.33, 0.56	[16]
ITO/PEDOT:PSS (30 nm)/ NPB (15 nm)/TCTA (5 nm)/mCP (5 nm) /1:1 mCP:PO-T2T (20 nm)/PO-T2T (45 nm)/Liq (0.5 nm)/Al	—	2.0	472	8.0	15.5	18.4	0.17, 0.23	[40]
ITO/PEDOT:PSS (30 nm)/ NPB(20 nm)/TCTA (5 nm) /1:1 TCTA:PO-T2T (20 nm)/PO-T2T (45 nm)/Liq (0.5 nm)/Al	—	2.0	552	6.2	18.6	12.9	0.41, 0.54	[40]
ITO/PEDOT:PSS (30 nm)/TAPC (20 nm)/mCP (15 nm)/1:1 DTAF:PO-T2T (20 nm)/PO-T2T (45 nm)/Liq (0.5 nm)/Al	—	2.0	572	5.7	15.1	14.6	0.47, 0.51	[40]
ITO/PEDOT:PSS (30 nm)/TAPC (20 nm)/1:1 TAPC:PO-T2T (20 nm)/PO-T2T (45 nm)/Liq (0.5 nm)/Al	—	2.0	586	3.7	8.9	7.5	0.51, 0.48	[40]
ITO/PEDOT:PSS (30 nm)/NPNPB (20 nm)/1:1 NPNPB:PO-T2T (20 nm)/PO-T2T (45 nm)/Liq (0.5 nm)/Al	—	3.0	657	0.2	0.1	0.1	0.64, 0.36	[40]
ITO/PEDOT:PSS (30 nm)/NPB (20 nm)/TCTA (5 nm)/3 P-T2T (75 nm)/Liq (0.5 nm)/Al	—	2.0	554	7.8	23.6	26.0	0.40, 0.55	[41]
ITO/TAPC (30 nm)/CDBP (10 nm)/1:1 CDBP:PO-T2T (30 nm)/PO-T2T (40 nm)/LiF (1 nm)/Al (100 nm)	51.0	2.5	476	13.0 (7.4)	26.6	27.8	0.17, 0.29	[42]
ITO/4% ReO ₃ :CPF (60 nm)/CPF (15 nm)/1:1 CPTBF:PO-T2T (25 nm)/PO-T2T (10 nm)/CN-T2T (40 nm)/Liq (0.5 nm)/Al (100 nm)	44.0	2.2	—	12.5 (9.1)	27.5	33.2	0.17, 0.29	[43]
ITO/4% ReO ₃ :CPF (60 nm)/CPF (15 nm)/1:1 CPF:PO-T2T (25 nm)/PO-T2T (10 nm)/CN-T2T (40 nm)/Liq (0.5 nm)/Al (100 nm)	41.0	2.2	—	9.5 (8.5)	21.9	22.9	0.18, 0.31	[43]
ITO/4% ReO ₃ :DTAF (60 nm)/DTAF (15 nm)/1:1 DSDTAF:3 N-T2T (25 nm)/CN-T2T (50 nm)/Liq (0.5 nm)/Al (100 nm)	59.0	2.0	535	13.2 (13.0)	42.9	47.3	0.37, 0.58	[43]
ITO/4% ReO ₃ :DTAF (60 nm)/DTAF (15 nm)/1:1 DTAF:3 N-T2T (25 nm)/CN-T2T (50 nm)/Liq (0.5 nm)/Al (100 nm)	51.0	2.0	551	11.6 (11.6)	35.3	41.3	0.42, 0.55	[43]
ITO/TAPC (50 nm)/mCP (10 nm)/CPTBF:3,4-CN (1:1, 20 nm)/PO-T2T (50 nm)/LiF (0.8 nm)/Al	18	5.74	524	6.87	23.8	22.6	0.35, 0.58	[44]
ITO/TAPC (50 nm)/mCP (10 nm)/ α -CPTBF:3,4-CN (1:1, 20 nm)/PO-T2T (50 nm)/LiF (0.8 nm)/Al	21	5.62	508	7.57	25.2	25.9	0.30, 0.56	[44]
ITO/TAPC (50 nm)/mCP (10 nm)/ β -CPTBF:3,4-CN (1:1, 20 nm)/PO-T2T (50 nm)/LiF (0.8 nm)/Al	25	5.60	510	7.34	24.4	24.7	0.30, 0.56	[44]
ITO/4% ReO ₃ :mCP (60 nm)/mCP (15 nm)/1:1 CN-Cz2:PO-T2T (20 nm)/PO-T2T (10 nm)/CN-T2T (40 nm)/Liq/Al	55.0	2.3	480	16.0 (14.7)	37.8	47.5	0.20, 0.40	[45]
ITO/TAPC (35 nm)/13AB (10 nm)/1:1 13AB:PO-T2T (30 nm)/PO-T2T (45 nm)/LiF (1 nm)/Al (100 nm)	—	2.3	540	12.4 (11.6)	40.4 (38.1)	35.6 (31.4)	0.37, 0.57	[46]
ITO/TAPC (35 nm)/13AB (10 nm)/1:1:1 13AB:PO-T2T:CDBP (30 nm)/PO-T2T (45 nm)/LiF (1 nm)/Al (100 nm)	—	2.3	532	15.5 (14.1)	49.9 (46.0)	43.8 (38.0)	0.32, 0.56	[46]
ITO/TAPC (35 nm)/DBT-SADF (10 nm)/6:4 DBTSADF:PO-T2T (30 nm)/PO-T2T (45 nm)/LiF (1 nm)/Al (100 nm)	—	2.4	524	16.9 (10.7)	52.4 (32.9)	55.9 (22.9)	0.29, 0.55	[46]
ITO/TAPC (35 nm)/CDBP (10 nm)/2:5:3 DBTSADF:PO-T2T:CDBP (30 nm)/PO-T2T (45 nm)/LiF (1 nm)/Al (100 nm)	—	2.4	516	20.5 (14.2)	60.0 (41.4)	61.0 (28.9)	0.26, 0.53	[46]
ITO/MoO ₃ (0.4 nm)/NPB (30 nm)/TCTA (15 nm)/ FCF (10 nm)/1:1 FCF:PO-T2T (10 nm)/PO-T2T (10 nm)/TPBi (60 nm)/LiF (0.4 nm)/Al (60 nm)	—	—	492	6.2	—	—	—	[47]
ITO/MoO ₃ (0.4 nm)/NPB (30 nm)/TCTA (15 nm)/ FCF (10 nm)/1:1 TCz1:PO-T2T (10 nm)/TPBi (60 nm)/LiF (0.4 nm)/Al (60 nm)	—	—	524	18.0	—	—	—	[47]
ITO/HAT-CN (10 nm)/TAPC (50 nm)/TCTA (5 nm)/1:1:3 TCTA:PO-T2T:mCP (10 nm)/PO-T2T (45 nm)/LiF (1 nm)/Al (100 nm)	—	2.2	523	8.0 (5.4)	23.7	28.0	—	[48]
ITO/TAPC (50 nm)/mCP (10 nm)/1:1 2-Ac:PO-T2T (30 nm)/PO-T2T (45 nm)/LiF (1 nm)/Al (100 nm)	—	—	546	8.0	26.9	24.4	0.39, 0.57	[49]

(continued on next page)

Table 1 (continued)

Device structure (the exciplex component is underlined)	Φ_{film} (%)	V_{on} (V)	λ_{EL}^{max} (nm)	EQE (%)	CE (cd A ⁻¹)	PE (lm W ⁻¹)	CIE	Ref
ITO/TAPC (50 nm)/mCP (10 nm)/1:1 4-Ac:PO-T2T (30 nm)/PO-T2T (45 nm)/LiF (1 nm)/Al (100 nm)	—	—	542	8.2	29.5	29.1	0.38, 0.57	[49]
ITO/MoO ₃ (3 nm)/TAPC (15 nm)/1:1 TAPC:3 P-T2T (12 nm)/3 P-T2T (25 nm)/LiF/Al (single)	—	2.1	570	6.86	18.1	18.9	—	[50]
ITO/MoO ₃ (3 nm)/TAPC (15 nm)/1:1 TAPC:3 P-T2T (12 nm)/3 P-T2T (25 nm)/3 P-T2T:Cs ₂ CO ₃ (10 nm)/Al (1 nm)/MoO ₃ (5 nm)/TAPC (15 nm)/TAPC:3 P-T2T (12 nm)/3 P-T2T (25 nm)/LiF/Al (tandem)	—	4.1	570	14.4	38.1	19.6	—	[50]
ITO/4% ReO ₃ :Tris-PCz (60 nm)/Tris-PCz (15 nm)/1:1 Tris-PCz:CN-T2T (25 nm)/CN-T2T (50 nm)/Liq (0.5 nm)/Al (100 nm)	53.0	2.0	530	11.9 (11.1)	37.0	46.5	0.33, 0.57	[51]
ITO/HATCN (10 nm)/TAPC (35 nm)/BCzPh (10 nm)/1:1 BCzPh:CN-T2T (25 nm)/CN-T2T (40 nm)/LiF (1 nm)/Al (100 nm)	—	2.4	537	21.1 (16.8)	57.3	68.5	0.36, 0.56	[52]
ITO/HATCN (10 nm)/TAPC (35 nm)/BCzPh (10 nm)/1:1 BCzPh:B3PYMPM (25 nm)/CN-T2T (40 nm)/LiF (1 nm)/Al (100 nm)	—	2.5	523	4.9	5.8	4.5	0.31, 0.51	[52]
ITO (100 nm)/HAT-CN (10 nm)/Tris-PCz (30 nm)/1:1 Tris-PCz:T2T (30 nm)/SF3-TRZ (10 nm)/50 wt% Liq:SF3-TRZ (20 nm)/Liq (2 nm)/Al (100 nm)	45.3	3.2	518	11.5 (11.1)	34.4	33.8	0.28, 0.54 (LT ₅₀ = 66 h)	[53]
ITO (100 nm)/HAT-CN (10 nm)/Tris-PCz (30 nm)/1:1 Tris-PCz: SF3-TRZ (30 nm)/SF3-TRZ (10 nm)/50 wt% Liq:SF3-TRZ (20 nm)/Liq (2 nm)/Al (100 nm)	34.7	3.2	504	8.7 (8.0)	25.0	24.6	0.25, 0.52 (LT ₅₀ = 93 h)	[53]
ITO/HATCN (5 nm)/TAPC (55 nm)/TCTA:Tm3PyBPZ (30 nm)/Tm3PyBPZ (40 nm)/Liq (2 nm)/Al (100 nm)	—	2.4	514	13.1	44.2	54.5	—	[54]
ITO/TCTA (10 nm)/1:1 TCTA:B3PYMPM (30 nm)/BPhen (20 nm)/Cs ₂ CO ₃ (1 nm)/Al (1 nm)	36.0	—	490	0.93 (0.75)	21.4	—	—	[58]
ITO/MoO ₃ (1 nm)/1:1 TAPC:24iPBIOXD (70 nm)/LiF (1 nm)/Al (100 nm)	—	2.8	519	9.3	28.8	32.3	0.31, 0.55	[59]
ITO/MoO ₃ (1 nm)/1:1 TAPC: iTPBIOXD (70 nm)/LiF (1 nm)/Al (100 nm)	—	2.8	556	7.0	22.1	23.4	0.43, 0.54	[59]
ITO/MoO ₃ (1 nm)/TAPC (40 nm)/1:1 TCTA:24iPBIOXD (30 nm)/TmPyPB (40 nm)/LiF (1 nm)/Al (100 nm)	—	3.0	—	4.0	10.1	10.6	0.26, 0.43	[59]
ITO/MoO ₃ (1 nm)/TAPC (40 nm)/1:1 TCTA: iTPBIOXD (30 nm)/TmPyPB (40 nm)/LiF (1 nm)/Al (100 nm)	—	3.0	—	3.9	10.6	10.2	0.25, 0.44	[59]
ITO/MoO ₃ (1 nm)/TAPC (40 nm)/TCTA (10 nm)/1:1 mCP:24iPBIOXD (30 nm)/TmPyPB (40 nm)/LiF (1 nm)/Al (100 nm)	—	3.8	—	0.65	0.8	0.66	0.19, 0.20	[59]
ITO/MoO ₃ (1 nm)/TAPC (40 nm)/TCTA (10 nm)/1:1 mCP: iTPBIOXD (30 nm)/TmPyPB (40 nm)/LiF (1 nm)/Al (100 nm)	—	3.8	—	0.63	0.9	0.74	0.20, 0.23	[59]
ITO/PEDOT:PSS:m-MTADATA (20 nm)/1:1 m-MTADATA:3TPYMB (60 nm)/3TPYMB (15 nm)/LiF(0.8 nm)/Al(100 nm)	—	2.4	—	—	42.1 (40.1)	—	—	[62]
ITO/m-MTADATA (20 nm)/1:1 m-MTADATA:BPhen (27 nm)/BPhen (20 nm)/LiF (1 nm)/Al (80 nm)	17.0	—	—	5.49	14.7	9.08	—	[69]
ITO/m-MTADATA (30 nm)/1:1 m-MTADATA:TPBi (17 nm)/TPBi (27 nm)/(BCP) (7 nm)/LiF (1 nm)/Al (80 nm)	17.0	—	—	6.85	18.80	6.10	—	[69]
ITO/TCTA (10 nm)/1:1 m-MTADATA:OXD-7 (30 nm)/BPhen (20 nm)/Cs ₂ CO ₃ (1 nm)/Al (1 nm)	28.0	2.3	545	3.76	90.3	—	—	[69]
ITO/CuI (8 nm)/DPNC (30 nm)/BPhen (30 nm)/Ca (50 nm)/Al (200 nm)	—	4.0	580	3.3	10.5	3.6	—	[71]
ITO/CuI (4 nm)/DPNC (60 nm)/TPBi (60 nm)/Ca (50 nm)/Al (240 nm)	—	2.3	540	1.2	8.5	2.2	—	[71]
ITO/NPB (30 nm)/1:1 NPB:TPBi (35 nm)/TPBi (35 nm)/LiF(1 nm)/Al (100 nm)	28.0	2.5	450	2.7	—	—	0.15, 0.13	[72]
ITO/α-NPD (30 nm)/TCTA(10 nm)/1:1 HAP-3MF:mCP (20 nm)/DPEPO (10 nm)/TPBi (40 nm)/LiF (0.8 nm)/Al (100 nm)	66.1	4.0	550	11.3	—	—	—	[74]
ITO/MoO ₃ (5 nm)/TCTA (60 nm)/NPB (45 nm)/5:1 TPBi:PPh ₃ O (14 nm)/PPh ₃ O (15 nm)/BPhen (30 nm)/CsF (1.5 nm)/Al (110 nm)	—	3.6	435	4.0	—	2.23	0.15, 0.08	[75]
Exciplexes in the blend of donor or acceptor material with a donor-acceptor bipolar material as the emitters								
ITO/TAPC (35 nm)/TCTA or NPB (5 nm)/1:1 TAPC:DPTPCz (30 nm)/TmPyPB (40 nm)/LiF (1 nm)/Al (100 nm)	68.0	—	503	15.4	—	—	0.27, 0.52	[20]
ITO/TAPC (35 nm)/TCTA or NPB (5 nm)/1:1 TCTA:DPTPCz (30 nm)/TmPyPB (40 nm)/LiF (1 nm)/Al (100 nm)	55.0	2.8	502	11.9	34.2	35.8	—	[20]
ITO/TAPC (35 nm)/TCTA or NPB (5 nm)/1:1 NPB:DPTPCz (30 nm)/TmPyPB (40 nm)/LiF (1 nm)/Al (100 nm)	15.0	—	491	0.6	—	—	—	[20]
ITO (100 nm)/HAT-CN (10 nm)/Tris-PCz (30 nm)/1:1 Tris-PCz:3Cz-TRZ (30 nm)/SF3-TRZ (10 nm)/50 wt% Liq:SF3-TRZ (20 nm)/Liq (2 nm)/Al (100 nm)	45.0	3.0	511	8.9 (8.4)	26.1	27.4	0.26, 0.53 (LT ₅₀ = 337 h)	[53]
ITO (100 nm)/HAT-CN (10 nm)/Tris-PCz (30 nm)/1:1 Tris-PCz:BCz-TRZ (30 nm)/SF3-TRZ (10 nm)/50 wt% Liq:SF3-TRZ (20 nm)/Liq (2 nm)/Al (100 nm)	50.0	3.2	499	11.9 (11.3)	33.6	33.0	0.26, 0.50 (LT ₅₀ = 292 h)	[53]
ITO (100 nm)/HAT-CN (10 nm)/Tris-PCz (30 nm)/1:1 Tris-PCz:Cz-TRZ (30 nm)/SF3-TRZ (10 nm)/50 wt% Liq:SF3-TRZ (20 nm)/Liq (2 nm)/Al (100 nm)	40.3	3.0	517	9.5 (9.1)	29.1	30.6	0.29, 0.55 (LT ₅₀ = 123 h)	[53]
ITO/MoO ₃ (3 nm)/TAPC (25 nm)/4:6 TAPC:T2T (15 nm)/T2T (5 nm)/BPhen (30 nm)/LiF (1 nm)/Al (100 nm)	—	2.4	528	11.6 (9.4)	40.4	42.2	—	[53]
ITO/NPB (60 nm)/38% t-Cbz-SO:TAPC (30 nm)/TPBi (10 nm)/BCP (20 nm)/LiF (1 nm)/Al (100 nm)	53.0	—	540	14.0	26.3	20.3	—	[77]
ITO/MoO ₃ (3 nm)/mCBP (20 nm)/1:1 DMAC-DPS:T2T (25 nm)/T2T (40 nm)/LiF (0.8 nm)/Al (100 nm)	—	—	480	4.4	—	—	—	[78]
ITO/MoO ₃ (3 nm)/mCBP (20 nm)/1:1 DMAC-DPS: B4PyMPM (25 nm)/B4PyMPM (40 nm)/LiF (0.8 nm)/Al (100 nm)	—	—	493	4.4	—	—	—	[78]
ITO/MoO ₃ (3 nm)/mCBP (20 nm)/1:1 DMAC-DPS:PO-T2T (25 nm)/PO-T2T (40 nm)/LiF (0.8 nm)/Al (100 nm)	—	—	535	9.1	—	—	—	[78]
	—	—	550	1.6	—	—	—	[78]

(continued on next page)

Table 1 (continued)

Device structure (the exciplex component is underlined)	Φ_{film} (%)	V_{on} (V)	λ_{EL}^{max} (nm)	EQE (%)	CE (cd A $^{-1}$)	PE (lm W $^{-1}$)	CIE	Ref
ITO/MoO ₃ (3 nm)/TPD (20 nm)/1:1 TPD:DMAC-DPS (25 nm)/PO-T2T (45 nm)/LiF (0.8 nm)/Al								
ITO (95 nm)/HATCN (5 nm)/TAPC (20 nm)/1:1 m-MTADATA:26DCzPPy (20 nm)/TmPyPB (50 nm)/LiF (1 nm)/Al (100 nm)	20.3	—	520	5.0	15.9	—	—	[79]
ITO (95 nm)/HATCN (5 nm)/TAPC (20 nm)/1:1 TAPC:26DCzPPy (20 nm)/TmPyPB (50 nm)/LiF (1 nm)/Al (100 nm)	5.7	—	450	1.1	2.2	—	—	[79]
ITO/PEDOT:PSS (60 nm)/TAPC (20 nm)/mCP (20 nm)/1:1 DMAC-DPS:TCzTrz (25 nm)/TSPO1 (5 nm)/TPBi (30 nm)/LiF (1 nm)/Al (200 nm)	54.0	—	500	15.3 (10.7)	41.2 (28.5)	31.4 (13.6)	0.25, 0.46	[80]
ITO/PEDOT:PSS (60 nm)/TAPC (20 nm)/mCP (20 nm)/1:1 DMAC-DPS:DDCzTrz (25 nm)/TSPO1 (5 nm)/TPBi (30 nm)/LiF (1 nm)/Al (200 nm)	49.0	—	521	13.4 (10.5)	40.4 (31.3)	35.8 (15.0)	0.31, 0.53	[80]
ITO/TAPC (40 nm)/mCP (10 nm)/5:5 MAC:PO-T2T (20 nm)/PO-T2T (45 nm)/LiF (1 nm)/Al (150 nm)	—	2.4	516	13.3 (10.3)	39.0 (30.6)	35.0 (19.5)	0.31, 0.55	[81]
ITO/TAPC (40 nm)/mCP (10 nm)/7:3 MAC:PO-T2T (20 nm)/PO-T2T (45 nm)/LiF (1 nm)/Al (150 nm)	—	2.4	516	17.8 (12.3)	52.1 (35.6)	45.5 (21.5)	0.31, 0.55	[81]
ITO/PEDOT:PSS (60 nm)/TAPC (30 nm)/1:1 TCTA:CzTrz (25 nm)/TSPO1 (5 nm)/TPBi (30 nm)/LiF (1 nm)/Al (200 nm)	55.0	—	510	12.6	—	27.5	0.27, 0.53	[82]
ITO/PEDOT:PSS (60 nm)/TAPC (30 nm)/1:1 TCTA:DTrz (25 nm)/TSPO1 (5 nm)/TPBi (30 nm)/LiF (1 nm)/Al (200 nm)	37.0	—	515	5.5	—	11.0	0.35, 0.52	[82]
ITO/PEDOT:PSS (60 nm)/TAPC (30 nm)/1:1 TAPC:CzTrz (25 nm)/TSPO1 (5 nm)/TPBi (30 nm)/LiF (1 nm)/Al (200 nm)	36.0	—	515	8.9	—	19.7	0.30, 0.55	[82]
ITO/PEDOT:PSS (60 nm)/TAPC (30 nm)/1:1 TAPC:DTrz (25 nm)/TSPO1 (5 nm)/TPBi (30 nm)/LiF (1 nm)/Al (200 nm)	16.0	—	530	3.3	—	7.0	0.39, 0.51	[82]
ITO/TAPC (40 nm)/TCTA (20 nm)/3:1 DPSTPA:2CzPN (30 nm)/3TPYMB (80 nm)/LiF (1 nm)/Al (100 nm)	—	3.0	544	19.0	59.9	62.7	0.38, 0.55	[84]
ITO/TAPC (40 nm)/TCTA (20 nm)/3:1 DPSTPA:4CzIPN (30 nm)/3TPYMB (80 nm)/LiF (1 nm)/Al (100 nm)	—	3.1	590	3.8	8.3	7.5	0.50, 0.48	[84]
ITO/TAPC (40 nm)/TCTA (20 nm)/3:1 DPSTPA:CzDBA (30 nm)/3TPYMB (80 nm)/LiF (1 nm)/Al (100 nm)	—	2.9	592	14.6	29.6	31.0	0.53, 0.46	[84]
ITO/CuI (7 nm)/TCTA (40 nm)/DTS-XA (40 nm)/TPBi (20 nm)/Ca:Al	—	6.2	433	9.1	—	—	—	[85]
ITO/CuI (7 nm)/m-MTADATA (40 nm)/DTS-XA (40 nm)/TPBi (20 nm)/Ca:Al	—	4.2	524	8.3	—	—	—	[85]
ITO (50 nm)/PEDOT:PSS (60 nm)/TAPC (10 nm)/SiCz (20 nm)/99:1 DMAC-DPS:PO-T2T (25 nm)/DPEPO (5 nm)/TPBi (20 nm)/LiF (1 nm)/Al (200 nm)	—	6.9	—	15.3 (12.3)	22.0 (17.1)	—	0.20, 0.41	[86]
ITO (50 nm)/PEDOT:PSS (60 nm)/TAPC (10 nm)/SiCz (20 nm)/90:10 DMAC-DPS:PO-T2T (25 nm)/DPEPO (5 nm)/TPBi (20 nm)/LiF (1 nm)/Al (200 nm)	—	6.7	—	13.0 (11.3)	21.8 (18.3)	—	0.24, 0.51	[86]
ITO (50 nm)/PEDOT:PSS (60 nm)/TAPC (10 nm)/SiCz (20 nm)/50:50 DMAC-DPS:PO-T2T (25 nm)/DPEPO (5 nm)/TPBi (20 nm)/LiF (1 nm)/Al (200 nm)	—	7.2	—	10.8	28.6	—	0.32, 0.58	[86]
ITO/TAPC (35 nm)/TCTA (5 nm)/1:1 TPAFPO:PO-T2T (45 nm)/PO-T2T (60 nm)/LiF (0.8 nm)/Al (80 nm)	—	2.4	540	17.0	—	—	—	[88]
ITO/HAT-CN (10 nm)/TAPC (35 nm)/TCTA (5 nm)/1:1 TCTA:TRZSFX (35 nm)/TmPyPB (35 nm)/LiF (1 nm)/Al (120 nm)	—	2.7	520	22.5 (15.2)	79.6 (53.7)	78.1 (41.8)	0.35, 0.60	[89]
ITO/HAT-CN (10 nm)/TAPC (35 nm)/TCTA (5 nm)/1:1 TCTA:DTRZSFX (35 nm)/TmPyPB (35 nm)/LiF (1 nm)/Al (120 nm)	—	3.0	560	9.7 (1.4)	28.7 (4.0)	27.7 (2.0)	0.44, 0.51	[89]
ITO/TAPC (30 nm)/Pra-2DMAC (10 nm)/40:60 Pra-2DMAC:PO-T2T (30 nm)/PO-T2T (50 nm)/LiF (0.8 nm)/Al (80 nm)	—	2.4	540	15.0 (13.9)	49.2 (45.8)	—	0.36, 0.56	[90]
ITO/TAPC (30 nm)/Prm-2DMAC (10 nm)/40:60 Prm-2DMAC:PO-T2T (30 nm)/PO-T2T (50 nm)/LiF (0.8 nm)/Al (80 nm)	—	2.9	512	10.3 (2.86)	26.9 (7.8)	—	0.25, 0.45	[90]
ITO/TAPC (40 nm)/TAPC:CzT2.1 (7:3, 20 nm)/TmPyPB (50 nm)/LiF (0.8 nm)/Al (120 nm)	62	2.6	537	12.5	39.2	41.4	0.30, 0.60	[92]
ITO/TAPC (40 nm)/TCTA:CzT2.1 (7:3, 20 nm)/TmPyPB (50 nm)/LiF (0.8 nm)/Al (120 nm)	48	2.6	514	9.6	27.9	29.1	0.26, 0.56	[92]
ITO/TAPC (40 nm)/TAPC:CzT2.2 (7:3, 20 nm)/TmPyPB (50 nm)/LiF (0.8 nm)/Al (120 nm)	58	2.5	514	15.0	45.7	50.0	0.25, 0.59	[92]
ITO/TAPC (40 nm)/TCTA:CzT2.2 (7:3, 20 nm)/TmPyPB (50 nm)/LiF (0.8 nm)/Al (120 nm)	57	2.6	514	11.7	35.2	37.0	0.22, 0.55	[92]

the donors (Fig. 4) and 3 N-T2T as the acceptor (Fig. 2) in their 1:1 blend. The difference between the two donor structures is the attachment of two bulky SiPh₃ substituents on the fluorene fragment of DSDTAF [43]. Compared with that in DTAF, the enhanced steric bulkiness in DSDTAF increases the effective contact between the donor and acceptor counterparts in the blend, thereby rendering high PLQY of the exciplex, which is indeed found to be the case. The remote substitution causes a slight change in emission color, 551 nm for DTAF:3N-T2T vs 535 nm for DSDTAF:3N-T2T-based device. The device efficiency of the OLED based on the sterically congested donor DSDTAF is higher (13.2 %, 42.9 cd A $^{-1}$, 45.5 lm W $^{-1}$) than that of the device based on DTAF:3N-T2T exciplex (11.6 %, 35.3 cd A $^{-1}$, 41.3 lm W $^{-1}$) under the same device structure. The concept of emission enhancement by remote steric effect is further extended to another pair of donor molecules to examine its validity. Therefore, two carbazole-fluorene hybrid donors, CPF and CPTBF (Fig. 4), differ by attachment of two bulky tert-butyl

groups on the fluorene core of CPTBF, are investigated. When these two donors are individually combined with an appropriate acceptor, PO-T2T, the EQE enhancement from 9.5 % (CPF:PO-T2T) to 12.5 % (CPTBF:PO-T2T) is determined, thereby consolidating the theory [43]. The replacement of carbazole in CPTBF with α - and β -carboline led to two lower HOMO energy level donors, α -CPTBF and β -CPTBF (Fig. 4), respectively, which were blended with a new triazine acceptor, 4-(4,6-diphenyl-1,3,5-triazin-2-yl)phthalonitrile (3,4-CN, Fig. 4), to form green exciplex systems [44]. The devices employing α -CPTBF:3,4-CN and β -CPTBF:3,4-CN blends as EMLs exhibit better device characteristics as compared to those of the parent CPTBF:3,4-CN blend mainly due to the higher triplet energy of carboline for giving the higher delay fluorescence contributions.

Exciplexes have transient existence only in the excited state. Thus, the information regarding their structures is lacking, impeding the realization of efficient luminescence from the exciplex OLEDs for

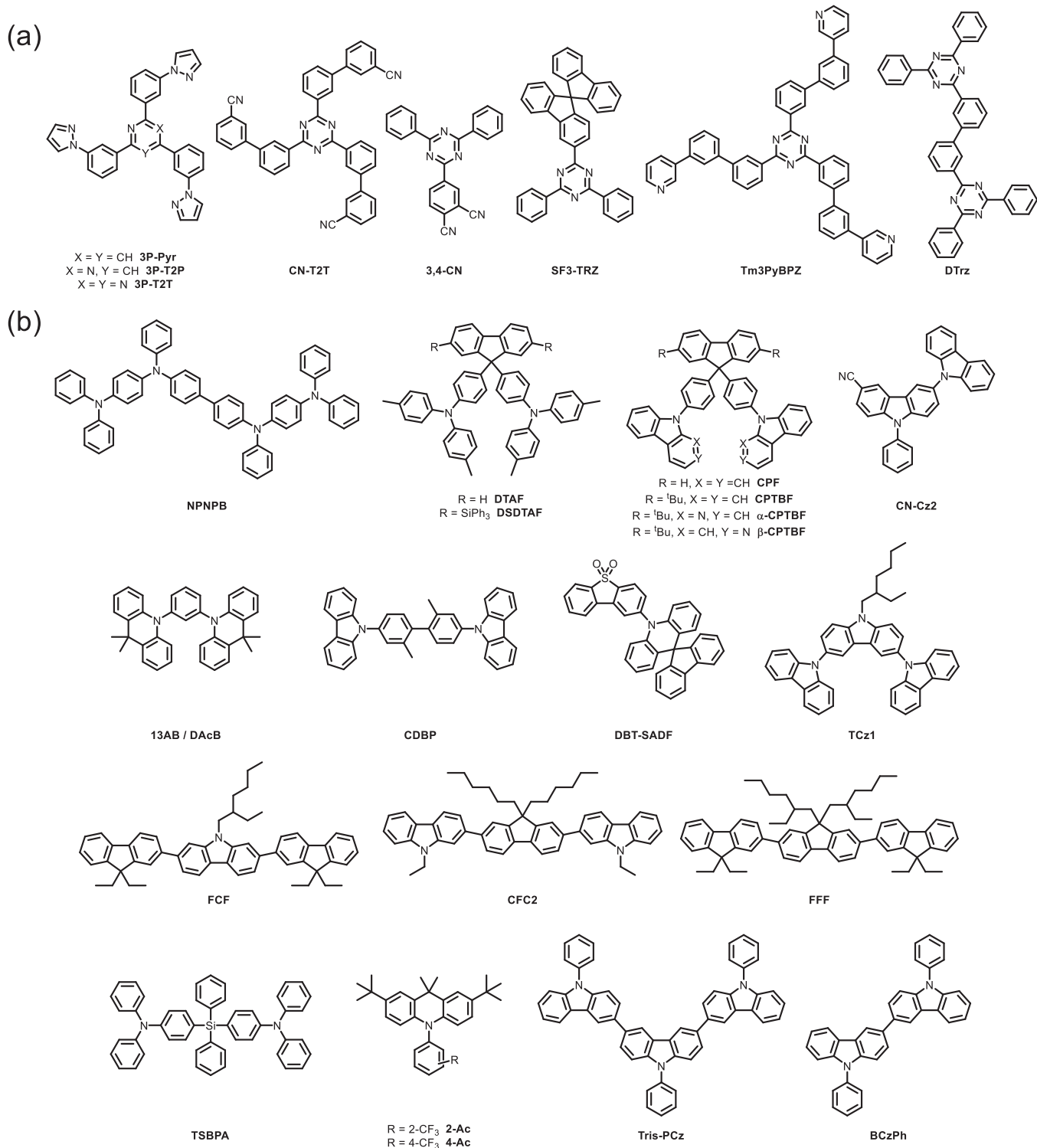


Fig. 4. (a) Molecular structures of the triazine acceptors and (b) the reported donors that were paired with the triazine acceptors.

decades. The geometric and electronic structures of the emitting states of the conventional luminophores can be easily modeled by advanced quantum chemical methods, such as time-dependent density-functional theory (TDDFT) and configuration interaction singles (CIS). However, the emitting states of the exciplexes are heteromolecular and complex. Thus, simple excited-state calculations are not enough for yielding structural information about the exciplexes. We attempted to solve this problem by employing the step-scan Fourier-transform infrared (FTIR) spectroscopic technique and density functional theory methods on an

exciplex consisting of a newly synthesized carbazole-based donor (CN-Cz2, Fig. 4) and PO-T2T as the acceptor [45]. The cyano-functionalized substance is selected primarily because of the strong and sharp infrared (IR) absorption ($2200\text{--}2500\text{ cm}^{-1}$), which can be used as a marker for transient Fourier transform infrared spectroscopy (FTIR) spectroscopy alongside modulation of the electronic structure of the material by the electron-withdrawing cyano group. The relevant exciplex-based (CN-Cz2:PO-T2T) cyan OLED exhibits outstanding performance, such as a low turn-on voltage of 2.3 V and high EQE (16 %, 37.8 cd A^{-1} ,

47.5 lm W⁻¹) with low-efficiency roll-off. The subsequent step-scan FTIR analysis is performed on a vacuum-deposited film on CaF₂ substrate using the following setup: 266 nm fourth harmonic of an Nd:YAG laser as the pump pulse, IR probe beam at an angle of ~45°, and sample thickness of ~1 nm. Absorptions due to the exciplex, which follows the same dynamics as the TADF emission obtained by the time-correlated single-photon counting technique, are observed (Fig. 5). The investigation suggested polaron pair formation in the exciplex, which can either recombine radiatively or dissociate. The latter leads to ionic polarons, which inhibit light emission. This scenario further explains the reason behind quantum yields in the exciplex-based systems that are lower than those in the conventional emitters. The grazing incident x-ray diffraction study indicated that the interplanar distance between the components in the films is larger than that in the films of the individual components, indicating an interaction between the counterparts. Moreover, in-plane intercalation-like interaction prevails the π-π stacking interaction between the D and A molecules in the exciplex [45].

Despite considerable progress, the device efficiency of the exciplex OLEDs remains far from the theoretical limit of 30 %. The overall quantum yield of any TADF-emitting material is a factor of RISC and fluorescence quantum efficiency. Zhang *et al.* underlined that the efficacy of conventional TADF emitters is limited by only one RISC channel, which mitigates the triplet harnessing ability of the system. The group also developed an interesting methodology to overcome the shortcoming. They synthesized two tricomponent exciplex systems based on different donor molecules and PO-T2T acceptors, viz., 13AB:PO-T2T:CDBP and DBT-SADF:PO-T2T:CDBP (Fig. 4), and compared their performance with that of the bicomponent analogs [46]. The former is a D:A:D type exciplex system having two RISC channels, one for each of the D:A equivalence, whereas the latter is a DA:A:D prototype exciplex system adopting three such channels, one for the TADF molecule itself and two for the D:A counterparts. The PLQY and k_{RISC} of the

tricomponent exciplexes are considerably high. For example, the PLQY and k_{RISC} for 13AB:PO-T2T:CDBP exciplex system is 40 % and 0.64 × 10⁵, whereas the analogous bicomponent system, 13AB:PO-T2T, exhibits only 15 % and 0.05 × 10⁵, respectively. The corresponding values for the system with three RISC channels, i.e., DBT-SADF:PO-T2T:CDBP, are 38.0 % and 1.17 × 10⁵, manifesting the importance of the high number of RISC channels on the subsequent rate constant. Similarly, the EQE of the tricomponent device 13AB:PO-T2T:CDBP (15.5 %) is higher than that of the bicomponent one at the same device configuration (12.4 %). However, the device efficiency of the DBT-SADF:PO-T2T:CDBP exciplex system having three RISC channels is 20.5 %, remarkably higher than that of its bicomponent partner DBT-SADF:PO-T2T (16.9 %) [46].

The exciplex emission has some intricacy, such as the formation of emissive states with different donor-acceptor distances, which adversely affect the emission color purity. Therefore, a broad emission range is observed where the systems with less D-A separation emit at a long wavelength, and those with great intermolecular distance have emissions at high energies. This finding demands a comprehensive investigation of the exciplex emission from organic solid films. Grazulevicius and coworkers reported a dual nature of exciplexes where two different emission bands (sky blue and orange) are shown by the mCP:PO-T2T exciplex system [47]. The alien orange emission persists along with the blue emission in the mCP|PO-T2T interface exciplex OLED. However, only one emission color is observed for the relevant annealed or nonannealed devices containing the volume exciplex (1:1 blend) of the same components. The authors suggested that the fraction of the high and low energy emitting exciplex systems is influenced by the energy barrier between the corresponding locally excited (LE) and exciplex states and justified their statement by probing four different systems based on 3,6-di(9-carbazolyl)-9-(2-ethylhexyl)carbazole (TCz1), 2,7-bis(9,9-diethylfluoren-2-yl)-9-(2-ethylhexyl)carbazole (FCF), 2,7-bis

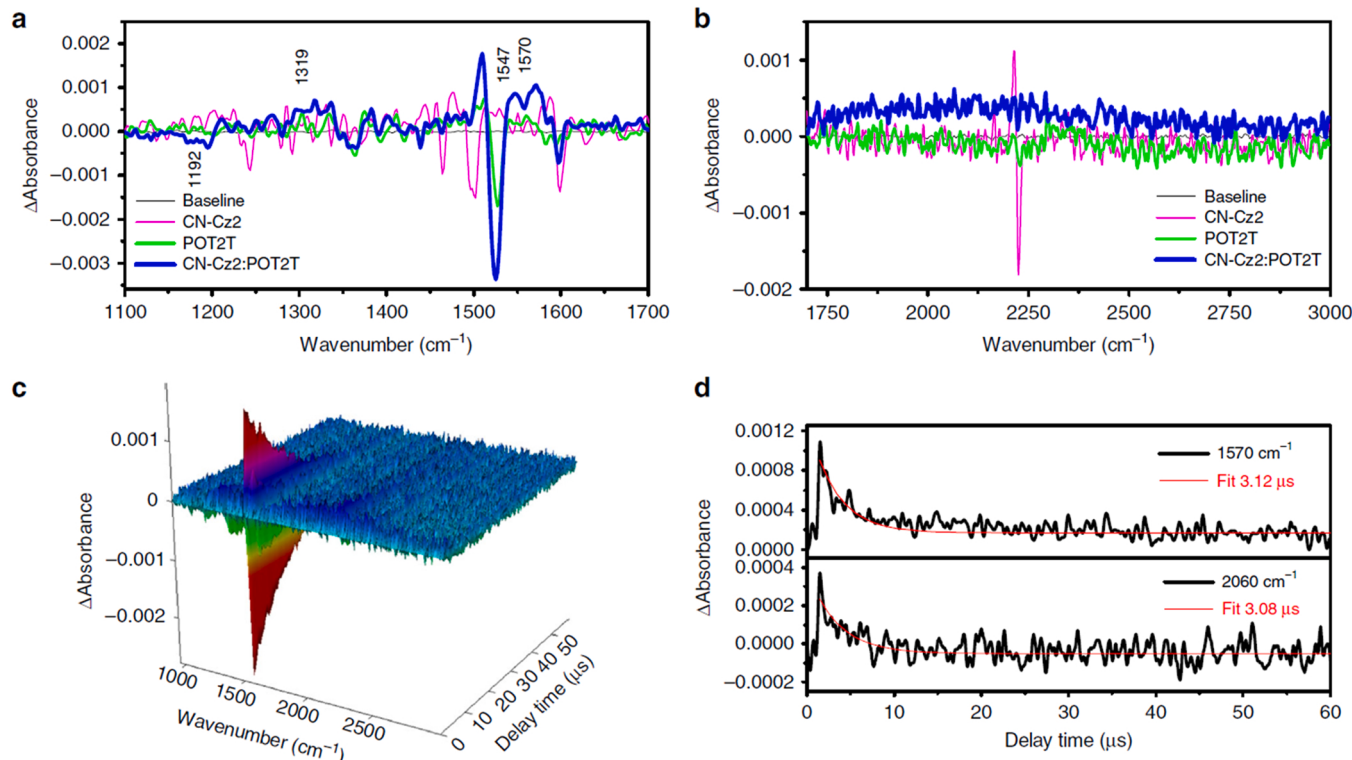


Fig. 5. (a-b) Transient IR spectra of thin films of CN-Cz2, PO-T2T, and CN-Cz2:PO-T2T (1:1) with a delay time of 1.6 μs in different spectral ranges. (c) Absorbance-frequency-time 3D plot for the CN-Cz2:POT2T (1:1) blend film. (d) Relaxation dynamics of 1570 and 2060 cm⁻¹ for the CN-Cz2:PO-T2T (1:1) film with λ_{ex} of 266 nm. Copyright 2018.

Reproduced with permission from [45] Springer Nature publishing group.

(9-ethylcarbazol-2-yl)-9,9-dihexylfluorene (CFC2), and 2,7-bis(9,9-diethylfluoren-2-yl)-9,9-di(2-ethylhexyl)fluorene (FFF) as the donors (Fig. 4) for PO-T2T acceptor. The systems where the low energy exciplexes prevailed have inferior device performance compared with those with minimized contribution from the low energy exciplexes due to leakage of energy in the former. This apparent problem is solved by thermal annealing, and exciplex OLEDs with EQE as high as 18 % were reported [47].

Given the critical role of the donor-acceptor distance in the exciplex emission, the systems with distance flexibility are interesting models to understand the details of the complicated emission. Adachi and co-workers designed and demonstrated such a system with long-range radiative coupling between electrons and holes for the first time in 2016 [26]. In a recent article, Yuan *et al.* opted for another approach to obtain high-efficiency exciplex OLEDs utilizing the long-range coupling phenomenon [48]. The donor-acceptor separation can be modulated either by inserting a thin layer of spacer molecules between the D and A layers or by doping the spacer directly into the D:A blend. Yuan *et al.* chose the codoping method using TCTA as the donor, PO-T2T as the acceptor, and mCP as the spacer. mCP is selectively chosen because of its large energy gap and unlikely interference in the exciplex emission. The TCTA:PO-T2T:mCP film exhibits emission characteristics of exciplexes between TCTA and PO-T2T. The exciplex formation between mCP and PO-T2T can be observed at an mCP layer thickness of more than 1 nm in the case of interfacial OLED. However, no such undesirable emission is detected even at a high doping concentration of the spacer in the D:A blend, suggesting the superiority of the blend OLEDs compared with the interfacial devices. The EQE, current, and PE of the blend mode devices are gradually increased with the mCP richness of the blend. For example, the device with a 1:1:3 doping ratio of TCTA:PO-T2T:mCP displays a high EQE of 8.0 % (23.7 cd A⁻¹, 28.0 lm W⁻¹) compared with only 3.9 % (11.6 cd A⁻¹, 13.1 lm W⁻¹) for the blend of 1:1:0 concentration ratio [48].

Chapran *et al.* depicted some high-performance exciplex OLEDs based on a range of triphenylamine-based donors and PO-T2T as the acceptor with emission tunability from the blue to the orange region in the visible spectrum. The relevant exciplex OLEDs show excellent device performance. For example, the TSBPA:PO-T2T (Fig. 4) exciplex-based green device is outstanding at η_{ext} of 20 % (60.9 cd A⁻¹, 71 lm W⁻¹) [15]. Then, Keruckiene *et al.* developed two acridine-based molecules 2-Ac and 4-Ac (Fig. 4) and demonstrated their exciplex-forming ability with PO-T2T. The OLEDs using these exciplexes as emitters exhibit EQEs of as high as ~8 % [49]. Besides PO-T2T, triazine-based acceptors are useful. Zhao *et al.* carefully picked donor and acceptor counterparts based on their carrier mobility and FMOs to fabricate blue, orange, and white exciplex OLEDs [50]. Accordingly, the TCTA:BPhen (Fig. 2) combination is selected for the blue emission, whereas the TAPC:3 P-T2T blend is preferred for the orange emission because the HOMO of TAPC (5.5 eV) is shallower than that of TCTA (5.8 eV). Both the single and tandem devices are fabricated for comparison purposes. The tandem device outperforms the single device. The TAPC:3 P-T2T-based orange single device shows EQE of 4.8 % and current efficiency of 12.6 cd A⁻¹, whereas those for the tandem device are 14.4 % and 38.1 cd A⁻¹, respectively. The performance of the TCTA:BPhen-based blue exciplex is relatively poor at 2.7 % and 3.6 cd A⁻¹. A tandem white OLED is then fabricated by employing the blue and the orange exciplexes using a specially designed charge generation layer. The relevant white OLED displays an EQE of 9.2 % (25.4 cd A⁻¹) [50].

We developed another triazine-based star-shaped acceptor material CN-T2T (Fig. 4) by incorporating benzonitrile fragments onto 2,4,6-triphenyl-1,3,5-triazine and then blended this acceptor with a hole-transporting material Tris-PCz (Fig. 4) [51]. The donor and acceptors possess high triplet energy and balanced electron and hole mobility that would lead to adequate carrier density at the D:A interface for simple generation of exciplexes. Then, a device is configured with the structure of ITO/4 % ReO₃:Tris-PCz (60 nm)/Tris-PCz (15 nm)/Tris-PCz:CNT2T

(1:1) (25 nm)/CN-T2T (50 nm)/Liq (0.5 nm)/Al (100 nm), which generates green emission (530 nm) and exhibits device efficiency as high as 11.9 % (37 cd A⁻¹ and 46.5 lm W⁻¹) with low driving voltage. Another device is fabricated with TCTA exhibiting similar energy levels as Tris-PCz to realize the effect of charge balance on the exciplex formation. However, this device has hole mobility that is slightly higher than that of Tris-PCz. The TCTA-based device has EQE lower than that of the Tris-PCz device, indicating the importance of charge balance on exciplex formation [51].

The relationship between SOC, singlet-triplet gap, and polarization is crucial to designing novel materials for light-emitting applications. Wang *et al.* addressed this issue on exciplex-based TADF emitters using MPL, photoinduced electron paramagnetic resonance (EPR), and time-resolved PL (TRPL) techniques [52]. The models used for this study are the exciplexes based on a carbazole donor material BCzPh (Fig. 4) and B3PYMPM (Fig. 2) and CN-T2T acceptors. The exciplexes are selected because they have similar energy levels leading to comparable emission characteristics, although at a considerably different singlet-triplet gap. The SOC is studied by MPL by monitoring at different PL emission wavelengths, and the formation of the radical ions is detected by photoinduced EPR (Fig. 6). The BCzPh:CN-T2T exciplex OLED exhibits outstanding device performance with a low turn-on voltage of 2.4 V, a maximum brightness of 10655 cd m⁻² (8 V), and a high EQE of 21.05 % with a low-efficiency roll-off. The other OLED based on BCzPh:B3PYMPM does not perform well and displays a considerably low EQE of only 4.89 % and low brightness. This striking difference between the device performances of the two exciplex OLEDs is then probed by MPL, which demonstrates the role of SOC on their performance. The authors concluded after analyzing the MPL data at a magnetic field of above 10 mT that the superior performance of the BCzPh:CN-T2T compared with that of the BCzPh:B3PYMPM exciplex system is due to the cumulative effect of the horizontal orientation preference and SOC in the former that is higher than that in the latter (Fig. 6). The SOC is facilitated by asymmetrically polarized orbital wavefunction of the exciplex system, which is proved by the presence of an EPR signal upon photoexcitation. The extent of SOC is inversely dependent on the singlet-triplet gap of the emitter, indicating the cooperation among SOC, singlet-triplet gap, and polarization [52].

BCzPh:CN-T2T appears to be a promising system; however, we have continued investigating and revealed some interesting details recently [16]. We opted for the techniques such as TRPL, capacitance-voltage (CV), impedance spectroscopy (IS), and transient EL measurements to understand the mechanism of exciplex formation in the interface as well as in bulk. The study determined a 26.4 % efficiency of the bulk device, whereas the EQE of the interface device is low at only 7.7 %. The considerable difference between the devices is assessed by comparing the charge accumulation at the interfaces with EML. The TRPL data, obtained by monitoring the spectra from short to long wavelengths, are used to examine the triplet harnessing efficiency. A distinct delayed fluorescence from the bulk exciplex system is observed in contrast to the interface device. This observation correlates with the transient EL. The data indicate a rapid reduction of the accumulated charge in the bulk exciplex, thereby boosting efficiency.

Thus far, several positive outcomes of the exciplex-based OLEDs have been discussed. However, a serious issue is rarely raised, that is, the device operational stability, which is a crucial parameter in evaluating the devices for practical applications. Undesirable carrier recombination during the device operation usually leads to the accumulation of triplet excitons on the acceptor, thereby deteriorating exciplex system stability. However, a clear strategy to overcome this problem has remained elusive thus far. Nguyen *et al.* addressed this issue by examining various exciplexes using Tris-PCz (Fig. 4) as the donor and a range of triazine-based acceptors of the conventional (T2T (Fig. 2), SF3-TRZ (Fig. 4)), bipolar (Cz-TRZ, Fig. 8), and TADF types (BCz-TRZ, 3Cz-TRZ, Fig. 8) [53]. All the acceptors utilized in this investigation share a common electron-deficient triazine group and differ only in the attached

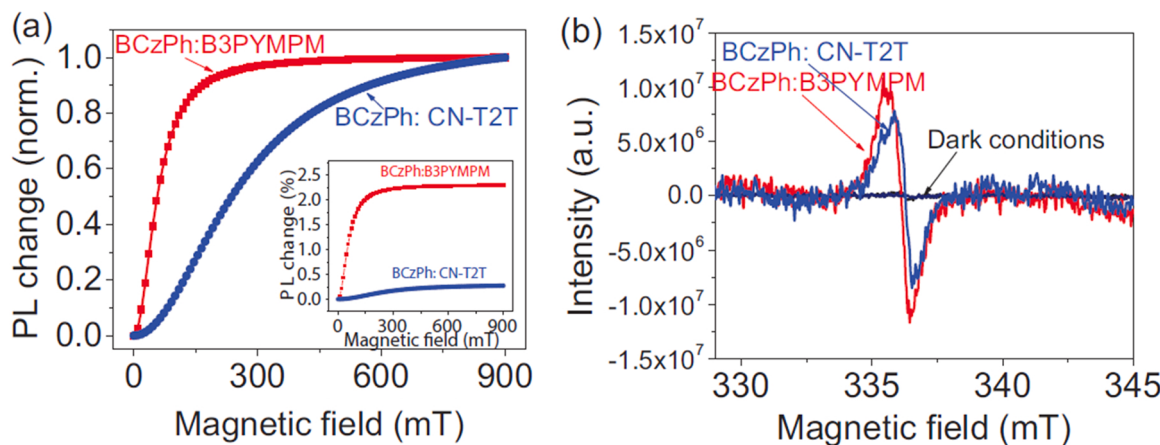


Fig. 6. (a) Normalized magneto-PL for BCzPh:CN-T2T and BCzPh:B3PYMPM exciplex thin films; the inset shows the original magneto-PL signals. (b) EPR signals for BCzPh:CN-T2T and BCzPh:B3PYMPM exciplex thin films under dark and 405 nm photoexcitation conditions.

Reproduced with permission from [52], Copyright 2019. John Wiley and Sons.

functionalities. The turn-on voltage and EQE of all the devices are in the comparable range (3.0–3.2 V and 8.7–11.9 %, respectively). However, the operational lifetime (LT_{50}) values of the devices vary greatly in each system, following the order TADF acceptor > D-A acceptor > conventional acceptor. For example, the LT_{50} of the TADF acceptor 3Cz-TRZ-based device is 337 h, whereas that of the conventional acceptor T2T-based device is considerably low at only 66 h because of the rapid degradation of the latter class of OLEDs. The remarkable stability in the TADF acceptor-based devices is due to RISC within the acceptors, which impedes the triplet exciton accumulation and degradation, as mentioned above. In 2016, Su *et al.* reported a highly efficient TADF OLED based on the exciplex of TAPC:T2T films. [53] The optimized device with EL centered at 528 nm exhibits a turn-on voltage as low as 2.4 V, high CE and PE of 40.4 cd A^{-1} and 42.2 lm W^{-1} , respectively, and a maximum EQE of 11.6 %. The device displays low-efficiency roll-off, which is attributed to the small ΔE_{ST} and the short delayed fluorescence lifetime of TAPC:T2T exciplex, thereby retaining η_{ext} of 9.4 % even at a high luminescence of 1000 cd/m^2 [2].

As mentioned, the successful confinement of the exciplex triplet excitons occurs only if the donor and acceptor molecules fulfill the necessary condition of higher triplet energy than the exciplex. Zhang *et al.* depicted a green exciplex OLED based on TCTA as the donor and Tm3PyBPZ (Fig. 4) as the acceptor material, which has an elongated conjugation compared with PO-T2T. Both the prompt and delayed components are observed in the photophysics of the exciplex system, confirming TADF. The EL maximum of the relevant exciplex OLED is 514 nm, and the EQE is as high as 13.1 % (44.2 cd A^{-1} , 54.5 lm W^{-1}) with a low turn-on voltage of 2.4 V [54].

2.2.1.2. Oxadiazole acceptors. The materials containing electron-deficient oxadiazole group are popularly electron transport and/or hole-blocking materials in OLEDs. The introduction of the oxadiazole group enhances the material thermal stability, which is a vital property for OLED material development [55].

In exciplex investigation, Kawabe *et al.* demonstrated a method to measure the electron mobility in organic materials by fabricating a bilayer OLED composed of a donor (TPD, Fig. 3) and oxadiazole-based acceptor materials (PBD, Fig. 2), exhibiting exciplex emission at 470 nm. The highest light emission (0.45 mW/cm^2) is obtained under the bias of 7 V with the EQE of only 0.24 % and a current density of 69 mA/cm^2 . The maximum quantum efficiency of the device is 1.1% when 3.5 V is applied [56]. In a further advancement to the exciplex formation, Su *et al.* investigated the effect of acceptors' LUMO on exciplex emissions as well as on η_{ext} in D/A interfacial-type devices. The triarylamine *m*-MTDATA is used as a donor, whereas several

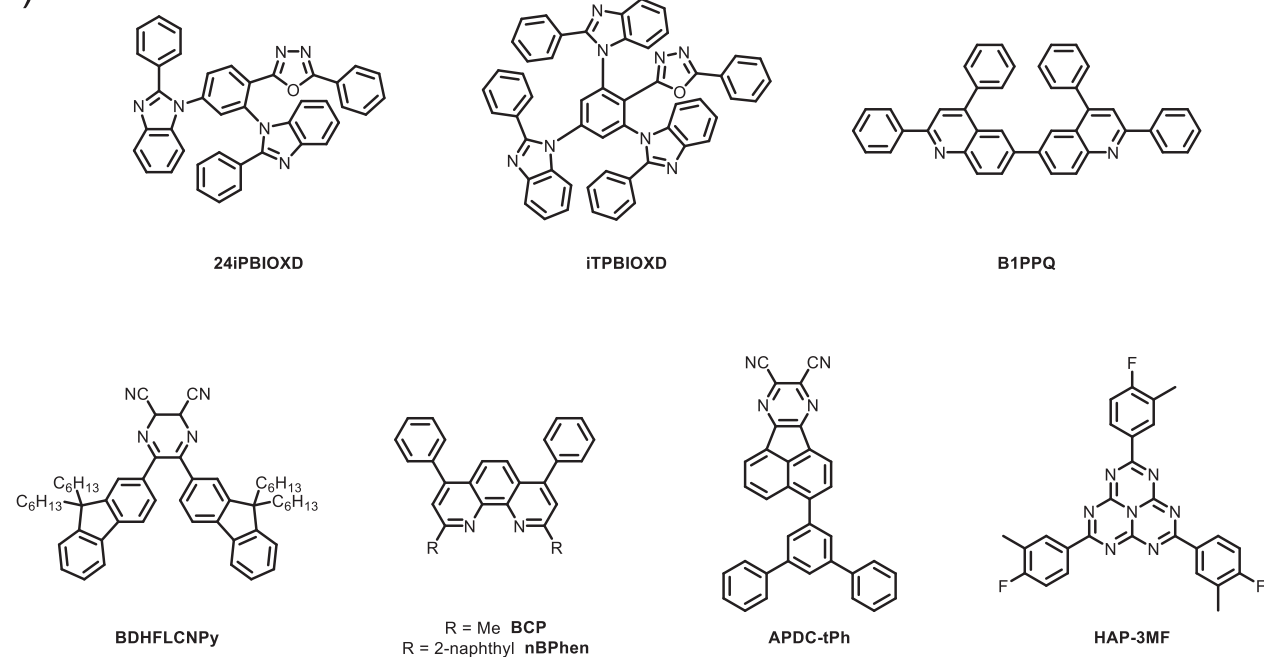
compounds, viz., 2,9-Dimethyl-4,7-diphenyl-1,10-phenanthroline (BCP, Fig. 7), 2-(4-Biphenyl)-5-(4-tert-butyl phenyl)-1,3,4-oxadiazole (PBD, Fig. 2), and 1,3,5-Tris(1-phenyl-1Hbenzimidazol-2-yl)benzene (TPBi, Fig. 3), are chosen as acceptor moieties. Efficient exciplex EL emission is governed by the electron transfer process from the donor moiety to the acceptor, which requires matched LUMOs and suitable intermolecular interactions between the donor and acceptor counterparts, i.e., low acceptor LUMO with compact D/A intermolecular contacts is highly favored. A nearly linear relationship between acceptor LUMOs and efficiency in exciplex-type devices with a fixed donor moiety mixing with different acceptors is observed. Thus, Su *et al.* concluded that the lower the LUMO of the acceptor is, the greater the EL efficiency of the exciplex would be; this finding is a remarkable addition to the exciplex research [57].

Jankus *et al.* conducted a detailed photophysical investigation on exciplex systems. They observed that little distinction exists between the prompt and delayed components of a 1:1 blend of *m*-MTDATA and PBD (Fig. 2) and that the singlet-triplet energy gap is nearly zero ($\Delta E_{ST} = 5 \text{ meV}$). Although the *m*-MTDATA:PBD blended film is an inefficient emitter system, they concluded that exciplex with a high PLQY and similar singlet-triplet splitting should present high-efficiency blue emitters. They also concluded that abundant red-shifted exciplexes are observed at long delay times. This finding is ascribed to the high degree of conformational disorder dictating the degree of charge transfer within an exciplex. A complete charge transfer contributes to a low coupling between the ground and excited state, thereby resulting in a red shift in emission and enhancing the radiative lifetime of the exciplex [19].

The donor to acceptor ratio is also essential to obtaining superior device performance. Song *et al.* demonstrated this finding by including exciplex TADF emitters in heterostructured organic light-emitting field-effect transistors to harvest the triplet excitons [58]. The authors first tested an exciplex system, TCTA:B3PYMPM, which exhibits weak performance. However, the scenario improves when the exciplex system is changed to *m*-MTDATA:OXD-7 because of the enhanced TADF of the latter compared with that of the former. The D:A ratio is important to tune the photoluminescent quantum yield of the film. However, this method affected the device's performance negatively. Moreover, the hole injection barrier of the *m*-MTDATA:OXD-7 exciplex system is lower than that of the TCTA:B3PYMPM system augmenting the exciton utilization ability of the system. However, the EQE of the *m*-MTDATA:OXD-7 exciplex OLED is on the light side, exhibiting only 3.8 % because of the low PLQY of the relevant film. Thus, the PL of the relevant materials should be high for practical brightness even though the oxadiazole group improves the thermal stability of the acceptor material [58].

Tao *et al.* synthesized two benzimidazole-oxadiazole hybrids,

(a)



(b)

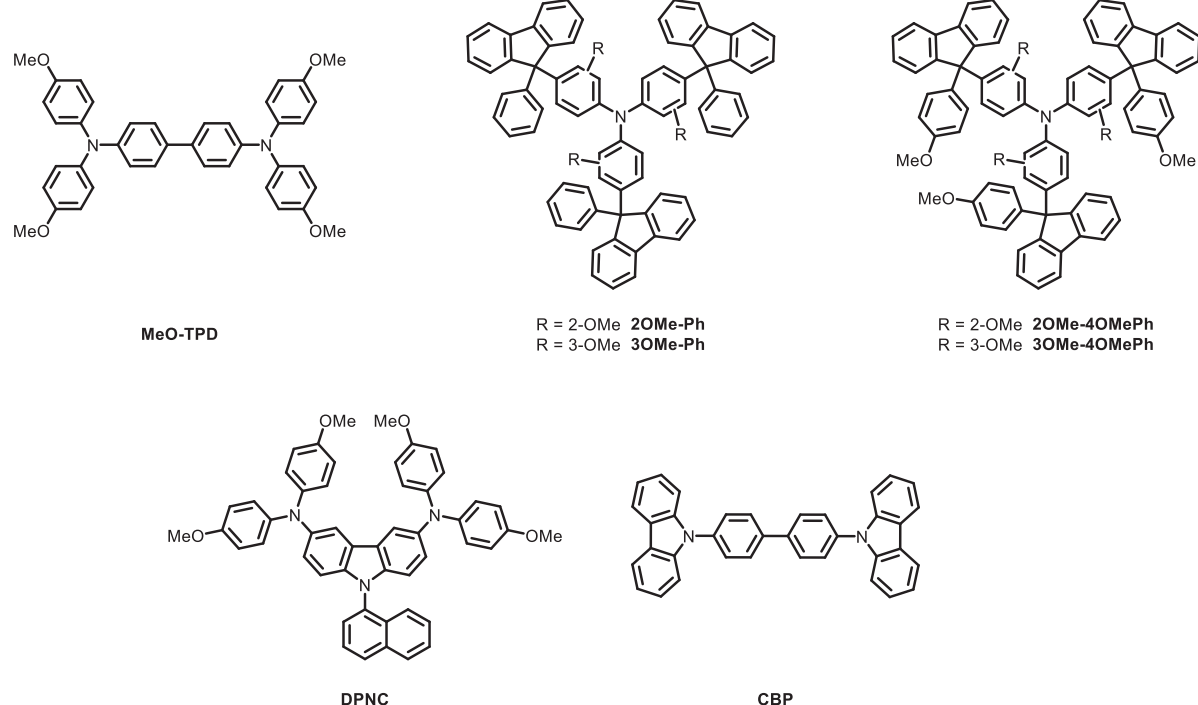


Fig. 7. (a) Molecular structures of the azole- and other *N*-heterocyclic-based materials used as acceptors and (b) related donor materials for exciplex-forming systems.

namely, 2-(2,4-bis(2-phenyl-1 H-benzo[d]imidazol-1-yl)phenyl)-5-phenyl-1,3,4-oxadiazole (24iPBIOXD) and 2-phenyl-5-(2,4,6-tris(2-phenyl-1 H-benzo[d]imidazol-1-yl)phenyl)-1,3,4-oxadiazole (iTPBIOXD), and employed them as electron-accepting units in the exciplex OLEDs (Fig. 7) [59]. The FMOs of these materials are compatible with donors, such as TAPC, TCTA, and mCP. The subsequent OLEDs exhibit variable performance. The TAPC-based devices have higher device efficiencies (EQE, CE, and PE) and lower turn-on voltage than the others,

with the 24iPBIOXD-based devices having an edge.

2.2.1.3. Triarylboron acceptors. Triarylboron compound has a vacant p orbital on the central boron atom, making the boron center inherently electron deficient. In the D-A system, a triarylboron acceptor that is conjugated with an electron donor can lead to a considerable charge delocalization and exhibit strong intramolecular charge transfer (ICT) properties. The charge transfer character in triarylboron-based D-A

compounds strongly influences their photophysical properties; some of them even demonstrate efficient TADF features [60]. Without strong coupling to the electron-donating group, triarylboron compounds can be used as effective electron acceptors in various photonic and organic optoelectronic materials. In particular, tris-[3-(3-pyridyl)mesityl] borane (3TPYMB, Fig. 2) is well studied and known as an ETL for OLEDs. Devices employing 3TPYMB as ETL possess current density and luminance that are larger and higher than those of devices with a conventional electron-transport material, tris(8-quinolinolato)aluminum (Alq_3 , Fig. 3), because of the electron mobility of 3TPYMB that is 10 times higher than that of Alq_3 [61].

Huang *et al.* reported a series of OLEDs based on an *m*-MTDATA:3TPYMB (1:1) exciplex system to improve OLED efficiency by altering ETL thickness [62]. In this study, increasing the ETL thickness leads the EL (due to exciplex emission) to be red-shifted. The device based on this exciplex system exhibits a low V_{on} of 2.1 V, a high CE of 36.8 cd A⁻¹, and a remarkably high luminescence of 17100 cd m⁻², with considerably low-efficiency roll-off. Such superior performance is credited to (i) the high E_T for the confinement of the triplet state of the exciplex in the *m*-MTDATA:3TPYMB EML and (ii) the aptitudes of the EML matrix for transporting both holes and electrons, thereby resulting in intrinsic suppression of the exciplex triplet quenching. In 2015, Xiong *et al.* studied the magneto-field effects of the MTDATA:3TPYMB blend and reported large magneto-conductance exceeding 60 % and MEL of more than 110 % at room temperature in the *m*-MTDATA:3TPYMB exciplex system [63]. The large magnetic field effects (MFEs) are attributed to the field-modulated RISC process, which can also alter the current and EL efficiency in devices.

The effect of electric field on the exciplex states studied by Monkman *et al.* using the same exciplex system consisting of the acceptor core (3TPYMB) was reported in 2016. They used a simple but novel approach to examine the evolution of the relaxed exciplex when an external electric field diminishes the separation of electron-hole, thereby leading to an enhanced emission at an abrupt D-A interface. The OLED devices employed in this approach constitute a D-A interface having a comparatively high HOMO-LUMO energy offset. The injected electrons and holes that cannot overcome the high-interface potential barrier form a considerable density of exciplex states pinned across the interface. Therefore, as the separation between the electron holes decreases with the increase of the applied field, the exciplexes also gain local excited state character, which upsurges the radiative decay rate, thereby increasing emission efficiency. Herein, the effect of electric field on the exciplex states is studied using single-layer (SL) and DL OLED devices. The SL device structure is ITO/PEDOT:PSS (40 nm)/1:1 MTDATA:3TPYMB (30 nm)/3TPYMB (30 nm)/LiF/Al, whereas the DL “abrupt interface” device structure is ITO/PEDOT:PSS (40 nm)/*m*-MTDATA (30 nm)/3TPYMB (30 nm)/LiF (0.8 nm)/Al (100 nm). The emission for the blend film peaks at 540 nm because of the exciplex formation. The brightness and device efficiency of the SL device are considerably higher than those of the DL device because of the substantial effective interface area in the blended system [64].

In addition to the electric effect on exciplex, the study of the MFE by Kwon *et al.* is extended in D-A exciplex materials comprising MeO-TPD (Fig. 7) and 3TPYMB (Fig. 2) [65]. The exciplex emission for the blend is observed at ~492 nm, extending over a broad spectral range up to ~700 nm. In this study, the EL in such exciplex-based OLEDs is considerably increased (up to ~40 %) when a magnetic field is applied. This scenario occurs owing to the existence of an additional spin-mixing channel between singlet and triplet states in the exciplex. In this new class of OLEDs, the magnetic field influences two spin-mixing channels operating at two energy levels, (i) the upper energy channel of polaron pairs and (ii) the lower energy channel of exciplexes, where magnetic field-enhanced RISC is feasible. The magneto-electroluminescent response may be improved by reducing the ΔE_{ST} value in the lower energy exciplex channel. Both processes, namely, MEL and MPL, are thermally activated, signifying the dominant role of RISC in the system.

Thus, such findings seem to be highly promising for the practical applications of the MFE on exciplex-based OLEDs to improve device efficiency.

2.2.1.4. Pyridine/pyrimidine/pyrazine acceptors. The N-embedding heteroarenes, known for their electron-deficient nature, are usually used as acceptor cores in D-A-type materials. In addition to the excellent electron transport properties, good electron injection and hole-blocking abilities are imparted to the molecules containing these heterocycles. The low-lying LUMO and HOMO energy levels can be feasibly achieved by incorporating one or more nitrogen atoms into the heterocyclic system. Therefore, the number of nitrogen atoms introduced can be adapted to modulate the HOMO and LUMO energy levels. Therefore, N-heterocyclic compounds have substantial potential for the development of high-performance OLEDs.

In 2013, Kim *et al.* reported the utilization of B3PYMPM (Fig. 2), a pyrimidine/pyridine-cored acceptor, to achieve high-efficiency exciplex-based OLED. The co-deposited film of TCTA:B3PYMPM exhibits efficient delayed fluorescence, and the PL efficiency increases from 36 % at room temperature (RT) to nearly 100 % at 35 K. Therefore, the EQE of the OLEDs with structure ITO/TAPC (30 nm)/TCTA (10 nm)/(1:1) TCTA:B3PYMPM (30 nm)/B3PYMPM (20–40 nm)/LiF (1 nm)/Al (100 nm) increases from 3.1 % at RT to 10 % at 195 K. The η_{ext} of 10 % is considered one of the highest values obtained back then using exciplexes, and a considerable proportion of the triplet exciplexes is harvested through RISC process [14].

Jenekhe *et al.* studied the PL and EL of exciplex forming blends and bilayers of a blue-emitting oligoquinoline acceptor (A) in conjunction with donors (D) with varying ionization potential [30]. Based on the exciplex formation between the pertinent donor/acceptor pairs, the EL emission ranges from blue-green to yellow-orange to white. In this study, the exciplex emission in D/A bilayers is electrically driven, whereas that in the blends is both optically and electrically driven. Herein, the blue-green exciplex EL with CIE coordinates of (0.16, 0.34) and brightness of up to 2900 cd/m² is obtained from both blends and bilayers of B1PPQ (Fig. 7) with TAPC. However, for binary blends of B1PPQ and MTDATA (Fig. 2), exciplex EL having bright yellow with CIE (0.41, 0.52) to orange with CIE (0.57, 0.42) is obtained with a brightness of up to 1900 cd/m². For bilayers of B1PPQ and MTDATA, white OLEDs with CIE (0.35, 0.32) are attained. The best device performance among them is obtained from the 10 mol% B1PPQ in the blend. The results obtained in this study revealed that a blend composition is an effective approach for tuning the exciplex EL colors for a given set of D/A pairs.

Then, a novel fluorene-containing derivative BDHFLCNPy (Fig. 7) was reported by Yu *et al.* to demonstrate exciplex emission in OLEDs [66]. The exciplex emission is observed at 657 nm at the NPB|BDHFLCNPy interface with the devices fabricated as the structure of ITO/NPB (30 nm)/BDHFLCNPy (x, nm)/Mg:Ag (200 nm), where x = 5, 10, 30 nm. The devices with a thick acceptor layer have high luminance efficiency because of the exciplex formation that offers “barrier-free” electron capture. The device with the thinnest acceptor layer has high luminance and current density because numerous electrons are injected into the device. The barrier-free capture first encompasses indirect hole-electron capture into the exciplex state. In the second step, endothermic transfer from the exciplex generates the excitons. Thus, the exciplex can either decay radiatively or transfer endothermically to the bulk exciton state at the heterojunction interface. This process probably yields a high-efficiency device with low turn-on voltage when energy transfer from exciplex to exciton is effective.

2.2.1.5. Phenanthroline acceptors. 1,10-Phenanthroline and its derivatives are usually used as electron-transporting and hole-blocking materials in electroluminescent devices because of their electron-deficient nature and low-lying HOMO. The most well-known examples are 2,9-dimethyl-4,7-diphenyl-1,10-phenanthroline (BCP, Figs. 7) and

4,7-diphenyl-1,10-phenanthroline (BPhen, Fig. 2). However, their relatively low triplet energies limit their usage as universal electron transport materials for PhOLEDs, particularly blue and white PhOLEDs. This problem was later circumvented by Kido *et al.*, who established a design strategy for high-performance N-heterocyclic electron transport materials (ETMs) using the combination of pyridine and triphenylbenzene moieties [67].

In 2008, Wang *et al.* obtained *m*-MTDATA/BPhen-based OLED exhibiting pure green exciplex emission. The exciplex composite (*m*-MTDATA:BPhen) exhibits a green PL band with a peak centered at 530 nm. Three kinds of OLED devices are fabricated for the study, including (i) a bilayer device comprising ITO/*m*-MTDATA/BPhen/LiF/Al, (ii) a three-layer device comprising ITO/*m*-MTDATA/BPhen/Alq₃/LiF/Al, (iii) a four-layer device structure comprising ITO/*m*-MTDATA/*m*-MTDATA:BPhen (1:1)/BPhen/Alq₃/LiF/Al. The EL performance is boosted by introducing an Alq₃ layer between the BPhen layer and cathode. Herein, the three-layer device displays a peak current efficiency of 7.6 cd/A at 2.38 mA/cm² with a maximum luminance of 5512 cd/m² at 6.8 V. In the blend device (four-layer device), a peak current efficiency of 4.9 cd/A at 4.33 mA/cm² and high luminance of 6620 cd/m² at 8.7 V is obtained. The absence of competition between the exciplex and monomer electronic transitions (as *m*-MTDATA and BPhen are competently low for monomer emission) results in highly efficient exciplex emission [68].

Zhang *et al.* demonstrated exciplex OLEDs based on blend films of *m*-MTDATA:BPhen and *m*-MTDATA:TPBi. The performance of the former device is better than that of the latter with a maximum EQE of 7.79 % at 10 mA cm⁻² and PE 12.97 lm W⁻¹. The high device efficiency of the BPhen device is attributed to nearly zero singlet-triplet gaps for the *m*-MTDATA:BPhen exciplex system, which is further verified by transient EL experiments. The presence of an unbalanced charge in the exciplex causes quenching of the singlet excited states, thereby lowering the EQE. The charge balance depends on the carrier mobility of the organic layers, the thickness of the layers, D:A molar ratio of the blend, and other operational reasons. Positive MEL and magneto conductivity are observed when the exciplex device is placed under a 100 mT magnetic field. This study showed that the exciplex EL originates only from TADF, whereas the TTA remains a trivial decay channel for the triplet excitons [69].

Grazulevicius *et al.* reported star-shaped phenylfluorenyl-substituted triphenylamines, namely, 2OMe-Ph, 3OMe-Ph, 2OMe-4OMePh, and 3OMe-4OMePh (Fig. 7), as the donors for blending with acceptors BPhen and BCP (Fig. 7). Among these combinations, the blend of 2OMe-Ph:BCP exhibits a deep blue emission with the maximum centered at 427 nm, whereas the emission maximum of the 2OMe-Ph:BPhen exciplex is slightly red-shifted and observed at 440 nm. A wOLED is successfully fabricated by combining the blue-emitting 2OMe-Ph:BPhen and green *m*-MTDATA:BPhen exciplexes. The blue exciplex is formed within the EML, whereas the green exciplex is formed at the interface between the EML and the hole-transporting layer of *m*-MTDATA. This new D/A pair results in a deep blue OLED with CIE chromaticity coordinates of (0.179; 0.104) and η_{ext} of 1.2 %, whereas the cold white devices display η_{ext} of 2.6 % after introducing a high concentration of BPhen for facilitating electron transport to reach the HTL/EML interface for green exciplex formation [70]. Furthermore, the same group reported an ambipolar material 3,6-di(4,4'-dimethoxy diphenyl aminyl)-9-(1-naphthyl) carbazole (DPNC, Fig. 7) as the donor for exciplex formation. An SL OLED with device structure ITO/CuI/DPNC/Ca:Al and bilayer OLEDs with structures ITO/CuI/DPNC/BPhen/Ca:Al (Bilayer I) and ITO-/CuI/DPNC/TPBi/Ca/Al (Bilayer II) are fabricated [71]. The bilayer OLED with DPNC/BPhen as exciplex emitter exhibits η_{ext} of 3.3 % with a maximum brightness of 27000 cd/m². The bilayer device employing DPNC/TPBi as exciplex emitter exhibits η_{ext} of 1.2 % with a maximum brightness of 983 cd/m² at 15 V. The inferior maximum η_{ext} of the DPNC/TPBi-based bilayer device is possibly ascribed to the shorter lifetime of the DPNC:TPBi exciplex compared with that of DPNC:BPhen

exciplex, thereby leading to the RISC efficiency of the former that is lower than that of the latter. The fabricated OLEDs exhibit voltage-dependent EL in a short range of applied bias, indicating that device emission can be fine-tuned by the adjustment of applied voltage.

2.2.1.6. Other nitrogen- and phosphine oxide acceptors. Adachi *et al.* reported that an exciplex formed between *m*-MTDATA and diphenylphosphine oxide-based molecule PPT as donor and acceptor, respectively. The emission band of the *m*-MTDATA:PPT exciplex is located at around 510 nm, considerably red-shifted compared with the emission observed from its counterparts. The results determined that the efficiency of delayed fluorescence is enhanced if the acceptor has high triplet energy [13].

TPBi, a benzimidazole derivative (Fig. 3), is a well-known and studied electron-transporting material. Jankus *et al.* reported an interesting strategy to achieve deep blue OLED using exciplex from the blend of NPB:TPBi. The device configures as ITO/NPB (30 nm)/NPB:TPBi (35 nm)/TPBi (35 nm)/LiF (1 nm)/Al (100 nm) present η_{ext} of 2.7 % with (CIE) coordinates of (0.15, 0.13) and brightness of 600 cd m⁻². The majority of the deep blue EL is harvested from triplet excitons via the triplet fusion (TF) process instead of thermally assisted delayed fluorescence (E-DF). Therefore, the importance of TF in producing efficient deep blue fluorescent OLEDs is worth noting, and the η_{ext} can consequently increase to 12 % with enhanced PLQY of the exciplex state [72].

Yu *et al.* revealed the importance of donor character for exciplex formation when TPBi (Fig. 3) is employed as an acceptor [73]. The absence of red-shifted emission in the PL of CBP:TPBi blend film indicated that no exciplex is generated between CBP (Fig. 7) and TPBi because of the moderate electron-donating nature of CBP. However, TCTA:TPBi mixed film exhibits exciplex emission, as TCTA has a strong electron-donating aromatic amine unit. In addition, the TCTA/TPBi exciplex emission suitably overlaps with the absorption of rubrene, rendering the efficient energy transfer highly feasible. A thin layer of pure rubrene with different thicknesses is inserted between TCTA and TPBi to achieve OLED with EL emission transferred from the exciplex. The best device with maximum luminescence of 18,311 cd m⁻² is achieved with a rubrene thickness of 0.2 nm. The device exhibits a low turn-on voltage of 3.1 V. Such a low turn-on voltage is distinctive of exciplex-based OLED, wherein holes on the HOMO of TCTA and electrons on the LUMO of TPBi recombine at the interface.

Adachi and coworkers reported an efficient exciplex system consisting of a heptazine derivative (HAP-3MF, Fig. 7) as the electron acceptor for the mCP electron donor [74]. Heptazine is an efficient electron-accepting core, and the 2-fluorotoluene groups are attached to the heptazine core to increase the solubility of the compound, leaving its electron deficiency untouched. The PLQY of the exciplex system is close to 56 %, and an OLED fabricated using the material illustrates excellent performance (11.3 % EQE). The EQE of the mCP:HAP-3MF-based device decreases with the increase of the fraction of the acceptor, perhaps as a result of concentration quenching owing to the planar structure of the molecule.

Although many milestones have been achieved thus far, numerous challenges engrossed with the blue OLEDs remain for obvious reasons. Phenyl phosphine oxides possess some exciting properties, such as a large HOMO–LUMO gap, high IE, excellent electron-transporting ability, and high triplet energy, to name a few. They can act as good electron acceptors to generate blue-emitting exciplexes. Shinar and coworkers recently demonstrated deep blue exciplex OLEDs based on TPBi:PPh₃O [75]. The relevant device with the configuration of ITO/MoO₃ (5 nm)/TCTA (60 nm)/NPB (45 nm)/5:1 TPBi:PPh₃O (14 nm)/PPh₃O (15 nm)/BPhen (30 nm)/CsF (1.5 nm)/Al (110 nm) exhibits bright exciplex emission at 435 nm. Although the EQE of the device is low (~ 4 %), the paper presented a scope of exploring the phosphine oxide-based materials in exciplex OLEDs. Hu *et al.* developed a near-IR exciplex OLED based on TCTA and a newly synthesized acceptor material 3-[{[1,

1^{''}:3^{':}1^{''}-terphenyl]-5'-yl)acenaphtho[1,2-*b*]pyrazine-8,9-dicarbonitrile (APDC-tPh, Fig. 7). An OLED with the configuration of ITO (150 nm)/MoO₃ (3.5 nm)/NPB (35 nm)/TCTA (10 nm)/1:1 TCTA:APDC-tPh (20 nm)/B4PYMPM (50 nm)/Liq (2 nm)/Al (120 nm) shows EL emission at 730 nm; however, an extremely low EQE of only 0.1 % is observed [76].

2.2.2. Exciplexes in the blend of donor or acceptor material with a donor-acceptor bipolar material as the emitters

The bipolar molecules are donor-acceptor dyads that usually emit from a charge-transfer state. The D or A functionality within them can undergo exciplex formation with another fragment of opposite polarity. This principle has been evaluated to improve the device performance of the exciplex OLEDs. The donor or acceptor counterparts should be carefully selected to drive the intrinsic charge transfer equilibrium of the bipolar molecule to the exciplex formation. In an interesting article, Jankus *et al.* demonstrated exciplex formation between a carbazole, namely, dibenzothiophene S,S dioxide hybrid, 9-[2,8]-9-carbazole-[dibenzothiophene- S,S -dioxide]-carbazole (t-Cbz-SO, Fig. 8), with TAPC as the donor. A 38 wt% blend of the compound in TAPC has a PLQY of 53 % and a relevant OLED emitted at 540 nm with a quantum efficiency of 14 % [77]. Li *et al.* demonstrated exciplex OLEDs based on the well-known TADF material 10,10'-4,4'-sulfonylbis(4,1-phenylene))bis(9,9-dimethyl-9,10-dihydroacridine (DMAC-DPS, Fig. 8) and various donor (TPD, Fig. 3) and acceptor (T2T, Fig. 2), B4PyMPM (Fig. 8), and PO-T2T, Fig. 2 materials, which show a wide range of emission color, namely, 480 nm (DMAC-DPS:T2T), 493 nm (DMAC-DPS:B4PyMPM), 535 nm (DMAC-DPS:POT2T), and 550 nm (TPD:DMAC-DPS). The DMAC-DPS:POT2T-based green OLED, where the TADF material is used as a donor, outperforms others with an EQE of 9.08 %, low-efficiency roll-off, and maximum luminance higher than 35,000 cd m⁻². On the contrary, the TADF material is unsuitable as an acceptor, as manifested by the poor performance of the TPD:DMAC-DPS-based system (EQE = 1.63 %) [78].

In another investigation, Su *et al.* delivered a novel strategy to fabricate highly efficient exciplex-based OLEDs by combining a bipolar transport material 2,6-bis(3-(carbazol-9-yl)phenyl)pyridine (26DCzPPy, Fig. 8) as acceptor and electron-rich *m*-MTDATA or TAPC (Fig. 2) as the donor. The *m*-MTDATA:26DCzPPy and TAPC:26DCzPPy blend films exhibit considerably red-shifted strong exciplex emission at 514 and 450 nm, respectively. The *m*-MTDATA:26DCzPPy-based green exciplex OLED displayed a maximum EQE of 5.03 % and a CE of 15.9 cd A⁻¹, whereas mixed exciplex and electropolex emissions are observed in the TAPC:26DCzPPy-based devices, with a maximum EQE of only 1.13 % and a CE of 2.19 cd A⁻¹ [79].

Employing two TADF materials, namely, one as the donor and the other as the acceptor has also proved beneficial. For example, Lee and coworkers demonstrated an efficient exciplex OLED using two TADF materials, DMAC-DPS (donor) and 9,9',9'',9'''-((6-phenyl-1,3,5-triazine-2,4-diyl)bis(benzene-5,3,1-triyl))tetrakis(9 H-carbazole) (DDCzTrz, acceptor) and 9,9',9'''-(5-(4,6-Diphenyl-1,3,5-triazin-2-yl)benzene-1,2,3-triyl) tris(9 H-carbazole) (TCzTrz, acceptor) (Fig. 8). The logic behind the material selection is that DMAC-DPS would serve as a suitable donor because of the electron abundance of its acridine moiety compared with the carbazole of the other two TADF molecules. Given that the electron-withdrawing nature of the triazine functionality of DDCzTrz and TCzTrz is stronger than that of the diphenyl sulfone moiety of DMAC-DPS, the former can be a suitable acceptor counterpart. Exciplex formation is observed, with the emission of the blend considerably red-shifted compared with that of the individual components. The EQEs of the relevant devices are 13.4 % (DMAC-DPS:DDCzTrz) and 15.3 % (DMAC-DPS:TCzTrz) [80].

The singlet and triplet energy levels of the TADF molecules are usually lower than that of the conventional fluorescent emitters. Therefore, engaging TADF-type materials as one of the exciplex components activates two RISC routes, namely, one in the TADF material

itself and another within the exciplex system. This scenario can lead to enhanced device efficiency due to the involvement of increased triplet excitons in the emission. Liu *et al.* examined exciplex formation partnered by a TADF emitter, 6-(9,9-dimethylacridin-10(9 H)-yl)-3-methyl-1 H-isochromen-1-one (MAC) as the donor (Fig. 8), and PO-T2T as the acceptor to consolidate the theory. An OLED fabricated using these components displays a low turn-on voltage (2.4 V) and high device efficiency (17.8 %, 52.1 cd A⁻¹, 45.5 lm W⁻¹); these values are higher than those from an mCP:PO-T2T device (EQE = 3.2 %), indicating the importance of using TADF materials as one of the exciplex forming components [81]. In a separate report, Lee and coworkers described new bipolar material based on carbazole and triazine (CzTrz) and its subsequent usage in exciplex formation. An all-acceptor reference material, DTrz (Fig. 4), is also prepared by replacing the carbazole of CzTrz with triazine to investigate the acceptor influence on the exciplex formation. The relevant exciplex systems have TCTA and TAPC as the donors, where the DTrz-based devices emit at wavelengths longer than those of the CzTrz-based devices because of the strong electron-accepting propensity of DTrz, leading to a low energy gap between donor HOMO and acceptor LUMO. The TCTA-based devices emit energy higher than that of the TAPC-based devices, perhaps because of the weaker electron-donating ability of TCTA than TAPC. The TCTA:CzTrz exciplex-based green OLED exhibits notable performance at 12.6% EQE [82].

Another interesting article by Zhang and coworkers reported utilizing a carbazole-triazine hybrid molecule, DPPTCz (Fig. 8), as the acceptor core to donors, such as TAPC, TCTA, and NPB (Fig. 3). The emission due to the concerned blends is at 503, 502, and 491 nm with a distribution of PLQY of 68 %, 55 %, and 15 %. The TAPC:DPPTCz-based device is the best in the series with EQE of 15.4 %, high PE of 47.9 lm W⁻¹, and low turn-on voltage of 2.7 V. These results are obtained possibly because of the high PLQY and low singlet-triplet gap of the blend. The TCTA:DPPTCz-based device also performs well at 11.9 %, 35.8 lm W⁻¹, and 2.8 V. However, the considerably low quantum efficiency of only 0.6 % is obtained from the NPB:DPPTCz-based device. This result is perhaps due to the low PLQY of the system because of the leakage of the exciplex triplet caused by the low-lying T₁ of NPB [20].

In 2016, Angioni *et al.* reported a linear bipolar molecule, 4,4'-(benzo[1,2,5]thiadiazole-4,7-diyl)bis(3-methoxybenzoate) (BT, Fig. 8), based on benzene–benzothiadiazole–benzene architecture. An interfacial exciplex formation is observed between BT and the hole-transporting layer TPD (Fig. 3). The emission is centered at approximately 580 nm. The twisted nature of BT makes self-stacking slightly probable, thereby enhancing the likelihood of hetero interactions with an adjacent molecule. Therefore, the electronic interaction of the acceptor (BT) and donor (TPD) molecules is highly feasible for exciplex formation at the interface upon photo- and/or electro-excitation. The device exhibits a turn-on voltage of 5.8 V with an EQE of 2.4 %, PE of 2.6 lm W⁻¹, a maximum brightness of 5219 cd m⁻² (at 15 V), and CIE coordinates of (0.38, 0.45) [83].

The recent report by Wu *et al.* echoed the importance of bipolar materials to obtain high-efficiency exciplex OLEDs. A triphenylamine-diphenyl sulfone hybrid, 2,2'-dimethyl-N,N-diphenyl-4'- (phenylsulfonyl)-[1,1'-biphenyl]- 4-amine (DPSTPA), is synthesized and tested as a donor to known acceptor materials (2CzPN, 4CzIPN, and CzDBA) (Fig. 8). The DPSTPA:2CzPN-based green device exhibits a remarkably high device efficiency of 20 %. The DPSTPA:CzDBA exciplex-based orange device also performs excellently at 14.6 %. However, the DPSTPA:4CzIPN exciplex OLED underperforms possibly because of the low PLQY of the relevant film [84]. Grazulevicius and coworkers synthesized a series of donor-acceptor molecules based on phenothiazine, phenoxythiine, and xanthene moieties as donors and sulfone substituents as acceptors. The material, DTS-XA (Fig. 8), stands out, and its interfacial exciplex OLED with TCTA (blue-emitting device) and *m*-MTDATA (orange emitting device) exhibits maximum EQE of 9.1 % and 8.3 %, respectively [85]. Lee and coworkers aimed to obtain

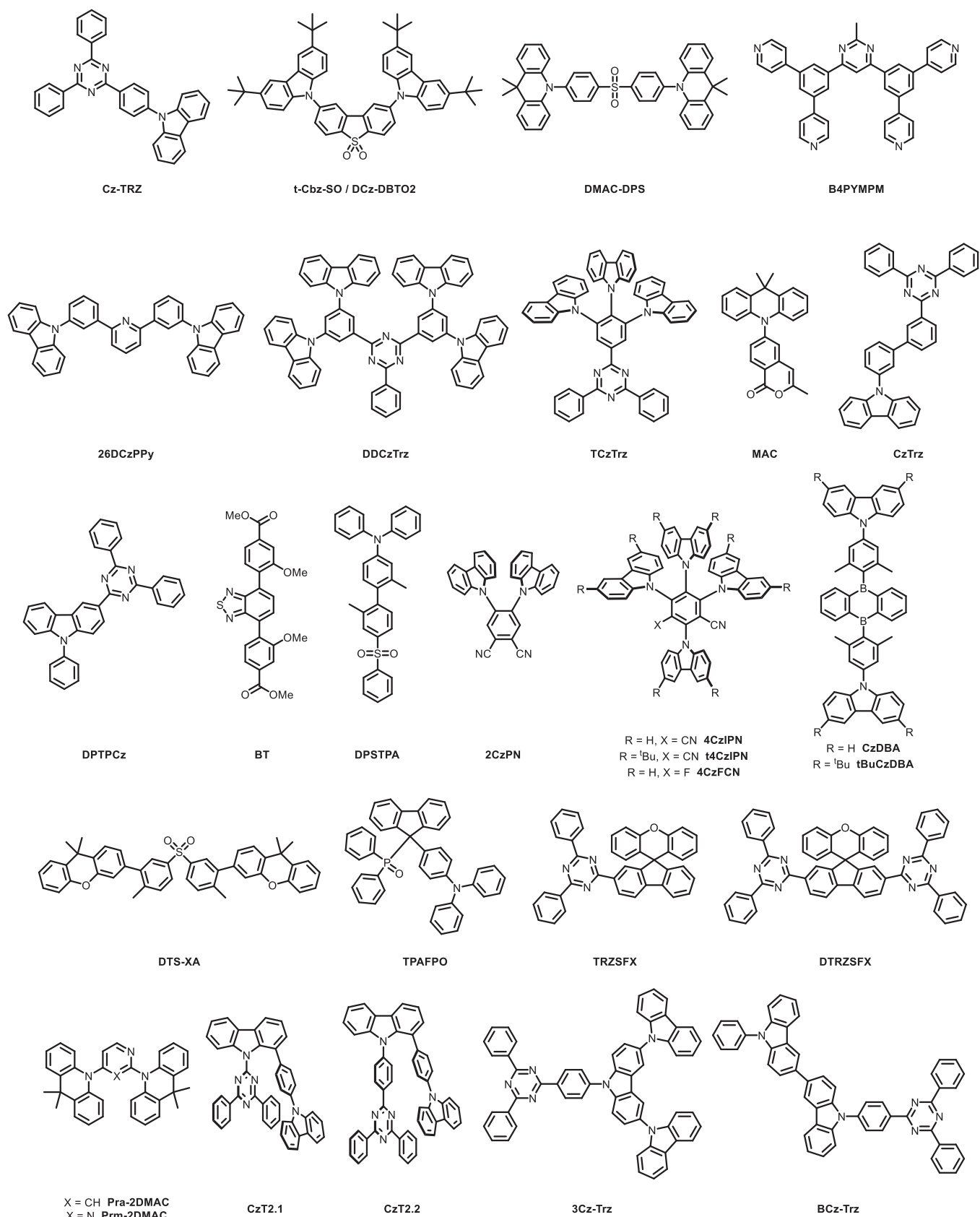


Fig. 8. Chemical structures of bipolar materials for exciplex-forming systems.

high-efficiency exciplex OLEDs based on already known materials instead of synthesizing new ones. In a recent report, they demonstrated a new strategy to enhance the EQE of exciplex OLEDs using the well-known TADF material DMAC-DPS (Fig. 8) as the donor and PO-T2T as the acceptor. Their idea is to use the TADF material both as an exciplex-forming component and a host. By maintaining the acceptor ratio below 10 wt % in DMAC-DPS, they achieved two motives simultaneously, that is, exciplex formation followed by exciplex dispersion in the TADF host. The EQE of the device employing 1 wt% of PO-T2T in DMAC-DPS is as high as 15.3 %, which is considerably higher than that of the 50:50 DMAC-DPS:PO-T2T-based device (10.8 %); this finding emphasized the importance of the dispersion of the exciplexes in the TADF host [86]. Some recent reports where exciplex emission accompanies the component emission in OLEDs are found, but these articles are included in this review because they do not demonstrate dedicated exciplex-based devices [87].

Zhao *et al.* designed and synthesized a bipolar material 9-(4-(diphenylamino)phenyl)-9 H-fluoren-9-yl)diphenylphosphine oxide (TPAFPO, Fig. 8) containing TPD and diphenylphosphine oxide acceptor. A 1:1 blend film of TPAFPO with POT2T exhibits a small singlet-triplet gap of approximately 80 meV. A green exciplex OLED based on this emitter shows a low turn-on voltage of 2.4 V and a high EQE of 17.0 %. When employed as the host in a TADF near-infrared (NIR) OLED, the relevant device exhibits a turn-on voltage of 3.0 V and a high EQE of 9.2 % [88]. Cao *et al.* reported two xanthene-triazine hybrid bipolar materials, namely, 2-(4,6-diphenyl-1,3,5-triazine-2-yl)-spiro[fluorene-9,9'-xanthene] (TRZSFX, Fig. 8) and 2,7-bis(4,6-diphenyl-1,3,5-triazine-2-yl)-spiro[fluorene-9,9'-xanthene] (DTRZSFX, Fig. 8), and their performance in exciplex OLEDs using TCTA as the donor. The TCTA:TRZSFX device exhibits excellent performance (22.5 %, 79.6 cd A⁻¹, 78.1 lm W⁻¹) [89]. Zhang *et al.* tested two DMAC-type donor-acceptor materials, namely, 10,10'-(pyridine-2,4-diyl)bis(9,9-dimethyl-9,10-dihydroacridine) (Pra-2DMAC, Fig. 8) with vertical configuration and 10,10'-(pyrimidine-2,4-diyl)bis(9,9-dimethyl-9,10-dihydroacridine) (Prm-2DMAC, Fig. 8) as the donor counterparts in exciplex OLEDs. The performance of an exciplex OLED based on the former is better than that of an exciplex OLED based on the latter [90].

The traditional exciplex systems usually comprise a 1:1 ratio of donor and acceptor counterparts. This arrangement sometimes poses concentration quenching or quenching due to the TTA of the electrically generated exciplex emitters. Lee and their coworkers proposed a strategy to address this issue. They mixed bipolar n-type materials with p-type materials, where the concentration of the former is high enough to behave like a host to the generated exciplexes between the bipolar and p-type materials. In the subsequent systems, the generated exciplex resembles the dopant and the excess bipolar material as the host. The luminance of the blend is governed by the HOMO-LUMO offset of the relevant n- and p-type materials. The performance of this host-dopant mimicked system is better than that of the devices with exciplexes dispersed in a host matrix [91]. Very recently, Chang and Wong *et al.* reported the carbazole-linked bipolar materials 1-(4-(9H-carbazol-9-yl)phenyl)-9-(4,6-diphenyl-1,3,5-triazin-2-yl)-9H-carbazole (CzT2.1, Fig. 8) and 1-(4-(9H-carbazol-9-yl)phenyl)-9-(4-(4,6-diphenyl-1,3,5-triazin-2-yl)phenyl)-9H-carbazole (CzT2.2, Fig. 8) as acceptors to blend with a conventional donor TAPC (Fig. 2) for exciplex-forming system [92]. They found that the emissions of the D:A blends are ascribed to the bipolar acceptor and the exciplex system, in which the ratio of these two emissive processes depends on the efficiency of exciplex formation as well as the donor-acceptor distances within the bipolar skeleton that governs the intrinsic relaxation behavior of the bipolar acceptors. The device with CzT2.2:TAPC blend as EML performs better characteristics with EL $\lambda_{\text{max}} = 514 \text{ nm}$ and EQE of 15.0 % (45.7 cd A⁻¹, 50.0 lm W⁻¹) due to the cooperation of exciplex emission and inherent emission from the bipolar acceptor.

Exciplex emission has also been tested to improve the efficiency of

light-emitting electrochemical cells (LECs), which are another type of surface-emitting device, such as the OLEDs. However, unlike OLEDs, that is, devices with multilayer stacked configuration, LECs have a simple operating structure of electrode/active layer/electrode. The active layer in the LECs is usually a mixture of small molecule or polymer emitter material and an ionic electrolyte, and the device can be fabricated using low-cost printing methods. Given that exciplex emission is usually broad, it has been tested in LECs to produce high color rendering, white-emitting devices. Compared with exciplex OLEDs, exciplex LECs have gained less research attention despite their great potential. A recent review article by Uchida and Nishikitani documented the recent progress of exciplex LECs, which will surely encourage the research community to delve into the topic [93].

Exciplex emitters are the new generation of OLED-emitting materials with potentials, such as (a) accessibility in a physical mixture of commercially available donor and acceptor material, (b) enhancement of electrical conductivity of the device due to the bipolar character of the emission layer, and (c) simple device structure. The increase in the number of articles on this topic since its inception by Adachi and co-workers is indicative of the dedication of the researchers. The highest device efficiency of exciplex OLEDs, where the exciplexes have been used as the emitter, is still not on par with that of TADF OLEDs, which already crossed the 35% EQE landmark. However, the effort by the research community is laudable. Among the exciplex forming agents, the DA-type TADF materials and the triazine acceptor-based materials appear special. Both of these materials have been proved to offer excellent device performances and deserve special attention.

3. Exciplexes as hosts and cohosts in OLEDs

Like any other materials, exciplexes also possess both pros and cons. Exciplex emission often occurs with low quantum yield, perhaps because of the small oscillator strength of the relevant transition due to limited orbital overlap. The emission spectra of the exciplexes are commonly broad owing to the charge transfer character of the emitting states, impeding the color purity of the devices where exciplexes are employed as emitters. The opposite is true for their application as hosts or sensitizers in electroluminescent devices. [8,21,94–96] The high efficiency of the exciplex OLEDs caused by efficient charge injection, balanced charge transportation, low driving voltage, efficiency roll-off, high triplet harnessing ability, and low singlet-triplet gap makes these virtual emitters useful as hosts in the light-emitting devices. The electronic properties of the exciplexes must resemble those of the conventional hosts to allow these exciplex hosts to fulfill their role. For example, the exciplexes must have confined triplet exciton systems at higher energy than the dopants to prevent leakage of the triplet excitons from the EMLs. In addition, a considerable overlap between the emission spectra of the exciplexes and the absorption spectra of the emitters must exist for a successful energy transfer. Exciplex formation at either the HTL|EML or the EML|ETL interface is often observed in the earlier OLEDs. The singlet and triplet states of the exciplexes in those devices are at lower energy than those of the emitters; thus, the back energy transfer from the emitter to the exciplexes drops the device efficacy.

The intrinsic triplet harnessing ability of the exciplexes due to the extremely narrow singlet-triplet gap prompts quantitative conversion of the electrically generated triplet excitons to the singlets, followed by subsequent transfer of the excitation energy to the dopant. Both the singlet-singlet (Förster) and triplet-triplet (Dexter) energy transfer (ENT) modes can operate, depending on the nature of the dopant, as shown in Fig. 9. At this point, we should briefly pause for a short discussion of the differences between conventional and exciplex hosts. The traditional host materials—both unipolar and bipolar—owe a large singlet-triplet gap that hinders the RISC. However, the intersystem crossing (ISC) can operate to convert some of the singlet excitons to the triplets. Both Förster and Dexter ENT modes can activate to excite the dopant. The exciplexes have a slight advantage over the conventional

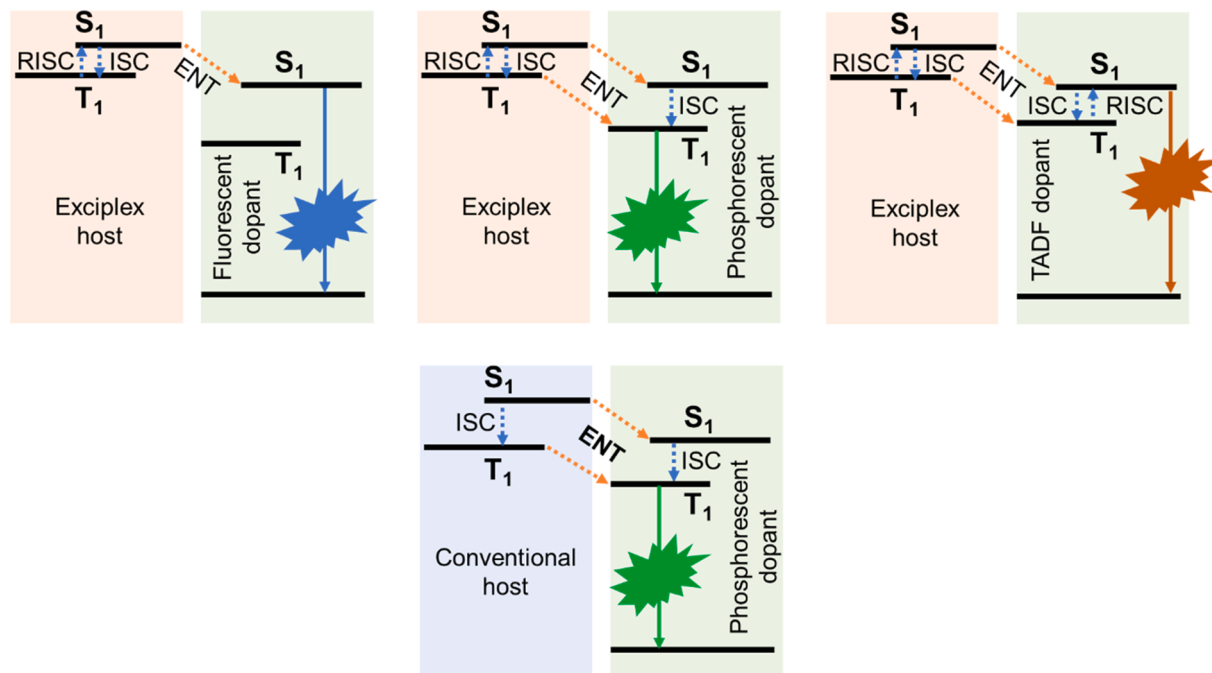


Fig. 9. Energy transfer (ENT) mechanisms in exciplex-hosted OLEDs for fluorescent, phosphorescent, and TADF dopants. The figure at the bottom represents the same mechanism in the case of conventional hosts and phosphorescence dopants. The broken arrows indicate nonradiative processes.

hosts because of the operation of both ISC and RISC within the host, thereby lowering the driving voltage of the device. Maintaining the optimal concentration ratio of the host and the dopant is important to extract the best device efficiency. The progress of the exciplex-hosted OLEDs is reviewed in this section, and the relevant device data are summarized in Table 2. The section is further divided into three subsections according to the dopants to keep the discussion organized.

3.1. Fluorescent OLEDs hosted by exciplexes

Although fluorescent OLEDs are nearly obsolete now, devices with high internal quantum efficiency are still possible using the exciplexes as hosts, provided that two important criteria are met: (a) exciton formation exclusively within the exciplex host, with minimal exciton trapping by the dopant and (b) restricted triplet energy transfer from the host to the guest to prevent the electrical energy loss (the triplet excitons are dark in fluorescence OLEDs). The dominant mode of energy transfer from the host to the dopant is Förster, which requires a decent overlap between the host emission and the dopant absorption spectra. ISC/RISC are usually inactive because of the large singlet-triplet gap in the typical fluorescent materials. Therefore, the efficiency of populating the S_1 state of the fluorescent dopant through energy transfer from an exciplex host can be expressed by the following equation:

$$\Phi_{S_1}^{Dopant} = 0.25 \times \Phi_{ENT}^{S-S} \sum_{k=0}^{\infty} (\Phi_{ISC} \Phi_{RISC})^k + 0.75 \times \Phi_{RISC} \times \Phi_{ENT}^{S-S} \times \sum_{k=0}^{\infty} (\Phi_{ISC} \Phi_{RISC})^k,$$

where Φ_{ENT}^{S-S} , Φ_{ISC} , and Φ_{RISC} are the quantum efficiencies of the exciplex for the singlet energy transfer, ISC, and RISC, respectively [21]. Various Φ terms have the following formulations:

$$\Phi_{ENT}^{S-S} = \frac{k_{ENT}^{S-S}}{k_{ENT}^{S-S} + k_r + (k_{IC} + k_{ISC})}$$

$$\Phi_{ISC} = \frac{k_{ISC}}{k_{ISC} + k_{ENT}^{S-S} + k_{fluo} + k_{IC}}$$

$$\Phi_{RISC} = \frac{k_{RISC}}{k_{RISC} + k_{ENT}^{t-t} + k_{phos} + k_{IC}}$$

Here, the k terms represent the appropriate rate constants, and k_{ENT}^{t-t} is the triplet energy transfer (Dexter) component. The dopant concentration must be optimized to check the undesired triplet energy transfer from the exciplex host. The molecular structures discussed in this subsection are shown in Fig. 10.

Zhang *et al.* fabricated fluorescent devices by employing Rubrene as the emitter at different doping concentrations to probe the energy transfer process from the mCBP:PO-T2T exciplex to the dopant [97]. No exciplex emission can be observed from the device with 1.0 wt% dopant concentration. Warm wOLED is obtained (CIE: 0.3161, 0.4269) with 6.1 % EQE (9.2 lm W^{-1}) at a low dopant concentration of ~0.4 wt%. The pure Rubrene-based orange device displays only a low EQE of 3.9 %, which is considerably lower than the EQE of the exciplex-hosted Rubrene-doped wOLED. This finding demonstrated the contribution of energy transfer in the white light-emitting device. The device efficiency reaches 7.1% (11.4 lm W^{-1}) when a two-EML device consisting of the blue-emitting exciplex and the orange-emitting fluorescent dopant is fabricated. Replacing the orange-emitting Rubrene with red-emitting dopant 4-(Dicyanomethylene)-2-tert-butyl-6-(1,1,7,7-tetramethyljulolidin-4-yl-vinyl)-4 H-pyran (DCJTB) improves the efficiency of the single EML-based device. The color temperature of the mCBP:PO-T2T exciplex-hosted white device depends on the doping concentration of DCJTB. The relevant warm and cold wOLEDs display high EQE of 6.2 % and 5.8% with a low turn-on voltage of less than 3 V. However, unsatisfactory results are produced when the efficient exciplex system is combined with the TADF emitter, 4CzTPN-Ph (Fig. 10). Zhao *et al.* reported an OLED based on the exciplex system TCTA:3 P-T2T as the host for DCJTB [98]. A maximum luminance of 22767 cd m^{-2} , with CE of 22.7 cd A^{-1} , PE of 21.5 lm W^{-1} , and EQE of 10.2 % can be realized from the relevant optimized device. The high efficiency of the device is due to the effective triplet up-conversion of the exciplex host system and consequent energy transfer from the host to the dopant. The energy transfer efficiency is further verified by dopant concentration-dependent spectral shift and the TADF of DCJTB. Kim *et al.* demonstrated a red

Table 2

Device data table – exciplexes as hosts/cohosts in fluorescent, phosphorescent and TADF OLEDs (the values in the parenthesis indicate data at 1000 nit).

Device structure (the exciplex component is underlined)	Φ_{film} (%)	V_{on} (V)	λ_{EL}^{max} (nm)	EQE (%)	CE (cd A ⁻¹)	PE (lm W ⁻¹)	CIE	Ref
Exciplexes as hosts/cohosts in fluorescent OLEDs								
ITO/4% ReO ₃ :Tris-PCz (60 nm)/Tris-PCz (15 nm)/1 wt% rubrene in 1:1 Tris-PCz:CN-T2T (25 nm)/CN-T2T (50 nm)/Liq (0.5 nm)/Al (100 nm)	—	2.0	—	6.9 (6.6)	21.4	28.1	0.49, 0.50	[51]
ITO/4% ReO ₃ :Tris-PCz (60 nm)/Tris-PCz (15 nm)/1 wt% DCJTB in 1:1 Tris-PCz:CN-T2T (25 nm)/CN-T2T (50 nm)/Liq (0.5 nm)/Al (100 nm)	—	2.0	—	9.7 (9.1)	19.3	23.3	0.59, 0.40	[51]
ITO/MoO ₃ (3 nm)/mCBP (20 nm)/0.4 wt% Rubrene in 1:1 mCBP:PO-T2T (20 nm)/PO-T2T (40 nm)/LiF (0.8 nm)/Al	—	—	—	7.1 (6.1)	18.2 (15.6)	11.4 (7.6)	0.31, 0.41	[97]
ITO/MoO ₃ (3 nm)/mCBP (20 nm)/mCBP:PO-T2T (20 nm)/1.0 wt% Rubrene in 1:1 mCBP:PO-T2T (5 nm)/PO-T2T (40 nm)/LiF (0.8 nm)/Al	—	—	—	6.1 (5.8)	18.2 (15.6)	11.4 (7.6)	0.31, 0.41	[97]
ITO/MoO ₃ (3 nm)/mCBP (20 nm)/DCJTB in 1:1 mCBP:PO-T2T (20 nm)/PO-T2T (40 nm)/LiF (0.8 nm)/Al	—	—	—	6.2 (5.5)	13.3 (11.9)	10.4 (7.4)	0.45, 0.39	[97]
ITO/MoO ₃ (3 nm)/mCBP (20 nm)/0.2 wt% DCJTB in 1:1 mCBP:PO-T2T (20 nm)/PO-T2T (40 nm)/LiF (0.8 nm)/Al	—	—	—	5.8 (3.6)	11.89 (7.5)	9.3 (3.9)	0.29, 0.32	[97]
ITO/MoO ₃ (3 nm)/mCBP (20 nm)/mCBP:PO-T2T (20 nm)/0.5 wt% 4CzTPN-Ph in PO-T2T (10 nm)/PO-T2T (40 nm)/LiF (0.8 nm)/Al	—	—	—	4.8 (4.0)	11.2 (8.7)	7.3 (3.9)	0.41, 0.42	[97]
ITO/MoO ₃ (3 nm)/NPB (20 nm)/TCTA (8 nm)/0.5 wt% DCJTB in 1:1 TCTA:3 P-T2T (15 nm)/3 P-T2T (45 nm)/LiF (1 nm)/Al	—	2.2	586	7.5 (7.3)	19.9 (19.6)	18.6 (15.8)	—	[98]
ITO/MoO ₃ (3 nm)/NPB (20 nm)/TCTA (8 nm)/1.0 wt% DCJTB in 1:1 TCTA:3 P-T2T (15 nm)/3 P-T2T (45 nm)/LiF (1 nm)/Al	—	2.2	605	10.1 (10.0)	22.7 (22.4)	21.5 (18.9)	—	[98]
ITO/MoO ₃ (3 nm)/NPB (20 nm)/TCTA (8 nm)/0.5 wt% DCJTB in 1:1 TCTA:3 P-T2T (15 nm)/3 P-T2T (45 nm)/LiF (1 nm)/Al	73.0	2.4	600	10.6	20.5	26.8	—	[99]
ITO/TAPC (30 nm)/B4PYMPM (50 nm)/LiF (0.7 nm)/Al (100 nm)	—	—	—	23.7	—	—	—	[100]
ITO (100 nm)/TAPC (65 nm)/TCTA (10 nm)/0.5 wt% DCJTB and 8 wt% Ir(ppy) ₂ (tmd) in 1:1 TCTA:B4PYMPM (30 nm)/B4PYMPM (55 nm)/LiF (0.7 nm)/Al (100 nm)	—	—	—	—	—	—	—	[100]
ITO/TAPC (40 nm)/0.2 wt% C545T in TAPC:DPTPCz (30 nm)/TmPyPB (50 nm)/LiF (1 nm)/Al (100 nm)	—	2.8	—	14.5	44.0	46.1	0.24, 0.55	[101]
ITO/TAPC (40 nm)/1.0 wt% C545T in TAPC:DPTPCz (30 nm)/TmPyPB (50 nm)/LiF (1 nm)/Al (100 nm)	—	3.0	—	7.5	23.1	18.2	0.24, 0.58	[101]
ITO/TAPC (40 nm)/mCP (5 nm)/1 wt% C545T in DPTPCz (30 nm)/TmPyPB (50 nm)/LiF (1 nm)/Al (100 nm)	—	3.9	—	3.9	12.8	8.0	0.26, 0.60	[101]
ITO/NPB (50 nm)/TCTA (15 nm)/C4FS1 (20 nm)/TPBi (65 nm)/LiF (0.5 nm)/Al	—	9.1	496	1.7	4.5	—	0.20, 0.40	[102]
ITO/NPB (50 nm)/TCTA (15 nm)/C4FS1 (10 nm)/mCP (5 nm)/POT2T (5 nm)/C4FS1 (10 nm)/TPBi (65 nm)/LiF (0.5 nm)/Al	—	8.1	496	2.2	6.2	—	0.19, 0.38	[102]
ITO (80 nm)/HAT-CN (10 nm)/TAPC (30 nm)/BCzPh (10 nm):2:1 BCzPh:3 P-T2T (30 nm)/3 P-T2T (70 nm)/LiF (1 nm)/Al (100 nm)	68.0	2.8	532	13.5 (11.7)	—	45.9 (44.9)	(LT ₇₅ = 2 h)	[103]
ITO (80 nm)/HAT-CN (10 nm)/TAPC (30 nm)/BCzPh (10 nm)/1 wt% C545T in 2:1 BCzPh:3 P-T2T (30 nm)/3 P-T2T (70 nm)/LiF (1 nm)/Al (100 nm)	97.0	2.3	—	15.5 (15.2)	—	66.5 (58.3)	(LT ₇₅ = 282 h)	[103]
ITO/HAT-CN (10 nm)/TAPC (30 nm)/TCTA (5 nm)/5 wt% DTPBT in 1:1 TCTA:3 P-T2T (30 nm)/3 P-T2T (65 nm)/LiF (1 nm)/Al (100 nm)	65.0	2.5	591	14.8 (11.0)	25.6	32.1	0.52, 0.46	[104]
ITO/HAT-CN (10 nm)/TAPC (30 nm)/TCTA (5 nm)/5 wt% DTPNT in 1:1 TCTA:3 P-T2T (30 nm)/3 P-T2T (65 nm)/LiF (1 nm)/Al (100 nm)	34.0	2.5	647	9.9 (8.1)	11.3	14.2	0.59, 0.41	[104]
ITO/HAT-CN (10 nm)/TAPC (30 nm)/TCTA (5 nm)/5 wt% DTPNBT in 1:1 TCTA:3 P-T2T (30 nm)/3 P-T2T (65 nm)/LiF (1 nm)/Al (100 nm)	35.0	3.5	689	8.8 (3.6)	0.9	0.9	—	[104]
ITO/4 wt% ReO ₃ :Tr-Ph (60 nm)/Tr-Ph (15 nm)/10 wt% (DT) ₂ BTh2CN in 1:1 Tr-Ph:3 P-T2T (20 nm)/3 P-T2T (10 nm)/CN-T2T (40 nm)/Liq (0.5 nm)/Al (100 nm)	—	1.8	674	4.6 (1.0)	1.2 (0.3)	2.0 (0.2)	0.69, 0.31	[104]
ITO/4 wt% ReO ₃ :Tr-Ph (60 nm)/Tr-Ph (15 nm)/10 wt% (DT) ₂ BTh2CN in 1:1 Tr-Ph:3 P-T2P (20 nm)/3 P-T2P (10 nm)/CN-T2T (40 nm)/Liq (0.5 nm)/Al (100 nm)	—	2.3	671	5.5 (0.8)	1.7 (0.2)	2.1 (0.1)	0.68, 0.31	[104]
ITO/4 wt% ReO ₃ :Tr-Tol (60 nm)/Tr-Tol (15 nm)/10 wt% (DT) ₂ BTh2CN in 1:1 Tr-Tol:3 P-T2T (20 nm)/3 P-T2T (10 nm)/CN-T2T (40 nm)/Liq (0.5 nm)/Al (100 nm)	—	1.8	669	3.4 (0.7)	1.0 (0.2)	1.5 (0.1)	0.69, 0.31	[104]
ITO/4 wt% ReO ₃ :Tr-Tol (60 nm)/Tr-Tol (15 nm)/10 wt% (DT) ₂ BTh2CN in 1:1 Tr-Tol:3 P-T2P (20 nm)/3 P-T2P (10 nm)/CN-T2T (40 nm)/Liq (0.5 nm)/Al (100 nm)	—	2.3	667	4.4 (0.6)	1.7 (0.3)	2.2 (0.1)	0.67, 0.32	[104]
ITO/4 wt% ReO ₃ :Tr-iBu (60 nm)/Tr-iBu (15 nm)/3 DPy2CN in Tr-iBu:PO-T2P (1:2, 20 nm)/PO-T2P (50 nm)/Liq (0.5 nm)/Al (100 nm)	44	2.5	674	6.28	1.84	2.32	0.63, 0.35	[104]
ITO/4 wt% ReO ₃ :PTCz-9'Cz (15 nm)/10% iCzPNT in PTCz-9'Cz:PO-T2T (2:1, 20 nm)/PO-T2T (10 nm)/CN-T2T (40 nm)/Liq/Al	67	2.2	578	7.8	19.5	25.5	0.53, 0.46	[104]
ITO/4 wt% ReO ₃ :TCTA (60 nm)/PTCz-9'Cz (15 nm)/10% iCzBTh2CN in PTCz-9'Cz:PO-T2T (2:1, 20 nm)/PO-T2T (10 nm)/CN-T2T (40 nm)/Liq/A	64	2.3	618	8.0	9.9	12.0	0.63, 0.37	[104]
ITO/HAT-CN (30 nm)/TAPC (70 nm)/DPSF (15 nm)/DPSF:CN-T2T:TTDSF (46.5 wt%: 46.5 wt%: 7 wt%, 30 nm)/CN-T2T (100 nm)/LiF (1 nm)/Al (100 nm)	26	3.9	774	5.3	—	—	—	[104]
ITO/HAT-CN (30 nm)/TAPC (70 nm)/DTSF (15 nm)/DTSF:CN-T2T:TTDSF (46.5 wt%: 46.5 wt%: 7 wt%, 30 nm)/CN-T2T (100 nm)/LiF (1 nm)/Al (100 nm)	25	4.1	774	4.0	—	—	—	[104]
	—	—	—	12.2 (11.8)	—	—	0.33, 0.59	[105]

(continued on next page)

Table 2 (continued)

Device structure (the exciplex component is underlined)	Φ_{film} (%)	V_{on} (V)	λ_{EL}^{max} (nm)	EQE (%)	CE (cd A ⁻¹)	PE (lm W ⁻¹)	CIE	Ref
ITO/HATCN (5 nm)/NPB (40 nm)/TCTA (10 nm)/1 wt% PhtBuPAD in 2:8 TCTA:CzTrz (20 nm)/TPBi (40 nm)/LiF (0.5 nm)/Al (150 nm)	—	—	—	16.5 (16.2)	—	—	0.32, 0.59	[105]
ITO/HATCN (5 nm)/NPB (40 nm)/TCTA (10 nm)/1 wt% PhtBuPAD in 2:8 tBuTCTA:CzTrz (20 nm)/TPBi (40 nm)/LiF (0.5 nm)/Al (150 nm)	—	—	—	11.2 (9.7)	36.8 (31.7)	24.8 (16.8)	0.25, 0.59	[106]
ITO (50 nm)/PEDOT:PSS (60 nm)/TAPC (20 nm)/mCP (10 nm)/1 wt% 6tBPA in 1:1 TCTA:Cz-Trz (25 nm)/TSPO1 (5 nm)/TPBi (30 nm)/LiF (1 nm)/Al (200 nm)	—	—	—	11.2 (9.7)	36.8 (31.7)	24.8 (16.8)	0.25, 0.59	[106]
ITO/HATCN (5 nm)/NPB (20 nm)/TCTA (8 nm)/3 wt% 2 in 1:1 TCTA:3 P- T2T (15 nm)/3 P-T2T (30 nm)/LiF (0.5 nm)/Al (100 nm)	56	2.9	608	8.0 (6.1)	12.4 (10.3)	12.1 (5.3)	0.56, 0.43	[110]
ITO/HATCN (5 nm)/NPB (20 nm)/TCTA (8 nm)/6 wt% 2 in 1:1 TCTA:3 P- T2T (15 nm)/3 P-T2T (30 nm)/LiF (0.5 nm)/Al (100 nm)	64	2.6	612	10.2 (8.0)	16.4 (13.5)	18.1 (8.6)	0.62, 0.37	[110]
ITO (100 nm)/HAT-CN (20 nm)/TAPC (30 nm)/TCTA (10 nm)/1 wt% 67dTPA-FQ in 4:1 TCTA:PO-T2T (30 nm)/TPBi (40 nm)/LiF (1 nm)/Al (100 nm)	28	4.8	552	8.4	25.7	26.4	—	[111]
ITO (100 nm)/HAT-CN (20 nm)/TAPC (30 nm)/TCTA (10 nm)/1 wt% 267TPA-FQ in 4:1 TCTA:PO-T2T (30 nm)/TPBi (40 nm)/LiF (1 nm)/Al (100 nm)	43	4.3	524	9.6	23.8	34.3	—	[111]
ITO (120 nm)/PEDOT: PSS (32 nm)/BCC-36: PO-T2T (5:1) + 1% C545T (25 nm)/PO-T2T (30 nm)/LiF (1 nm)/Al (100 nm), Exciplexes as hosts/cohosts in phosphorescent OLEDs	—	3.5	—	12.5	28.5	25	0.24, 0.57	[224]
ITO (130 nm)/TAPC (25 nm)/TCTA (5 nm)/11 wt% FIrpic in BTPS (10 nm)/B3PyPB (50 nm)/Liq (1 nm)/Al (100 nm)	60.0	2.8	—	22.1 (18.0)	47.9 (38.9)	45.5 (30.9)	—	[112]
ITO (70 nm)/mCP:ReO ₃ (45 nm)/mCP (15 nm)/10 wt% FIrpic in 1:1 mCP: B3PYMPM (15 nm)/B3PYMPM (20 nm)/B3PYMPM:Rb ₂ CO ₃ (55 nm)/ LiF (0.7 nm)/Al (100 nm)	—	3.0	—	29.5	62.2	55.4	—	[113]
ITO/MoO ₃ (8 nm)/TAPC (40 nm)/mCP (5 nm)/8 wt% FIrpic in 1:1 mCP: iTPyBIB (10 nm)/iTPyBIB (5 nm)/TmPyPB (40 nm)/LiF (1 nm)/Al (120 nm)	—	3.3	—	11.5	23.4	14.2	0.15, 0.29	[114]
ITO/MoO ₃ (8 nm)/TAPC (40 nm)/mCP (5 nm)/8 wt% FIrpic in 1:1 mCP: iTPBiPy (10 nm)/iTPBiPy (5 nm)/TmPyPB (40 nm)/LiF (1 nm)/Al (120 nm)	—	3.2	—	19.3	38.5	36.9	0.15, 0.29	[114]
ITO/MoO ₃ (8 nm)/TAPC (40 nm)/mCP (5 nm)/8 wt% FIrpic in 1:1 mCP: iTPyBiPy (10 nm)/iTPyBiPy (5 nm)/TmPyPB (40 nm)/LiF (1 nm)/Al (120 nm)	—	3.2	—	13.5	28.0	25.5	0.22, 0.32	[114]
ITO (70 nm)/6% ReO ₃ in mCP (45 nm)/mCP (15 nm)/10 wt% FIrpic in mCP:PO-T2T (30 nm)/PO-T2T (20 nm)/4% Rb ₂ CO ₃ :PO-T2T (25 nm)/Al (100 nm)	—	—	—	30.3 (29.4)	—	66.0	—	[115]
ITO/HATCN (10 nm)/NPB (10 nm)/TCTA (5 nm)/1:1 TCTA: BTDCb-PCz (5 nm)/8 wt% FIrpic in BTDCb-PCz (20 nm)/TmPyPB (50 nm)/Liq (1 nm)/Al	—	2.7	500, 475	23.6 (18.6)	55.6 (45.4)	52.9 (33.9)	0.19, 0.46	[116]
ITO/HATCN (10 nm)/NPB (10 nm)/TCTA (5 nm)/1:1 TCTA: BTCz-PCz (5 nm)/8 wt% FIrpic in BTCz-PCz (20 nm)/TmPyPB (50 nm)/Liq (1 nm)/Al	—	2.9	500, 475	23.0 (16.6)	44.8 (33.0)	43.7 (23.6)	0.15, 0.35	[116]
ITO/HATCN (10 nm)/NPB (10 nm)/TCTA (5 nm)/1:1 TCTA: DCb-PCz (5 nm)/8 wt% FIrpic in DCb-PCz (20 nm)/TmPyPB (50 nm)/Liq (1 nm)/ Al	—	2.8	500, 475	24.6 (22.8)	46.4 (42.9)	44.6 (31.6)	0.15, 0.34	[116]
ITO/HATCN (10 nm)/NPB (10 nm)/TCTA (5 nm)/1:1 TCTA: CzBPDCb (5 nm)/8 wt% FIrpic in CzBPDCb (20 nm)/TmPyPB (50 nm)/Liq (1 nm)/Al	—	3.2	500, 475	21.9 (19.7)	44.2 (41.7)	38.9 (29.1)	0.15, 0.35	[116]
ITO (180 nm)/HAT-CN (10 nm)/TAPC (60 nm)/TCTA (5 nm)/mCBP (5 nm)/15 wt% in FIrpic 2:1:1 mCBP:PO-T2T:B4PyPPM (10 nm)/PO- T2T (45 nm)/LiF (1 nm)/Al(100 nm)	—	—	—	25.6 (24.6)	45.8 (44.3)	54.3 (37.3)	—	[117]
ITO (180 nm)/HAT-CN (10 nm)/TAPC (60 nm)/TCTA (5 nm)/mCBP (5 nm)/15 wt% FIrpic in 1:1 mCBP:B4PyPPM (10 nm) /PO-T2T (45 nm)/LiF (1 nm)/Al(100 nm)	—	—	—	21.1 (20.3)	39.8 (38.2)	44.7 (32.3)	—	[117]
ITO (50 nm)/PEDOT:PSS (40 nm)/TAPC (20 nm)/mCP (10 nm)/5 wt% FCNir in 1:1 TCTA:DBFTrz (25 nm)/TSPO1 (5 nm)/TPBi (20 nm)/LiF (1.5 nm)/Al (200 nm)	—	—	—	22.6 (20.5)	41.4 (37.9)	46.8 (31.6)	—	[118]
ITO (50 nm)/PEDOT:PSS (40 nm)/TAPC (20 nm)/mCP (10 nm)/5 wt% FCNir in t-DCPDA:DBFTrz (25 nm)/TSPO1 (5 nm)/TPBi (20 nm)/LiF (1.5 nm)/Al (200 nm)	—	—	—	16.4	25.2	—	0.14, 0.20	[118]
ITO (50 nm)/PEDOT:PSS (40 nm)/TAPC (20 nm)/mCP (10 nm)/5 wt% FCNir in DCDPA:DBFTrz (25 nm)/TSPO1 (5 nm)/TPBi (20 nm)/LiF (1.5 nm)/Al (200 nm)	—	—	—	15.3	22.5	—	0.14, 0.19	[118]
ITO (70 nm)/6 wt% ReO ₃ in mCP (30 nm)/mCP (20 nm)/12 wt% FCNir in 1:1 mCP:BM-A10 (20 nm)/BM-A10 (20 nm)/12 wt% Rb ₂ CO ₃ in BM-A10 (20 nm)/Al (100 nm)	82.0	2.9	—	24.0 (21.0)	—	41.0 (26.0)	0.15, 0.21 LT ₅₀ ~ 1 h	[119]
ITO/MoO ₃ (8 nm)/TAPC (40 nm)/mCP (5 nm)/8 wt% FIrpic in 1:1 TAPC: CzPyCN (10 nm)/TmPyPB (40 nm)/LiF (1 nm)/Al	—	2.9	472, 516	6.2	17.0	15.6	0.29, 0.43	[120]
ITO/MoO ₃ (8 nm)/TAPC (40 nm)/mCP (5 nm)/8 wt% FIrpic in 1:1 mCP: CzPyCN (10 nm)/TmPyPB (40 nm)/LiF (1 nm)/Al	—	3.0	471	19.1	37.9	33.0	0.15, 0.28	[120]
	—	2.7	472	13.3	30.9	33.7	0.19, 0.36	[120]

(continued on next page)

Table 2 (continued)

Device structure (the exciplex component is underlined)	Φ_{film} (%)	V_{on} (V)	λ_{EL}^{max} (nm)	EQE (%)	CE (cd A ⁻¹)	PE (lm W ⁻¹)	CIE	Ref
ITO/MoO ₃ (8 nm)/TAPC (40 nm)/mCP (5 nm)/8 wt% Flrpic in 1:1 TAPC: CbPyCN (10 nm)/TmPyPB (40 nm)/LiF (1 nm)/Al	—	2.8	472	21.4	43.0	48.2	0.14, 0.30	[120]
ITO/MoO ₃ (8 nm)/TAPC (40 nm)/mCP (5 nm)/8 wt% Flrpic in 1:1 mCP: CbPyCN (10 nm)/TmPyPB (40 nm)/LiF (1 nm)/Al	54.1	2.6	—	13.7 (12.7)	25.2 (23.3)	22.2 (15.8)	—	[121]
ITO (130 nm)/TAPC (30 nm)/SiDMAC (5 nm)/16 wt% (dppy) ₂ Ir(acac) in 1:1 SiDMAC:BPSPF (30 nm)/BPSPF (5 nm)/B3PyPB (50 nm)/Liq (1 nm)/Al(100 nm)	90.2	—	—	17.7 (14.3)	—	50.8 (44.4)	—	[26c]
ITO (80 nm)/HAT-CN (10 nm)/TAPC (30 nm)/BCzPh (10 nm)/8 wt% Ir (ppy) ₂ (acac) in 2:1 BCzPh:3 P-T2T (30 nm)/3 P-T2T (70 nm)/LiF (1 nm)/Al (100 nm)	85.0	2.2	—	29.7 (25.8)	—	143.4 (123.9)	(LT ₇₅ = 48 h)	[103]
ITO (80 nm)/HAT-CN (10 nm)/TAPC (30 nm)/BCzPh (10 nm)/8 wt% Ir (ppy) ₂ (acac) in CBP (30 nm)/3 P-T2T (70 nm)/LiF (1 nm)/Al (100 nm)	96.0	2.6	—	29.5 (27.3)	—	112.2 (98.9)	(LT ₇₅ = 44 h)	[103]
ITO (50 nm) BCFN:HATCN (40 nm:30%)/BCFN (10 nm)/mCBP (10 nm)/ 15 wt% CNIM in mCBP:CnMSi-Trz (30 nm)/ DBFTRZ (5 nm)/ ZADN (20 nm)/LiF (1.5 nm)/Al (200 nm)	—	5.3	—	23.1	45.4	44.1	0.16, 0.29	[122]
ITO (50 nm) BCFN:HATCN (40 nm:30%)/BCFN (10 nm)/mCBP (10 nm)/ 15 wt% CNIM in mCBP:CnMSi-2DBF-Trz (30 nm)/ DBFTRZ (5 nm)/ ZADN (20 nm)/LiF (1.5 nm)/Al (200 nm)	—	5.0	—	23.8	48.9	51.2	0.16, 0.28	[122]
ITO (50 nm) BCFN:HATCN (40 nm:30%)/BCFN (10 nm)/mCBP (10 nm)/ 15 wt% CNIM in mCBP:CnMSi-4DBF-Trz (30 nm)/ DBFTRZ (5 nm)/ ZADN (20 nm)/LiF (1.5 nm)/Al (200 nm)	—	5.6	—	19.0	37.8	40.4	0.16, 0.30	[122]
ITO (150 nm)/3 wt% p-doped NPD in BCFA (10 nm)/BCFA (125 nm)/SDI (10 nm)/ HT4 (5 nm)/ BP (5 nm)/10% IrE in 1:1 HT3:ET7 (40 nm)/ET3 (10 nm)/1:1 NET:NDN (30 nm)/Al (100 nm)	—	4.1	462	25.1	—	—	—	[122]
ITO (150 nm)/3 wt% p-doped NPD in BCFA (10 nm)/BCFA (125 nm)/SDI (10 nm)/ HT4 (5 nm)/ BP (5 nm)/10% IrE in 1:1 HT4:ET7 (40 nm)/ET3 (10 nm)/1:1 NET:NDN (30 nm)/Al (100 nm)	—	3.9	462	24.2	—	—	—	[122]
ITO (150 nm)/3 wt% p-doped NPD in BCFA (10 nm)/BCFA (125 nm)/SDI (10 nm)/ HT4 (5 nm)/ BP (5 nm)/10% IrE in 1:1 HT3:ET8 (40 nm)/ET3 (10 nm)/1:1 NET:NDN (30 nm)/Al (100 nm)	—	3.4	462	21.9	—	—	—	[122]
ITO (150 nm)/3 wt% p-doped NPD in BCFA (10 nm)/BCFA (125 nm)/SDI (10 nm)/ HT4 (5 nm)/ BP (5 nm)/10% IrE in 1:1 HT4:ET8 (40 nm)/ET3 (10 nm)/1:1 NET:NDN (30 nm)/Al (100 nm)	—	3.5	462	22.4	—	—	—	[122]
ITO (120 nm)/TAPC (75 nm)/TCTA (10 nm)/8 wt% Ir(ppy) ₃ in 1:1 TCTA: TPBi /BmPyPb/LiF/Al	—	—	—	20.5	—	—	—	[124]
ITO (120 nm)/TAPC (75 nm)/TCTA (10 nm)/8 wt% Ir(ppy) ₃ in 1:1 CBP: TPBi/BmPyPb/LiF/Al	—	—	—	21.2	—	—	—	[124]
ITO (70 nm)/TAPC (60 nm)/TCTA (10 nm)/8 wt% Ir(ppy) ₂ (acac) in 1:1 TCTA:B3PYMPM (30 nm)/B3PYMPM (40 nm)/Al (100 nm)	—	2.4	—	30.2	106.0	—	—	[126]
ITO (70 nm)/TAPC (60 nm)/TCTA (10 nm)/8 wt% Ir(ppy) ₂ (acac) in 1:1 TCTA:B3PYMPM (30 nm)/B3PYMPM (40 nm)/LiF (0.7 nm)/Al (100 nm)	—	2.4	—	29.1 (28.7)	—	124.0 (112.5)	—	[127]
ITO (70 nm)/TAPC (75 nm)/TCTA (10 nm)/8 wt% Ir(ppy) ₂ (acac) in 1:1 TCTA:B3PYMPM (30 nm)/ B3PYMPM (40 nm)/LiF (0.7 nm)/Al (100 nm)	—	2.5	—	30.0	—	—	—	[128]
ITO (70 nm)/MoO ₃ (1 nm)/CBP (90 nm)/8 wt% Ir(ppy) ₂ (acac) in CBP (15 nm)/TPBi (65 nm)/LiF (0.7 nm)/Al (100 nm)	—	3.0	—	25.0	—	—	—	[128]
ITO (60 nm)/HATCN (50 nm)/TAPC:ReO ₃ (10 nm)/TAPC (5 nm)/TCTA (5 nm)/8 wt% Ir(ppy) ₂ (tmd) in 1: TCTA:B3PYMPM (30 nm)/B3PYMPM (15 nm)/B3PYMPM:Rb ₂ CO ₃ (30 nm)/Al (70 nm)	—	—	—	31.9 (27.6)	—	—	—	[129]
ITO/HATCN (10 nm)/TAPC (55 nm)/Ir(ppy) ₂ (acac) (0.8 nm)/TmPyPB (40 nm)/1:1 BPhen:LiNH ₂ (10 nm)/HATCN(10 nm)/TAPC (55 nm)/Ir (ppy) ₂ (acac)(0.8 nm)/TmPyPB (40 nm)/Liq (2 nm)/Al(120 nm)	—	5.8	528	36.8	135.7	59.9	0.35, 0.61	[130]
ITO (110 nm)/HAT-CN (10 nm)/TAPC (10 nm)/TCTA (10 nm)/ Ir (ppy) ₂ acac (0.2 nm)/B3PyMPM (70 nm)/Liq (0.2 nm)/Al (120 nm)	—	2.8	—	25.9 (18.0)	83.0 (55.6)	93.0 (50.2)	—	[131]
ITO (80 nm)/HAT-CN (10 nm)/TAPC (30 nm)/TCTA (10 nm)/8 wt% Ir (ppy) ₂ (acac) in 1:1 TCTA:3 P-T2T (20 nm)/3PT2T (70 nm)/LiF (1 nm)/ Al (100 nm)	96.0	2.3	525	28.1 (28.0)	107.0 (106.0)	132.0 (108.0)	(LT ₈₀ = 1020 min)	[133]
ITO (80 nm)/HAT-CN (10 nm)/TAPC (30 nm)/TCTA (10 nm)/8 wt% Ir (ppy) ₂ (acac) in 1:1 TCTA:B3PYMPM (30 nm)/B3PYMPM (50 nm)/LiF (1 nm)/Al (100 nm)	—	2.5	—	31.7 (31.4)	119.0 (120.0)	127.0 (101.0)	(LT ₈₀ = 18 min)	[133]
(ITO) (80 nm)/HATCN (30 nm)/TAPC (30 nm)/PhCNCzp-Me (15 nm)/ 8 wt% Ir(ppy) ₂ (acac) in 1:1 PhCNCzp-Me:B3PyMPM: (25 nm)/ B3PyMPM (50 nm)/LiF (1 nm)/Al (120 nm)	—	4.7	—	15.7 (11.5)	60.8 (43.7)	37.6 (20.1)	0.33, 0.62	[134]
(ITO) (80 nm)/HATCN (30 nm)/TAPC (30 nm)/PhCzp-Me (15 nm)/8 wt% Ir(ppy) ₂ (acac) in 1:1 PhCzp-Me:B3PyMPM: (25 nm)/B3PyMPM (50 nm)/LiF (1 nm)/Al (120 nm)	—	3.1	—	27.8 (27.1)	106.1 (104.0)	85.5 (78.5)	0.34, 0.63	[134]
(ITO) (80 nm)/HATCN (30 nm)/TAPC (30 nm)/PhCNCzp-MeCzPh (15 nm)/8 wt% Ir(ppy) ₂ (acac) in 1:1 PhCNCzp-MeCzPh:B3PyMPM: (25 nm)/B3PyMPM (50 nm)/LiF (1 nm)/Al (120 nm)	—	3.8	—	25.6 (24.8)	99.4 (95.8)	69.4 (59.4)	0.34, 0.63	[134]
(ITO) (80 nm)/HATCN (30 nm)/TAPC (30 nm)/PhCNCzm-Me (15 nm)/ 8 wt% Ir(ppy) ₂ (acac) in 1:1 PhCNCzm-Me:B3PyMPM: (25 nm)/ B3PyMPM (50 nm)/LiF (1 nm)/Al (120 nm)	—	3.1	—	29.4 (28.3)	106.0 (105.5)	93.5 (80.2)	0.33, 0.63	[134]

(continued on next page)

Table 2 (continued)

Device structure (the exciplex component is underlined)	Φ_{film} (%)	V_{on} (V)	λ_{EL}^{max} (nm)	EQE (%)	CE (cd A ⁻¹)	PE (lm W ⁻¹)	CIE	Ref
(ITO) (80 nm)/HATCN (30 nm)/TAPC (30 nm)/PhCNCzm-MeCzPh (15 nm)/8 wt% Ir(ppy) ₂ (acac) in 1:1 PhCNCzm-MeCzPh:B3PyMPM: (25 nm)/B3PyMPM (50 nm)/LiF (1 nm)/Al (120 nm)	—	3.5	—	31.5 (30.2)	113.1 (112.2)	99.4 (77.8)	0.32, 0.64	[134]
ITO/HATCN (30 nm)/TAPC (30 nm)/BCzPh-pimi (15 nm)/8 wt% Ir(ppy) ₂ (acac) in 1:1 BCzPh-pimi: B3PyMPM (30 nm)/B3PyMPM (40 nm)/LiF (1 nm)/Al (120 nm).		2.9		22.3 (21.7)	84.1 (81.8)	77.3 (70.6)	0.31, 0.64	[134]
ITO/HATCN (30 nm)/TAPC (30 nm)/BCzPh-mimi (15 nm)/8 wt% Ir(ppy) ₂ (acac) in 1:1 BCzPh-mimi: B3PyMPM (30 nm)/B3PyMPM (40 nm)/LiF (1 nm)/Al (120 nm).		3.1		18.7 (18.5)	70.4 (69.0)	64.7 (59.3)	0.30, 0.65	[134]
ITO (100 nm)/TAPC (75 nm)/NPB (10 nm)/5 wt% Ir(mphq) ₂ (tmd) in 1:1 NPB:PO-T2T (30 nm)/POT2T (10 nm)/0.5% Rb ₂ CO ₃ :PO-T2T (40 nm)/Al (100 nm)	—	1.9	—	34.1 (32.4)	—	62.2 (42.0)	(LT ₉₀ = 2243 h)	[135]
ITO (100 nm)/TAPC (75 nm)/NPB (10 nm)/5 wt% Ir(MDQ) ₂ (acac) in 1:1 NPB:PO-T2T (30 nm)/POT2T (10 nm)/0.5% Rb ₂ CO ₃ :PO-T2T (40 nm)/Al (100 nm)	—	1.9	—	26.8 (25.9)	—	48.9 (33.8)	(LT ₉₀ = 1102 h)	[135]
ITO (130 nm)/PPBI/α-NPD (20 nm)/1 wt% (DPQ) ₂ Ir(dpm) in 1:1 α-NPD:4DBF46PM (40 nm)/4DBF46PM (20 nm)/DPB (30 nm)/20 wt% Liq-doped DPB (20 nm)/Liq (1 nm)/Al (80 nm)	—	2.6	675	13.4 (9.8)	2.2 (1.7)	1.8 (0.9)	0.63, 0.30	[137]
ITO (130 nm)/PPBI/α-NPD (20 nm)/1 wt% (DPQ) ₂ Ir(dpm) in 1:1 α-NPD:4DBF26PM (40 nm)/4DBF26PM (20 nm)/DPB (30 nm)/20 wt% Liq-doped DPB (20 nm)/Liq (1 nm)/Al (80 nm)	—	3.1	675	13.4 (10.7)	2.5 (2.0)	1.8 (1.0)	0.64, 0.30	[137]
ITO (130 nm)/PPBI/α-NPD (20 nm)/1 wt% (DPQ) ₂ Ir(dpm) in 1:1 α-NPD:4DBF46TRZ (40 nm)/4DBF46TRZ (20 nm)/DPB (30 nm)/20 wt% Liq-doped DPB (20 nm)/Liq (1 nm)/Al (80 nm)	—	2.4	675	13.4 (10.8)	2.1 (1.7)	1.9 (0.9)	0.71, 0.29	[137]
ITO (130 nm)/PPBI/α-NPD (20 nm)/3 wt% (DPQ) ₂ Ir(dpm) in 1:1 α-NPD:4DBF46TRZ (40 nm)/4DBF46TRZ (20 nm)/DPB (30 nm)/20 wt% Liq-doped DPB (20 nm)/Liq (1 nm)/Al (80 nm)	—	2.4	675	13.4 (11.1)	1.8 (1.4)	1.5 (0.7)	0.72, 0.28	[137]
ITO (130 nm)/PPBI/α-NPD (20 nm)/5 wt% (DPQ) ₂ Ir(dpm) in 1:1 α-NPD:4DBF46TRZ (40 nm)/4DBF46TRZ (20 nm)/DPB (30 nm)/20 wt% Liq-doped DPB (20 nm)/Liq (1 nm)/Al (80 nm)	—	2.4	675	13.4 (9.5)	1.5 (1.2)	1.3 (0.6)	0.72, 0.28	[137]
ITO (150 nm)/ TAPC (20 nm)/TCTA (10 nm)/3 wt% Ir(mphq) ₂ (acac) in 1:1 TCTA:B3PYMPM (10 nm)/8 wt% Ir(ppy) ₂ (acac) in TCTA:B3PYMPM (20 nm)/B3PYMPM (45 nm)/LiF (0.7 nm)/Al (100 nm)	—	2.4	—	23.3	—	57.0	0.53, 0.45	[138]
ITO (150 nm)/ TAPC (20 nm)/ TCTA (10 nm)/8 wt% Ir(ppy) ₂ (acac) + 0.5% Ir(mphq) ₂ (acac) in TCTA:B3PYMPM (30 nm)/B3PYMPM (45 nm)/ LiF (0.7 nm)/ Al (100 nm)	—	2.4	—	25.4	—	—	0.56, 0.43	[139]
ITO/MoO ₃ (4 nm)/mCP (20 nm)/1.5 wt% Ir(pq) ₂ (acac) in 1:1 mCP:PO-T2T (25 nm)/DEPEO (3 nm)/Bepp2 (40 nm)/LiF (1.5 nm)/Al (100 nm).	—	3.0	596	18.7	35.3	31.0	—	[140]
ITO/MoO ₃ (5 nm)/NPB (50 nm)/(btb) ₂ Ir(acac) (0.5 nm)/TPBi (10 nm)/BPhen (40 nm)/Mg:Ag (100 nm)	—	3.0	595, 551	7.9 (5.4)	21.3 (14.4)	17.7	—	[141]
ITO/MoO ₃ (5 nm)/NPB (40 nm)/TCTA (10 nm)/(btb) ₂ Ir(acac) (0.5 nm)/TPBi (10 nm)/BPhen (40 nm)/Mg:Ag (100 nm)	—	3.6		14.3 (11.5)	40.5 (33.1)	37.4	—	[141]
ITO (50 nm)/DNTPD (60 nm)/BPBPB (20 nm)/PCZAC (10 nm)/5 wt% PO-01 in 1:1 mIDIDP:TPBi (30 nm)/DBFTrz (5 nm)/ZADN (30 nm)/LiF (1.5 nm)/Al (200 nm)	—	5.6	561	21.4 (20.9)	70.1 (67.7)	52.4 (37.8)	0.49, 0.51 (LT ₈₀ = 227 h)	[142]
ITO (50 nm)/DNTPD (60 nm)/BPBPB (20 nm)/PCZAC (10 nm)/5 wt% PO-01 in 1:1 TCTA:TPBi (30 nm)/DBFTrz (5 nm)/ZADN (30 nm)/LiF (1.5 nm)/Al (200 nm)	—	5.7	561	22.2 (21.5)	71.9 (69.6)	52.4 (38.2)	0.49, 0.51 (LT ₈₀ = 17 h)	[142]
ITO/TAPC (30 nm)/CDBP (10 nm)/6 wt% Ir(ppy) ₂ (acac) in 1:1 CDBP:PO-T2T (30 nm)/PO-T2T (40 nm)/LiF (1 nm)/Al (100 nm)	—	2.5	—	28.6 (23.3)	98.3	110.2	0.29, 0.64	[42]
ITO/TAPC (30 nm)/CDBP (10 nm)/2 wt% Ir(MDQ) ₂ (acac) in 1:1 CDBP:PO-T2T (30 nm)/PO-T2T (40 nm)/LiF (1 nm)/Al (100 nm)	—	2.5	—	28.0 (18.9)	54.3	63.1	0.58, 0.41	[42]
ITO (130 nm)/PPBI (20 nm)/NPD (20 nm)/10 wt% (DPQ) ₂ Ir(dpm) in 1:1 NPD: DBT-TRZ (40 nm)/DBT-TRZ (20 nm)/DPB (30 nm)/20 wt% Liq doped in DPB (20 nm)/Liq (1 nm)/Al (80 nm)	2.8	675	10.9 (6.9)	1.3 (0.7)	1.5 (0.3)	0.70, 0.29 (LT ₈₀ = 280 h)	[144]	
ITO (130 nm)/PPBI (20 nm)/NPD (20 nm)/10 wt% (DPQ) ₂ Ir(dpm) in 1:1 DBTPB: DBT-TRZ (40 nm)/DBT-TRZ (20 nm)/DPB (30 nm)/20 wt% Liq doped in DPB (20 nm)/Liq (1 nm)/Al (80 nm)	52.0	2.4	675	11.5 (6.3)	1.2 (0.7)	1.5 (0.3)	0.72, 0.28 (LT ₈₀ = 750 h)	[144]
ITO (130 nm)/PPBI (20 nm)/NPD (20 nm)/10 wt% (DPQ) ₂ Ir(dpm) in 1:1 BTBTPDF: DBT-TRZ (40 nm)/DBT-TRZ (20 nm)/DPB (30 nm)/20 wt% Liq doped in DPB (20 nm)/Liq (1 nm)/Al (80 nm)	48.0	2.2	675	11.7 (7.5)	1.1 (0.8)	1.6 (0.4)	0.72, 0.28 (LT ₈₀ = 1480 h)	[144]
ITO/HATCN (5 nm)/TAPC (30 nm)/DMIC-CZ (5 nm)/8 wt% Ir(mpqi) ₂ dmbm-d ₁ in 1:1 DMIC-Cz:ET24 (30 nm)/BPhen (70 nm)/LiF (1 nm)/ Al		2.5	633	16.4 (16.2)	9.3 (9.3)	8.2 (4.8)	—	[145]
ITO/HATCN (5 nm)/TAPC (30 nm)/DMIC-CZ (5 nm)/8 wt% Ir(mpqi) ₂ dmbm-d ₁ in 1:1 DMIC-Cz:ET24 (30 nm)/BPhen (70 nm)/LiF (1 nm)/ Al	—	2.2	634	14.0 (13.9)	7.6 (7.6)	7.2 (4.6)	—	[145]
ITO (130 nm)/polymer buffer (20 nm)/NPD (20 nm)/ 1 wt% (DPQ) ₂ Ir(dpm) in 1:1 α-NPD:DPB (40 nm)/DPB (50 nm)/ 20 wt% Liq doped DPB (20 nm)/Liq (1 nm)/Al (80 nm).	45	2.7	—	14.0 (9.8)	1.6 (1.1)	1.9 (0.4)	0.71, 0.29	[146]
ITO (130 nm)/polymer buffer (20 nm)/NPD (20 nm)/ 3 wt% (DPQ) ₂ Ir(dpm) in 1:1 α-NPD:DPB (40 nm)/pDPB (50 nm)/ 20 wt% Liq doped pDPB (20 nm)/Liq (1 nm)/Al (80 nm).	45	2.6	—	15.7 (11.7)	1.8 (1.3)	2.2 (0.5)	0.71, 0.29	[146]
	57	2.4	—	16.7 (10.8)	1.6 (0.5)	2.2 (0.5)	0.27, 0.28	[146]

(continued on next page)

Table 2 (continued)

Device structure (the exciplex component is underlined)	Φ_{film} (%)	V_{on} (V)	λ_{EL}^{max} (nm)	EQE (%)	CE (cd A ⁻¹)	PE (lm W ⁻¹)	CIE	Ref
ITO (130 nm)/polymer buffer (20 nm)/NPD (20 nm)/ 3 wt% (DPQ) ₂ Ir (dpm) in 1:1 α -NPD:nBPhen (40 nm)/nBPhen (50 nm)/ 20 wt% Liq doped nBPhen (20 nm)/Liq (1 nm)/Al (80 nm).	—	—	—	—	—	—	—	[147]
ITO/TAPC (30 nm)/TCTA (20 nm)/4 wt% Isq-1 in 1:1 TCTA:T2T (25 nm)/ TmPyPB (70 nm)/LiF(1 nm)/Al	28	—	760	6.29	—	—	—	[147]
ITO/TAPC (30 nm)/TCTA (20 nm)/4 wt% Isq-2 in 1:1 TCTA:T2T (25 nm)/ TmPyPB (70 nm)/LiF(1 nm)/Al	48	—	750	10.32	—	—	—	[147]
ITO/TAPC (30 nm)/TCTA (20 nm)/4 wt% Isq-3 in 1:1 TCTA:T2T (25 nm)/ TmPyPB (70 nm)/LiF(1 nm)/Al	41	—	755	9.58	—	—	—	[147]
ITO/MoO ₃ (2 nm)/15 wt% MoO ₃ :m-MTDATA (30 nm)/m-MTDATA (10 nm)/2 wt% Ir(ppy) ₃ in 1:1 m-MTDATA:TmPyPB (30 nm)/TmPyPB (30 nm)/LiF (1 nm)/Al (100 nm)	—	2.2	—	11.5	39.1 (30.4)	27.9 (26.8)	0.32, 0.61	[148]
ITO/MoO ₃ (2 nm)/15 wt% MoO ₃ :m-MTDATA (30 nm)/m-MTDATA (10 nm)/2 wt% Ir(bt) ₂ (acac) in 1:1 m-MTDATA:TmPyPB (30 nm)/TmPyPB (30 nm)/LiF (1 nm)/Al (100 nm)	—	2.5	602, 560	18.5	50.7 (44.9)	57.6 (22.4)	0.51, 0.49	[148]
ITO/MoO ₃ (2 nm)/15 wt% MoO ₃ :m-MTDATA (30 nm)/m-MTDATA (10 nm)/2 wt% (pq) ₂ Ir(acac) in 1:1 m-MTDATA:TmPyPB (30 nm)/TmPyPB (30 nm)/LiF (1 nm)/Al (100 nm)	—	2.7	—	10.8	9.4 (8.1)	9.6 (4.9)	0.67, 0.33	[148]
ITO/HATCN (10 nm)/NPB (10 nm)/TCTA (10 nm)/6 wt% Flrpic in 4-PhCz- δ -aza-SBF (20 nm)/6 wt% Flrpic in 4-DPhT- γ -aza-SBF (20 nm)/ TmPyPB (40 nm)/Liq (1 nm)/Al (80 nm)	—	3.9	—	22.5 (21.9)	47.9 (46.6)	15.8 (14.4)	0.16, 0.34 (LT ₉₀ = 9.3 h)	[149]
ITO/HATCN (10 nm)/NPB (10 nm)/TCTA (10 nm)/ 4-PhCz- δ -aza-SBF (20 nm)/Flrpic (5 nm)/4-DPhT- γ -aza-SBF (20 nm)/TmPyPB (40 nm)/Liq (1 nm)/Al (80 nm)	—	3.4	—	26.2 (14.1)	60.3 (34.2)	52.7 (19.4)	0.16, 0.33 (LT ₉₀ = 5.8 h)	[149]
ITO/HATCN (10 nm)/NPB (5 nm)/TAPC (30 nm)/8 wt% Ir(ppy) ₂ (acac) in 4-PhCz- δ -aza-SBF (20 nm)/8 wt% Ir(ppy) ₂ (acac) in 4-DPhT- γ -aza-SBF (20 nm)/TmPyPB (30 nm)/Liq (1 nm)/Al (80 nm)	—	3.0	—	22.5 (19.1)	78.1 (67.9)	43.4 (31.1)	0.32, 0.62 (LT ₉₀ = 11.3 h)	[149]
ITO/HATCN (10 nm)/NPB (5 nm)/TAPC (30 nm)/4-PhCz- δ -aza-SBF (20 nm)/Ir(ppy) ₂ (acac) (5 nm)/4-DPhT- γ -aza-SBF (20 nm)/TmPyPB (30 nm)/Liq (1 nm)/Al (80 nm)	—	2.3	—	24.6 (19.0)	87.4 (67.4)	101.6 (59.2)	0.36, 0.61 (LT ₉₀ = 5.8 h)	[149]
ITO/TPAF (15 nm)/10 wt% Ir(ppy) ₂ (acac) in 1:1 TPAF:B3PYMPM (30 nm)/B3PYMPM (45 nm)/LiF (0.8 nm)/Al (80 nm)	—	2.2	—	20.1 (19.5)	77.0 (74.6)	97.5 (72.1)	0.34, 0.63	[150]
ITO/TPAF (40 nm)/1.5 wt% Ir(MDQ) ₂ (acac) in 1:1 TPAF: B3PYMPM (30 nm)/B3PYMPM (45 nm)/LiF (0.8 nm)/Al (80 nm)	—	2.4	—	19.2 (11.2)	34.0 (20.9)	44.3 (14.9)	0.60, 0.39	[150]
ITO (50 nm)/PEDOT (60 nm)/ TAPC (20 nm)/ mCP (10 nm)/ BPBPCz: SBFTz: Ir(ppy) ₂ (acac) (25 nm: 5%)/ TSPO1 (5 nm)/ TPBi (40 nm)/ LiF (1.5 nm)/ Al (200 nm)	—	3.3	523	22.0	83.2	65.9	0.33, 0.63	[151]
ITO (50 nm)/ PEDOT (60 nm)/ TAPC (20 nm)/ mCP (10 nm)/ BPBPCz: SBFTz: Ir(mphmq):tmd (25 nm: 5%)/ TSPO1 (5 nm)/ TPBi (40 nm)/ LiF (1.5 nm)/ Al (200 nm)	—	3.4	610	26.2	37.9	32.7	0.65, 0.35	[151]
Exciplexes as hosts/cohosts in TADF OLEDs								
ITO (70 nm)/(4 wt% ReO ₃):mCP (50 nm)/mCP (15 nm)/ 5 wt% 4CzIPN in 1:1 mCP:B3PyMPM (30 nm)/B3PYMPM (20 nm)/(4 wt% Rb ₂ CO ₃): B3PYMPM (35 nm)/Al (100 nm)	~100.0	3.0	—	29.6 (27.8)	94.5 (88.0)	88.6 (49.0)	—	[154]
ITO (130 nm)/TAPC (35 nm)/TCTA (5 nm)/5 wt% 4CzIPN in 1:1 CBP: B4PyPPM (10 nm)/B4PyPPM (65 nm)/LiF (0.8 nm)/Al (100 nm)	73.1	2.3	—	25.7 (24.8)	83.0 (80.1)	106.9 (79.4)	—	[155]
ITO (50 nm)/PEDOT:PSS (60 nm)/TAPC (20 nm)/mCP (10 nm)/3 wt% 4CzIPN in 1:1 TAPC:TPBI (25 nm)/TSPO1 (35 nm)/LiF (1 nm)/Al (200 nm)	—	—	502	3.3	—	8.2	0.36, 0.44	[156]
ITO (50 nm)/PEDOT:PSS (60 nm)/TAPC (20 nm)/mCP (10 nm)/3 wt% 4CzIPN in 1:1 TCTA:TPBI (25 nm)/TSPO1 (35 nm)/LiF (1 nm)/Al (200 nm)	—	—	502	5.6	—	14.3	0.27, 0.50	[156]
ITO (50 nm)/PEDOT:PSS (60 nm)/TAPC (20 nm)/mCP (10 nm)/3 wt% 4CzIPN in 1:1 mCP:TPBI (25 nm)/TSPO1 (35 nm)/LiF (1 nm)/Al (200 nm)	—	—	502	13.0 (6.7)	—	34.1 (7.4)	0.23, 0.54	[156]
ITO (50 nm)/PEDOT:PSS (60 nm)/TAPC (20 nm)/mCP (10 nm)/3 wt% 4CzIPN in 1:1 mCP:TPBI (25 nm)/TSPO1 (35 nm)/LiF (1 nm)/Al (200 nm)	—	—	502	25.8 (22.2)	—	58.6 (29.2)	0.22, 0.55	[156]
ITO (50 nm)/PEDOT:PSS (60 nm)/TAPC (20 nm)/mCP (10 nm)/3 wt% 4CzIPN in 1:1 mCP:BmPyPb (25 nm)/TSPO1 (35 nm)/LiF (1 nm)/Al (200 nm)	—	—	502	28.6 (23.1)	—	56.6 (29.6)	0.21, 0.53	[156]
ITO/4 wt% ReO ₃ :dCzPSi (60 nm)/dCzPSi (15 nm)/10 wt% 4CzIPN in dCzPSi:PO-T2T (20 nm)/PO-T2T (10 nm)/CN-T2T (40 nm)/Liq/Al	—	2.2	—	21.1 (20.1)	56.4	59.1	0.21, 0.49	[158]
ITO/4 wt% ReO ₃ :mCP (60 nm)/mCP (15 nm)/10 wt% 4CzIPN in dCzPSO ₂ : PO-T2T (20 nm)/PO-T2T (10 nm)/CN-T2T (40 nm)/Liq/Al	—	2.2	—	18.7 (17.6)	56.6	68.5	0.26, 0.54	[158]
ITO (100 nm)/HATCN(1 nm)/TAPC (65 nm)/TCTA (5 nm)/9 wt% DACT-II in 1:1 CBP:B4PyPPM (10 nm)/B4PyPPM (50 nm)/Liq (1 nm)/Al (80 nm)	—	2.2	534	28.6 (27.5)	97.9 (94.2)	127.2 (107.3)	—	[159]
ITO (100 nm)/HATCN(1 nm)/TAPC (65 nm)/TCTA (5 nm)/9 wt% DACT-II in 1:1 CBP:B4PyPPM (10 nm)/B4PyPPM (50 nm)/Liq (1 nm)/Al (80 nm)	—	2.2	534	29.8 (27.7)	101.9 (94.6)	134.9 (108.2)	—	[159]
ITO (100 nm)/HATCN(1 nm)/TAPC (65 nm)/TCTA (5 nm)/9 wt% DACT-II in 1:1 TCTA:B4PyPPM (10 nm)/B4PyPPM (50 nm)/Liq (1 nm)/Al (80 nm)	—	2.2	534	30.3 (28.5)	103.7 (97.8)	136.6 (111.1)	—	[159]
	—	2.2	534	31.7 (28.5)	—	—	—	[159]

(continued on next page)

Table 2 (continued)

Device structure (the exciplex component is underlined)	Φ_{film} (%)	V_{on} (V)	λ_{EL}^{max} (nm)	EQE (%)	CE (cd A ⁻¹)	PE (lm W ⁻¹)	CIE	Ref
ITO (100 nm)/HATCN(1 nm)/TAPC (65 nm)/TCTA (5 nm)/9 wt% DACT-II in 1:1 CBP:B4PyMPM (10 nm)/B4PyPPM (50 nm)/Liq (1 nm)/Al (80 nm)					108.4 (97.5)	145.4 (111.5)		
ITO/HAT-CN (10 nm)/TAPC (40 nm)/TCTA (10 nm)/CBP (10 nm)/15 wt % TPA-PZCN in 1:1 CBP:PO-T2T (20 nm)/PO-T2T (55 nm)/Liq (2 nm)/Al (120 nm)	—	2.4	648	28.1	—	—	0.66, 0.34	[160]
ITO/MoO _x (6 nm)/CDBP (60 nm)/CDBP:2DBSOSPO:3 % 4CzTPNBu (25 nm)/2DBSOSPO (60 nm)/LiF (1 nm) Al (100 nm)	97	2.6	564	30.3	98.8	114.9	0.48, 0.49	[162]
ITO/MoO _x (6 nm)/CDBP (60 nm)/CDBP:3DBSOSPO:3 % 4CzTPNBu (25 nm)/3DBSOSPO (60 nm)/LiF (1 nm) Al (100 nm)	91	2.5	564	23.3	75.8	91.5	0.47, 0.51	[162]
ITO/MoO _x (6 nm)/CDBP (60 nm)/CDBP:4DBSOSPO:3 % 4CzTPNBu (25 nm)/4DBSOSPO (60 nm)/LiF (1 nm) Al (100 nm)	79	2.7	568	15.9	65.1	73.0	0.48, 0.51	[162]
ITO/TAPC (35 nm)/TCTA (10 nm)/CBP (10 nm)/CDBP:PO-T2T (1:1):DBBPZ-DPXZ (6 wt%) (20 nm)/PO-T2T (45 nm)/LiF (1 nm) Al	—	2.8	628	20.8	—	25.6	0.62, 0.38	[163]
ITO/NPD (40 nm)/DCDPA (15 nm)/TDBA-DI 20 %-doped in DBFPO (30 nm)/TSP01 (30 nm)/LiF (1 nm) Al (100 nm)	—	2.5	458	37.8	68.0	82.1	0.15, 0.28	[164]
ITO/NPD (40 nm)/T2fQ (15 nm)/TDBA-DI 20 %-doped in DBFPO (30 nm)/TSP01 (30 nm)/LiF (1 nm) Al (100 nm)	—	2.5	458	41.2	72.2	87.2	0.15, 0.28	[164]
ITO/HAT-CN (10 nm)/TAPC (40 nm)/TCTA (10 nm)/CBP (10 nm)/15 wt % PT-TPA in 1:1 CBP:B4PyMPM (20 nm)/B4PyMPM (65 nm)/Liq (2 nm) Al (120 nm)	—	2.8	648	28.8	20.0	24.9	0.66, 0.33	[165]
ITO/HAT-CN (10 nm)/TAPC (40 nm)/TCTA (10 nm)/CBP (10 nm)/10 wt % PT-Az in 1:1 CBP:B4PyMPM (20 nm)/B4PyMPM (65 nm)/Liq (2 nm) Al (120 nm)	—	3.4	628	9.7	10.0	11.3	0.63, 0.36	[165]

fluorescent OLED with an unusually high efficiency of 10.6 % based on the emitter DCJTB and an exciplex-forming cohost, TCTA:B4PYMPM (Fig. 8) [99]. The emission maximum of the exciplex is at 509 nm and that of the DCJTB-doped film is considerably red-shifted at 596 nm. The origination of the delayed DCJTB PL is indeed from the RISC of the exciplex triplet and not from the TTA, as evidenced by transient PL experiments. Another reason for the high device efficiency is the horizontal orientation preference of the emitter to the substrate. However, low device efficiency, as well as red-shifted EL, is observed at high doping concentrations, presumably because of emitter molecule aggregation, concentration quenching, and increased possibility of Dexter energy transfer (DET) from the exciplex to dopant. Hung *et al.* reported an exciplex system by mixing a hole-transporting material, Tris-PCz, with a star-shaped electron-transporting material, CN-T2T; the former acts as the donor, whereas the latter acts as the acceptor [51]. As mentioned earlier the relevant exciplex is employed as the emitter to construct green OLED with high device efficiency, where the high efficiency is primarily due to the balanced hole and electron mobility of the relevant constituent materials. The exciplex host is efficient in hosting fluorescent dopants, such as Rubrene and DCJTB. The Rubrene-doped yellow device is excellent at 6.9 % EQE (21.4 cd A⁻¹, 28.1 lm W⁻¹), whereas the DCJTB-doped red device exhibited an EQE as high as 9.7 % (19.3 cd A⁻¹, 23.3 lm W⁻¹).

Kim *et al.* demonstrated an interesting strategy to realize high-efficiency fluorescent OLEDs by combining the sensitizing effect and the induced heavy atom effect in an exciplex host system. A phosphorescent dopant, Ir(ppy)₂(tmd) (Fig. 10), is introduced as a sensitizer into an exciplex-hosted DCJTB-doped device to enhance fluorescent OLED efficiency [100]. An efficient energy transfer from the host and the phosphorescent dopant to the fluorescent dopant is anticipated because of the large spectral overlap between the emission spectra of the exciplex host, Ir(ppy)₂(tmd), and the absorption spectra of DCJTB. The prompt PL decay rate of a 0.5 wt% DCJTB blended film in TCTA:B4PYMPM is faster than that of the exciplex without the dopant, signaling the energy transfer from the host to the dopant. The exciplex decay rate further increases with the doping concentration of the phosphorescent dopant. The combined influence of the sensitizing effect and the induced heavy atom effect in the DCJTB-doped exciplex OLED is phenomenal. An EQE as high as 23.7 % is also extracted from the relevant device.

Zhang *et al.* reported a green OLED using an exciplex host TAPC:DPTPCz and a green fluorescent dopant C545T. The host possesses FMO

characteristics close to those of the dopant that can mitigate exciton trapping [101]. The dopant concentration is maintained at a low value to reduce the unwanted host to dopant triplet-triplet energy transfer. A high EQE of 14.5 % can be extracted from the relevant green OLED. A considerable drop of device performance ($V_{on} = 3.9$ V, EQE = 3.9 %, CE = 12.8 cd A⁻¹, and PE = 8.0 lm W⁻¹) is observed when the emitter is doped in a conventional host (DPTPCz). The result suggests the possibility of harnessing 100 % triplet excitons in conventional fluorescent OLEDs by energy transfer from the exciplex system.

Fluorescent OLEDs share a common mitigating factor, that is, concentration quenching of their emission. Aggregation-induced emission (AIE) may be a valuable method to overcome this issue. The AIE probes have a typical group attached to their backbone that moderates their emission. These probes are non-luminescent in solution but highly emissive in the aggregated state. Thus, the concentration quenching problem in fluorescent OLEDs can be theoretically circumvented by employing AIE-type chromophores as emitters. Nondoped OLEDs with slightly complicated device structures can also be strategically developed using such types of emitters. Grazulevicius and coworkers worked in this direction to design and synthesize two derivatives of tetra-fluorophenyl carbazole and tri/tetraphenylethylene that exhibit AIE (C4FS1 and C4FS2, Fig. 10) [102]. C4FS1 and C4FS2 are thermally stable, and they have similar HOMO and luminescence in the solid-state (PLQY = 57 % and 27 %, respectively). The non-doped OLEDs based on these materials as emitters are mediocre compared with the contemporary devices (EQE = 1.08 % and 0.34 % only), perhaps because of low PLQY and charge recombination. The device efficiency improved slightly upon employing the materials as the emitters in interfacial exciplex OLEDs. Although the concept is novel, it fails to come up with a novel device.

Our group has been working in this direction for years now and has added some notable contributions to OLED research. We reported a new exciplex system based on a carbazole-based donor, BCzPh (Fig. 4), triazine-based acceptor, 3P-T2T (Fig. 4), and relevant fluorescent (C545T) and phosphorescent (Ir(ppy)₂(acac)) emitter-doped devices [103]. All the devices, including the one with the exciplex as emitter, excel in device efficiency, which is a possible outcome for quantitative energy transfer from the exciplex to the green dopants. As the emitter device, exciplex exhibits device efficiency as high as 13.5 % (45.9 lm W⁻¹). The device efficiency of the fluorescent and phosphorescent devices is 15.5 % (58.3 lm W⁻¹) and 29.7 % (123.9 lm W⁻¹),

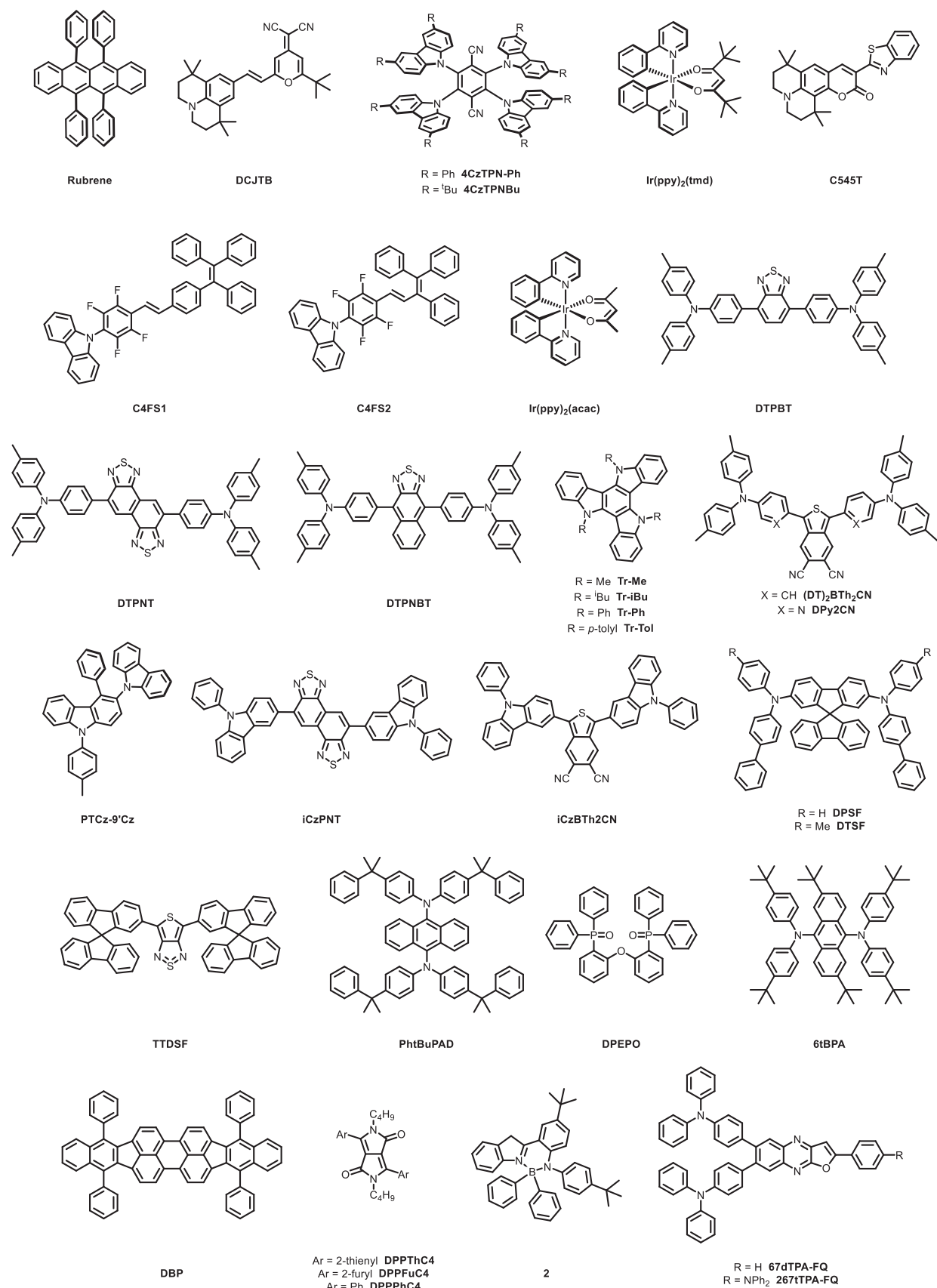


Fig. 10. Molecular structures of the donor and acceptor materials used for the exciplex hosts and fluorescent emitters that are discussed in subsection 3.1.

respectively. Moreover, the operational lifetime of the exciplex-hosted C545T device is longer than that of the traditional single-host system (Alq_3 :C545T). This finding is explained based on transient EL, CV characterization, and impedance–voltage experiments. All these studies determined that the reasons for the long operational lifetime of the exciplex-hosted device are superior carrier injection and transportation, outstanding charge balance, excellent exciton confinement, and effective energy transfer to the dopants. Another article from our group described red and NIR OLEDs based on fluorescent dopants and exciplex hosts [104]. The TCTA:3P-T2T exciplex system is chosen to host three newly synthesized long-wavelength-emitting dopants with D-A-D configuration (DTPBT: 628 nm; DTPNT: 659 nm; DTPNBT: 710 nm). The 5 wt % emitter-doped devices are remarkable at 15 %, 10 %, and 9 % EQE for the DTPBT-, DTPNT-, and DTPNBT-based devices, respectively. These results are attributed to the effective harvesting of triplet excitons and simple energy transfer from the exciplex host to the fluorescent dopants. In another recent report, we described red fluorescent OLEDs based on exciplex hosts. Three triazatruxene-based molecules, namely, Tr-Me, Tr-Ph, and Tr-Tol, with methyl, phenyl, and p-tolyl pendant groups, respectively, are coupled with three acceptors, namely, 3P-T2T, 3P-T2P, and 3P-Pyr (Fig. 4), consisting of phenylpyrazole peripherals and triazine, pyrimidine, and pyridine core, respectively [104]. The exciplex emissions depend on the feature of N-heteroarene cores of acceptors. Of the nine exciplex-forming D:A combinations, the green device comprising Tr-Tol:3P-T2P blend as the EML outperforms others and offers a maximum EQE of up to 12.8 %. The Tr-Ph:3P-T2P blend exhibits the best performance when employed as the host in fluorescent OLEDs containing newly developed fluorescent emitter ($(\text{DT})_2\text{BTh}_2\text{CN}$). The relevant red fluorescent OLED (EL_{max} ~670 nm) offers EQE higher than 5 %. Based on time-resolved fluorescence, we concluded that the light emission is dominated by singlet energy transfer with simultaneous quenching from triplet energy transfer. The aggregation of Tr-Me donor can be suppressed by introducing a bulkier alkyl chain such as iso-butyl (iBu) onto triazatruxene core [104]. Indeed, the new donor Tr-iBu was found to efficiently form exciplex systems with various heteroarene-based acceptors with diphenylphosphine oxide (-POPh₂) peripherals such as PO-T2T, PO-T2P and PO-Pyr (Fig. 2). The emission energy can be well manipulated by the feature of heteroarene cores. The devices with the Tr-iBu:PO-T2P and Tr-iBu:PO-Pyr blends were as the EMLs can achieve moderate EQE_{max} of 8.27 % and 7.54 %, respectively. Upon introducing a new fluorescence molecule, DPY2CN (Fig. 10), as emitter for the Tr-iBu:PO-T2P exciplex-based device, a deep-red OLED device with EL $\lambda_{\text{max}} = 674$ nm and EQE_{max} of 6.28 % was achieved via efficient FRET between the exciplex host and the fluorescent emitter. In addition, PO-T2T was utilized to examine the exciplex forming systems comprising 4-phenyl-9-(p-tolyl)-9 H-carbazole (PTCz)-based donors (Fig. 10) with various C3-substituents for tuning HOMOs [104d]. The exciplex blend PTCz-9'Cz:PO-T2T (2:1) was utilized to serve as the EML for a sky-blue (490 nm) exciplex-OLED device with EQE_{max} of 10.9 %. Upon introducing a D-A-D-type fluorescent emitter, iCzPNT (Fig. 10), a yellow emission device with EL $\lambda_{\text{max}} = 578$ nm and EQE_{max} of 7.8 % was achieved. This exciplex system was also employed to make an efficient (EQE_{max} 8.0 %) red device (EL $\lambda_{\text{max}} = 578$ nm) as iCzBTh2CN (Fig. 10) was incorporated as the fluorescent dopant. The excitons formed at exciplex host can be efficiently extracted by introduced fluorescent dopants. However, the triplet-triplet quenching is inevitable as the doping concentration increases, limiting the ultimate device efficiency. For this exciplex-hosted fluorescent device strategy to achieve highly efficient and high stability near-infrared (NIR) OLED devices, the emission of exciplex needs to extend to orange or red range in order to have a good spectral overlap with the absorption of a NIR emitter for efficient FRET process. Very recently, Liu and Wong *et al.* reported new orange and red exciplex-forming systems with spirobifluorene (SF)-cored triarylamine type donors, DPSF and DTSF (Fig. 10), and CN-T2T acceptor (Fig. 4) [104e]. These donors were found to form aggregation for quenching exciplex emission, leading to low

exciplex PLQYs. However, in the EL device with DPSF:CN-T2T blend, the charge recombinations occur at lower energy exciplex state that leads the device (EL $\lambda_{\text{max}} = 584$ nm) to perform EQE_{max} up to 6.0 %, which is unexpected basically from the observed PLQY. This exciplex system was further employed as host to achieve a high efficiency (EQE_{max} of 5.3 %) NIR OLED (EL $\lambda_{\text{max}} = 774$ nm) by doping a D-A-D-type fluorescence emitter TTDSF (PLQY 26 %) (Fig. 10). The device performs promising stability with excellent operation lifetime (LT₉₅ > 200 h), indicating the bright prospect of adopting exciplex host and tailor-made NIR dopant to realize NIR OLED for future lighting applications.

Song *et al.* adopted a different strategy to obtain a small singlet-triplet gap in exciplex systems. They synthesized a sterically congested TCTA analog, containing tertiary butyl groups (tBuTCTA, Fig. 2), to reduce the donor-acceptor contact and subsequent lowering of the singlet-triplet gap [105]. The PhtBuPAD-doped fluorescent device employing tBuTCTA: CzTRZ (Fig. 8) exciplex system as the host outperforms the other devices where TCTA is used as the donor component to the exciplex system. Lee and coworkers recently reported high-efficiency green fluorescent OLEDs by utilizing a ternary sensitizing host based on exciplex that inhibits nonradiative exciton decay of the exciplexes [106]. DPEPO is added as the third component in the relevant TCTA: Cz-TRZ exciplex to increase the donor-acceptor separation that controls the nonradiative decay rate. The relevant green OLEDs are fabricated using 6tBPA as the dopant. Adding DPEPO in the exciplex system enhances the PLQY, which directly influences the EQE of the pertinent devices. For example, the device efficiency increases from 11.2 % to 13.65 % when the DPEPO concentration increases from 0 % to 50 %. The authors concluded that the efficiency enhancement is due to the minimization of nonradiative exciton loss by the externally added component, DPEPO. In a recent report, Ledwon *et al.* demonstrated some fluorescent OLEDs based on some quinoxaline acceptor-based dopants, which show EQE of up to 7 % [107].

In 2016, Kyon *et al.* reported a new OLED exhibiting enhanced operational stability with EQE approaching 100 %. In the pertinent work, MFEs, that is, MEL is investigated in super fluorescent OLED (SF-OLED) devices and MPL in thin films of (MeO-TPD:3TPYMB) exciplex-based host doped with fluorescent emitter (DBP, Fig. 10) [108]. The PL emission of MeO-TPD:3TPYMB exciplex and DBP covers a broad spectral range center at ≈ 418 and ≈ 694 nm, respectively. The enhanced quantum efficiency in SF-OLED devices is attributed to the decrease in the MFE activation energy (E_{act}) compared with that of the undoped exciplex. In addition, both MPL and MEL responses decrease considerably with the increase of emitter concentration. This decrease in MFE is ascribed to the existence of a DET process from the exciplex triplet state to the lowest triplet state of the dopant (dark exciton), thereby draining the magneto-RISC process in the exciplexes. The enhanced quantum efficiency in SF-OLED devices is attributed to a decrease in MFE activation energy compared with that of the pristine D:A exciplex blend. However, both MPL and MEL responses decrease as the concentration of emitter increases above ~ 1 %. This finding is attributed to the DET from the triplet CT state of the exciplex blend to the lowest triplet state of the additive emitter molecules (non-luminescent).

For the first time, Data *et al.* reported that diketopyrrolopyrrole (DPP) derivatives can be used as emitters in OLED devices. The previously explored t-Cbz-SO (Fig. 8):TAPC exciplex is selected as the exciplex host owing to its high efficiency (>15 %) with emitters being DPPPhC4, DPPFuC4, or DPPThC4. In all the cases, high overall efficiency is observed for the exciplex-enhanced devices, that is, an EQE of 11.2 % for DPPFuC4 and 11.1 % for DPPThC4 at 100 cd/m² [2]. However, the best overall efficiency is achieved with DPPFuC4-based devices with a 12.1 % EQE and 28.4 cd A⁻¹ device efficiency [109]. The doping strategy is generally suffering from the concentration quenching problem. In this regard, the molecular design of emitter for reducing the propensity of concentration quenching is crucial for obtaining high efficiency device. In 2021, Wang *et al.* reported the use of the boron-chelation between indole and carbazole to make a fluorescent

emitter 2-(tert-butyl)-5-(4-(tert-butyl)phenyl)-6,6-diphenyl-6,12-dihydro-5 H-6λ [4],7λ [4]-benzo[4,5][1,3,2]diazaborinino[1,6-a]indole (2, Fig. 10) featuring planarity and rigidity as well as bulky substituents for suppressing the intermolecular interactions. [110] The device employing TCTA:3P-T2T blend as exciplex cohost for such B-chelated dopant can achieve a red device (EL $\lambda_{\text{max}} = 612 \text{ nm}$) and EQE_{max} up to 10.2 % with a relatively high doping concentration of 6 wt %. In addition to the concentration quenching issue, the triplet energy of fluorescent dopant is equally important. Very recently, Wang and Ma *et al.* demonstrated the importance of a fluorescent dopant with a suitably aligned triplet energy respect to the exciplex cohost to perform better device characteristics [111]. They used TCTA:PO-T2T as the exciplex cohost ($T_1 = 2.35 \text{ eV}$) and two green-light-emitting molecules, 67dTPA-FQ ($T_1 = 2.19 \text{ eV}$) and 267TTPA-FQ ($T_1 = 2.32 \text{ eV}$) (Fig. 10), using 2-phenylfuro[2,3-b]quinoxaline (FQ) as an acceptor and triphenylamine (TPA) as a donor unit, as emissive dopants to explore the device performance. In which, 267TTPA-FQ doped device achieved EQE_{max} of 9.6 % that outperforms the counterpart device employing 67dTPA-FQ as dopant with EQE_{max} of 8.4 %.

3.2. PhOLEDs hosted by exciplexes

The discovery of PhOLEDs provided an impetus to the then-new technology toward commercialization. In the exciplex-hosted devices, the emission of dopant is activated by exciplex formation in the host followed by transfer of excitation energy from the host to the dopant through both Förster and Dexter mechanisms, as shown in Fig. 9. In this context, the exciplex hosts have an edge over the conventional hosts because both ISC and RISC simultaneously operate in the former, whereas only ISC operates in the latter. The major advantages of using exciplex hosts in PhOLEDs include (a) driving voltage reduction, (b) device efficiency augmentation, (c) broadening of the recombination zone and (d) minimization of efficiency roll-off and operational lifetime betterment [94]. Similarly, the higher device efficiency of the PhOLEDs compared with that of the fluorescent OLEDs is due to an efficient energy transfer from the exciplex host to the dopant and reduced triplet-polaron-quenching effects. Given that the emitting state of the phosphorescent dopant is a triplet, the most important mode of energy transfer from the host is triplet-triplet energy transfer; the singlet energy transfer adds excitons to the emission. Therefore, unlike the cases where the singlet energy transfer is the dominant mode, the PhOLEDs offer some relaxation of the spectral overlap criterion between the host emission and the dopant absorption, enabling a versatile selection of dopant materials. The molecular structures of the PhOLED-based OLEDs in this subsection are presented in Fig. 11 and Fig. 14. This subsection is divided further according to the emission color for an organized presentation.

3.2.1. Blue PhOLEDs

The color purity and stability issues of the blue OLEDs have caused problems for the research community for years. Despite their remarkable progress, blue devices still attract researchers to search for high-performing ones. Among many blue phosphorescent emitters, Flrpic has remained the most popular because of its benchmark performance. Therefore, this emitter frequently appears in blue PhOLED-related papers.

Sasabe, Kido, and coworkers reported highly efficient blue PhOLEDs utilizing energy transfer from exciplex host to dopant [112]. The relevant exciplex system comprises TAPC as the donor and a sulfone-based host material 5',5''''-sulfonyl-di-1,1':3',1''-terphenyl (BTPS, Fig. 11) with a large energy gap as the acceptor. Two types of devices are fabricated—one with a thin layer of TCTA and another without it—both showing similar performance. For example, the device with TCTA exhibits high PE of 50.1 lm W^{-1} and a high EQE of 21.7 % at 100 cd m^{-2} , whereas the values for the device without TCTA are 45.5 lm W^{-1} and 22.1 %, respectively. The exciplex emission is observed at a low doping

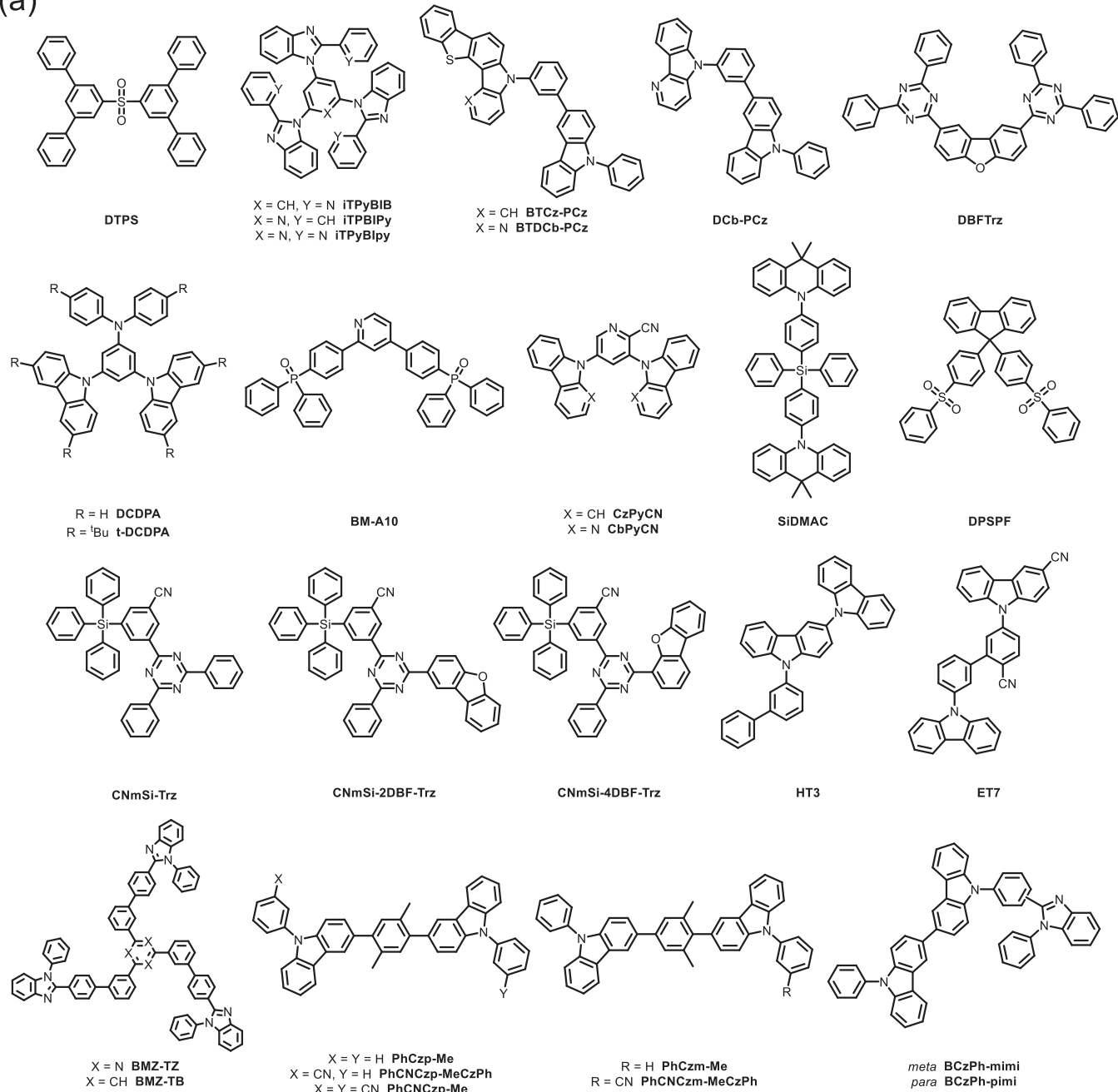
concentration of the emitter, revealing incomplete energy transfer at a low dopant concentration. In another report, Kim *et al.* described a high-efficiency blue PhOLED based on Flrpic (Fig. 2) and mCP:B3PYMPM (Fig. 2) exciplex system [113]. Similar to other papers from the Kim group, this article demonstrated horizontal orientation preference by the emitter molecules (horizontal: vertical = 0.76:0.24) that enhance the light out-coupling and, consequently, device efficiency. The relevant device exhibits an EQE of 29.5 %, which is close to the theoretical limit.

Chen *et al.* developed exciplex-forming hosts based on three benzimidazole-containing new electron acceptor materials with isomerized N-linkage to the central phenyl or pyridine ring (iTPyBIB, iTPBiPy, and iTPyBiPy, Fig. 7) [114]. All the materials form exciplex systems when blended with the hole-transporting materials (mCP, TCTA, and TAPC) in a 1:1 molar ratio. The blue PhOLEDs containing the exciplex systems are then fabricated. Of all the systems, the mCP:iTPBiPy exciplex-forming cohost device exhibits the best performance with maximum efficiencies of 38.5 cd A^{-1} , 36.9 lm W^{-1} , and 19.3 % with satisfactory CIE of (0.15, 0.29), which is considerably higher than that of single mCP (33.5 cd A^{-1} , 27.9 lm W^{-1} , and 17.0 %) and that of mCP:TPBI (26.9 cd A^{-1} , 26.4 lm W^{-1} , and 13.4 %) under similar device conditions. This result is considered one of the best results obtained by employing electron-accepting materials containing benzo-imidazole in exciplex-based devices. Lee *et al.* demonstrated a blue PhOLED based on Flrpic as the emitter and mCP:PO-T2T exciplex system as the host [115]. Fig. 12a clearly shows exciplex formation between the two components, where the triplet energy of the exciplex is lower than that of the components but higher than that of the dopant, facilitating the confinement of the triplet excitons within the exciplex system and subsequent energy transfer to the dopant. Thus far, this blue PhOLED has been one of the most efficient blue PhOLEDs, employing a physical mixture of commercially available materials as the exciplex host. The other device characteristics are shown in Fig. 12b-d. The relevant exciplex OLED features EQE and PE as high as 30.3 % and 66 lm W^{-1} , respectively, besides low driving voltage. The high device efficiency is attributed to the exciplex system together with the low LUMO of PO-T2T that aids electron injection.

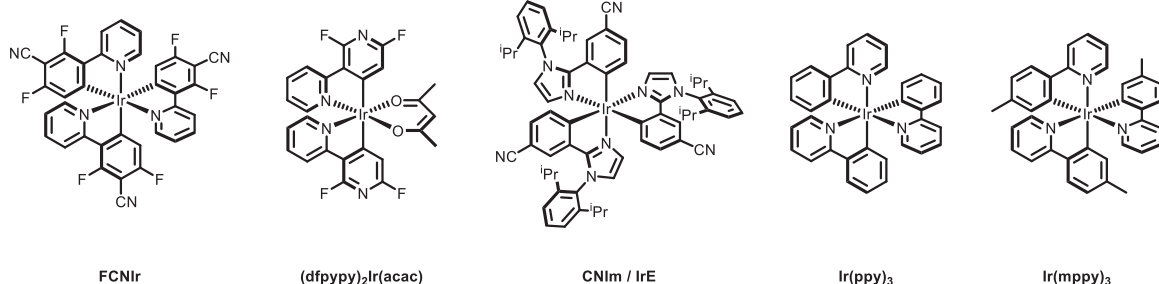
Wang *et al.* synthesized new δ-carboline donors (BTCz-PCz, BTDCb-PCz, and DCb-PCz, Fig. 11) with high triplet energies and glass transition temperatures for exciplex formation [116]. The relevant exciplexes provide pure deep blue emission with a low device efficiency when combined with TmPyPB as the acceptor. However, the exciplex systems are proved to be valuable hosts to blue phosphorescent dopants. Flrpic and the relevant OLEDs offer good device performance (EQE 22–24 %). Ma and coworkers introduced the concept of double exciplex forming host for the phosphorescent emitters in the quadruple-doped EMLs. Compared with that in the single-host systems with only one energy transfer channel, the exciton utilization through multiple energy transfer channels in the double-host systems offers efficiency enhancement. Therefore, the efficiency of a blue PhOLED employing the double host is 1.25 times higher than the relevant device with a single exciplex host. The device also has a low-efficiency roll-off [117].

A few studies also reported other blue phosphors, excluding Flrpic. Lee *et al.* developed high triplet energy exciplex hosts TCTA:DBFTrz, DCDPA:DBFTrz, and t-DCDPA:DBFTrz (Fig. 11) for deep blue PhOLEDs [118]. In contrast to the TCTA:DBFTrz exciplex system with triplet energy of 2.8 eV, the other two new exciplex host systems (DCDPA:DBFTrz and t-DCDPA:DBFTrz) display high triplet energies of ~2.9 eV. This result demonstrated that the pertinent exciplex host systems are highly beneficial as hosts for a deep blue triplet emitter (FCNir). Thus, the FCNir-doped DCDPA:DBFTrz and t-DCDPA:DBFTrz deep blue devices display high EQEs of 15.3 % and 16.4 %, respectively, with a color coordinate of (0.14, 0.19). However, the EQE of the TCTA:DBFTrz exciplex-based device exhibits only 8.7 %, which is attributed to the triplet energy of the TCTA:DBFTrz exciplex (2.8 eV) which is lower than that of the FCNir emitter (2.9 eV). This scenario results in the

(a)



(b)

**Fig. 11.** Molecular structures of (a) the exciplex-forming host systems and (b) blue and green phosphors of PhOLEDs.

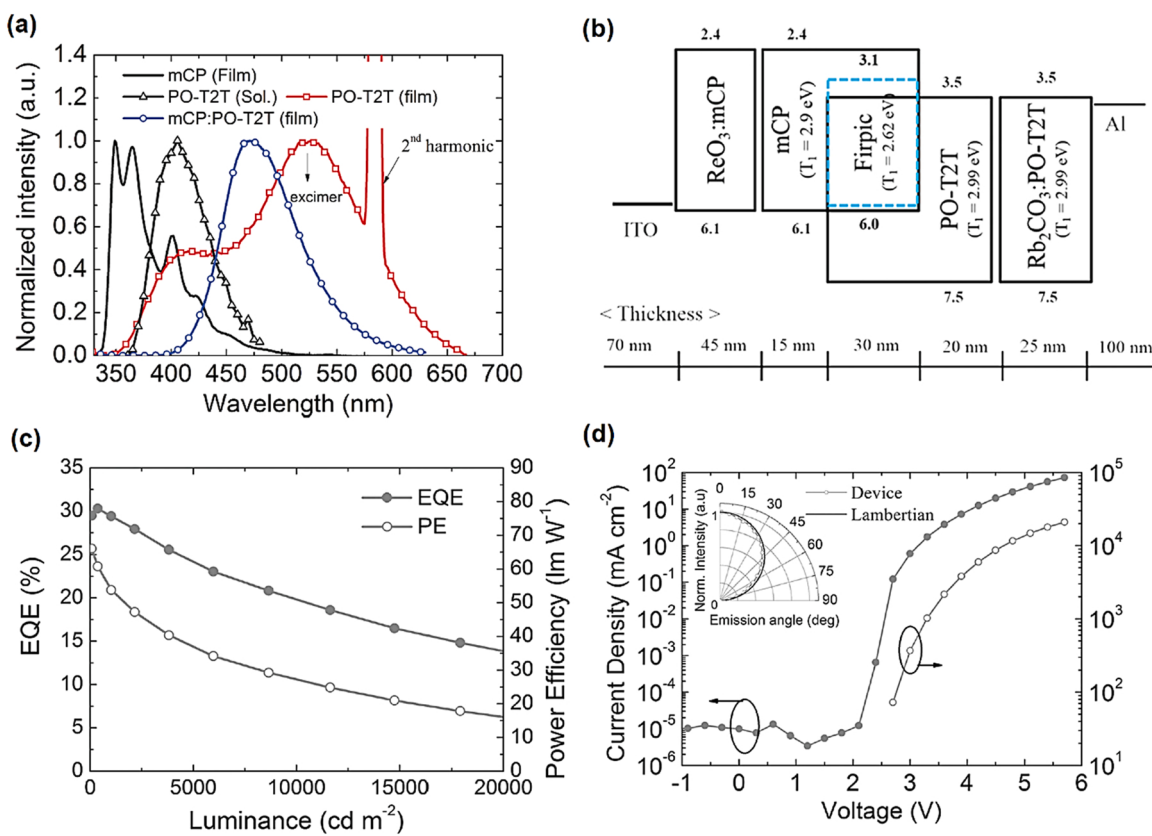


Fig. 12. (a) Fluorescence spectra of mCP, PO-T2T, and their 1:1 blend, indicating the formation of exciplex between the two. (b) Energy level diagram of the FIrpic:mCP:PO-T2T-based blue PhOLED. (c) Variation of EQE and PE with luminance. (d) Current density–voltage–brightness plot of the blue PhOLED. Reproduced with permission from [115] Copyright 2014. John Wiley and Sons.

incomplete energy transfer from the exciplex host to the FCNIr emitter, which is validated from the transient PL decay data. In another research, Kim *et al.* reported a blue PhOLED consisting of mCP as the donor, a phosphine oxide-based compound, BM-A10 (Fig. 11), as the acceptor for the exciplex system, and the deep-blue dopant FCNIr (Fig. 11) [119]. Both the exciplex components and the exciplex itself have a small singlet-triplet gap and high triplet energy (~3.0 V), enough to host a deep-blue emitter. The photoluminescent quantum yield of the exciplex is as low as 17 %; however, that of the FCNIr-doped film is approximately 82 %. The corresponding exciplex OLED exhibits a turn-on voltage of 2.9 V and a maximum EQE of 24 %.

Sun, Tao, and coworkers synthesized two cyanopyridine derivatives, namely, CzPyCN and CbPyCN (Fig. 11), by simple catalyst-free nucleophilic aromatic substitution reactions and employed them as acceptors to form exciplexes with TAPC and mCP [120]. The emissions of the two donor-acceptor combinations are dramatically different from each other. For example, the steady-state and the time-resolved fluorescence of the TAPC-based systems are characterized by emission at a wavelength (520–530 nm) longer than that of the components (330–360 nm) with a long decay time. These characteristics are the signatures of exciplex formation. On the contrary, no exciplex formation is observed with mCP as the donor component ($\lambda_{PL} = 425\text{--}450 \text{ nm}$). When employed as the hosts in PhOLEDs comprising the blue emitter FIrpic, the mCP:acceptor-based devices outperform the TAPC:acceptor-based devices. Although the TAPC-based exciplex systems emit at a wavelength (520–530 nm) longer than that in FIrpic (~470 nm), the reason for using this exciplex system as a host for a blue emitter is not clear to us at the moment of writing this article. Mu and coworkers adopted an unusual strategy to obtain high-efficiency blue PhOLEDs. They inserted an ultra-thin (0.3 nm) neat phosphorescent dopant layer between the donor (mCP) and the acceptor (TmPYPB) layers [26]. The ultra-thin layer is

not expected to impede the interfacial exciplex formation between mCP and TmPYPB. The relevant OLED exhibits a high EQE of up to 18 %, which is comparable to that obtained from a much more complicated host: guest-based devices. The authors believed that alleviation of the issues like TF and triplet diffusion due to simple device structure along with effective energy transfer from the exciplex to the dopant increases the device performance.

In 2016, Sasabe and Kido *et al.* also reported a wide-energy-gap exciplex consisting of SiDMAC and BPSPF (Fig. 11) as a host material for blue PhOLEDs. The emission of the SiDMAC:BPSPF blend is observed at 437 nm, with the PLQY of the blue phosphor-doped (dfppy)₂Ir(acac) exciplex host being 54 %. The resulting blue PhOLED is achieved to present a low driving voltage of 2.67 V with an η_{ext} of 13.7 % (22.2 lm W⁻¹, 25.2 cd A⁻¹) at 100 cd m⁻² and 12.7 % (15.8 lm W⁻¹, 23.3 cd A⁻¹) at 1000 cd m⁻² [121]. The triplet energy of exciplex-forming cohost is always a crucial issue for realizing high efficiency blue phosphorescent device. In this regard, Lee group utilized benzonitrile to modify the design of acceptors with triazine core. Three triazine-based acceptors with a bulky triphenylsilyl group 3-(4,6-diphenyl-1,3,5-triazin-2-yl)-5-(triphenylsilyl)benzonitrile (CNMSi-Trz), 3-(4-(dibenzo[b,d]furan-2-yl)-6-phenyl-1,3,5-triazin-2-yl)-5-(triphenylsilyl)benzonitrile (CNMSi-2DBF-Trz) and 3-(4-(dibenzo[b,d]furan-4-yl)-6-phenyl-1,3,5-triazin-2-yl)-5-(triphenylsilyl)benzonitrile (CNMSi-4DBF-Trz) (Fig. 11), were reported to form exciplex systems with a typical high triplet donor mCBP. Among them, the CNMSi-2DBF-Trz:mCBP exciplex blend exhibits a high triplet energy of 2.9 eV, which is beneficial to confine the triplet excitons on the dopant [122]. A *fac*-tris(3-(1-(2,6-diisopropylphenyl)-1 H-imidazol-2-yl)benzonitrile)iridium (CNIm, Fig. 11)-doped blue PhOLED with CIE coordinates of (0.16, 0.28) was fabricated to achieve EQE_{max} over 23.8 %. More importantly, the exciplex-hosted device revealed superior

device lifetimetime. In addition to the point of triplet energy, by the judicious selection of donor and acceptor, the use of exciplex-forming cohost can lead a lower operation voltage of blue PhOLEDs, which is beneficial not only for high efficiency but also device lifetime. For example, Choi *et al.* recently reported a systematic screening of D:A blends with various structural features and properties to find a suitable HT3:ET7 (Fig. 11) blend as the exciplex-forming cohost. The exciplex cohosted device doped with IrE (Fig. 11) as a phosphorescent dopant to achieve high-performance blue PhOLED with a low operating voltage (4.1 V), high EQE_{max} (23.4 %, at 500 cd m⁻²) and a promising operation lifetime (LT₉₅ = 232 h) [122].

3.2.2. Green PhOLEDs

Green is another primary color in display devices, and research effort to produce pure green OLEDs is valuable. Among various green emitters, Ir(ppy)₂(acac) (Fig. 10) and Ir(ppy)₃ (Fig. 11) have been the researchers' favorite choices since their discovery, although other emitters have also been utilized.

In an early attempt, Park and coworkers probed energy transfer from exciplex hosts to the phosphorescent dopants using CBP (Fig. 7) as the donor and B3PYMPM as the acceptor and fabricated highly efficient OLEDs using green phosphorescent dopant, Ir(ppy)₃ [123]. Exciplex formation occurs at the donor=acceptor interface, which is employed as the host and electron-transporting layer for the phosphorescent emitter. The exciplex emission intensity drops with the increase of donor dose, invoking a possibility of an energy transfer mechanism from the exciplex host to the dopant. The intensity of exciplex luminescence is nearly proportional to the inverse square of dopant concentration in the emission layer. Furthermore, the quantum efficiency of the OLEDs improves with the increase of dopant concentration. This result is attributed to the high rate of energy transfer from the exciplex host to the guest emitter molecules. An EQE as high as 20.1 % is observed at a dopant concentration of 6 wt%. Moreover, the exciplex emission ratio of the OLEDs enhances with an increase in current density, benefitting additional efficiency roll-off at high current.

The exciplex system BCzPh:3P-T2T (Fig. 4) and its performance in fluorescent OLEDs have been mentioned earlier. When deployed as the host in green PhOLED comprising Ir(ppy)₂(acac) as the emitter, the relevant device displays good performance, for example, low turn-on voltage (2.2 V), high EQE (29.7 %), and high PE (143.4 lm W⁻¹) [118]. Although the EQEs of the exciplex-hosted device and analogous traditional host CBP-based device are comparable, the former outperforms the latter (2.6 V, 29.5 %, 112.2 lm W⁻¹).

Song *et al.* established the light emission mechanism in exciplex-hosted PhOLEDs by monitoring the current density and luminance with exciplex and exciplex-free cohosts. The relevant report suggested the prevalence of energy transfer in the devices that use exciplexes as the hosts. On the contrary, charge trapping dominates the traditional host-based devices [124]. After testing two donor:acceptor blends, namely, TCTA:TPBi and CBP:TPBi (Fig. 3), the authors realized that the composition of the blend is crucial for exciplex formation and subsequent light emission. For example, among the two tested systems, only TCTA:TPBi blend undergoes exciplex formation, perhaps because of the more powerful electron-donating ability of TCTA than CBP. Moreover, exciplex emission is feasible only at a 1:1 D:A concentration ratio and exciplex quenching by charge trapping at any other proportion are noted. When employed in green PhOLEDs consisting of Ir(ppy)₃ as the dopant, the TCTA-containing device outperforms the CBP-based device because of the improved hole injection and transportation of the former compared with the latter. This report is particularly surprising because the CBP-containing OLEDs are known to offer excellent device efficiencies. Other reports mention the excellent performance of other hosts containing OLEDs compared with CBP-based devices. An article by Zhou *et al.*, documenting tandem OLEDs using exciplex-forming host m-MTADATA:TPBi, is another ironic example of the poor performance of CBP-containing devices [125]. The authors of the pertinent article

fabricated two sets of OLEDs, namely, one with exciplex-forming cohosts and another with common hosts, such as CBP, to investigate the EL of Ir(ppy)₃. Compared with the single-host device, the exciplex-hosted device delivers higher current efficiency and PE because of the high charge carrier mobility in the exciplex-based EML. In addition, the turn-on voltages of the relevant devices are affected by the band gap of the host materials, for example, 3.3 V for the CBP-based device, whereas 2.2 V for the exciplex OLED. In accordance to the observation of the single devices, tandem OLED is also fabricated using the multilayer structure: ITO/MoO₃ (5 nm)/m-MTADATA (35 nm)/6 mol% Ir(ppy)₃ in 1:1 m-MTADATA:TPBi (15 nm)/TPBi (30 nm)/1:1 BPhen:LiNH₂ (10 nm)/MoO₃ (10 nm)/m-MTADATA (30 nm)/6 mol % Ir(ppy)₃ in 1:1 m-MTADATA:TPBi (15 nm)/TPBi (40 nm)/LiF (1 nm)/Al (60 nm). The current efficiency of the tandem device is higher than that of the single devices. However, the PE of the former worsens, perhaps because of the amplification of the driving voltage as the two EL cells are stacked in the tandem device.

Kim and coworkers successfully developed highly efficient exciplex-based green PhOLED using Ir(ppy)₂(acac) as the emitter and TCTA:B3PYMPM (Fig. 2) exciplex system as the host [126]. The maximum current efficiency and PE of the relevant devices are 106 cd A⁻¹ and 127.3 lm W⁻¹, respectively, with maximum η_{ext} climbing as high as 30.2 %. The authors concluded from the simulation studies that the high efficiencies are due to negligible electrical loss. They also preferred the horizontal orientation of the emitters. In another article in the same year, Kim *et al.* reported a high-efficiency PhOLED with small driving voltage and low-efficiency roll-off employing the same host and dopant system, i.e., TCTA:B3PYMPM and Ir(ppy)₂(acac) [127]. The exciplex emission disappears at a dopant concentration higher than 4 %, indicating complete energy transfer from the host to the dopant only at the high concentration ratio. The energy transfer is further boosted by a nearly negligible singlet-triplet gap in the exciplex. The pertinent OLEDs turn on at 2.4 V and achieve a high EQE of 29.1 % with a PE of 124.0 lm W⁻¹. The concept of preferred horizontal ratio ($\Theta_{||} = 77\%$) and subsequent minimal electrical loss is again invoked to explain the high efficiency of the devices. The trap-assisted recombination within the EML has a detrimental effect on OLED efficiency. Thus, the energy transfer-dominated light emission, employing exciplex hosts, is proved to be useful to minimize trap-induced efficiency degradation. Kim and coworkers tested the TCTA:B3PYMPM host and Ir(ppy)₂(acac) dopant combination again in the following year to study the charge recombination mechanism in phosphorescent devices [128]. Another reference device using CBP as the host is also fabricated. The performance of the exciplex-based device is better than that of the CBP-based device. The reason is that the charge balance in the exciplex-hosted device is better than that in the single-hosted device. Moreover, the low turn-on voltage of the exciplex device is attributed to efficient charge injection at the electrodes and charge transportation to the EML under a low external bias in the exciplex-hosted device. The authors determined that the Langevin recombination in the exciplex device is responsible for its enhanced performance compared with that of the other device, which favors the trap-assisted recombination on emitter molecules. The fall in charge density in the exciplex is linked to the low-efficiency roll-off of the device. The TCTA:B3PYMPM exciplex system is also explored as a host to other phosphorescent emitters, such as the green-emitting (ppy)₂Ir(tmd) (Fig. 10), to fabricate highly efficient inverted top-emitting OLED [129]. The concerned device reaches an incredible EQE of 31.9 % with a small efficiency roll-off. For example, the EQE and current efficiencies are 27.6 % and 120.7 cd A⁻¹ at 1000 cd m⁻² and 24.5 % and 107.6 cd A⁻¹ at 20,000 cd m⁻². This result verifies the preferred horizontal orientation of the emitter molecules (horizontal: vertical = 0.78:0.22).

Xu *et al.* reported a basic design strategy to obtain a novel tandem OLED comprising an ultra-thin emitter layer and interface exciplex. The emitter is the green phosphorescent dopant, Ir(ppy)₂(acac), and the exciplex system is TAPC:TmPyPB, which are interconnected by the 1:1

BPhen:LiNH₂ layer [130]. The study aims to demonstrate the energy transfer mechanism in the interface exciplex OLEDs with ultra-thin emission layers versus that in the traditional host–dopant systems. The majority of the carriers in interface exciplex OLED form excitons at the interfaces, with donor and acceptor, and the relevant excitation energy is transferred to the dopant. The authors fabricated both single and tandem OLEDs using the same components and observed that the tandem device exhibits luminance that is approximately twice that of the single device. However, a compromise with the driving voltage is determined. The tandem green OLED offers a maximum CE of 135.7 cd A⁻¹ and a high EQE of 36.8 %, which are nearly twice that of the single emitter device (66.2 cd A⁻¹, EQE = 17.97 %). According to the authors, the high efficiency of the tandem device is due to the combined reinforcement by plasmon quenching effect, a high-quality charge generation unit, and electric field-induced quenching effect.

OLEDs with a non-doped emission layer are less intricate and cheaper to produce than those with a doped EML. Replacing the traditional doped emitting layer (EML) with a non-doped ultra-thin EML (UEML) is a relatively new device engineering strategy that has been proved promising. Although the EQEs of the UEML-containing devices are comparable with those of the conventional EML-containing devices, UEMls have gained minimal research attention, perhaps because of their unsatisfactory PE and roll-off characteristics. Li *et al.* opted for green PhOLED using UEML, together with an interfacial exciplex system with a multi-quantum (MCQ) well structure, to address the PE and roll-off related issues [131]. The concerned device comprises TCTA, B3PyMPM, and Ir(ppy)₂(acac) as the donor, acceptor, and emitter, respectively. The MCQ structure broadens the recombination zone, thereby reducing the efficiency roll-off, perhaps because of the TF suppression due to the proper arrangement of the triplet excitons at the interfaces. Devices with a various number of quantum wells (QWs) are

shown in Fig. 13. In the typical non-MCQ devices, exciton formation selectively occurs at the TCTA:B3PyMPM interface, where high triplet density and exciton quenching becomes pronounced. On the contrary, the carriers are effectively dispersed across a wide recombination zone with the increasing number of QWs, thereby reducing carrier accumulation at each TCTA:B3PyMPM interface. This scenario immediately results in TTA containment and efficiency roll-off improvement. Under this condition, EQE is related to the current density by the following equation:

$$\frac{\eta_{ext}^{TT}(j)}{\eta_0} = \frac{j_c}{4j} \left(\sqrt{1 + 8 \frac{j}{j_c}} - 1 \right)$$

where η_{ext}^{TT} is the EQE in the presence of TTA, and η_0 is the EQE at extremely low current density. The authors found that a reasonable agreement exists between theoretical and experimental results. For example, the non-MCQ device exhibits 30.5 % EQE roll-off at 1000 cd m⁻², whereas the relevant values for the devices with 3, 5, and 7 QWs are 16.5 %, 9.7 %, and 5.2 %, respectively.

Lu *et al.* designed and synthesized two benzimidazole-based materials, namely, BMZ-TB and BMZ-TZ (Fig. 11), by Suzuki coupling between the appropriate fragments to develop exciplex hosts for PhOLEDs [132]. These materials have tripodal structures, exhibit high triplet energy and are employed as the acceptors to form exciplexes with *m*-MTDATA, TAPC, and TCTA. All these exciplex systems are tested as hosts for the green phosphorescent dopant, Ir(mppy)₃ (Fig. 11). The device performance of the triazine-based compound BMZ-TZ is better than that of the non-triazine analog, BMZ-TB. The result is attributed to the high EA of the triazine core in the former. Another article by Shih *et al.* reported green PhOLED based on Ir(ppy)₂(acac) as the emitter and an exciplex system composed of TCTA and 3P-T2T as the host [133].

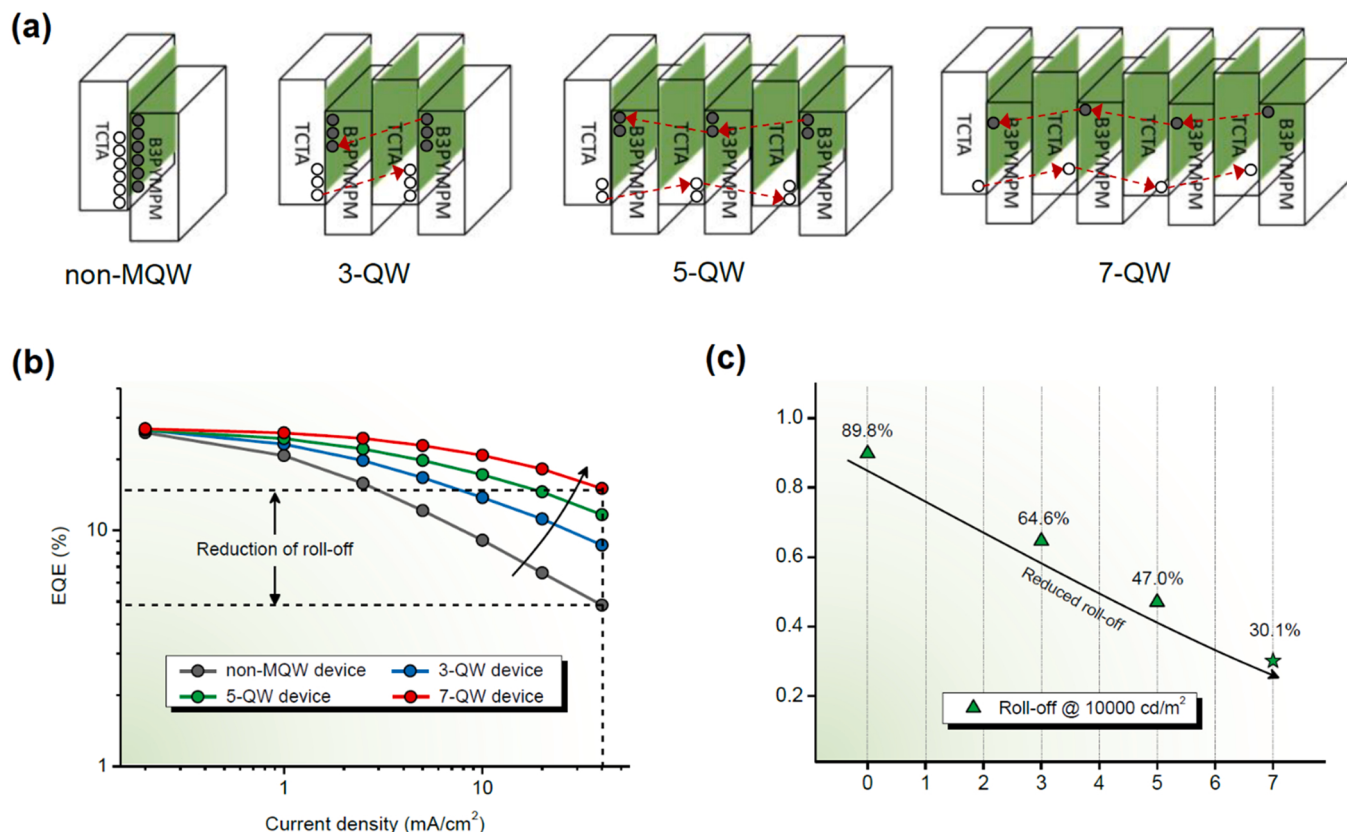


Fig. 13. (a) EML structure with non-MQW, 3-QW, 5-QW, and 7-QW. The green color represents the UEML consisting of Ir(ppy)₂(acac). (b) EQE-current density characteristics of the non-MQW and MQW devices. (c) Roll-off characteristics of the devices with different numbers of QW. Reproduced with permission from [131] Copyright 2013. Royal Society of Chemistry.

From the authors' perspective, the components are selected because of their appropriate energy levels that would facilitate carrier injections and mitigate the driving voltage-related issues. Moreover, the appropriate energy levels of the relevant donor and acceptor aid the charge confinement and accumulation at the interface, thereby facilitating exciplex formation and eliminating the undesired charge-trapping effect. A green PhOLED is obtained with a low turn-on voltage of 2.3 V, high PE of 132 lm W⁻¹, and high EQE of 28.1 with low-efficiency roll-off. Moreover, the TCTA:3P-T2T exciplex-hosted device exhibits a high operational lifetime ($L_{T80} = 1020$ min) with an initial brightness of 2000 cd m⁻². The device lifetime is two orders longer than that of the reference device based on the TCTA:B3PYMPM exciplex system. The authors argued that the stability of exciplex emission can be responsible for the observed result. In addition, the acceptor B3PYMPM was found by Liu and Chen *et al.* to form exciplex systems with diphenylcarbazole-based donors PhCzp-Me, PhCzm-Me, PhCNCzp-Me, PhCNCzp-MeCzPh, and PhCNCzm-MeCzPh (Fig. 11) with different phenyl linkage patterns (*para* vs. *meta*) [134]. The meta-bridged donors exhibit highly twisted conformations that lead the corresponding exciplex systems to have higher triplet energies and longer D-A distances, which contribute to the final device performance. Among them, the optimal exciplex PhCNCzm-MeCzPh:B3PyMPM blend was found to achieve a high efficiency green PhOLED with EQE_{max} up to 31.5 % when Ir(ppy)₂(acac) was introduced as dopant. Very recently, the same group reported two new exciplex-forming systems with bipolar donors BCzPh-pimi, BCzPh-mimi (Fig. 11) and B3PYMPM [134]. Interestingly, the introduction of electron-withdrawing benzimidazole moiety onto 9, 9'-diphenyl-9H,9'H-3,3'-bicarbazole (BCzPh) gives the resulting materials bipolar character, but reduces the hole mobility of donor for balancing the carrier transporting feature in EML. Therefore, the green PhOLED device employing BCzPh-pimi:B3PyMPM as cohost and Ir(ppy)₂(acac) as dopant showed EQE_{max} of 22.31 %. More importantly, the device can retain its EQE_{max} at 22.16 % at a high luminance of 10 000 cd m⁻², corresponding to the efficiency roll-off of only 0.67 %.

3.2.3. Red, orange, and yellow PhOLEDs

The electromagnetic wave of long wavelengths, such as deep red to NIR, is beneficial for plant growth and is applicable in health monitoring systems. Therefore, light-emitting devices with emission peaks post 660 nm are desired and stimulate an active research field. Barrier-free charge injection into the EML with a broad recombination zone normally boosts the device efficiency of PhOLEDs; however, the short operational lifetime of the majority of these devices is a serious concern. Kim and coworkers came up with red PhOLEDs with long operational stability using an exciplex host and two red phosphorescent dopants, namely, Ir(mphmq)₂(tmd) and Ir(MDQ)₂(acac) (Fig. 14) [135]. The relevant devices exhibit the general multilayer structure of ITO (100 nm)/TAPC (75 nm)/NPB (10 nm)/5 wt% emitter in 1:1 NPB:PO-T2T (30 nm)/POT2T (10 nm)/0.5 % Rb₂CO₃:PO-T2T (40 nm)/Al (100 nm). Some other host-based reference devices are also prepared for comparison. The results reveal that exciplex-hosted devices have low turn-on voltage. The Ir(mphmq)₂(tmd) in NPB:PO-T2T device offers the highest EQE of 34.1 % with a PE of 62.2 lm W⁻¹. The device efficiency increases by 1.5 % upon replacing PO-T2T with B3PYMPM. The research also determined the high operation stability of the Ir(mphmq)₂(tmd)-based device ($L_{T90} > 2200$ h).

Liao *et al.* attempted to examine phosphorescent and fluorescent OLEDs using an exciplex-forming host consisting of *m*-MTDATA and BPhen as the hole- and electron-transporting materials, respectively, using PL (steady-state and time-resolved) and delayed EL [136]. The first batch device structure consists of ITO/MoO₃ (2.5 nm)/*m*-MTDATA (30 nm)/EML (10 nm)/BPhen (30 nm)/LiF (1 nm)/Al (60 nm). The exciplex emission in the system is observed regardless of whether the hole- and electron-transporting materials are present in discrete adjacent layers or intermixed in one layer. Doping the *m*-MTDATA:BPhen layer with Ir(piq)₃ leads to a short exciplex lifetime, signifying efficient

energy transfer from the exciplex to Ir(piq)₃ (Fig. 14). The second batch of devices having the structure ITO/MoO₃ (2.5 nm)/*m*-MTDATA (30 nm)/*m*-MTDATA:Ir(piq)₃ (10 nm, 5 % by volume)/*m*-MTDATA (x nm)/BPhen (35 nm)/LiF (1 nm)/Al (60 nm) is fabricated to examine the exact energy transfer mechanism from the exciplex to dopant. The emission bands at 620 and 560 nm are attributed to the emission of Ir(piq)₃ and the exciplex, respectively. The study revealed that the electron-hole recombination occurs across the *m*-MTDATA/BPhen interface yielding the exciplex and that the energy is transferred from the exciplex to Ir(piq)₃. With the increase in thickness of the *m*-MTDATA spacer, the Ir(piq)₃-doped layer becomes gradually far from the exciton formation region, thereby making the energy transfer from the exciplex to dopant inefficient. This energy transfer occurs predominantly via the DET mechanism.

Sasabe, Kido, and coworkers developed three dibenzofuran-based n-type exciplex host materials, namely, 4DBF26PM, 4DBF46PM, and 4DBF46TRZ (Fig. 14), by simple Suzuki–Miyaura cross-coupling reactions between the appropriate fragments [137]. The exciplex host partners have high triplet energy (>2.9 eV). Deep-red PhOLEDs with high EQE is obtained when these host partners are combined with the p-type material α -NPD (Fig. 3) together with the phosphorescent emitter, (DPQ)₂Ir(dpm). The authors also investigated the influence of doping concentration and the D:A ratio on the device performance and operational stability. They determined that the optimized device has a lifetime six times longer than that of the other benchmark red OLEDs. Among the synthesized compounds, the triphenyl triazine derivative 4DBF46TRZ outperforms others with an EQE of approximately 15 % and L_{80} of 3300 h.

Kim *et al.* developed an orange OLED comprising two separate layers of two different phosphors, namely, red Ir(mphq)₂(acac) (Fig. 14) and green Ir(ppy)₂(acac), hosted by TCTA:B3PYMPM exciplex. In the relevant two EML OLEDs, the doping concentrations of the green and the red emitters are 8 wt% and 3 wt%, respectively, and the thickness values of the EMLs vary. The device efficiency relies on the thickness of the two EMLs. The total thickness is fixed at 30 nm. For example, the orange device with a red and green EML thickness combination of 5 and 25 nm offers a high EQE of 22.8 %, whereas the EQE of the other device with a 10 and 20 nm thickness combination is increased by 23.3 %. The device efficiency roll-off is low, perhaps because of the minimization of triplet exciton quenching by dispersing the recombination zone all over the EML [138]. In another paper in the same year, Kim and coworkers used the same set of materials mentioned above. They described the effect of changing the concentration of the red dopant on the device efficiency of the orange OLED. In the new article, the concentration of the green dopant is fixed at 8 %, whereas that of the red dopant varies from 0.3 % to 2.0 % by weight. The relevant device with a red EML dopant concentration of 0.5 wt% displays a low turn-on voltage of 2.4 V and a high EQE of 25.4 % [139].

Xi and coworkers reported an orange OLED based on mCP:PO-T2T exciplex host and (pq)₂Ir(acac) emitter (Fig. 14) [140]. At an optimized 1.5 % doping concentration of the emitter, the OLED delivers 18.7 % EQE together with the current efficiency and PE of 35.3 cd A⁻¹ and 31.0 lm W⁻¹. At a low doping concentration (0.1 wt%), the energy transfer from the exciplex host to the dopant is incomplete, and the blue exciplex emission observed is mixed with the dopant emission (orange) to obtain wOLED. At an optimal device configuration, an EQE of 7.5 % corresponding to current efficiency and PE of 15.5 cd A⁻¹ and 13.7 lm W⁻¹, respectively, is achieved. Yu and coworkers adopted the donor–phosphor–acceptor arrangement, where a thin layer of the emitter is sandwiched between the donor and acceptor layers to fabricate orange emitting PhOLEDs. [141] The authors fabricated two devices comprising NPB (Fig. 3) and TCTA as the donor counterpart, with the common acceptor equivalent being TPBi. The OLEDs based on interfacial exciplexes and a 0.5 nm-thick emitter layer display a PE, current efficiency, and EQE of 37.4 lm W⁻¹, 40.5 cd A⁻¹, and 14.3 %, respectively, that are approximately two times higher than those based

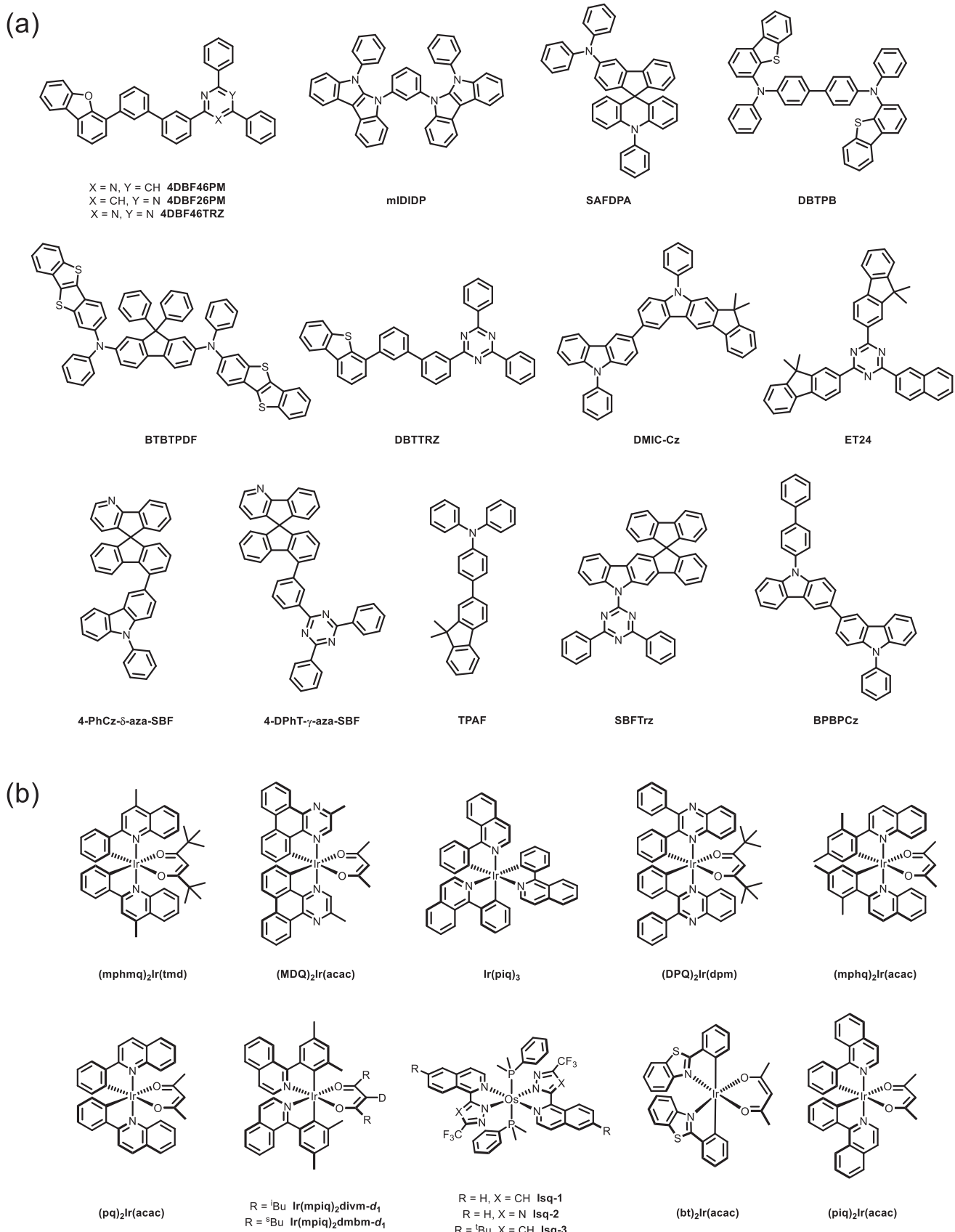


Fig. 14. Molecular structures of (a) the exciplex-forming host systems and (b) other phosphors of PhOLEDs.

on non-exciplex systems. The improved device performance is attributed to suppression of triplet leakage, efficient energy up-conversion of triplet excitons, and completion of energy transfer. Lee and coworkers synthesized a new indoloindole derivative, 1,3-bis(6-phenylindolo[2,3-*b*]indol-5(6 H-yl)benzene (mIDIPD, Fig. 14), as a p-type exciplex component [142]. Although exhibiting an mCP-like molecular structure, the material is very electron-rich because of the fusion of the two indole units. An exciplex system based on this material, together with TPBi as the acceptor, is used as the host for the yellow phosphorescent emitter PO-01 (Fig. 18). At a doping concentration of 5 wt%, the mIDIPD:TPBi-hosted device has a lifetime 10 times longer than that of another device based on TCTA:TPBi. Both devices display comparable EQE that is higher than 20 %.

In 2017, Meng *et al.* reported a novel exciplex-forming host by blending N,N-10-triphenyl-10 H-spiro [acridine-9,9'-fluoren]-3'-amine (SAFDPA, Fig. 14) with BPhen (Fig. 2), which was then utilized to develop a highly simplified orange-red phosphorescence OLED. The T_1 energy of the exciplex is higher than that of the trivalent iridium complex, Ir(MDQ)₂(acac) (Fig. 14), thereby leading to efficient energy transfer to the dopant. The exciplex-hosted reddish-orange OLED realizes a high PE of 31.80 lm W⁻¹ with a low turn-on voltage of 2.2 V. With an exciplex-forming host, the PE of the device is enhanced by 36.2 % compared with that of the reference device (23.54 lm W⁻¹) probably because of low operating voltage. Moreover, the exciplex-hosted OLED with EQE of 11.01 % displays a reddish-orange color with CIE coordinates of (0.628, 0.372) at 500 cd m⁻² and an extraordinarily low CE roll-off of 1.41 % with the brightness from 500 cd m⁻² to 5000 cd m⁻² [143].

Saito *et al.* demonstrated a highly efficient and stable deep-red OLED based on the exciplex host system. They determined that the p-type host materials played a major role in the stability of the devices while investigating the effect of different types of p-type host materials on the performance of red PhOLEDs. The authors used three p-type materials, viz., NPD (Fig. 3), DBTPB, and BTBTPDF (Fig. 14), combined with a triazine-based n-type material DBT-TRZ to generate the exciplexes. They found that the BTBTPDF:DBT-TRZ exciplex system outperforms others with a maximum EQE of 12 %, LT80 of approximately 1500 h, and low power consumption. When employed as the host in a red PhOLED using (DPQ)₂Ir(dpm) (Fig. 14) as the dopant, this exciplex system exhibits the longest device lifetime, presumably because of the preferable location of the recombination zone near the ETL side of the EML. This orientation may prevent the chemical degradation of the HTL by the electron carriers [144]. In addition to efficiency; the device stability is a very crucial parameter in considering the practical application of PhOLEDs. One of the strategies for improving the stability of phosphorescent emitter is to introduce deuterium (D) effect for the ligand design. A recent example disclosed by Sun and Hang *et al.* reveals the importance of selectively deuterating on alkenyl H atoms of ancillary anionic diketone ligands for making Ir-centered red phosphorescent emitters. The devices employing exciplex-forming cohost composing of 7,7-dimethyl-5-phenyl-2-(9-phenyl-9 H-carazole-3-yl)-5,7-dihydroindeno[2,1-*b*]carbazole (DMIC-Cz, Fig. 14) as donor and 2,4-bis(9,9-dimethyl-9 H-fluoren-2-yl)-6-(naphthalen-2-yl)-1,3,5-triazine (ET24, Fig. 14) as acceptor and deuterated red emitters Ir(mpqi)₂dvm-d₁ and Ir(mpqi)₂dbbm-d₁ (Fig. 14) outperform the devices with non-deuterated parent emitters in efficiency and stability without significantly altering the emission profiles [145].

Recently, the OLED with deep-red and NIR emission drew many attentions due to their potential lighting applications for plant growth, health monitor, light communication, and biomedical imaging etc. Along this line, researchers have made great progress in this regard. For example, Kido *et al.* reported to use exciplex cohost system comprising a phenanthroline derivative, nBPhen (Fig. 7), as acceptor and a famous HTM, α -NPD (Fig. 3), as donor and a deep-red Ir dopant, (DPQ)₂Ir(dpm) (Fig. 14), to achieve a high efficiency device with EQE_{max} of 17 % and a low operation voltage of 2.37 V, representing the best PhOLED device in

this emission range [146]. In addition to Ir-based phosphors, Os-based complexes can also serve as good dopants for PhOLEDs. In this regard, Chi and Lee *et al.* recently reported the utilization of an exciplex-forming blend TCTA:T2T as cohost for isoquinolinyl azolate based Os(II) complexes. [147] The NIR emission wavelengths (> 745 nm) with short radiative decay lifetimes (in hundreds of ns) and PLQY up to 48 % in doped thin films ensure the device to perform EQE_{max} of 9.66 % at a current density of 300 mA cm⁻², where the devices employing Os-centered dopants Isq-2 and Isq-3 (Fig. 14) can perform maximum radiance over 170 W sr⁻¹ m⁻², revealing the potential of exciplex-hosted NIR PhOLEDs for future applications.

3.2.4. Multicolor OLEDs

Discussing separately the papers that aimed to utilize the same hosts in different color-emitting devices is valuable. The performance of the CDBP:PO-T2T-based exciplex OLED has been discussed earlier [42]. In addition to using the exciplex system as the emitter, the authors developed green and red PhOLEDs, utilizing the exciplex as the host and Ir(ppy)₂(acac) (Fig. 10) and (MDQ)₂Ir(acac) (Fig. 14) as the emitters. The optimized doping concentrations of the dopants are 6 wt% and 2 wt%. Both the devices exhibit a low turn-on voltage of 2.5 V. The CE, PE, and EQE for the green device are 98.3 cd A⁻¹, 110.2 lm W⁻¹, and 28.6 %, respectively, and those for the red device are 54.3 cd A⁻¹, 63.1 lm W⁻¹, and 28.0 %, respectively. These values are comparable with those of the benchmark devices known back then, indicating the competency of the relevant exciplex system, not only as a blue emitter but also as an efficient host. Based on transient EL decay studies, the authors suggested the activation of the phosphorescent dopants by energy transfer from the host instead of direct charge trapping. Chen and coworkers reported multicolor PhOLEDs based on an exciplex host consisting of *m*-MTDATA as the donor and TmPyPB as the acceptor [148]. The relevant dopants are Ir(ppy)₃ (Fig. 11, green), (bt)₂Ir(acac) (Fig. 14, yellow), and (piq)₂Ir(acac) (Fig. 14, red). The yellow device excels at a low turn-on voltage of 2.5 V and a high EQE of 18.5 %. The green and red devices also perform well at low turn-on voltages (<2.7 V) and high EQEs (>10 %), further demonstrating the effectiveness of the exciplex host system. Current density–voltage–brightness plots of the relevant devices are shown in Fig. 15. Based on theoretical studies, the authors concluded that the matched FMOs of the exciplex-forming components and high oscillator strength of the exciplex emission augment the device performance. Zhang, Wang, and coworkers came up with two new 4-substituted aza-SBFs, namely, 4-PhCz- δ -aza-SBF and 4-DPhT- γ -aza-SBF (Fig. 14), with high triplet energy (>2.8 eV) and high glass transition temperature (>140 °C) to determine exciplex hosts for multicolor OLEDs [149]. A physical mixture of the components using the former as the donor and the latter as the acceptor forms deep blue exciplex with TADF character ($\lambda_{PL} = 418$ nm, $\Phi_{PL} = 23.9$ %). The new exciplex system is further deployed as the host in blue and green PhOLED using Flripic (Fig. 2) and Ir(ppy)₂(acac) (Fig. 10) as the dopants, respectively. Both the non-doped and doped devices are tested. The non-doped blue PhOLED exhibits CE, PE, and EQE of 60.3 cd A⁻¹, 52.7 lm W⁻¹, and 26.2 %, respectively, whereas those of the non-doped green PhOLED are 87.4 cd A⁻¹, 101.6 lm W⁻¹, 24.6 %, respectively, both with a low turn-on voltage of 2.3 V. The doped devices have comparable device efficiencies.

Tao *et al.* synthesized a triphenylamine–fluorene hybrid electron donor TPAF (Fig. 14) with appropriate HOMO to blend with the known electron acceptor B3PYMPM and simplify the devices based on exciplex hosts. The relevant exciplex system (D:A = 3:7) emits bluish-green light with its emission spectrum centered at 496 nm and exhibits ambipolar transporting property [150]. Two phosphors, namely, the green-emitting Ir(ppy)₂(acac) (Fig. 10) and the red-emitting (MDQ)₂Ir(acac) (Fig. 14), are chosen to construct green and red OLEDs, which show excellent device performance owing to simple barrier-free structures, ambipolar transporting property, and complete energy transfer from the host to the dopant. Very recently, Lee *et al.* reported a novel donor unit SBFCbz by fusing carbazole with 9,9'-spirobifluorene (SBF),

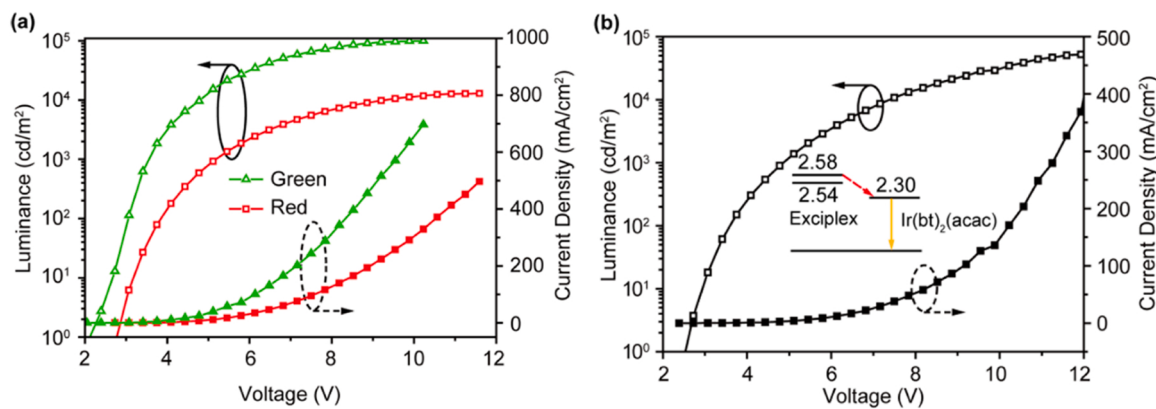


Fig. 15. Current density–voltage–brightness plots of m-MTADATA:TmPyPB exciplex-hosted (a) red, green, and (b) yellow devices. Reproduced with permission from [148], Copyright 2018. American Chemical Society.

which was then coupled with triazine to form a bipolar acceptor, namely 5’-(4,6-diphenyl-1,3,5-triazin-2-yl)-5’H-spiro[fluorene-9,11’-indenol[1,2-b]carbazole] (SBFTrz, Fig. 14). The exciplex system of the donor 9-[(1,1’-biphenyl)-4-yl]-9’-phenyl-9H,9’H-3,3’-bicarbazole (BPBPCz, Fig. 14) and SBFTrz displayed a triplet energy of 2.59 eV, which was suitable as an exciplex cohost for the green [Ir(ppy)₂(acac)] (Fig. 10) and red [Ir(mphmq)₂tdm] (Fig. 14) doped PhOLEDs [151]. The charge balance in SBFTrz:BPBPCz exciplex cohost allows green and red PhOLEDs performing high efficiency and limited efficiency roll-off at high luminance as well as higher operational lifetime as compared to those of corresponding device employing SBFTrz as single host.

Therefore, the exciplex-hosted PhOLEDs have considerably improved since their introduction. The energy transfer channel is most important in utilizing the electrically generated excitons in these devices. However, the role of SOC interaction between the heavy metal atom of the phosphorescent molecule and the exciplex host is considerable in realizing a high-performing device. However, this factor is often overlooked. Guo *et al.* demonstrated the synergistic effects of energy transfer and intermolecular SOC (ISOC) in an exciplex-hosted PhOLED by MEL experiment. They found a broadening of MEL line shape at the high field because of the ISOC effect that stimulates a fast transition process between singlet and triplet states of the exciplex host. The energy transfer process from the exciplex host to the phosphorescent dopant is highly efficient, as confirmed by the different line widths of MELs [152].

3.3. TADF OLEDs hosted by exciplexes

In addition to PhOLEDs, devices employing TADF emitters can achieve 100 % internal quantum efficiency, because both the triplet and singlet excitons can be brought into emission. The emission in PhOLEDs is phosphorescence, which utilizes the electrically generated triplet excitons. However, TADF is a delayed fluorescence that involves both the singlet and triplet excitons in the emission. RISC brings the dark triplet excitons into the emission channel by upconverting them into the singlets. Given the participation of the triplet states, TADF dopants, like the PhOLEDs, are required to be dispersed in a host matrix to avoid unnecessary shortcomings. Exciplexes are proved to be good hosts for TADF dopants. In this subsection, we review the research activity on this topic. Although both the Förster and DET mechanisms can theoretically operate between the exciplex host and the TADF dopant, the predominant mode of energy transfer is the former because the host itself can upconvert the triplet excitons formed within it because of the self-TADF character (Fig. 9). The low doping concentration of the emitter further wanes the triplet energy transfer. However, unlike in PhOLEDs, where emission occurs from the triplet states, the emission in the TADF OLEDs is from the singlet states. Thus, RISC (emitter) is very important in the

TADF OLEDs, whereas ISC is much more important in PhOLEDs. The TADF dopant structures and that of the relevant hosts are provided in Fig. 16, and the relevant data are summarized in Table 2.

Sperlich and coworkers demonstrated a kinetic model for TADF OLEDs, including radiative and nonradiative first- and second-order effects, to analyze the effect of efficiency limiting in OLEDs. The transient PL of exciplexes is intricated by their nonabsorbing nature. The authors modeled the m-MTADATA:3TPYMB exciplex system and found that the TTA is the dominant second-order effect. TTA is unambiguously an efficiency-limiting process in OLEDs because it depletes the triplet exciton density. The EL is contaminated with a contribution of emitting states formed via TTA in addition to that formed via RISC because of the increasing influence of TTA at a high temperature [153]. In 2014, Kim and coworkers demonstrated a green fluorescent OLED with EQE of as high as 30 % using 1:1 mCP:B3PyMPM as the host for the TADF emitter 4CzIPN (Fig. 8) [154]. The blend film of the dopant shows an emission band centered at 515 nm with an almost unity quantum yield, which is attributed to an efficient energy transfer from the host to the dopant and efficient blockage of radiationless decay processes of the TADF emitter. Moreover, the angle-dependent PL studies revealed that the horizontal transition dipole ratio is 0.73, pointing at the preferred horizontal orientation of the emitter molecules. The relevant OLED exhibits a turn-on voltage of 3.0 V, a high EQE of 29.6 %, and maximum current efficiency of 94.5 cd A⁻¹. These values are comparable with those of a typical PhOLED. A moderate efficiency roll-off exists, perhaps because of the TTA during the long exciton lifetime of 4CzIPN. Sasabe, Kido, and coworkers documented a green TADF OLED using 4CzIPN as the emitter and a 1:1 blend of CBP and B4PyPPM as the host [155]. The exciplex formation in the blend is identified by red-shifted emission at 443 nm. The energy transfer is most efficient at a 5 % dopant concentration based on doped films of various emitter concentrations. The optimized OLED offers an EQE of 25.7 %, a low turn-on voltage of 2.3 V, and a high PE of 107 lm W⁻¹. The relevant data for an analogous PhOLED using Ir(ppy)₃ (Fig. 11) are 25.3 %, 3.0 V, and 108.9 lm W⁻¹, indicating the potential of the exciplex-hosted TADF devices.

Exciplex hosts are proved to be efficient in augmenting the EQE of PhOLEDs. However, they may not be appropriate for TADF OLEDs because TADF emitters possess deep energy levels. Lee *et al.* tested four exciplex systems, namely, TAPC:TPBi, TCTA:TPBi, CBP:TPBi, and mCP:TPBi, as hosts for the green TADF dopant 4CzIPN; they reported a high-efficiency TADF OLED based on these systems. [156] The PL spectra revealed that CBP:TPBi and mCP:TPBi would not form exciplexes, whereas TAPC:TPBi and TCTA:TPBi blends readily formed exciplexes. Among the four systems, the emission of the mCP:TPBi blend overlapped considerably with the absorption spectrum of the dopant. The PLQYs of the doped films of the mCP:TPBi, CBP:TPBi, TCTA:TPBi, and TAPC:TPBi are 97 %, 66 %, 15 %, and 6 %, respectively, indicating the most efficient

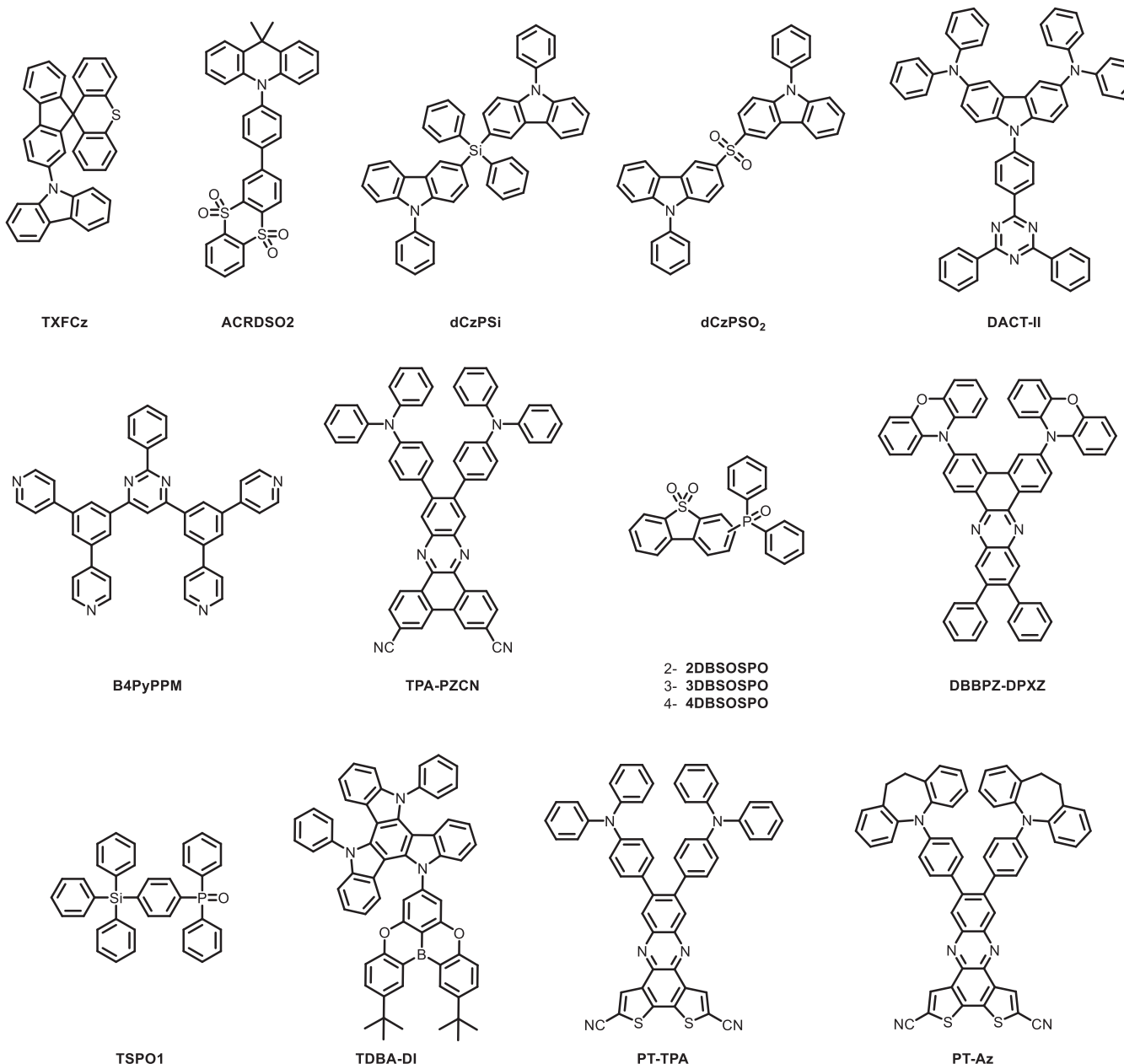


Fig. 16. Molecular structures of the materials used in TADF-doped exciplex-based OLEDs.

energy transfer in mCP:TPBI. The authors concluded that energy transfer occurs for the mixed host systems but not for those that form exciplexes. The EQEs of the relevant OLEDs are 25.8 % (mCP:TPBI), 13.0 % (CBP:TPBI), 5.6 % (TCTA:TPBI), and 3.3 % (TAPC:TPBI), which verify the PLQYs of the doped films. Another electron transport material, BmPyPb (Fig. 2), is tested with mCP to enhance further the device efficiencies. The mCP:BmPyPb mixed host behaves like the mCP:TPBI host system.

Su *et al.* reported an active planar p-n heterojunction platform based on two p-type materials, DAcB and TXFCz (Fig. 16), and a tripodal triazine-based n-type material TmPyTz (Fig. 2). [157] The exciplex system, DAcB (Fig. 4):TmPyTz, performs well as a host in a fluorescent OLED, and then it is extended to a TADF OLED containing a yellow dopant, ACRDSO₂ (Fig. 16). The corresponding OLED provides good device efficiency, such as an EQE of as high as 20 % and a PE of 70 lm W⁻¹. The emission color of the OLED can be changed by modifying the doping position of the p-n heterojunction.

RISC is an essential parameter for the TADF emitter. Thus, its magnitude can be increased, and efficiency roll-off can be consequently

suppressed by spin mixing between the exciplex host and the TADF dopant in the excited state. Hung *et al.* synthesized two high triplet energy materials, namely, dCzPSi and dCzPSO₂ (Fig. 16); they comprise π -conjugation blockers, such as diphenyl silane ($>\text{SiPh}_2$) or sulfone ($>\text{SO}_2$), linking two 9-phenylcarbazole (PCz) units [158]. They are individually tested as hosts for the green TADF dopant, 4CzIPN, which exhibits device efficiency of as high as 19 % and low roll-off. The exciplex systems dCzPSi:PO-T2T and dCzPSO₂:PO-T2T are then employed as the hosts for the same dopant, and these OLEDs are superior to the single-host OLEDs based on the individual donors. For instance, the maximum EQE of the dCzPSi:PO-T2T-based OLED is as high as 21.1 %.

The green TADF emitter, 4CzIPN, has been the most popular among researchers. However, thus far, only a few research articles have demonstrated green TADF OLEDs that are hosted by high-PE exciplex. Sasabe *et al.* have recently demonstrated the strategical use of two different types of pyrimidine-based electron-transporting materials as the exciplex component to realize high-efficiency exciplex-hosted TADF OLEDs based on the emitter DACT-II (Fig. 16) [159]. The article

demonstrated the alteration of electron-transporting properties of pyrimidine derivatives with a slight variation of structure using three compounds, such as B4PyMPM (Fig. 8), B4PyPPM (Fig. 16), and B3PyMPM (Fig. 2). For example, 4-pyridine derivatives, such as B4PyMPM and B4PyPPM, display electron mobility and electron injection property that are ten times higher than those of the 3-pyridine analogs, such as B3PyMPM. This result is reflected in their OLED performance, as shown in Fig. 17 which shows that the chemical structures of the pyridine derivatives have upshot in other device parameters except for the EL maxima. Green TADF OLED using B3PyMPM as one of the exciplex components exhibits excellent device performance, such as a low driving voltage of 2.5 V at 100 cd m⁻², a high EQE of 29.2 %, and a high PE of 133.2 lm W⁻¹, without any additional light out-coupling enhancement.

Most of the research attention on TADF OLEDs has been focused on blue- and green-emitting devices, which have recorded thus far an EQE of as high as 30 %. However, only a handful of high-efficiency red TADF devices are known to date, perhaps because of the intrinsic low quantum yield of the red emitters due to the energy gap law. However, non-radiative transitions can be minimized by adopting a suitable molecular design strategy, such as a strong donor and acceptor and rigid molecular backbone. In addition, red-emitting devices with high EQE can be generated. Zhang *et al.* synthesized a new red TADF emitter, TPA-PZCN (Fig. 16), comprising TPD and dicyano-substituted phenazine as the acceptor to achieve high-efficiency red TADF OLEDs [160]. The material has a small singlet-triplet gap (0.13 V), high PLQY (97 %), and effective RISC. An OLED based on the emitter doped in CBP achieves a maximum EQE of 27.4 %, with the EL spectrum centered at approximately 628 nm. Replacing CBP with an exciplex host (CBP:PO-T2T) causes the device to

glow at a slightly long-wavelength (648 nm) with comparable EQE (28.1 %) but at a low driving voltage (3.0 V vs 2.4 V).

Traskovskis *et al.* demonstrated a novel strategy to obtain exciplex systems with a high RISC rate ($>10^7$ s⁻¹). The concerned strategy chooses selective donor-acceptor pair, where the acceptor molecule can undergo fast intersystem crossing to form a locally excited triplet state (³LA). This controlled excitation transfer to the locally excited triplet state comes with optimal RISC that turns on TADF. The downside of this emission mechanism is the abnormal quenching of thermal PL triggered by metastable acceptor triplet state under room temperature. However, when the donor and acceptor counterparts are combined to form dyads, the latter forms intermolecular exciplexes in solid films that exhibit TADF character, balanced bipolar charge transportation, and the ability to host TADF emitters in exciplex-hosted TADF OLEDs [161].

Xu *et al.* reported a series of acceptor *m*DBSOSPO (*m*=2, 3, 4, Fig. 16) combining phosphine oxide (PO) and dibenzofuran-S,S-dioxide (DBSO) with different linkage topologies to study the exciplex formation with a donor 4,4'-bis(9-carbazolyl)-2,2'-dimethylbiphenyl (CDBP). The CDBP:*m*DBSOSPO exciplex blends show typical TADF behaviors [162]. Among them, the device employing CDBP:2DBSOSPO as exciplex cohost doped with 3 % of a yellow TADF emitter (4CzTPNBu, Fig. 10) exhibits outstanding EL characteristics including $\text{EQE}_{\text{max}} = 30.3$ % and power efficiency of 114.9 lm W⁻¹. The introduction of exciplex cohost benefits the RISC efficiency up to 99% and effectively reduce triplet nonradiative rate constant, leading to a tenfold increase singlet radiative/nonradiative ratio as compared to that of single host system. An exciplex-forming CDBP:PO-T2T (Fig. 4) blend that can host a red TADF emitter 10, 10'-(11,12-diphenyldibenzo[*a,c*]phenazine-3,6-diyl)bis (10 H-phenoxyazine) (DBBPZ-DPXZ) (Fig. 16) was recently reported by

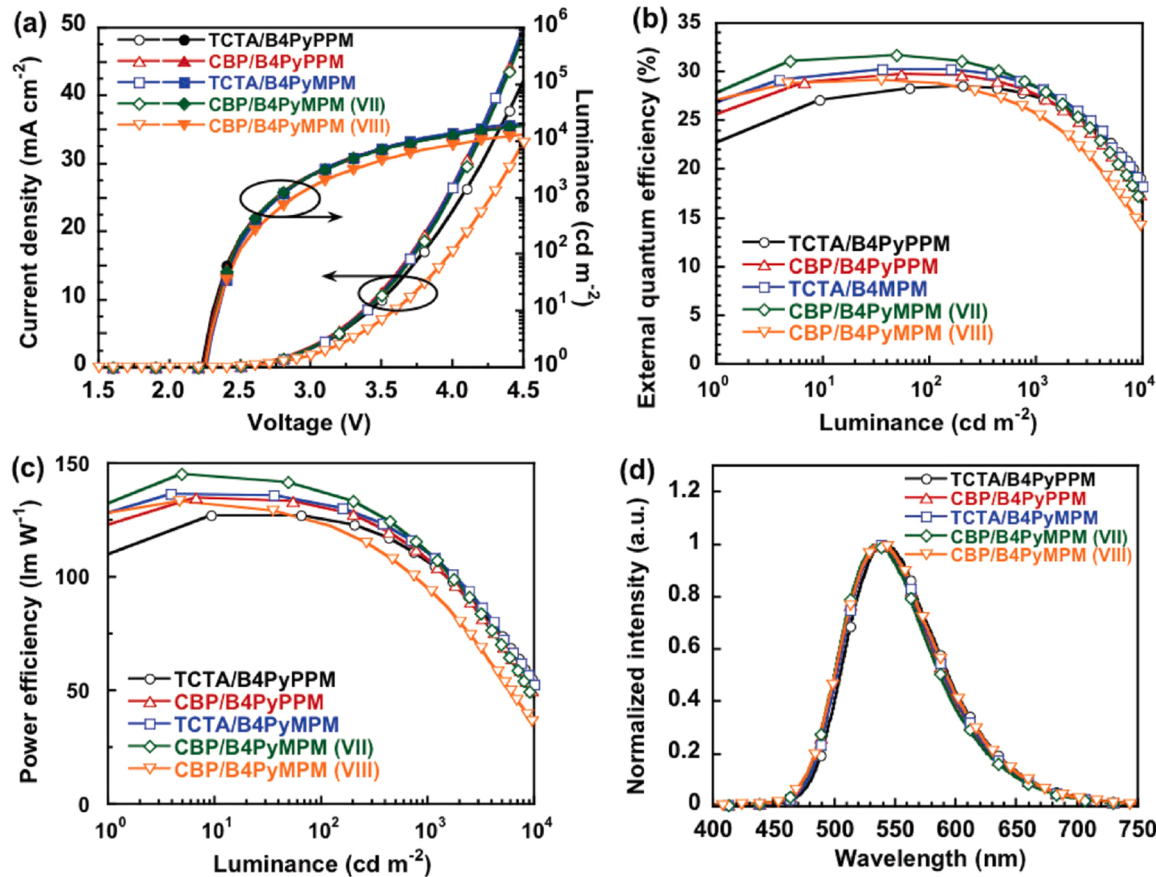


Fig. 17. Performance of the exciplex-hosted DACTII-based devices: (a) J-V-L characteristics, (b) EQE-brightness characteristics, (c) PE-brightness characteristics, and (d) EL spectra.

Reproduced with permission from [159] Copyright 2018. John Wiley and Sons.

Wang and Zhang *et al.* [163] With 6 wt% doping of DBBPZ-DPXZ, the device undergoes completely energy transfer to give a red exciplex-hosted TADF device (EL $\lambda_{\max} = 628$ nm) with EQE_{max} up to 20.8%. By reducing the doping concentration to 0.2 wt%, a high efficiency (20.7%) wOLED with the residual blue exciplex host emission and red TADF emission was achieved.

Very recently, Gasparini *et al.* reported to introduce a high hole mobility (7.5×10^{-3} cm²V⁻¹s⁻¹) fluorinated thiophene-quinoxaline (TQ) copolymer that works together with the exciplex-forming interface between an ambipolar host bis(diphenylphosphine oxide)dibenzofuran (DBFPO, Fig. 2) and diphenyl[4-(triphenylsilyl)phenyl]phosphine oxide (TSPO1, Fig. 16) to confine the exciton formation zone at the host/ETM interface [164]. The confinedly formed excitons are transferred to a blue TADF emitter the 5-(2,12-di-tert-butyl-5,9-dioxa-13b-boranaphtho[3,2,1-de]anthracen-7-yl)-10,15-diphenyl-10,15-dihydro-5 H-diindolo[3,2-a:3',2'-c]carbazole (TDBA-DI, Fig. 16), resulting an extremely high efficiency blue (EL $\lambda_{\max} = 458$ nm) TADF device (EQE_{max} = 41.2 %) with a low turn-on voltage (2.5 V), low efficiency roll-off and long device lifetime. Wu and Fan *et al.* recently reported an interesting molecular design strategy to make efficient TADF emitter [165]. Instead of adopting rigid electron donor and acceptor as structural blocks to synthesize D-A type molecular TADF materials, a new red TADF compound (PT-TPA, Fig. 16) with free rotation of the terminal phenyl groups was reported to show high fluorescence radiative decay rate mainly due to a larger transition dipole moment that facilitates the S₁→S₀ transition as compared to that of a counterpart emitter PT-Az (Fig. 16) with ethylene-linked terminal phenyl groups. The device employing PT-TPA as dopant in an exciplex-forming host comprising CBP as donor and B4PyMPM as gave an EQE_{max} of 28.8% (EL $\lambda_{\max} = 648$ nm).

In brief, exciplexes are proved to be excellent hosts. The RISC within the exciplex framework upconverts triplet excitons, which are the majority. The subsequent energy transfer to the dopant is an effective channel to harness the electrically generated excitons. The conventional hosts are mostly RISC silent because of the large singlet-triplet gap. Compared with the traditional hosts, the exciplex-hosted devices can consequently operate at decreased driving voltage, which is advantageous. However, as shown in Table 2, the turn-on voltage of exciplex-hosted OLEDs varies widely with the nature of exciplexes, where a low turn-on voltage alludes to an appropriate combination of donor and acceptor. Although research in TADF OLEDs has achieved several important milestones, uncertainties remain. These ambiguities can be unveiled by theoretical modeling. Regnat and coworkers presented an electro-optical device model of fluorescent OLED with a TADF exciplex host, mainly accounting for charge carriers, excitons, and photons [166]. The model simulates current-voltage-luminance characteristics, angle-dependent EL spectra, EL decay, and determination of the emission zone. This simulation is important to set the exciton diffusion constant. The simulation reiterates the importance of ISC and TTA minimization for EQE enhancement and predicts a remarkably high efficiency of 42 %, which has not been achieved thus far. Finally, although exciplex hosts are sought after to obtain high-performing OLEDs, the exciplex formation between the emitter and host molecules occasionally broadens the emission profile, inducing color impurity [167].

4. White OLEDs based on exciplexes

The primary objective of any new technology in this era of rapidly depleting energy resources is saving energy. Likewise, the introduction of OLED technology intends not only to replace LCDs but also to produce energy-saving lighting modules as a substitute for power-hungry LED lighting units. OLED-based flat panel white lighting modules, which can potentially imitate daylight, are more power-efficient than the existing LED modules. Moreover, research on wOLEDs has been a popular topic in the context of the energy crisis, and enormous endeavor has been

given to develop advanced, power-efficient, and high-luminance wOLEDs since their discovery in the 90s [168]. Among trial methodologies, incorporation of exciplexes, either as emitters or as hosts, has been proved to please the researchers because of the promising performances of the subsequent wOLEDs. Some early reports on exciplex-based white OLEDs were made, but they all encountered low device efficiencies, high driving voltage, and low luminance [169]. In this section, we review the progress of exciplex-based wOLEDs. For an organized presentation, we divided this section into two parts, exciplexes as the emitters and exciplexes as the hosts. The relevant device data are summarized in Table 3.

4.1. Exciplex emitters in wOLEDs

Red, green, and blue colors are usually combined to produce white and the color temperature depends on the relative fraction of the individual colors. However, only two different emitting species in exciplexes can sometimes lead to white light because exciplex emissions are rather broad, covering an extensive wavelength range. Zucchi *et al.* reported a solid-state structural study of bimetallic lanthanide complexes, whose PL spectra display characteristic sharp emission lines of each ion. These complexes are used as dopants in OLEDs, and a broad emission covering the yellow-green region is observed in the EL spectra of the devices in addition to the emission from metal ions. The pertinent broad emission is ascribed to the exciplex formation between the CBP host and the dopant within the emission layer. The mixture of the [(Eu(acac)₃)₂(μ -bpm)] (acac = acetylacetone and bpm = 2,2'-bipyrimidine, Fig. 18) red emission and the exciplex emission offers an overall white EL from the devices when the Eu ion is used as a single dopant. [170] Zhao *et al.* reported a wOLED based on a simple electron-transporting type material, anthracene-9,10-diylbis(diphenylphosphine oxide) (DPPA, Fig. 18) [171]. Unlike PL, the EL of this material had not been known back then. In the relevant research, the authors intended to utilize DPPA as an emitter and as the electron-transporting material. The fluorescence spectrum of a 1:1 blend film of NPB and DPPA has a band in the blue region that correlates with the DPPA emission and a broad band in the red region that is due to the exciplex formation. The EL spectrum of the relevant OLED is similar to the PL spectrum, and an almost pure white light with CIE coordinates of 0.33, and 0.33 is obtained.

The first all-exciplex-based white OLED was reported by Hung *et al.* in 2014 [40]. Different exciplex systems are tested to produce a range of colors. Then, the suitable exciplexes are employed in a tandem device to obtain the white OLED. A similar concept was already known back then, the production of white light by inserting two blend layers of m-MTDATA:Al(DBM)₃ (Fig. 18) and TPD (Fig. 3):BPhen between HTL and ETL [172]. However, the device efficacy is inadequate, and the device lacks color stability. Hung *et al.* adopted the tandem structure comprising two individual blend layers of 1:1 D:A configuration by a charge generation layer configuration (Fig. 19a) to overcome the problem. In this configuration, the carriers are generated at the DTAF (Fig. 4)/MoO₃ interface and injected into the adjacent EMLs. The relevant wOLED displays a turn-on voltage of 4.0 V, a L_{max} of 50300 cd m⁻² at 24 V, and a maximum EQE of 11.6 % corresponding to CE of 27.7 cd A⁻¹, and PE of 15.8 lm W⁻¹. The two-color wOLED has broad emission peaks in the blue (mCP:PO-T2T) and yellow (DTAF:POT2T) region of the visible spectrum covering wavelengths from 430 nm to 730 nm (Fig. 19b). The color-rendering indices (CRI) of the device are as high as 70.1–70.6.

Grazulevicius and coworkers synthesized a bicarbazole derivative pCNBCzoCF₃ (Fig. 2) and fabricated a wOLED based on it [173]. The concept is similar to the wOLEDs reported early in the decade, i.e., combining emitter emission and the exciplex emission to generate white light. A non-doped OLED based on pCNBCzoCF₃ exhibits a sky blue color. Similarly, the m-MTDATA:pCNBCzoCF₃ exciplex system produces an orange-emitting device. The warm-white OLED is subsequently fabricated by combining these two OLEDs into one, which displays a brightness of 40900 cd m⁻² (at 15 V), the current efficiency of 53.8 cd

Table 3

Device data table – exciplex based white OLEDs (the values in the parenthesis indicate data at 1000 nit).

Device structure (the exciplex component is underlined)	Φ_{film} (%)	V_{on} (V)	λ_{EL}^{max} (nm)	EQE (%)	CE (cd A $^{-1}$)	PE (lm W $^{-1}$)	CIE	Ref
Exciplex based white OLEDs								
ITO/PEDOT:PSS (30 nm)/TPAC (20 nm)/mCP (15 nm)/ 1:1 mCP:PO-T2T (20 nm)/ PO-T2T (45 nm)/Liq (1 nm)/Al (1 nm)/ MoO ₃ (5 nm)/DTAF (20 nm)/1:1 DTAF: PO-T2T (20 nm)/PO-T2T (50 nm)/Liq (0.5 nm)/Al (100 nm).	—	4.0	—	11.6	27.7	15.8	0.29,0.35	[40]
ITO/TAPC (30 nm)/CDBP (10 nm)/0.1 wt% Ir(ppy) ₂ (acac) and 0.3 wt% Ir (MDQ) ₂ (acac) in 1:1 CDBP:PO-T2T (30 nm)/PO-T2T (40 nm)/ LiF (1 nm)/Al (100 nm).	—	2.5	—	25.5 (14.8)	67.0	84.1	0.40, 0.43	[42]
ITO/MoO ₃ (3 nm)/TCTA (15 nm)/1:1 TCTA:BPhen (12 nm)/BPhen (30 nm)/3 P- T2T:Cs ₂ CO ₃ (10 nm)/ Al (1 nm)/ MoO ₃ (5 nm)/ TAPC (15 nm)/TAPC:3 P-T2T (12 nm)/ 3 P-T2T (25 nm)/LiF/Al	—	4.6	451,570	9.17	25.4	11.5	0.41, 0.44	[75]
ITO/MoO ₃ (3 nm)/mCBP (20 nm)/0.5 wt% (bt) ₂ Ir(acac) in mCBP:PO-T2T (20 nm)/ PO-T2T (40 nm)/LiF (0.8 nm)/Al	—	2.5	—	22.2 (20.6)	58.4 (54.0)	52.3 (43.2)	0.42, 0.43	[97]
ITO/CuI/TCTA/pCNBCzoCF ₃ /m-MTADATA/ pCNBCzoCF ₃ /BCP/Ca:Al	—	6.8	—	18.8 (17.0)	53.8 (46.2)	19.3 (10.6)	0.40, 0.44	[173]
ITO/HAT-CN (10 nm)/TAPC (55 nm)/FIrpic/TmPyPB (40 nm)/1:1 BPhen:LiNH ₂ (10 nm)/HAT-CN (10 nm)/TAPC (55 nm)/PO-01/TmPyPB (40 nm)/Liq (2 nm)/ Al (120 nm)	—	6.9	—	18.6	41.5	19.1	—	[174]
ITO/MoO ₃ (1 nm)/mMTADATA (50 nm)/mCzPPQ (10 nm)/POT2T (10 nm)/TPBi (40 nm)/LiF (0.5 nm)/Al	—	6.0	—	3.2	8.9	4.4	0.21, 0.56	[175]
ITO/MoO ₃ (1 nm)/mMTADATA (50 nm)/pCzPPQ (20 nm)/PO-T2T (20 nm)/TPBi (40 nm)/LiF (0.5 nm)/Al	—	7.8	—	0.8	1.6	0.5	0.17, 0.45	[175]
ITO/MoO ₃ (1 nm)/TAPC (30 nm)/mCP (17 nm)/(MDQ) ₂ Ir(acac) (0.1 nm)/mCP (3 nm)/FIrpic (0.2 nm)/PO-T2T(15 nm)/BPhen (40 nm)/LiF (1 nm)/Al (120 nm)	—	—	—	20.0 (18.5)	41.0 (38.1)	30.7 (21.9)	0.41,0.40	[177]
ITO (120 nm)/TCTA (40 nm)/1:1 TCTA: BP4mPy (29 nm)/8:2 m-MTADATA: TmPyPB (1–3 nm)/ 26DCzPPY (3 nm)/1:9 m-MTADATA: B3PyMPM (3 nm)/ TmPyPB (50 nm)/LiF (0.8 nm)/Al (150 nm)	—	—	385, 462, 652	1.5	2.7	2.0	—	[178]
ITO/TAPC (35 nm)/1:1 TAPC:TPBi (80 nm)/TPBi (35 nm)/LiF (1 nm)/Al (100 nm)	—	5.0	—	0.5	1.0	0.4	0.42, 0.36	[180]
ITO/TAPC (35 nm)/1:1 TAPC:TPBi (50 nm)/TPBi (35 nm)/LiF (1 nm)/Al (100 nm)	—	3.0	—	0.7	1.9	1.1	0.33, 0.45	[180]
ITO/TAPC (35 nm)/1:1 TAPC:TPBi (80 nm)/TPBi (5 nm)/LiF (1 nm)/Al (100 nm).	—	85.0	—	0.6	1.3	0.5	0.45, 0.41	[180]
ITO/MoO ₃ (10 nm)/TAPC:MoO ₃ (10 %, 50 nm)/TAPC (20 nm)/PO-01 (0.06 nm)/ mCP:B3PYMPM:FIrpic (1:1:0.4, 10 nm)/B3PYMPM (15 nm)/B3PYMPM: Li ₂ CO ₃ (3 %, 40 nm)/Li ₂ CO ₃ (1 nm)/Al	—	2.4	—	20.0 (19.5)	64.5 (62.8)	75.3 (63.1)	—	[184]
ITO/HAT-CN (10 nm)/TAPC (55 nm)/FIrpic/TmPyPB (40 nm)/BPhen:LiNH ₂ (10 nm, 50 % by mole)/HAT-CN (10 nm)/TAPC (55 nm)/PO-01/TmPyPB (40 nm)/Liq (2 nm)/Al (120 nm),	—	6.9	—	18.6	41.5	19.1	—	[185]
ITO/HATCN (15 nm)/TAPC (60 nm)/TCTA (5 nm)/mCBP (5 nm)/1:1 mCBP:PO- T2T (4 nm)/Ir(ppy) ₂ (acac) (0.04 nm)/1:1 mCBP:POT2T (3 nm)/RD071 (0.06 nm)/1:1 mCBP: PO-T2T (9 nm)/PO-T2T (45 nm)/LiF (1 nm)/Al	—	2.4	—	21.2 (15.8)	50.6 (35.5)	66.2 (34.6)	0.40,0.46	[186]
ITO (180 nm)/HAT-CN (10 nm)/HAT-CN: TAPC (40 nm)/TAPC (5 nm)/mCBP (5 nm)/PO-01 (0.03 nm)/mCBP:FIrpic (15 %, 2 nm)/PO-T2T (8 nm)/PO-T2T: Liq (10 %, 30 nm)/Liq (1 nm)/Al (150 nm)	—	2.6	—	28.4 (18.2)	72.2 (46.3)	87.2	0.35, 0.44	[187]
ITO/TAPC (40 nm)/TCTA (10 nm)/15 wt% FIrpic + 0.25 wt% (MDQ) ₂ Ir(acac) in 1:1 m-CBP:B4PyPPM/TmPyPb (45 nm)/LiF (0.8 nm)/Al (80 nm)	—	2.6	—	23.9 (21.9)	52.0 (49.1)	64.1 (35.2)	0.40, 0.42	[190]
ITO/TAPC (40 nm)/TCTA (10 nm)/ 15 wt% F3Irpic + 0.25 wt% (MDQ) ₂ Ir(acac) in 1:1 m-CBP:B4PyPPM/TmPyPb (45 nm)/TmPyPb (45 nm)/LiF (0.8 nm)/Al (80 nm)	—	2.5	—	26.9 (23.7)	61.5 (56.8)	71.5 (37.2)	0.40, 0.48	[190]
ITO/TAPC (40 nm)/TCTA (5 nm)/m-CBP (5 nm)/15 wt% FIrpic in 1:1 m-CBP: B4PyPPM (12 nm)/4 wt% Ir(ppy) ₂ (acac) in m-CBP:B4PyPPM (3 nm)/2 wt% (MDQ) ₂ Ir(acac) in 1:1 m-CBP: B4PyPPM (15 nm)/B4PyPPM (45 nm)/LiF (0.8 nm)/Al (80 nm)	—	2.5	—	22.3 (21.4)	49.2 (46.3)	59.1 (30.8)	0.45, 0.44	[190]
ITO/TAPC (40 nm)/TCTA (5 nm)/m-CBP (5 nm)/15 wt% FIrpic in 1:1 m-CBP: B4PyPPM (12 nm)/4 wt% Ir(ppy) ₂ (acac) in m-CBP:B4PyPPM (3 nm)/2 wt% (MDQ) ₂ Ir(acac) in 1:1 m-CBP: B4PyPPM (15 nm)/B4PyPPM (45 nm)/LiF (0.8 nm)/Al (80 nm)	—	2.6	—	25.3 (23.5)	55.5 (49.6)	67.0 (29.4)	0.48, 0.45	[190]
ITO/HAT-CN (10 nm)/TAPC (40 nm)/TCTA (10 nm)/4 wt% PO-01 in 1:1 CNTPADPA:PO-T2T (3 nm)/15 wt% FIrpic in 1:1 mCP:PO-T2T (20 nm)/PO-T2T (45 nm)/Liq (2 nm)/Al (120 nm)	—	2.4	—	19.5 (16.0)	60.0 (49.5)	73.0 (41.9)	0.41, 0.48	[191]
ITO/HAT-CN (15 nm)/TAPC (60 nm)/TCTA (5 nm)/mCBP (5 nm)/10 wt% FIrpic in 1:1 4 P-NPB:PO-T2T (12 nm)/YDD01/PO-T2T (45 nm)/LiF (1 nm)/Al (150 nm)	—	2.1	—	21.9 (18.9)	60.4 (52.1)	85.0 (49.1)	0.53, 0.47	[192]
ITO/HAT-CN (15 nm)/TAPC (60 nm)/TCTA (5 nm)/10 wt% FIrpic in 1:1 mCBP:PO- T2T (5 nm)/2 wt% (tptpy) ₂ Ir(acac) in 1:1 mCBP:PO-T2T (4 nm)/2 wt% RD071 in 1:1 4 P-NPB:PO-T2T (3 nm)/PO-T2T (45 nm)/LiF (1 nm)/Al (150 nm)	—	2.3	—	23.5 (21.6)	45.1 (43.9)	65.3 (36.5)	0.46, 0.42	[192]
ITO/HAT-CN (15 nm)/TAPC (60 nm)/TCTA (5 nm)/10 wt% FIrpic in 1:1 mCBP:PO- T2T:FIrpic (5 nm)/1 wt% Ir(ppy) ₂ (acac) in 1:1 mCBP:PO-T2T (2 nm)/2 wt% (tptpy) ₂ Ir(acac) in 1:1 mCBP:PO-T2T (4 nm)/2 wt% RD071 in 1:1 4PNPB:PO-T2T (3 nm)/PO-T2T (45 nm)/LiF (1 nm)/Al (150 nm)	—	2.3	—	22.8 (21.4)	61.5 (55.0)	79.0 (48.0)	0.44, 0.47	[192]
ITO/MoO ₃ (3 nm)/mCP (45 nm)/12 wt% FIrpic in 1:1 mCP:B4PyPPM (20 nm)/5 wt % PO-01 in 1:1 mCP:B4PyPPM (10 nm)/B4PyPPM (35 nm)/Liq (0.8 nm)/Al	—	2.5	—	21.7 (20.9)	66.4 (61.8)	73.6 (42.3)	0.40, 0.45	[193]
ITO/TPAPB (30 nm)/1:1 TPAPB:TPBi (30 nm)/TPBi (40 nm)/LiF (1 nm)/Al	44.0	3.2	468	7.0	9.1	7.2	0.14, 0.18	[194]

(continued on next page)

Table 3 (continued)

Device structure (the exciplex component is underlined)	Φ_{film} (%)	V_{on} (V)	λ_{EL}^{max} (nm)	EQE (%)	CE (cd A ⁻¹)	PE (lm W ⁻¹)	CIE	Ref
ITO/TPAPB (30 nm)/ 4 wt% Ir(2-phq) ₃ in 1:1 TPAPB:TPBi (30 nm)/TPBi (40 nm)/ LiF (1 nm)/Al	—	2.9	—	18.5	49.5	44.3	0.53, 0.47	[194]
ITO/TPAPB (30 nm)/ 0.5 wt% Ir(2-phq) ₃ in 1:1 TPAPB:TPBi (30 nm)/TPBi (40 nm)/LiF (1 nm)/Al	—	3.2	—	15.7	42.5	29.6	0.46, 0.43	[194]
ITO/HATCN (15 nm)/TAPC (50 nm)/TCTA (5 nm)/mCBP (3 nm)/FIrpic (0.05 nm)/1:1 mCBP: (0.05 nm)/mCBP (2 nm)/1:1 mCBP:PO-T2T (2 nm)/FIrpic (0.2 nm)/1:1 mCBP: PO-T2T (2 nm)/Ir(ppy) ₂ (acac) (0.1 nm)/1:1 mCBP:PO-T2T (2 nm)/RD071 (0.05 nm)/1:1 mCBP:PO-T2T (2 nm)/FIrpic (0.1 nm)/PO-T2T (40 nm)/LiF (1 nm)/Al	2.4			26.1 (18.9)	40.0 (36.0)	50.1 (29.7)	0.46,0.43	[199]
ITO/MoO ₃ (3 nm)/mCP (30 nm)/(pq) ₂ Ir(acac) (1.1 nm)/1:1 mCP:PO-T2T (15 nm)/ (pq) ₂ Ir(acac) (1.1 nm)/PO-T2T (40 nm)/LiF (1 nm)/Al	—	3.8		22.5 (19.5)	44.9 (38.9)	47.4 (31.8)	0.56, 0.39	[200]
ITO/MoO ₃ (2 nm)/FSF4A (45 nm)/3 wt% Ir(MDQ) ₂ in FSF4A:PO-T2T (20 nm)/ MCP (4 nm)/FIrpic (0.2 nm)/PO-T2T (35 nm)/LiQ (1 nm)/Al (100 nm)	—	2.2	—	12.4 (10.6)	32.6 (30.3)	34.1 (21.4)	0.33, 0.34	[203]
ITO/HAT-CN (10 nm)/TAPC (40 nm)/TCTA (5 nm)/15 wt% FIrpic in 1:1 26DCzPPy:B4PyMPM (10 nm)/4 wt% Ir(ppy) ₂ (acac) in 1:1 CDBP:B4PyMPM (2 nm)/4 wt% Ir(MDQ) ₂ (acac) in 1:1 CDBP:B4PyMPM (5 nm) B4PyMPM (50 nm)/ LiQ (2 nm)/Al (120 nm)	—	2.6	—	30.9 27 (24.7)	55.0	61.3	0.42, 0.42	[204]
ITO/MoO ₃ (3 nm)/ m-MTDATAT (20 nm)/1:1 m-MTDATA:OCT (5 nm)/TCTA (X nm)/1:1 TAPC:OCT (5 nm)/TCTA (2 nm)/OCT (5 nm)/TPBi (40 nm)/ LiF (1 nm)/ Al (100 nm)	—	3.7	—	1.7	4.8	3.9	0.28, 0.33	[205]

A^{-1} , PE of 19.3 lm W⁻¹, and EQE of 18.8 %. Xu *et al.* have recently demonstrated simplified and efficient tandem wOLED using energy transfer from exciplexes to the complementary color non-doped ultra-thin EMLs containing FIrpic (Fig. 2, blue) and PO-01 (Fig. 18, yellow) emitters [174]. The EQE of the relevant device reaches 18.6 %, corresponding to high current efficiency of 41.5 cd A⁻¹.

In an unprecedented approach, Baek *et al.* developed wOLED without using emitting dopant of any type, but the exciplexes generated at the HTL=ETL interface were utilized. [175] The key role of HTL and ETL in an OLED is to obtain balanced transport of charge carriers to the EML. Moreover, the coexistence of these layers in an OLED aids exciplex formation and emission can be observed if the appropriate combination is used. This emission is normally broad and may be useful in developing wOLED with high CRI. Instead of using any fluorescent or phosphorescent dopant, the authors investigated wOLEDs with multiple EMLs. According to the authors, these wOLEDs have a carrier balance that is better than that of the SL device, and they can provide QW effect and charge control to confine excitons within the EML. The authors fabricated two-, three-, and four-layer exciplex devices, where TCTA is used as the donor, and TPBi, m-MTDATA, and BPhen are used as the acceptors. The relevant device structures are shown in Fig. 20. The two-layer devices generate two different types of emission patterns: devices A1 and A2, with blue emission stronger than that of yellow-green emission, and A3 and A4, showing only yellow-green emission (Fig. 20c). The emission peak at 460 nm is due to the TCTA:BPhen exciplex and that at 550–560 nm are attributed to m-MTDATA:TPBi and m-MTDATA:BPhen exciplexes. The three- and four-layer OLEDs are fabricated using a structure, as shown in Fig. 20b. The authors described the energy transfer process of excitons in three-layer devices as a combination of (a) exciton generation in each exciplex EML, (b) occurrence of delayed fluorescence, and (c) exciton movement from S₁ of blue exciplex (TCTA:BPhen) to the S₁ of yellow-green exciplex (m-MTDATA:TPBi or BPhen) and confining exciton transfer from blue to the other EML (Fig. 20d). The multi-EML structure is believed to enhance the exciton distribution in the whole EML to minimize exciton quenching and improve CRI. The device performance improves in the multiple-layer OLEDs. However, none of the devices delivers a notable efficiency (e.g., EQE < 5 %).

Sych *et al.* synthesized two bipolar quinoline–carbazole hybrids with different linking topologies, namely, mCzPPQ and pCzPPQ (Fig. 18), which form blue exciplex with PO-T2T and orange exciplex with the donor m-MTDATA [176]. The synthesized compounds individually emit violet fluorescence, where the meta substituted compound exhibits energy triplet and IE that are higher than those of the para derivative. The hole and electron mobilities of the two compounds exceed 10⁻⁴ cm² V⁻¹

s⁻¹ at electric fields exceeding 10⁵ V cm⁻¹. The authors fabricated wOLEDs by combining two interfacial exciplex emissions in a three-layered sandwich-type structure. The optimized device with a three-layer structure delivers white EL with a high CRI of 76, color temperature of 8400 K, and maximum EQE of 3.2 %.

He and coworkers studied the influence of bilayer interfacial exciplex structure and bilayer non-exciplex structure on the device performance of ultra-thin FIrpic-based blue OLEDs [177]. mCP and PO-T2T are chosen as the exciplex-forming partners, and the exciplex is believed to reduce interface charge accumulation and exciton quenching. The resulting blue device exhibits an EQE of 23.1 % and produces white emission when combined with an ultra-thin orange-red emitting dye (MDQ)₂Ir(acac) (Fig. 14). The position of the ultra-thin red EML influences the device's performance. When the layer is inserted at the mCP side of the device, an exciton suppression that directly formed on the red dopant is observed, enhancing spectral stability. The optimized white OLED displays a high EQE of 20 %.

Exciplex emission is also explored for its potential to imitate daylight artificially. Luo *et al.* have recently reported an exciplex-based white OLED with daylight-like emission using commercially available components, such as m-MTDATA and TCTA as the donors and TmPyPB (Fig. 2), B3PyMPM (Fig. 2), and BP4mPy (Fig. 18) as the acceptors [178]. The FMOs of each of these materials are at different energy from the others. Thus, an appropriate combination of the components results in the emission of different colors, which are mixed to generate white light. The authors intended to mimic the daylight emission by setting the main carrier recombination zone to the red emission layer. The donor-acceptor combination for the individual exciplex pixels is as follows: 1:1 TCTA:BP4mPy (blue), 8:2 m-MTDATA:TmPyPB (green), and 1:9 m-MTDATA:B3PyMPM (red). The researchers examined white OLED with two different architectures: one tandem device with the blue- and red-emitting components and another with a thin layer of (1–3 nm) of green components inserted between the red and blue pixels. The former type of device produces two peaks, i.e., blue and red, in its electroluminescent spectrum. The blue emission is slightly intense and dependent on the applied bias, producing an overall pinkish white color. The insertion of the green-EML improves the color rendition, and an emission spectrum close to the daylight is achieved. However, the device efficiency is substantially low at only 1.5 %, 2.7 cd A⁻¹, and 2.0 lm W⁻¹.

Nevertheless, the utilization of triplet excitons is vital to realize high-performing devices. Li *et al.* demonstrated a new methodology with stepped RISC to boost the upconversion of nonradiative triplet excitons. They used mCP:DMAC-DPS:PO-T2T:4CZPNPh (Fig. 18) ternary exciplex system to fabricate white LED, exhibiting an EQE of 22.7 %, PE of

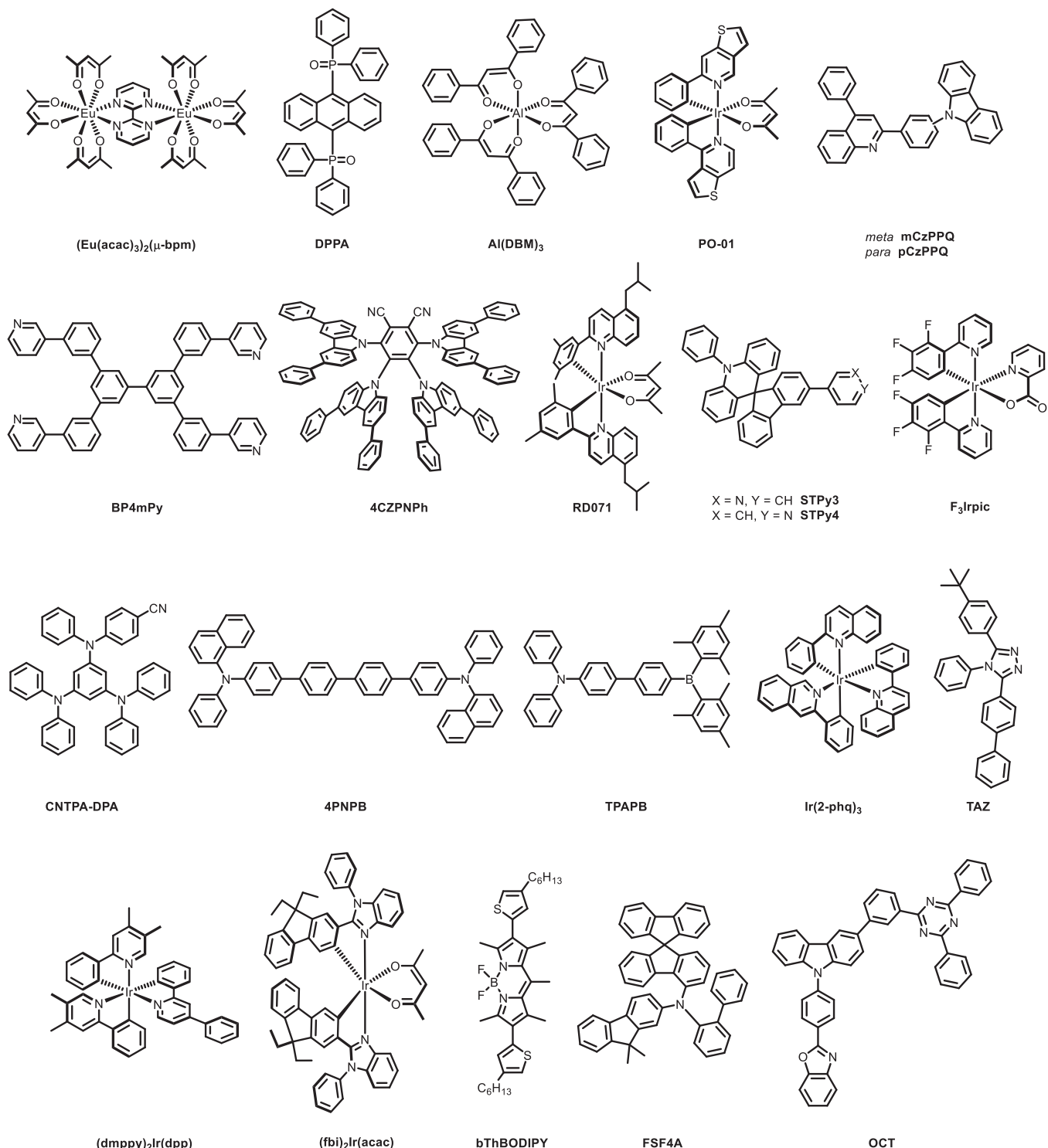


Fig. 18. Molecular structures that were used in exciplex-based wOLEDs.

62.5 lm W⁻¹, and low-efficiency roll-off. The authors concluded that diminished nonradiative depletion of triplet excitons suppresses triplet-triplet quenching and consequently augmented the device performance [179]. A very interesting wOLED device composed of the sky blue exciplex emission from the TAPC:TBPi (Fig. 3) blend and yellow electrophosphorescence at high voltages was recently reported by Namdas, Ajayaghosh, and Unni et al., pointing out a possible strategy to achieve a wide spectral coverage using different mechanisms [180].

4.2. Exciplexes as hosts in wOLEDs

The concept that the exciplexes are excellent hosts has been echoed multiple times throughout the article. Energy transfer from the exciplex host to the dopant is schematically represented in Fig. 9. The same strategy has been tested to develop high-performance white light-emitting devices. Consistent maintenance of high PE and color stability under the operating brightness is a huge challenge for wOLEDs. The reason is that, unlike other parameters, such as EQE, PE is much more sensitive to the driving voltage. Many designs and engineering strategies

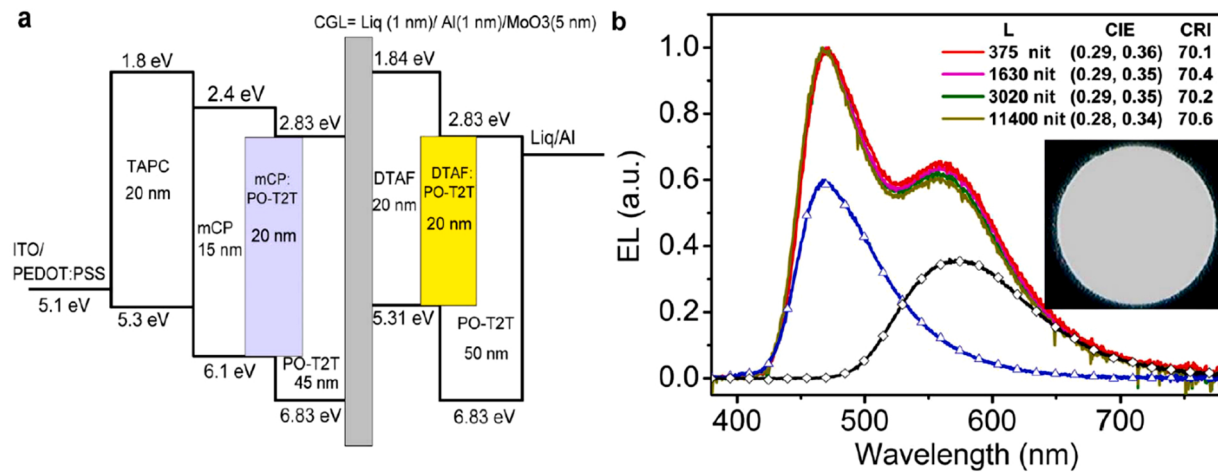


Fig. 19. All-exciplex-based wOLED by tandem structure. (a) The electronic level configurations of tandem wOLED. (b) EL spectra of device W at different brightness values and two decomposed bands corresponding to the blue and yellow exciplex emissions.
Reproduced with permission from [40]. Copyright 2014. Springer Nature publishing group. .

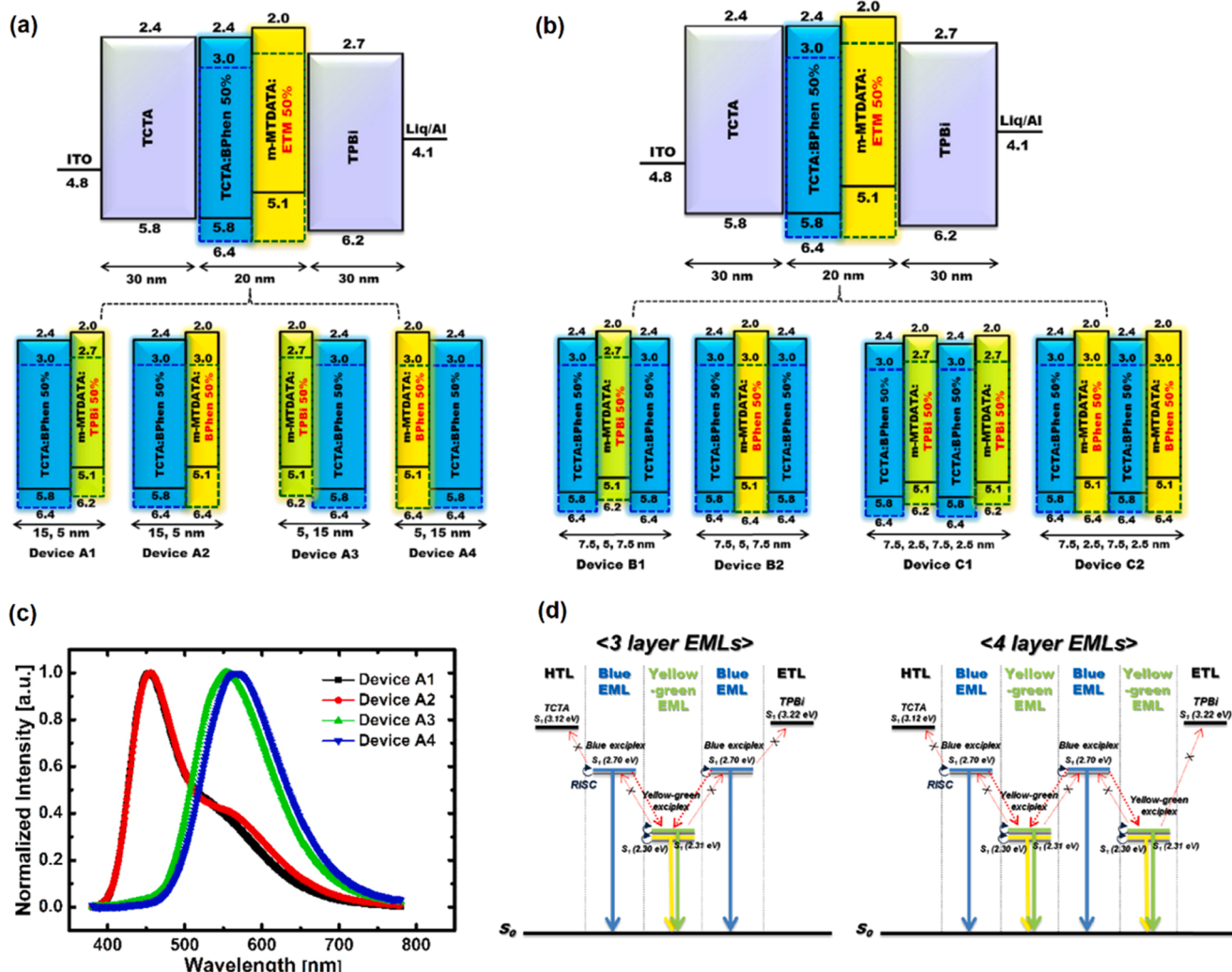


Fig. 20. Schematic energy level diagram and device structures of (a) two-layer devices and (b) three- and four-layer devices; (c) normalized emission spectra of the two-layer devices; (d) the singlet states (S₁) of materials and exciton transfer mechanism in wOLEDs.
Reproduced with permission from [175]. Copyright 2017. John Wiley and Sons. .

have been developed thus far to enhance the PE by achieving 100 % internal quantum efficiency, efficient exciton harnessing, and a low carrier injection barrier. Of several tested methodologies, devices based on phosphorescent emitters and exciplex hosts are proved to be the most efficient, as the phosphorescent materials have 100 % exciton harnessing ability, and the exciplex hosts can lower the driving voltage of the device. In this section, we review such devices and finally compare them with the wOLEDs based on the exciplex emitters.

The exciplex host system, CDBP:PO-T2T, was mentioned earlier. Individual OLEDs with $\text{Ir}(\text{ppy})_2(\text{acac})$ (Fig. 10) and $(\text{MDQ})_2\text{Ir}(\text{acac})$ (Fig. 14) doped in this exciplex host matrix emit green and red lights, and the exciplex itself emits in the blue region [42]. The blue OLED comprising the exciplex as the emitter exhibits a considerably high EQE of 13 %, whereas the EQE for the green and red devices is ~ 28 %. A single-EML wOLED, consisting of the exciplex system and the above-mentioned dopants, exhibits a low turn-on voltage of 2.5 V, a current efficiency of 67.0 cd A^{-1} , PE of 84.1 lm W^{-1} , and EQE of 25.5 %. The authors alluded to the high performance as a combined effect of (a) bipolar emission layer and a barrier-free structure of the exciplex system, (b) nearly unitary internal quantum efficiency due to the TADF nature of the exciplex host, and (c) effective sensitization due to triplet energy of the exciplex that is higher than that of the dopants.

Duan *et al.* reported a blue-emitting exciplex system by blending BPhen with TCTA, which was employed as the blue emitter and the host in fluorescent–phosphorescent wOLED consisting of the yellow phosphorescence emitter PO-01 (Fig. 18). The device exhibits a maximum EQE of 4.3 % and maximum PE of 9.0 lm W^{-1} [181]. In another report, the same group investigated the singlet and triplet energy transfers from exciplex to phosphors to realize an exciplex/phosphorescence hybrid white OLED. The exciplex is formed by simply blending the extensively used TCTA and BPhen. The TCTA:BPhen exciplex is used as the blue EML and the host for green and red phosphors. Energy transfer from the exciplex to the dopants is efficient owing to the large overlap between the PL spectrum of the TCTA:BPhen exciplex and the absorption spectra of the phosphors. This unique wOLED that utilizes the singlet-state exciplex as the blue emitter in combination with green and red phosphors exhibits η_{ext} of 10.5 % at 1000 cd m^{-2} and PE of 13.5 lm W^{-1} with CIE coordinates of (0:38, 0:43) [182].

Zhang *et al.* identified a new mechanism to comprehend exciplex–fluorescence and exciplex–phosphorescence hybrid wOLEDs with a simple device structure [97]. The work aimed to circumvent the low RISC efficiency of blue exciplex systems and complex device structure of the traditional wOLEDs, thereby promising to develop high-performance white light-emitting devices. In the beginning, a blue exciplex system mCBP:PO-T2T is used as the emitter to obtain an OLED with a high EQE of 7.7%. In this exciplex matrix, the phosphorescent dopant $(\text{bt})_2\text{Ir}(\text{acac})$ is doped, generating warm wOLED with a remarkably high EQE of 22.2%, a low turn-on voltage of 2.5 V, and a high power-efficiency of 52.3 lm W^{-1} . A low dopant concentration of 0.5 wt% is maintained, and the energy transfer is not complete, causing both the exciplex emission and the dopant emission to appear. This phenomenon leads to a white emission. The triplet energy of the components is higher than that of the exciplex, and a large spectral overlap between the exciplex emission and the dopant absorption spectra may have facilitated energy transfer from the host to the dopants. This scenario can be a possible reason for the high device performance.

Chang *et al.* examined the TCTA:BP4mPy (Fig. 18) combination to form a stable exciplex with an adequate energy gap and an EQE that was higher than that of the other exciplex blends [183]. Blue, green, and red PhOLEDs exhibit EQEs of 15.8 %, 14.1 %, and 8.8 %, respectively, using the pertinent exciplex as the host with dopants, such as FIripic (Fig. 2), $\text{Ir}(\text{ppy})_3$ (Fig. 11), and $\text{Ir}(\text{piq})_3$ (Fig. 14). Moreover, the blue, green, and red devices display turn-on voltages of 3.0, 3.2, and 3.6 V, respectively, which are lower than those of devices utilizing common host materials. Thus, the results obtained in such exciplex-based OLEDs indicate the efficient and balanced carrier transport in EML. Finally, a white

exciplex-based OLED is fabricated, and a maximum EQE of 11.3 % with PE of 16.3 lm W^{-1} and stable emission is realized.

Wang *et al.* demonstrated high-performance phosphorescent wOLED by inserting an ultra-thin layer of orange dopant (PO-01, Fig. 18) into a blue emission layer consisting FIripic in an exciplex host (mCPB: B3PYMPM) matrix [184]. The relevant OLED was among the top-performing phosphorescent white light-emitting device based on exciplex host back then and offered low working voltage and high efficiency (20 %, 64.5 cd A^{-1} , and 75.3 lm W^{-1}) with low roll-off. In this work, the authors first stabilized the blue device and explored the exciton density profile in the EML. They determined from their studies that the orange emission is the strongest by placing the non-doped orange EML at 3 nm from the interface between the electron blocking layer and the emission layer. The authors alluded to (a) 100 % exciton harvesting capability of the host, (b) appropriate device design, (c) excellent exciton confinement in the EML, and (d) electrical exciton energy lower than that of the conventional hosts for the high device performance. Xu *et al.* described highly simplified and efficient tandem wOLEDs based on the energy transfer from the exciplexes to the ultra-thin layers of phosphorescent dopants, such as FIripic (blue) and PO-01 (yellow). TAPC and TmPyPB are chosen as the exciplex-forming components, and the relevant wOLED shows a good performance (41.5 cd A^{-1} , 19.1 lm W^{-1} , 18.6 %) [185]. Ma and coworkers fabricated hybrid wOLED by inserting ultra-thin red and green phosphorescent emitters (RD071 (Fig. 18) and $\text{Ir}(\text{ppy})_2(\text{acac})$ (Fig. 10)) in blue exciplex (mCBP:PO-T2T). The use of ultra-thin phosphorescent layers keeps the electric transport properties of the device almost unchanged, favoring the efficient and stable exciton recombination in the EML. The relevant device offers maximum PE, CE, and EQE of 66.2 lm W^{-1} , 50.6 cd A^{-1} , and 21.2 %, respectively, with relatively low-efficiency roll-off. Moreover, the optimized devices exhibit stable electroluminescent spectra with a high CRI [186]. In another report, Ma and coworkers proposed an adaptive cohost structure that simplifies the device fabrication process while delivering high efficiency. The authors employed a thin layer (2 nm) of a blue phosphorescent dopant (FIripic) dispersed in mCBP that can extract the excitons from the interfacial exciplexes formed between mCBP and the cohost PO-T2T. The white device is then generated by introducing an ultra-thin layer of an orange phosphor (PO-01, Fig. 18) at the appropriate location around the exciton recombination zone. The relevant device structure enhances the exciton utilization through the multiple energy transfer routes, causing the device to excel (28.4 %, 72.17 cd A^{-1} , 87.17 lm W^{-1}) [187].

Tang *et al.* used a different approach, that is, allocation of gradient exciplexes (AGEs), to find a solution to the PE problem of wOLEDs. They synthesized two bipolar spiro-type materials with donor–spiro–acceptor topology, namely, STPy3, and STPy4 (Fig. 18), as the exciplex-forming agents [188]. In the relevant research work, the authors described the AGE as a slope between the single host and the exciplex cohost by adjusting the D:A ratio. The newly synthesized materials are employed as single hosts for the conventional blue (FIripic) and yellow (PO-01) bicolor phosphorescent wOLED, which achieves a maximum EQE of 27.8 %. However, the PE of the device is limited to only 50 lm W^{-1} because of the high driving voltage. This scenario is not rare but is one of the many reported wOLEDs with high EQE but with low PE. The authors hypothesized that serious energy loss during carrier injection together with exciton transfer from host to yellow phosphor results in the high driving voltage of the devices. The exciplexes based on STPy3 and STPy4 as the donors and PO-T2T as the acceptor are again proved unsuccessful in constructing wOLED because of insufficient triplet energy of the exciplex to host blue emitters. On the contrary, remarkable improvements in the driving voltage, efficiency roll-off at high brightness, and color stability are observed by employing AGE. According to the authors, the exciplex distribution in the EML due to the gradient mixing ratio of the D and A counterparts for AGE instead of a fixed D:A ratio in conventional exciplex systems mainly enhances device efficiency. Although a slight improvement of the device EQE (28.2 % for AGE vs

27.8 % in the other device) is determined, the PE of 72.7 lm W^{-1} at 1000 cd m^{-2} is increased by 45.4 % [188]. The color rendering index (CRI) is an important parameter for the white OLEDs. Since the colors of the objects are realized by shining light on them, the quality of the incident light is important to reveal the color of the object appropriately. If a wOLED is used as the source of the incident light, then a minimum CRI of 80 is required. A common trend among researchers to improve the CRI is to use a multiple emitter system to cover a wider spectral range. The downside of this strategy is the complexity of the devices that takes a toll on cost and fabrication simplicity. Also, insufficient energy transfer from the blue emitter in these multi-emitter systems sometimes causes a broadening of the spectrum that affects the color purity. This issue was fixed by Tang et al. in a recent publication using a strategy called the color remedy strategy. The relevant publication reported wOLED with CRI as high as 80 with high EQE and PE [189].

Zhao et al. have recently reported exciplex-based high-performance white OLEDs that deliver a remarkably high EQE of 21 % even at a brightness of 5000 cd m^{-2} [190]. The 1:1 blend of m-CBP as the electron donor (Fig. 2) and B4PyPPM as the electron acceptor (Figure 16) is employed as the host, which exhibits blue fluorescence. The exciplex system is excellent at hosting multicolor phosphorescent emitters. The blue, cyan, green, and red PhOLEDs based on the emitters Flrpic (Fig. 2), F₃Irpic (Fig. 18), Ir(ppy)₂(acac) (Fig. 10), and (MDQ)₂Ir(acac) (Fig. 14), respectively, exhibit high EQEs of 26.2 %, 26.1 %, 24.7 %, and 26.5 % (17.7 %, 18.1 %, 17.5 %, and 20.6 % in traditional hosts). Then, the authors constructed a single-EML wOLED by doping blue or cyan phosphorescent emitters with a red dopant in the exciplex host. The relevant devices exhibit high efficiencies, such as PE of 71.5 lm W^{-1} and high EQE of 26.9 %. They also fabricated a three-color multi-EML wOLED with a high color rendering index and high efficiencies (EQE = 21 %) at practical brightness.

Zhang and coworkers synthesized a new tripodal bipolar compound CNTPA-DPA (Fig. 18) to reduce the driving voltage and enhance the PE of wOLEDs and used this compound as a multi exciplex-forming cohost in wOLEDs [191]. The material forms exciplexes with mCP and PO-T2T, which are both beneficial. Flrpic and PO-01 are employed as the blue- and orange-emitting components in the white device. The high hole mobility and suitable HOMO of the material assist the orange emitting component of the OLED (PO-01) to achieve remarkably high efficiencies (2.1 V , 27 %, 115.5 lm W^{-1}). The authors believed that the multi exciplex forming host strategy alleviates high voltage and energy loss, which are common in traditional wOLEDs with single-exciplex forming co-hosts, and aids in achieving low operating voltage and enhanced efficiency. In particular, the optimized wOLEDs exhibit augmentation of PE by 45.7 % and EQE by 19.6 %. Moreover, the appropriate combination of materials with matching energy level alignment helps the device achieves a low operating voltage of 3.8 V at 1000 cd m^{-2} .

The importance of the PE of any electronic device is often surpassed by high EQE. Although the latter is a crucial device output parameter, the former is no less important when a certain device is picked out for commercialization. A device with low PE consumes a huge amount of electrical power and is unwelcoming in an era when the concept of renewability is high in academic and industrial research. Despite considerable milestones in white OLED development, devices with appreciably high color rendering index, luminance, and PE still have a huge demand. Ma and coworkers adopted a new design concept using exciplexes as hosts to obtain high-performing wOLEDs by varying phosphorescent emitters [192]. In the multiple-EML wOLEDs, EML order influences the emission behavior of the devices. The authors selected mCBP:PO-T2T and 4PNPB:PO-T2T (Fig. 18) exciplex systems as the hosts for blue and yellow emitters, respectively, and fabricated two types of two-color white devices of Y + B and B + Y prototype. The investigation proved that the latter is more useful than the former in constructing wOLEDs. The different behavior of the devices that differ only in the arrangement order of the emission layers may have been due to exciton degradation by unwanted carrier recombination in the former

device. Then, the blue-orange two-color white OLEDs are fabricated, thereby yielding good efficiencies due to barrier-free charge injection into the EMLs. The authors continue to fabricate three- and four-color wOLEDs to make a breakthrough (Fig. 21). The resulting OLEDs have low turn-on voltages ($\sim 2.3 \text{ V}$) and exhibit a large EQE of 22.5 % and a particularly large PE of 79 lm W^{-1} , without any light out-coupling technique. The color rendering index of the devices is as high as 81, and the authors credited their success to their sagacious device selection.

Another research endeavor by Chen and coworkers is worth mentioning. The authors explored the combination of mCP and B4PyPPM as the universal exciplex host for multicolor phosphorescent dopants and, finally, white OLED [193]. The emission spectrum of a 1:1 blend film of mCP and B4PyPPM shows a peak at 448 nm because of the exciplex. The triplet energy of the exciplex system is sufficient to host the dopants, such as Flrpic (blue), Ir(ppy)₃ (green), PO-01 (orange), and (MDQ)₂Ir(acac) (red). The subsequent one-color OLEDs deliver maximum EQE of 20.1 %, 26.3 %, 24.6 %, and 19.8 %, respectively, which are appreciably higher than those obtained from single host-based devices. Then, two-color white OLEDs are fabricated using Flrpic and PO-01 as the emitters. The concentration of the blue dopant (Flrpic) is fixed at 12 wt%, and that of the orange dopant (PO-01) is varied to comprehend the effect of the orange dopant on device performance. The relevant device performance is presented in Fig. 22, which clearly shows that the current densities of the devices are nearly independent of the doping concentration, perhaps because of negligible charge trapping in the exciplex host system. However, the device efficiencies change with the doping concentration of the orange dopant, and the highest efficiencies (21.7 %, 66.4 cd A^{-1} , 73.6 lm W^{-1}) are realized at a concentration of 5 wt%. The authors attributed the high device performance to balanced charge transport in the host and multiple energy transfer pathways between the host and the dopants.

Lee et al. reported another exciplex system containing TPBi and a bipolar boryl compound (TPAPB, Fig. 18) [194]. The 1:1 blend film of TPAPB and TPBi has an emission centered around 470 nm with a PLQY of 44 %. A subsequent blue OLED using this exciplex as the emitter displays an EQE of 7 %. Moreover, the blended film shows good bipolar transporting properties due to the effective hole and electron transport properties of the constituents, paving the way to explore the exciplex system as the host. Then, the authors continued to prepare orange PhOLED by doping 4 wt% Ir(2-phenylpyridine)₃ (Fig. 18) in the exciplex host, which exhibits good efficiencies (49.5 cd A^{-1} , 44.3 lm W^{-1} , 18.5 %). Finally, the authors constructed wOLED employing the exciplex system as the emitter and as the host for orange phosphorescent dopant. The relevant device exhibits warm white emission with a spectral characteristic distributed over the entire visible spectrum and displays excellent efficiencies without using any out-coupling enhancement technique (29.6 lm W^{-1} , 42.5 cd A^{-1} , 15.7 %).

Electrical excitation of p-n co-deposited films can result in the formation of either exciplexes, electroplexes, or both. These excited-state complexes are slightly different from one another in terms of the attraction among the components, which is strong in exciplexes. The exciplex formation is perceived both under photonic and electrical excitations. However, electroplexes are observed only under EL conditions [195]. Although some publications with electroplexes as the central concept can be found, the OLED community has consistently avoided electroplexes because of poor emission quantum yield and challenges in controlling the electroplex formation. The articles in this area describing electroplexes as the hosts are few [196]. However, broad emission of the electroplexes can be beneficial for achieving white light, and they can be utilized as hosts, like the exciplexes. Lou et al. worked in this direction and developed a hybrid wOLED by controlling exciplex and electroplex formation between TAPC:TmPyPB donor-acceptor pair [197]. Both the single- and two-emitter OLEDs are fabricated by employing the electroplex system as the host and (dmppy)₂Ir(dpp) and Ir(piq)₃ (Fig. 14) as the dopants. The single-emitter device exhibits high efficiency of 16.8 % (56.4 lm W^{-1}) and low-efficiency roll-off. The two-emitter wOLED is

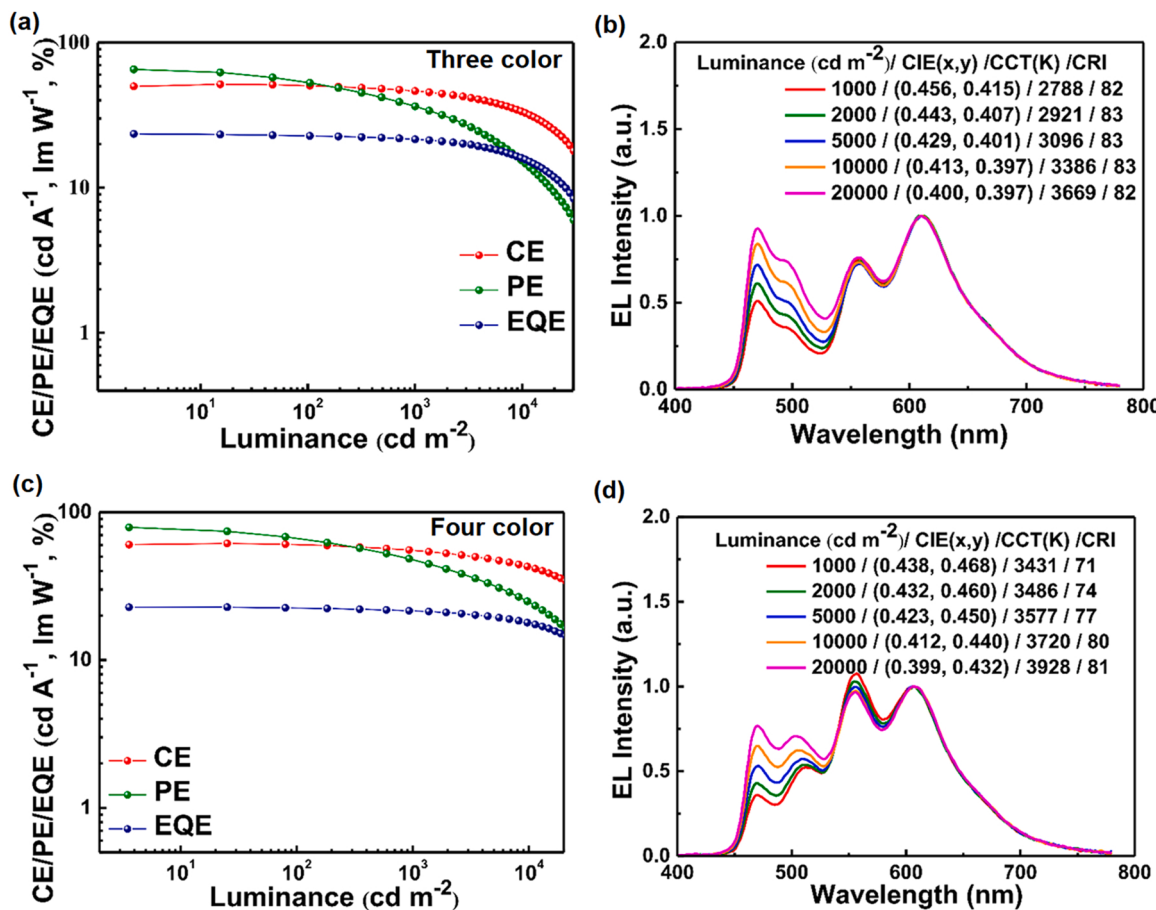


Fig. 21. EL characteristics of the (a)-(b) three-color wOLEDs and (c)-(d) four-color wOLEDs.
Reproduced with permission from [192], Copyright 2019. American Chemical Society.

also efficient (15.1 %, 28.2 lm W⁻¹) with the lowest correlated color temperature (CCT) of 2319 K and highest CRI of 92.1 among the doping-free (DF) wOLEDs.

The DF technology has become a favorable approach because this strategy potentially leads to simplified fabrication procedures and, consequently, lessened production costs. The blue emitter is an essential component for the wOLEDs. However, blue emission manipulation is always a difficult task, particularly for hybrid wOLEDs. Luo et al. reported DF-wOLEDs by managing a blue exciplex system without introducing a blue single molecular emitter for wOLEDs [198]. The blue exciplex system (*m*-MTDATA:TAZ (Fig. 18)) is initially combined with the orange phosphor, (fbi)₂Ir(acac) (Fig. 18), and then with the yellow phosphor, (dmppy)₂Ir(dpp) (Fig. 18), for improved performance to realize DF-wOLEDs without blue single molecular emitters and to achieve the white emission. They found that the device with a yellow emitter displays good performance with an EQE of 9.9 % and a CRI of 53 at 1000 cd/m². CRI and CCT are two important parameters to evaluate the quality of light emanating from wOLEDs. Thus, another device is fabricated using two thin layers of red Ir(pic)₃ and yellow Ir(dmppy)₂(dpp) iridium complexes together with the *m*-MTDATA:TAZ exciplex system. The device displays a maximum EQE of 11.3 %, CE of 20.9 cd A⁻¹, PE of 23.5 lm W⁻¹, CRI of 85, and CCT of 2376 K, suggesting its potential application for indoor lighting. Ma and coworkers fabricated high-efficiency and high-CRI phosphorescent white OLEDs by inserting phosphorescent dopants emitting three different colors into different locations of exciplex EML. The relevant dopants are Flrpic (Fig. 2, blue), Ir(ppy)₂(acac) (Fig. 10, green), and RD071 (Fig. 18, red). mCBP and PO-T2T are employed as the exciplex-forming components. Thus, the wOLED exhibits maximum EQE, CE, and PE of 21.1 %, 36.4 cd

A⁻¹, and 46.0 lm W⁻¹, respectively [199]. In another report, Liu et al. designed non-doped wOLED by combining the blue-emitting exciplex mCP:PO-T2T with the orange-red emitter (pq)₂Ir(acac) (Fig. 14). In the subsequent OLED, an ultra-thin layer of the phosphor is inserted at both sides of the exciplex. The group tested both the doped and non-doped devices. The latter exhibits reduced efficiency roll-off. The device efficiency and spectra of the non-doped device are modulated by the thickness of the ultra-thin phosphorescent layer. The relevant report indicated an EQE ranging from 15 % to 22 %, PE from 33 lm W⁻¹ to 47 lm W⁻¹, and CCT from 1600 K to 2600 K. The authors believed that efficient charge trapping and recombination contribute to the excellent performance of the pertinent devices [200]. Wang et al. reported a series of four-color hybrid wOLEDs by incorporating three ultra-thin green, orange, and red phosphorescent layers with a blue-exciplex emission layer (TCTA:TPBi). The authors believed that the location of the exciplex layer can alter the energy transfer path that would modify the spectrum and the CRI. An optimized hybrid wOLED delivers a high CRI of 97 at a luminance of 6000 cd m⁻² [201].

Lavrentovich et al. presented a unique interface engineering approach for the fabrication of efficient wOLEDs by inserting a layer with different thicknesses (100 nm vs 4 nm) of an ambipolar red emissive compound (bThBODIPY, Fig. 18) between layers of PPT and *m*-MTDATA (exciplex formation region) [202]. Compared with the device employing a thin bThBODIPY layer, the device with a thick bThBODIPY layer has a superior performance. The device with a thick bThBODIPY layer has CIE 1931 coordinates of (0.49, 0.42), high brightness (28, 829 cd m⁻²), PE of 4.75 lm W⁻¹, and maximum EQE of 6.8 %, whereas the device employing a thin bThBODIPY layer has a maximum EQE of 1.17 %, a brightness of 6579 cd m⁻² at 15 V, and PE of 1.2 lm W⁻¹ with

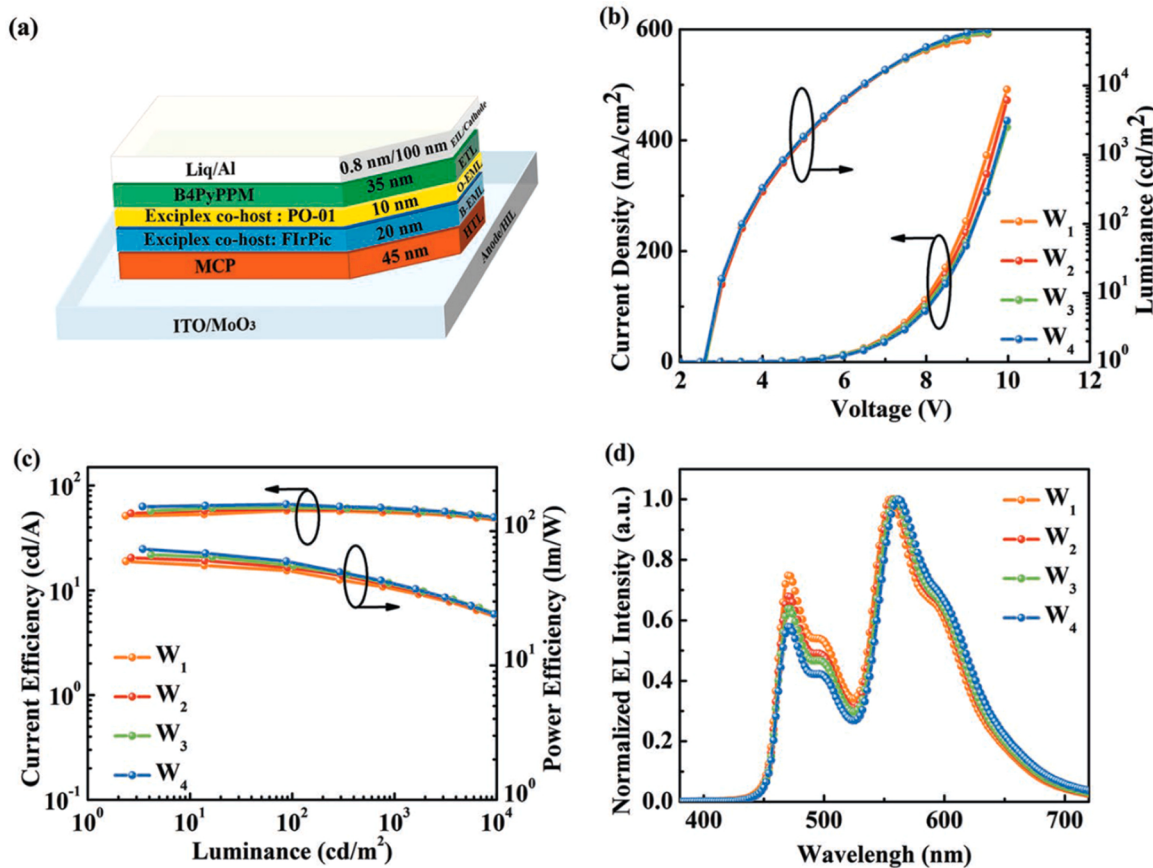


Fig. 22. Illustration of various device data of the two-color wOLEDs hosted by mCP:B4PyPPM exciplex system. The devices W1–W4 differ from one another by the doping concentration of the orange dopant and correspond to the concentrations of 0.8 %, 1.5 %, 3 %, and 5 %, respectively. Reproduced with permission from reference [193] Copyright 2019. John Wiley and Sons.

CIE 1931 coordinates of (0.39, 0.35). The enhanced device characteristics are most likely due to the effective recombination of holes and electrons in the transport layers in addition to the relatively high PLQY of bThBODIPY in solid-state. However, compared with the device with a high EQE, the device with a low EQE is more stable over a wide range of working current densities with almost negligible efficiency roll-off, thereby making it an efficient wOLED system.

Chen *et al.* reported the combination of a donor *N*-([1,1'-biphenyl]-2-yl)-*N*-(9,9-dimethyl-9*H*-fluoren-2-yl)-9,9'-spirobi[fluoren]-4-amine (FSF4A, Fig. 18) and an acceptor PO-T2T to form a new exciplex-forming system, which can be utilized as cohost to fabricate high efficiency red PhOLED upon doping with 3 wt% of Ir(MDQ)₂(acac) (Fig. 14) [203]. The exciplex cohosted red (EL $\lambda_{\text{max}} = 612 \text{ nm}$) PhOLED exhibits an ultralow turn-on voltage of 1.95 V, a maximum power efficiency of 38.5 lm W⁻¹, an EQE_{max} of 17.3 %. Then, an ultra-thin Flrpic layer was incorporated into the red device to make a wOLED with EQE_{max} = 12.4%, a low turn-on voltage of 2.2 V, a maximum power efficiency of 34.1 lm W⁻¹, and the (CIE) coordinate (0.33, 0.33) at 1000 cd m⁻². Fung *et al.* reported an interesting strategy of using multiple exciplex cohosts for phosphorescent dopants to achieve highly efficient wOLEDs [204]. The EML of the three-color wOLED with EQE_{max} up to 27 % comprises a three-layer structure of 26DCzPPy:B4PyMPM:Flrpic (1:1:15 %, 10 nm)/CDBP:B4PyMPM:Ir(ppy)₂(acac) (1:1:4 %, 2 nm)/CDBP:B4PyMPM:Ir(MDQ)₂(acac) (1:1:4 %, 5 nm) (Fig. 8). The suitable matching of the triplet energy between the exciplex host and phosphorescent dopant is very important. In this case, the higher T₁ energy exciplex 26DCzPPy:B4PyMPM blend can use to host Flrpic, whereas the lower energy exciplex CDBP:B4PyMPM can accommodate green and red phosphors. Very recently, Miao and Huang *et al.* reported an excellent bipolar deep-blue emissive acceptor 2-(4-(3-(3-(4,6-diphenyl-1,3-

5-triazin-2-yl)phenyl)-9*H*-carbazol-9-yl)phenyl)benzo[d]oxazole (OCT, Fig. 18) that can form green (524 nm) and orange-red (596 nm) exciplex with TAPC and *m*-MTDATA, respectively [205]. The wide emission feature of exciplex-forming system is highly suitable for developing high-color-quality white OLEDs.

Indeed, the integration of the intrinsic blue emission from OCT and complementary green and orange-red exciplex emissions, a wOLED was achieved with a record-high color-rendering index (CRI) of 97 among the three-color-based wOLEDs. In summary, the exciplex-based wOLEDs have gained pace in recent years because of their potential to deliver excellent device efficiency. Although substantial progress has been made in this area, many challenges remain, including those on efficiency, efficiency roll-off, PE, operational stability, and luminance. These challenges must be overcome before the commercialization of white light-emitting panels based on OLEDs.

5. Exciplex-based, solution-processed OLEDs

Any technology is a fine-tuned balance between possibility and practicability, and the OLEDs are no exception. Commercialization demands low device manufacturing costs and optimized output efficiency. The two most widely used device fabrication technology for OLEDs are vacuum deposition and solution process, each of which has its advantages and disadvantages. The solution processes, such as spin coating, inkjet printing, roll-to-roll coating, and spray coating, are low-cost options for the vacuum deposition technique and have the possibility of producing large-area devices at a low expense. Because of practicability, vacuum-deposited multilayer devices offer superior efficiency to solution-processed devices, although at a considerably high cost. Thus, most of the commercialized OLED panels currently use the vacuum

deposition device fabrication technique. Nevertheless, the solution process technology has become increasingly popular, and considerable research attention has been paid to making breakthroughs in this area. Like the vacuum-deposited devices, the solution-processed devices have multilayer structures that aid charge injection, transportation, and recombination, leading to the enhancement of device efficiency and stability [206].

As mentioned earlier, high PE is a paramount criterion for practical application of the OLEDs, thereby posing a major challenge to the solution-processed devices. The PE of solution-processed OLEDs is defined by the following equation:

$$\eta_{PE} = \frac{K_r E_{ph}}{e} \times \frac{\eta_{ext}}{V},$$

where K_r is the radiative luminous efficiency, E_{ph} is the average photon energy, and V is the driving voltage. Thus, the PE is directly proportional to the EQE and inversely proportional to the driving voltage. The exciplex host systems are proved to offer driving voltage lower than that of the other conventional host counterparts, and this scenario has prompted the research community to test exciplex systems in solution-processed OLEDs to achieve a high PE. [207].

Another challenge is device fabrication. The multilayer device structure has a high demand, as the role of each layer in device efficiency can be individually tuned. In the vacuum-deposited OLEDs, each layer is deposited seamlessly on top of others by thermal evaporation in a programmed manner. On the contrary, the multilayer device fabrication for solution-processed OLEDs must take care of interdiffusion and intermixing of the layers, complicating a simple technology. A detailed discussion on the device fabrication of solution-processed OLEDs is beyond the scope of the present article; hence, the readers are encouraged to go through an excellent recent review article on the topic published by Wang *et al.* [207]. In this section, we systematically review the research endeavors to obtain highly efficient solution-processed, exciplex-based OLEDs. The relevant device data are summarized in Table 4, and the relevant chemical structures are summarized in Figs. 23 and 26.

5.1. Exciplexes as the emitters

Efficient solution-processable exciplex emitters are sought after to construct low-cost OLEDs. The TADF materials are promising candidates in this case, but all solution-processed blue TADF OLEDs have been rarely achieved because of the critical role played by the molecular design. Ban *et al.* attempted to address the problem by synthesizing a series of TADF emitters X-4CzCN (Fig. 23) in which bulky substituents are introduced to the TADF emitting core through unconjugated linkers [208]. Therefore, the solubility of the materials is enhanced without affecting the TADF emitting feature. Moreover, the end-capping groups hinder the triplet-triplet and triplet-polaron quenching by separating the energy transfer and charge-transporting channels. The photoluminescent quantum efficiency of the materials varies with the alteration of end-capping groups. The authors predicted that the large volume of the peripheral units would hypsochromically shift the EL spectra, simultaneously enhancing the energy transfer of exciplex and inhibiting the energy leakage of the electromer. Therefore, solution-processed blue OLEDs using these materials achieve low turn-on voltage (2.9 V), high EQE (20.6 %), and CIE of 0.16, 0.27.

Comparable device efficiency from solution-processed OLEDs with that from vacuum-deposited devices is an important goal. Colella *et al.* reported solution-processed TADF exciplex OLED based on TAPC as the donor and a bipolar material DCz-DBTO2 (Fig. 23) as the acceptor [209]. The exciplex system based on these materials in a co-evaporated film (30 wt% of DCz-DBTO2 in TAPC) harvests nearly 100 % of the triplet excitons by TADF and has a PLQY higher than 50 %. Another advantage of using this exciplex system is the good solubility of the components in chlorinated solvents, such as chloroform and

chlorobenzene. The optimized solution-processed OLED exhibits a maximum EQE of 8.9 % (27.5 cd A⁻¹, 16.5 lm W⁻¹) with luminance higher than 4000 cd m⁻². These values are close to those of a vacuum-deposited OLED using the same exciplex system.

The majority of the research groups tend to demonstrate exciplex formation among small molecular systems, as they are easy to evaporate thermally. However, these small molecular systems are consistently avoided in the solution process because of the challenge they pose to casting a high-quality film. On the contrary, exciplex systems out of TADF polymers offer the efficient triplet-harnessing ability and are suitable for device fabrication by printing technologies. Pander *et al.* explored an exciplex system based on a polymer small molecule PVK as the donor and PO-T2T as the acceptor, and the concerned OLED displays a maximum EQE of 4.5 % [210].

In another article, Zhao *et al.* demonstrated exciplex-based solution-processed OLED using PO-T2T as the acceptor and a triphenylamine-containing bipolar material TPA-3 (Fig. 23) as the donor. The green emission from the TPA-3:PO-T2T film is accompanied by a small singlet-triplet gap and TADF character. The relevant solution-processed OLED exhibits a maximum EQE of 14.4 % [211]. The authors introduced two other donors, 3CzFDPhTz and 9PhFDPhTz (Fig. 23), to form exciplexes with PO-T2T and further improve the device efficiency. These ternary exciplex systems have RISC higher than that of traditional exciplexes, and the pertinent solution-processed exciplex OLED reaches a high EQE of 24 %. The authors determined that the ternary exciplexes are responsible for this scenario, and they were interested to explore the reason. Simplified energy level diagrams of the traditional and ternary exciplexes are shown in Fig. 24, which reveals extra RISC channels in the latter. The authors suggested that the extra upconversion channels in the ternary exciplexes mitigate the unwelcomed quenching processes, such as TTA, triplet-polaron annihilation, and singlet-triplet annihilation, which boost device efficiency.

This idea is further extended to ternary polymer-based exciplex OLED by the same group. The authors described that introducing a small donor molecule into the polymer matrix would change the scenario of exciplex formation [212]. This scenario is illustrated in Fig. 25. Two exciplexes would be expected now, that is, between the foreign donor and the acceptor and between the polymer and the acceptor. The former would have higher excitation energy than the latter, and the formation of this high-energy exciplex would be guided by strong intermolecular interaction among the small molecules. This scenario would open a new triplet harnessing channel, which would be completed by the energy transfer from the high-energy exciplex to the other. The authors predicted that the ternary system would assist excellent film-forming ability and film stability without the need for additional material. Based on these assumptions, the authors continued to investigate the PVK:PO-T2T:mCP ternary system, which turned out to be promising. The mCP:PO-T2T exciplex system has higher energy than the PVK:PO-T2T system. Thus, the emission of the ternary system is primarily due to the latter. The relevant ternary system has a high PLQY of 82 % and offers an EQE of as high as ~22 %.

In addition to use polymer as exciplex-forming component, Ban *et al.* reported an intriguing homojunction exciplex (ho-exciplex) forming system by linking the donor (CzTPA, Fig. 23) and acceptor (PhTRZ, Fig. 23) moieties, that are capable of forming exciplex by physically blending method, into a single molecule PhTRZ-CzTPA (Fig. 23) [213]. The solution-processed devices employing PhTRZ-CzTPA as a single component for exciplex-forming EML or host for green phosphorescent dopant achieved comparable electroluminescence characteristics with the devices using conventional CzTPA:PhTRZ blend. The superior solvent resistance to isopropanol of PhTRZ-CzTPA makes a better material for fully-solution-processed device. In addition, Burn and Pivrikas *et al.* recently reported three new oxadiazole-based acceptors deriving from the benchmark molecule OXD-7 for exploring their capability of forming exciplex with a typical donor *m*-MTDATA [214]. These new oxadiazole-based acceptors exhibit higher electron mobility as compared

Table 4

Device data table – exciplex based solution-processed OLEDs (the values in the parenthesis indicate data at 1000 nit).

Device structure (the exciplex component is underlined)	Φ_{film} (%)	V_{on} (V)	λ_{EL}^{max} (nm)	EQE (%)	CE (cd A $^{-1}$)	PE (lm W $^{-1}$)	CIE	Ref
ITO/PEDOT:PSS (20 nm)/MeCz-4CzCN (60 nm)/PHPO (40 nm)/Cs ₂ CO ₃ (2 nm)/Al (100 nm)	53.0	2.9	486	21.8 (19.0)	46.5	35.6	0.17, 0.35	[208]
ITO/PEDOT:PSS (20 nm)/PhCz-4CzCN (60 nm)/PHPO (40 nm)/Cs ₂ CO ₃ (2 nm)/Al (100 nm)	62.0	2.9	475	20.6 (18.2)	40.8	27.5	0.16, 0.27	[208]
ITO/PEDOT:PSS (20 nm)/PhDCz-4CzCN (60 nm)/PHPO (40 nm)/Cs ₂ CO ₃ (2 nm)/Al (100 nm)	65.0	3.1	465	10.0 (7.9)	18.9	11.2	0.19, 0.28	[208]
ITO/PEDOT:PSS (40 nm)/3:7 DCz-DBTO2:TAPC (60 nm)/TPBi (40 nm)/LiF (1 nm)/Al (100 nm)	—	5.5	—	8.9	27.5	15.0	—	[209]
ITO/HIL 1.3 N (45 nm)/PVKH (10 nm)/6:4 PVK:PO-T2T (27 nm)/PO-T2T (50 nm)/LiF (0.8 nm)/Al (100 nm)	20.0	4.9	510	4.5	13.3	—	—	[210]
ITO/PEDOT:PSS (30 nm)/TPA-3:PO-T2T (35 nm)/PO-T2T (55 nm)/LiF (0.8 nm)/Al (80 nm)	—	3.9	519	14.4 (11.0)	49.1 (37.3)	33.4 (20.0)	—	[211]
ITO/PEDOT:PSS (30 nm)/TPA-3:3CzFDPhTz/PO-T2T (35 nm)/PO-T2T (55 nm)/LiF (0.8 nm)/Al (80 nm)	—	3.1	524	18.8 (8.9)	63.0 (29.6)	43.0 (16.3)	—	[211]
ITO/PEDOT:PSS (30 nm)/TPA-3:9PhFDPhTz/PO-T2T (35 nm)/PO-T2T (55 nm)/LiF (0.8 nm)/Al (80 nm)	—	3.1	524	24.0 (10.1)	78.2 (32.7)	61.4 (24.7)	—	[211]
ITO/PEDOT:PSS (30 nm)/1:3 PVK:mCP (35 nm)/PO-T2T (45 nm)/LiF (0.8 nm)/Al (80 nm)	82.0	4.1	514	21.6	64.7	45.2	0.26, 0.51	[212]
ITO/PEDOT:PSS (10 nm)/CzTPA: PhTRZ (35 nm)/PhPO (40 nm)/Cs ₂ CO ₃ (1 nm)/Al	68	3.1	532	0.06	0.21	0.11	0.36, 0.55	[213]
ITO/PEDOT:PSS (10 nm)/CzTPA-PhTRZ (35 nm)/PhPO (40 nm)/Cs ₂ CO ₃ (1 nm)/Al	67	2.8	526	4.5	13.9	14.5	0.35, 0.55	[213]
ITO/PEDOT:PSS (10 nm)/20 % Ir(mppy) ₃ in CzTPA: PhTRZ (35 nm)/PhPO (40 nm)/Cs ₂ CO ₃ (1 nm)/Al	—	3.2	—	0.03	0.09	0.05	0.31, 0.58	[213]
ITO/PEDOT:PSS (10 nm)/20 % Ir(mppy) ₃ in CzTPA- PhTRZ (35 nm)/PhPO (40 nm)/Cs ₂ CO ₃ (1 nm)/Al	—	2.4	—	8.0	25.7	20.2	0.31, 0.61	[213]
ITO/(PEDOT:PSS) (30 nm)/3:5 m-MTDATA:1 (40 nm)/ TmPyPB (80 nm)/(LiF) (1 nm)/(Al) (100 nm)	—	2.5	—	5.3 (0.3)	15.5	17.5	0.40, 0.55	[214]
ITO/(PEDOT:PSS) (30 nm)/3:5 m-MTDATA:2 (40 nm)/ TmPyPB (80 nm)/(LiF) (1 nm)/(Al) (100 nm)	—	3.0	—	1.8	4.2	4.4	0.49, 0.50	[214]
ITO/(PEDOT:PSS) (30 nm)/3:5 m-MTDATA:3 (40 nm)/ TmPyPB (80 nm)/(LiF) (1 nm)/(Al) (100 nm)	—	3.1	—	1.2	4.0	3.9	0.49 0.49	[214]
ITO/(PEDOT:PSS) /1:1 PFB:F8BT (<80 nm)/Al (50 nm)	—	4.0	—	1.6	—	—	—	[215]
ITO/PEDOT:PSS (40 nm)/15 wt% Flrpic in TCTA:2PO (20 nm)/ TmPyPB (40 nm)/Liq (2 nm)/Al (120 nm)	—	—	—	14.6	29.2	—	—	[216]
ITO/PEDOT:PSS (40 nm)/15 wt% Flrpic in TCTA:3PO (20 nm)/ TmPyPB (40 nm)/Liq (2 nm)/Al (120 nm)	—	—	—	12.2	26.8	—	—	[216]
ITO/PEDOT:PSS (25 nm)/10 wt% Flrpic in 1:1 TAPC:POPH (35 nm)/TPBI (35 nm)/Ca (10 nm)/Ag	—	3.4	—	—	6.3 (6.2)	3.4	0.17, 0.38	[217]
ITO/PEDOT:PSS (25 nm)/10 wt% Flrpic in 1:1 TCTA:POPH (35 nm)/TPBI (35 nm)/Ca (10 nm)/Ag	—	2.7	—	—	25.8 (24.5)	22.5	0.15, 0.32	[217]
ITO/PEDOT:PSS (25 nm)/10 wt% Flrpic in 1:1 mCP:POPH (35 nm)/TPBI (35 nm)/Ca (10 nm)/Ag	—	4.4	—	—	13.5 (11.5)	6.0	0.15, 0.35	[217]
ITO / PEDOT:PSS /10 wt% Flrpic in 1:1 TCTA:TPBi /TmPyPB /Cs ₂ CO ₃ /Al	—	3.9	—	8.9 (8.2)	18.1 (16.7)	9.2	0.16, 0.34	[218]
ITO / PEDOT:PSS /10 wt% Flrpic in 1:1 TCTA:TPOB /TmPyPB /Cs ₂ CO ₃ /Al	—	2.8	—	13.8 (13.7)	28.2 (28.1)	22.0	0.15, 0.33	
ITO/PEDOT:PSS (35 nm)/PVK (15 nm)/5 wt% B2 in 1:1 TCTA:TPBi (30 nm)/TPBi (40 nm)/Ca (8 nm)/Al (100 nm)	—	—	451	3.7	5.1	—	0.17,0.18	[219]
ITO/PEDOT:PSS (40 nm)/40 nm)/10 wt% Flrpic in 1:3 Ph-O-TCTA:PhPO (60 nm)/TPBI (40 nm)/Cs ₂ CO ₃ (2 nm)/Al	89.1	—	—	16.5	33.6	20.6	—	[220]
ITO/PEDOT:PSS (40 nm)/10 wt% Flrpic in 1:1 TCTA:PhPO (60 nm)/TPBI (40 nm)/Cs ₂ CO ₃ (2 nm)/Al	50.2	—	—	9.0	20.1	10.1	—	[220]
ITO/PEDOT:PSS (40 nm)/10 wt% 5TCzBN in 1:3 Ph-O-TCTA:PhPO (60 nm)/TPBI (40 nm)/Cs ₂ CO ₃ (2 nm)/Al	81.5	—	—	15.2	35.3	21.6	—	[220]
ITO/PEDOT:PSS (40 nm)/10 wt% oPTBC in CBP (40 nm)/PO-T2T (60 nm)/LiF (1 nm)/Al (100 nm)	—	3.0	548	16.2 (13.0)	53.4 (42.5)	41.9 (25.2)	0.40, 0.56	[221]
ITO/PEDOT:PSS (40 nm)/10 wt% oPTBC in 1:1 CBP:PO-T2T (40 nm)/PO-T2T (60 nm)/LiF (1 nm)/Al (100 nm)	—	4.3	544	11.5 (10.6)	38.5 (35.5)	20.8 (17.4)	0.38, 0.56	[221]
ITO/PEDOT:PSS (40 nm)/10 wt% 4CzIPN in CBP (40 nm)/PO-T2T (60 nm)/LiF (1 nm)/Al (100 nm)	—	2.9	532	20.0 (13.3)	67.2 (44.1)	62.1 (29.1)	0.35, 0.58	[221]
ITO/PEDOT:PSS (40 nm)/10 wt% 4CzIPN in 1:1 CBP:PO-T2T (40 nm)/PO-T2T (60 nm)/LiF (1 nm)/Al (100 nm)	—	4.0	528	18.1 (14.9)	59.9 (49.4)	37.6 (25.9)	0.34, 0.58	[221]
ITO/PEDOT:PSS (40 nm)/H2:10 wt% tBuCzDBA (30 nm)/ B4PyMPM (60 nm)/LiF (1 nm)/Al (150 nm)	—	2.5	548	20.0	69.0	69.9	0.40, 0.57	[222]
ITO/PEDOT:PSS (40 nm)/H2:10 wt% tBuCzDBA (30 nm)/ B3PyMPM (60 nm)/LiF (1 nm)/Al (150 nm)	—	2.5	548	26.4	85.5	95.0	0.42, 0.55	[222]
ITO/PEDOT:PSS (40 nm)/PVK (20 nm)/18 wt% t4CzIPN in 1:1 P(Bn-DPAc):tPTRZ (15 nm)/TPBi (40 nm)/LiF (0.8 nm)/Al (100 nm)	—	3.5	—	31.2	107.3	84.3	0.33, 0.60	[223]
ITO/PEDOT:PSS (40 nm)/1 wt% Ir(Flpy-CF ₃) ₃ in m-MTDATA (40 nm)/TmPyPB (55 nm)/LiF (0.5 nm)/Al (100 nm)	—	2.3	—	25.2 (23.7)	74.3 (70.1)	97.2 (72.5)	0.52, 0.47	[225]
ITO/PEDOT:PSS (40 nm)/1 wt% Ir(Flpy-CF ₃) ₃ in 1:1 m-MTDATA:TmPyPB (40 nm)/TmPyPB (55 nm)/LiF (0.5 nm)/Al (100 nm)	—	4.1	—	19.5 (18.3)	57.6 (53.9)	35.2 (29.1)	0.52, 0.47	[225]

(continued on next page)

Table 4 (continued)

Device structure (the exciplex component is underlined)	Φ_{film} (%)	V_{on} (V)	λ_{EL}^{max} (nm)	EQE (%)	CE (cd A ⁻¹)	PE (lm W ⁻¹)	CIE	Ref
ITO/PEDOT:PSS (40 nm)/3 wt% (DPA-Flpy-CF ₃) ₂ Ir(acac) in m-MTADATA (40 nm)/TmPyPb (50 nm)/LiF (1 nm)/Al (100 nm)	—	2.3	606	19.3	32.4	44.5	0.64, 0.36	[226]
ITO/PEDOT:PSS (60 nm)/5:50:45 (pq) ₂ Ir(acac):m-MTADATA:DPIQ (60 nm)/TmPyPB (60 nm)/LiQ (1 nm)/Al (100 nm)	—	3.4	596	13.1 (11.6)	25.3 (21.9)	23.9 (10.9)	—	[227]
ITO/PEDOT:PSS (60 nm)/5:50:45 (pq) ₂ Ir(acac):m-MTADATA:SFIQ (60 nm)/TmPyPB (60 nm)/LiQ (1 nm)/Al (100 nm)	—	3.4	596	13.4 (11.8)	24.8 (22.4)	18.4 (11.3)	—	[227]
ITO/PEDOT:PSS (60 nm)/5:50:45 (pq) ₂ Ir(acac):m-MTADATA:DM-DHAIQ (60 nm)/TmPyPB (60 nm)/LiQ (1 nm)/Al (100 nm)	—	3.6	596	14.1 (12.2)	26.6 (22.6)	19.3 (11.2)	—	[227]
ITO/PEDOT:PSS (60 nm)/5:50:45 (piq) ₂ Ir(acac):m-MTADATA:SXIQ (60 nm)/TmPyPB (60 nm)/LiQ (1 nm)/Al (100 nm)	—	3.1	596	10.6 (9.6)	20.3 (18.3)	15.9 (9.5)	—	[227]
ITO/HIL 1.3 N (45 nm)/5 wt% Pt ₂ (bis-dthpym)(dpm) ₂ in 7:3 TCTA:PO-T2T (5 nm)/PO-T2T (50 nm)/LiF (0.8 nm)/Al	—	10.3	—	0.8	—	—	—	[229]
ITO/HIL 1.3 N (45 nm)/PVKH (10 nm)/5 wt% Pt ₂ (bis-dthpym)(dpm) ₂ in 3:2 TPD:PBD (5 nm)/TPBi (50 nm)/LiF (0.8 nm)/Al (100 nm)	—	5.6	—	3.6	—	—	—	[229]
ITO/PEDOT:PSS(40 nm)/10 wt% Flpic + 0.2 wt% (fbi) ₂ Ir(acac) in 1:1 TCTA:TPO (35 nm)/TmPyPB(40 nm)/Cs ₂ CO ₃ (2 nm)/Al (100 nm)	—	3.0	—	—	38.5	22.5	0.34, 0.41	[230]
ITO/PEDOT:PSS (25 nm)/1: 0.3: 0.15 (TPAF)3:OXD-7:Flpic (40 nm)/CBP (15 nm)/TPBI (35 nm)/Ca (10 nm)/Ag	—	5.4	—	5.3 (4.4)	22.6	—	0.27, 0.32	[231]
ITO/PEDOT:PSS (30 nm)/PVK (15 nm)/25 wt% 4CzFCN + 0.6 wt% (MDQ) ₂ Ir(acac) in CDBP (30 nm)/PO-T2T (50 nm)/LiF (0.8 nm)/Al (100 nm)	—	4.1	—	20.8 (11.8)	—	31.3	0.33, 0.39	[232]
ITO/PEDOT:PSS (20 nm)/PCz-4CzCN + 0.9 wt% PO-01 (60 nm)/PHPO (40 nm)/Cs ₂ CO ₃ (2 nm)/Al (100 nm).	—	2.8	—	15.6 (15.4)	35.8	28.1	0.41, 0.49	[233]

to that of parent OXD-7. Among them, the solution-processed simple bilayer OLED employing the blend of 4-(2-ethylhexyloxy)phenyl-oxadiazole (1, Fig. 23):m-MTADATA as EML gave the best overall performance with EQE_{max} = 5.6 %.

Recently, Zhang *et al.* reported a solution-processed OLED employing the blend of two polymers poly(9,9'-dioctylfluorene-co-bis-N,N'-(4-butylphenyl)-bis-N,N'-phenyl-1,4-phenylene-diamine) (PFB, Fig. 23) and poly[(9,9-dioctylfluoren-2,7-diyl)-alt-(benzo[2,1,3]thiadiazol-4,8-diyl)] (F8BT, Fig. 23) as the EML exhibited a wide EL spectral coverage from the green (500 nm) to the near-infrared (900 nm) [215]. In addition to the original exciton from F8BT, primary F8BT:PFB exciplex emission, the electromer emission from folded PFB molecules, and a new exciplex state (secondary exciplex) generated by the interaction between exciplex and electromer states was proposed. This work represents an alternative means to achieve broadband light-emitting devices.

5.2. Exciplexes as the hosts

The fluorescent–phosphorescent hybrid device structure has recently been proved to be useful in solution-processed wOLEDs because of the operational stability of the blue fluorescence and the high efficiency of phosphorescence. TADF materials are particularly useful in this context because of the 100 % exciton harnessing the ability of the emitters. However, unlike the vacuum-deposited devices, which prefer small molecules because of their ease of sublimation, the solution-processed devices favor large molecules to endure spin coating of the next layer, where the materials to be deposited in layers are usually dissolved in orthogonal solvents. Appropriate end-capping groups must be selected to maintain the TADF character of the emitter, and they should be dispersed in a host like most other TADF devices.

5.2.1. Blue and green OLEDs

Zhang *et al.* reported two new phosphine oxide-based acceptor materials, 2PO and 3PO (Fig. 26), with wide band gap and high triplet energy to fabricate TADF exciplexes [216]. Two exciplex hosts, TCTA:2PO and TCTA:3PO, are successfully designed by blending these acceptors with TCTA, and emission from these exciplexes can be observed. The molar ratio of the donor to the acceptor in the films is kept at 1:1, and the exciplex emissions of TCTA:2PO and TCTA:3PO are observed at 472 nm and 482 nm, respectively, typically red-shifted compared with their counterparts. Given that 2PO and 3PO have high triplet energies, the resulting exciplexes can be used as the host for blue

phosphors. Solution-processed blue PhOLEDs based on these exciplex systems doped with the well-known phosphor Flpic are subsequently fabricated. The pertinent devices of 2PO and 3PO exhibit maximum EQEs of 14.6 % and 12.2 % with current efficiencies of 29.2 and 26.8 cd A⁻¹, respectively, and they display relatively low current efficiency roll-off values of 3.5 % and 0.4 %. These values are considered one of the best results in blue PhOLEDs with solution-processed exciplex hosts.

Sun *et al.* also achieved high-performance solution-processed blue PhOLEDs by using the energy transferred from an exciplex-type host. Three exciplex host systems, TAPC:POPH, TCTA:POPH, and mCP:POPH, are developed by mixing the well-known hole-transporting materials, TAPC, TCTA, and mCP, with a newly synthesized highly stable electron-transporting molecule, (5-terphenyl-1,3-phenylene)bis(diphenylphosphine oxide) POPH (Fig. 26), in a 1:1 molar ratio [217]. Of all the mixed host systems, the best result is obtained with the TCTA:POPH-based exciplex host and its pertinent solution-processed blue PhOLEDs (Flpic dopant) displays an extremely low turn-on voltage of 2.7 V, a high PE of 22.5 lm W⁻¹, and a low-efficiency roll-off, even with the luminance of up to 10000 cd m⁻². A solution-processed device structure is used for the first time to attain a turn-on voltage of blue PhOLEDs below 3 V with a maximum luminance of 40000 cd m⁻². Such a device performance demonstrates a balanced charge transfer and an effective exciton formation in exciplex-type hosts.

For power-efficient solution-processed PhOLEDs, Sun *et al.* demonstrated an exciplex-type host in a 1:1 molar blend consisting of TCTA and a new electron-transporting material, TPOB (Fig. 26) [218]. The solubility and EA of TPOB are enhanced by incorporating DPPO groups at the edge of the TPBI core, while the triplet energy leakage from the exciplex state of TCTA:TPOB to the individual molecules is also productively eliminated. Furthermore, the twisted configuration of the components imparts the exciplex with good film-forming ability. The TCTA:TPOB blend film emission is observed at 464 nm with a PLQY of 19.6 %. However, the Flpic-doped TCTA:TPOB blend exhibits a PLQY of 75.2 %, which indicates that the exciplex system is highly efficient and that it would serve as a good host material to sensitize the dopant in the PhOLEDs. Thus, solution-processed PhOLEDs based on this exciplex system realize an η_{ext} of 13.8 %, high PE of 22 lm W⁻¹, and a low turn-on voltage of 2.8 V. Moreover, the TCTA:TPOB-based device exhibits a low-efficiency roll-off with a current efficiency of 28.1 cd A⁻¹ at 1000 cd m⁻² and 23.8 cd A⁻¹ at 10,000 cd m⁻², thereby signifying stable charge carrier balance and broad recombination zone in the emission layer. Peng *et al.* have recently demonstrated a blue

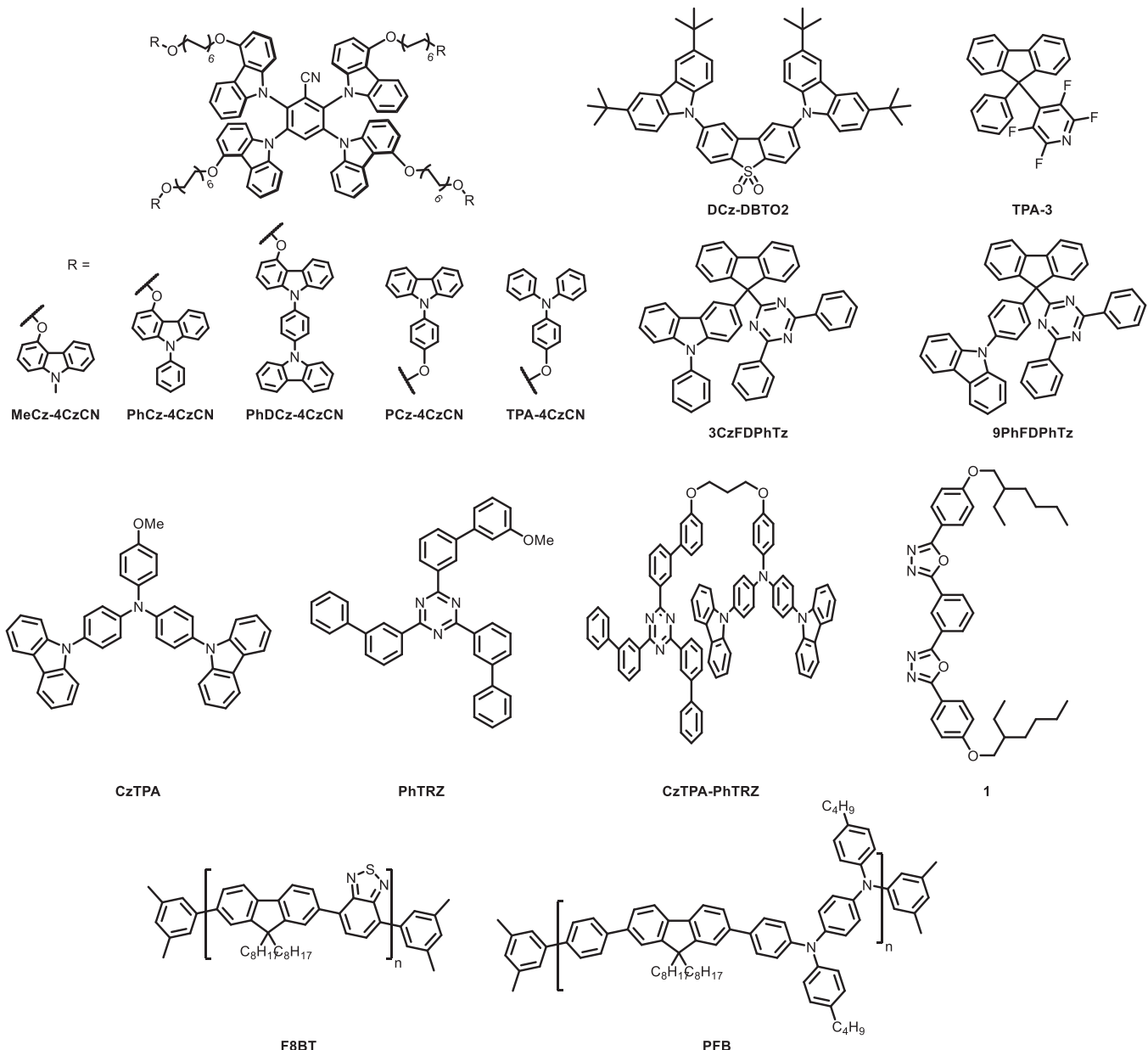


Fig. 23. Molecular structures of donor and acceptors that were used in solution-processed OLEDs with exciplexes as the emitters.

solution-processed exciplex OLED based on TCTA:TPBi that achieves an EQE of 3.7 % [219].

Feng *et al.* reported a modified TCTA analog, Ph-O-TCTA (Fig. 26), and solution-processed OLEDs based on it [220]. In this molecule, three TCTA units are connected to a benzene 1,3,5-triol core by nonconjugated alkyl chains. This design strategy helps authors improve the solubility of TCTA while simultaneously maintaining its intrinsic properties. Tris(4-(diphenyl phosphoryl)phenyl) benzene (PhPO, Fig. 26) is chosen as the acceptor, and the Ph-O-TCTA:PhPO exciplex system is employed as the host for blue phosphorescent dopant (FIrpic, Fig. 2) in a solution-processed device. The relevant device achieved a high EQE of 16.5% (33.6 cd A⁻¹, 20.6 lm W⁻¹), which is higher than that of the device based on the TCTA:PhPO exciplex host (9.0%, 20.1 cd A⁻¹, 10.1 lm W⁻¹). Furthermore, a solution-processed blue fluorescent OLED based on this host and 5TCzBN (Fig. 26) as the dopant offers excellent device output (15.2%, 35.3 cd A⁻¹, 21.6 lm W⁻¹).

Yang *et al.* reported a green solution-processed TADF OLED using CBP:PO-T2T as the exciplex host and oPTBC (Fig. 26) as the TADF

emitter [221]. The relevant device enjoys barrier-free carrier injection and effective energy transfer and offers a low turn-on voltage of 3.0 V and excellent efficiency (16.2 %, 53.4 cd A⁻¹, 41.9 lm W⁻¹). These values are better than those from the devices based on bulk CBP:POT2T and single CBP hosts. Another solution-processed device using 4CzIPN as the emitter (Fig. 8) yields a low turn-on voltage of 2.9 V, high maximum current, power, and external quantum efficiencies of 67.2 cd A⁻¹, 62.1 lm W⁻¹, and 20.0 %, respectively.

Wang *et al.* recently reported the use of a dendritic oligocarbazole donor (H2, Fig. 26) mixing with two pyridine-containing isomeric acceptors B4PyMPM (Fig. 8) and B3PyMPM (Fig. 2), respectively, to explore new exciplex-forming systems [222]. The carrier balance of interfacial exciplex is significantly influenced by the limited structural changes on acceptors, and thus the final device characteristics. The device employing H2/B3PyMPM interfacial exciplex host and a TADF emitter tBuCzDBA (Fig. 8) achieve an EQE_{max} of 26.4 and a record-high maximum power efficiency (PE) of 95.0 lm W⁻¹ among solution-processed TADF-OLEDs. In addition, Cho and Choi *et al.*

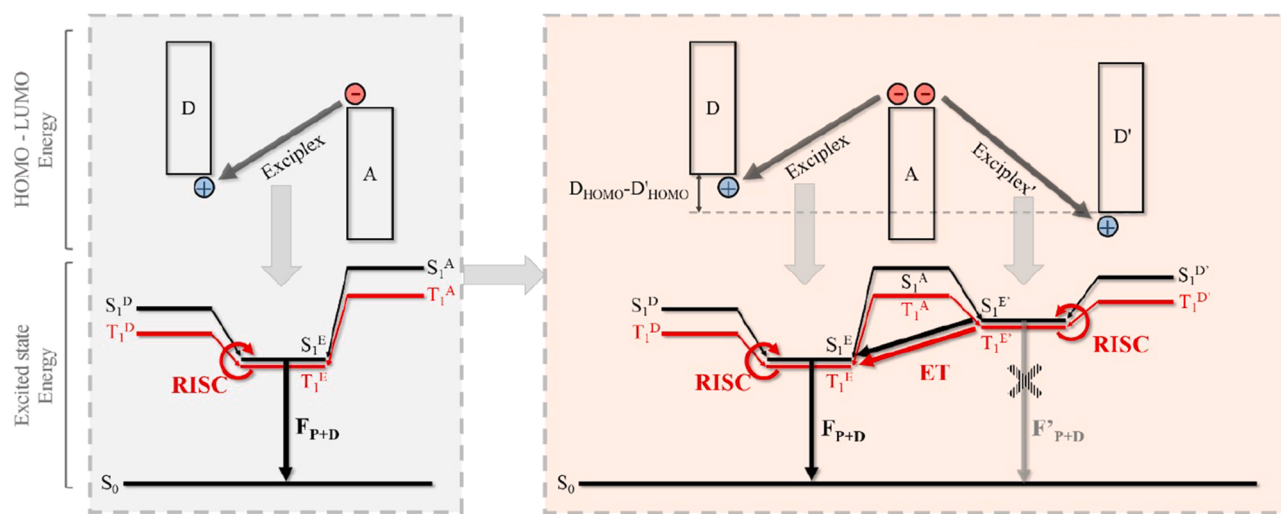


Fig. 24. Simplified energy diagram of common and ternary exciplexes. ET represents the energy transfer, and F_{P+D} stands for prompt and delayed fluorescence. Reproduced with permission from reference [211] Copyright 2014. Royal Society of Chemistry.

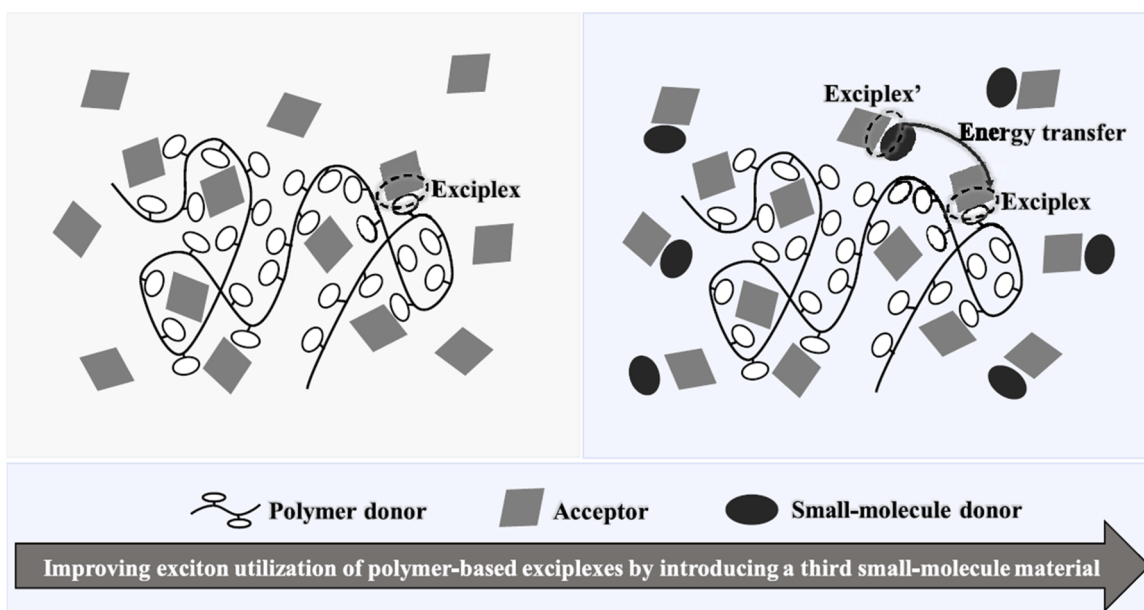


Fig. 25. Simplified exciplex formation diagrams of the conventional polymer small-molecule exciplex and ternary polymer-based exciplex. Reproduced with permission from [212] Copyright 2020. Elsevier.

reported the exciplex-forming blend composing of a new polymer donor, poly(9,9-diphenyl-10-(4-vinylbenzyl)-9,10-dihydroacridine) ($P(Bn-DPAc)$, Fig. 26), and a small-molecule acceptor, 2-(4'-(*tert*-butyl)-[1,1'-biphenyl]-4-yl)-4,6-diphenyl-1,3,5-triazine ($tPTRZ$, Fig. 26) [223]. The solution-processed device employing $P(Bn-DPAc):tPTRZ$ as the host doped with a green TADF emitter 2,4,5,6-tetra(3,6-di-*tert*-butylcarbazol-9-yl)-1,3-dicyanobenzene ($t4CzIPN$, Fig. 8) exhibited a high current efficiency of 107.3 cd A⁻¹ and a EQE_{max} of 31.2 %. The exciplex-hosted device significantly outperforms the counterpart device employing a unipolar polymer host $P(Bn-DPAc)$, verifying the beneficial effects on enhancing device efficiency with exciplex host.

Very recently, Jou *et al.* reported new exciplex-forming systems comprising 3 P-T2T and PO-T2T as acceptors and 3,6-bis(N-carbazolyl)-N-phenylcarbazole (BCC-36, Fig. 26) as donor [224], in which the BCC-36:PO-T2T blend was utilized to achieve high efficiency solution-processed exciplex-OLED with EQE up to 20 % and the current efficacy of 41 cd A⁻¹. This new exciplex blend was found to be excellent

host system for fluorescent emitter (C545T, Fig. 10), phosphorescent emitter [$\text{Ir}(\text{ppy})_2(\text{acac})$] (Fig. 10) as well as TADF emitter (4CzIPN, Fig. 8) for giving highly efficient OLED devices.

5.2.2. Yellow, orange, and red OLEDs

Scientists have been putting much effort into obtaining solution-processed OLEDs with low driving voltage and high PE. In many cases, unwanted charge trapping, high carrier injection barrier, and heterojunction barrier for bulk exciton formation lead to complications in driving voltage and PE that must be overcome. Sometimes, phase separation and self-aggregation of the phosphorescent dopants in solution-processed host:guest films further complicate the situation. Wang *et al.* developed a solution-processed yellow-emitting PhOLED by combining *m*-MTDATA and TmPyPB as an exciplex-forming host and Ir(Flpy-CF₃)₃ (Fig. 26) as the dopant displaying a record high PE of 97.2 lm W⁻¹ (25.2 %, 74.3 cd A⁻¹) [225]. The effective injection and transportation of both holes and electrons can be achieved using a good

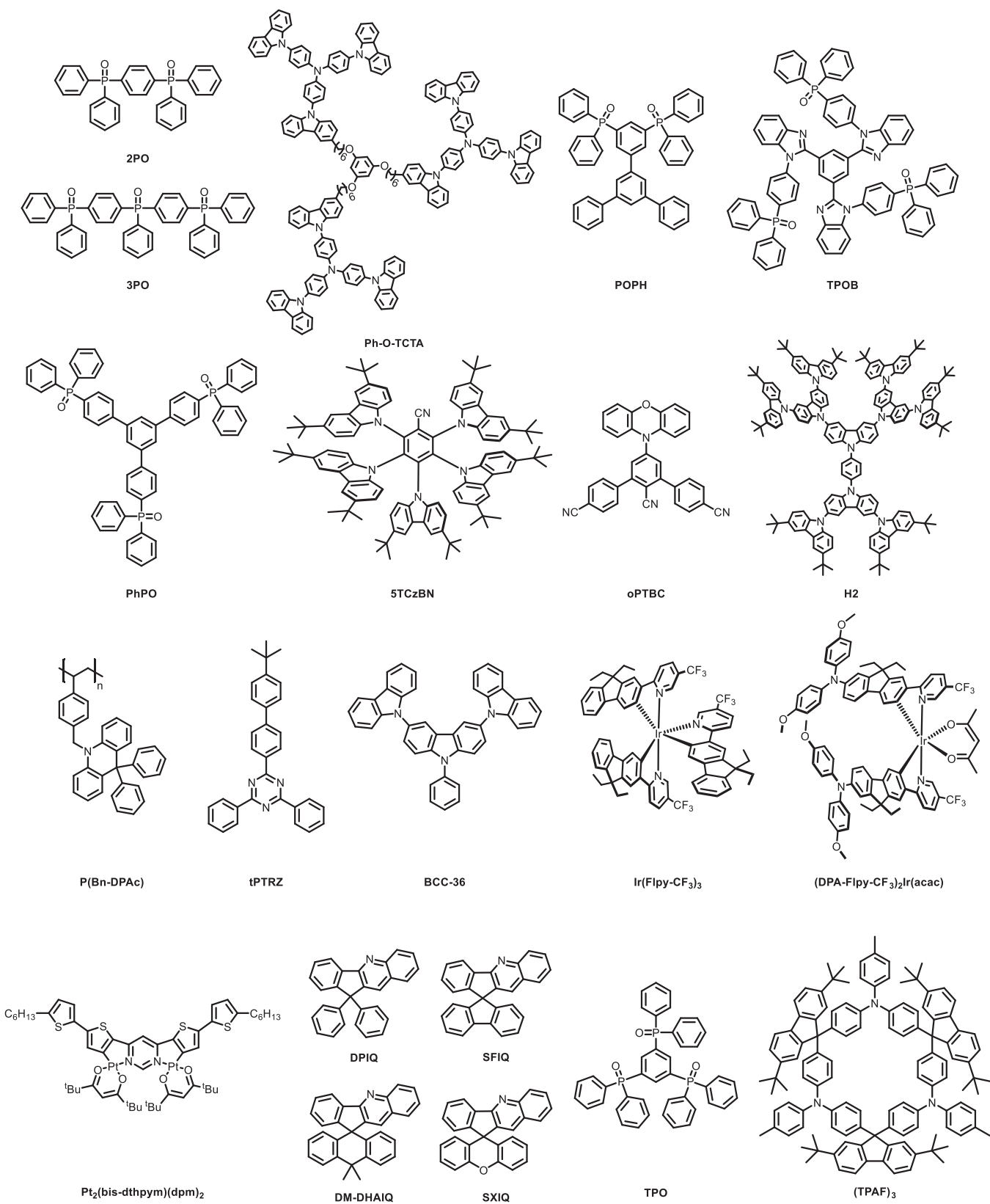


Fig. 26. Molecular structures of donor and acceptors that were used in solution-processed exciplex-hosted OLEDs.

hole-transporting host (*m*-MTDATA) and TmPyPB as ETL with good electron mobility. Thus, issues about high driving voltage caused by the large charge injection barrier and low charge mobility can be circumvented. In addition, carriers can follow a barrier-free process by directly

recombining at the *m*-MTDATA/TmPyPB interface to form the localized excited-state exciplex instead of surmounting the heterojunction barrier. Thus, energy transfer from the exciplex to the dopant is very efficient because the unwanted charge-trapping effect is successfully eradicated,

resulting in an extremely low turn-on voltage and a record high PE. The authors tested devices employing interfacial and bulk exciplexes and observed a dramatic difference between them, as shown in Fig. 27. As mentioned in Fig. 27, both devices A and B have similar device structures except for the EML composition. Pure *m*-MTDATA and binary *m*-MTDATA:TmPyPB are used as the hosts in devices A and B, respectively. In device A, the exciplexes form at the interface between EML and TmPyPB, whereas the exciplex generation is spread across the EML for device B. The performance of the device employing interface exciplex (device A) is better than that of the bulk exciplex-based device (device B), perhaps because of the slight charge-trapping effect in the former. Ultralow driving voltage green- and red-emitting s-PhOLEDs are also demonstrated by utilizing the same concept, exhibiting a peak PE of 81.1 lm W^{-1} (18.1 %, 62.0 cd A^{-1}) and 29.0 lm W^{-1} (16.3 %, 22.2 cd A^{-1}), respectively.

Liu et al. developed a red-emitting heteroleptic iridium complex (*DPA-Flpy-CF₃*)₂Ir(acac) (Fig. 26) to use the emitter as a dopant in a solution-processed OLED [226]. This red phosphor exhibits efficient PL with an emission band positioned at 602 nm, a high absorption coefficient in the wavelength range of 400–600 nm, and a measured PLQY of 42 % in degassed 2-MeTHF. The optimized red solution-processed PhOLEDs are fabricated by employing interfacial *m*-MTDATA-TA=TmPyPB exciplex as a host with a low doping concentration (1–3 wt %) of (*DPA-Flpy-CF₃*)₂Ir(acac) (Fig. 26). The corresponding OLED displays a maximum EQE of as high as 19.3 % and a PE of 44.5 lm W^{-1} with CIE coordinates of (0.64, 0.36). This performance is one of the highest values reported for red solution-processed PhOLEDs and is even similar to that of modern red thermally evaporated PhOLED counterparts.

Zhang et al. explored the role of the steric effect of host molecules on

the device performance of solution-processed OLEDs and synthesized four new acceptor materials, DPIQ, SFIQ, DM-DHAIQ, and DM-DHAIQ (Fig. 26) [227]. These materials form exciplexes with *m*-MTDATA, and the relevant exciplex systems are employed as the hosts in a red solution-processed device containing (pq)₂Ir(acac) as the emitter (Fig. 14). The relevant OLEDs achieve high EQEs ranging from 10.6 % to 14.1 %. Shahalizad et al. worked on solution-processed OLEDs with exciplex hosts and a neodymium complex as the emitter to push further the EL to the NIR region. The PLQY of the blend (1.2 %) and the EQE of the device (0.034 %) are inadequate [228].

The NIR phosphorescent emitters suitable for solution-processed OLEDs are relatively rare. Recently, Shafikov and Kozhevnikov et al. reported a novel molecular design strategy to make a dinuclear metal complex Pt₂(bis-dthpym)(dpm)₂ (Fig. 26) with intense NIR emission ($\lambda_{\text{max}} = 725 \text{ nm}$) [229]. The solution-processed OLEDs employing TBP:PBD exciplex cohost doped with 5 % w/w of Pt₂(bis-dthpym)(dpm)₂ achieved an EQE_{max} of 3.6 %, a turn-on voltage of 5.6 V (at 0.01 mW cm^{-2}), maximum radiosity of 2.7 mW cm^{-2} , which is particularly high compared to those of reported NIR-emitting phosphorescent OLEDs.

5.2.3. White OLEDs

Ban et al. designed and synthesized a high triplet energy phosphine oxide-based electron–acceptor material TPO (Fig. 26), which has a good film-forming ability via spin coating. The authors determined that this result is due to hindering of π – π stacking in the solid-state caused by the star molecular shape. An efficient exciplex is developed by blending TPO with the commonly used electron donor, TCTA [230]. One of the key factors to achieving high performance in wOLEDs is efficient blue

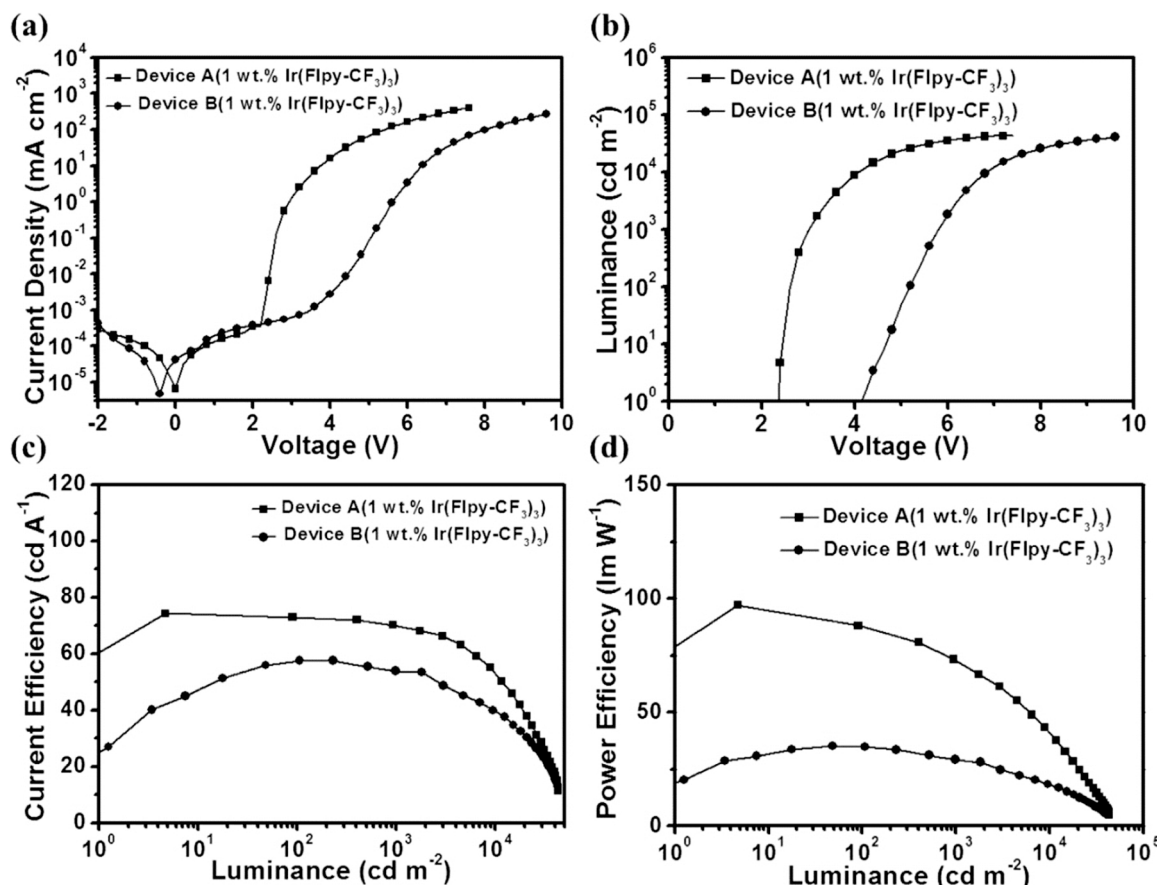


Fig. 27. Device performance of solution-processed yellow PhOLEDs based on Ir(Flpy-CF₃)₃ as the dopant and interface (device A) and bulk binary (device B) exciplexes of *m*-MTDATA and TmPyPB as the hosts.

Reproduced with permission from [225], Copyright 2015. Springer Nature.

emission. Therefore, a solution-processed blue PhOLED is initially fabricated, thereby exhibiting a maximum current efficiency of 23.8 cd A⁻¹ and a PE of 15.8 lm W⁻¹. A solution-processed white PhOLED is developed by employing this exciplex system (TCTA:TPO) as the host and by codoping it with 0.2 wt% orange phosphors (fbi)₂Ir(acac) (Figs. 18) and 10 wt% blue phosphors Flrpic. The developed white PhOLED shows a low turn-on voltage of 3.0 V, a maximum brightness of 46,500 cd m⁻² at 10 V, and maximum CE and PE of 38.5 cd A⁻¹ and 20.5 lm W⁻¹, respectively. The superiority of the pertinent exciplex system used for the solution-processed device is attributed to the high triplet energy of the exciplex host and the bipolar transporting nature of the emitter. Thus, such well-designed exciplex systems can be efficiently used as a host material for low-cost solution-processed OLEDs.

In 2014, Quan *et al.* designed a novel triphenylamine-fluorene oligomer (TPAF)₃ as a host (Fig. 26) to develop highly efficient solution-processed white PhOLEDs [231]. In addition to the hollow space within the molecule (TPAF)₃, the extended fluorene edges are expected to augment the compatibility of the host with the dopant, leading to a good film-forming ability. The host system is then blended with TPBI or CBP to form the exciplex, in which Flrpic is introduced as the dopant to achieve white light emission. The exciplex emission of the (TPAF)₃:CBP blend is observed at 575 nm, thereby combining the Flrpic emission to provide wOLED with a turn-on voltage of 5.4 V, a maximum CE of 22.6 cd A⁻¹, and luminance of 14213 cd m⁻². This device exhibits the current efficiency of 10.4 and 9.1 cd A⁻¹ at the practical brightness of 100 and 1000 cd m⁻², respectively. Thus, a new strategy is presented for developing efficient solution-processed white PhOLEDs.

He *et al.* chose three interfacial exciplexes, namely, CDBP|PO-T2T, mCP|PO-T2T, and m-CBP|PO-T2T, as hosts and 4CzFCN as the emitter (Fig. 8) to develop a solution-processed TADF OLEDs. [232] The blue solution-processed TADF OLED with 25 % doping concentration of

4CzFCN exhibits a low turn-on voltage of 3.6 V, maximum EQE of 21.0 % with low-efficiency roll-off, and a high maximum brightness of more than 10,000 cd m⁻². The authors then fabricated a hybrid white OLED with 4CzFCN and (MDQ)₂Ir(acac) (Fig. 14) as the dopants and the CDBP|PO-T2T interfacial exciplex system as the host. The relevant optimized wOLED reaches a high EQE of 20.8 % with a CIE coordinate of 0.33, 0.39.

Despite considerable progress in solution-processed wOLEDs, triplet-polaron quenching, low-energy exciplex state, and electromer formation between the bulky substituents often pose challenges in restraining energy leakage. As anticipated, fully solution-processed TADF-based hybrid wOLEDs are rare in literature. Ban *et al.* synthesized two TADF molecules, PCz-4CzCN and TPA-4CzCN (Fig. 23), to solve the above issues [233]. The former has four end-capping phenylcarbazoles, whereas the latter has four triphenylamine units. In both molecules, the central TADF core is 4CzCN. The efficiency of the relevant devices depends on these end-capping groups, although they are connected with the central emissive core by a nonconjugated backbone. For example, the PCz-4CzCN-based solution-processed blue OLED offers a maximum EQE of 22.6 %, which is nearly 20 times higher than that of the TPA-4CzCN-based device. The authors invoked the theory of electromers to explain such a remarkable performance difference between two related materials. Electromer formation in TPA-4CzCN-based devices induces energy leakage of the emissive core, which is responsible for inferior device performance. On the contrary, the rigid phenylcarbazole units in PCz-4CzCN are thought to block the energy leakage. The exciplex formation between phenylcarbazole units and the ETL layer is also thought to mitigate TTA and triplet-polaron quenching, providing an impetus to the device. The whole situation is illustrated in Fig. 28. The subsequent wOLED using PCz-4CzCN (Fig. 23) and PO-01 (Fig. 18) as the blue TADF and yellow phosphorescent dopants, respectively, offer a

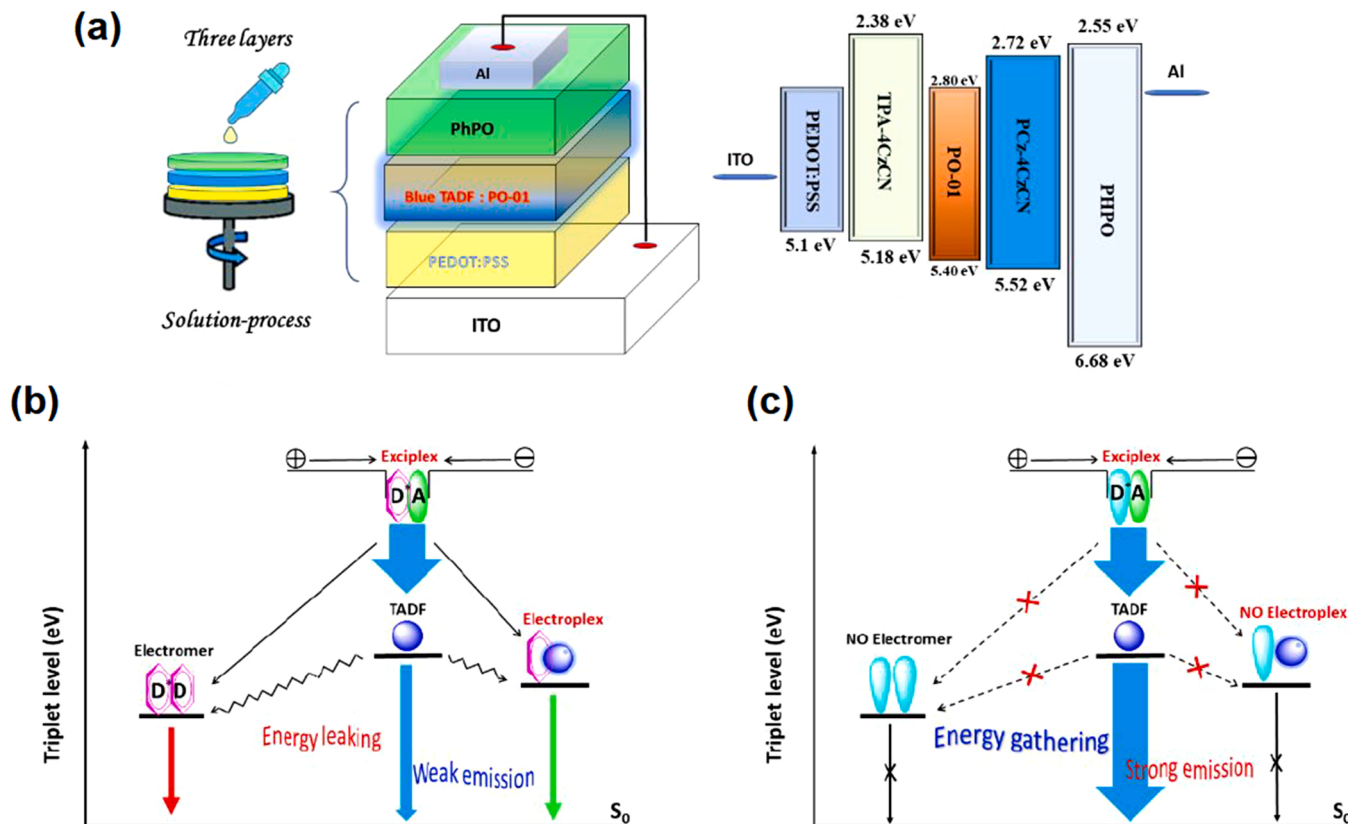


Fig. 28. (a) Device structure and energy-level diagram. Exciton formation and energy transfer diagram of (b) PCz-4CzCN- and (c) TPA-4CzCN-based solution-processed OLEDs. (Figs. 3 and 6).

Reproduced with permission from reference [233] Copyright 2020. American Chemical Society.

low turn-on voltage of 2.8 V and high EQE of 15.6 % (35.8 cd A^{-1} , 28.1 lm W^{-1}).

6. Some unconventional exciplexes in OLEDs – exciplexes between pure organic molecules and inorganic complexes

The conventional exciplex systems are made of organic donor and acceptor materials. However, there are some reports where exciplexes are generated in a mixture of organic material and inorganic complexes. Since the molecular systems of this type of exciplexes are different than those discussed so far, we dedicated a separate section for such materials.

Some interesting examples of unconventional exciplexes came from Baldo, Swagar, and coworkers. The researchers used supramolecular chemistry, particularly, the material science combinatorial approach, to design and synthesize the exciplexes. Exciplexes are supramolecular entities. Thus, the authors envisioned a lock-and-key approach for counterpart design. A special-shaped acceptor and a series of donor molecules are tested for exciplex formation, and EQE of up to 5.4 % is obtained from the relevant devices [234]. Qin *et al.* reported an exciplex system based on neutral manganese complexes [235]. The ionic manganese (II) complexes are efficient green emitters and have been proved to be useful as emitters in the PhOLEDs. The solid-state PL of such manganese complexes arises from metal-centered d-d radiative transition. However, their photophysical excellences are tainted by intrinsic low solubility and hydrolysis propensity in the air, which must be mitigated to apply these materials in the OLEDs. Qin *et al.* fixed the issues by synthesizing air-stable neutral Mn(II) complexes DBFDPO-MnX₂, X = Cl or Br (Fig. 29) with 4,6-bis(diphenyl phosphoryl) dibenzofuran (DBFDPO) as the ligand. These tetrahedral complexes are highly phosphorescent in the solid-state, with PLQY exceeding 80 %. They can be evaporated without considerable loss due to dissociation, and vacuum-deposited OLEDs can be fabricated by employing them as emitters. A red exciplex OLED using the complex exhibits 8.3 % EQE (18.64 cd A^{-1} , 17.92 lm W^{-1}).

The key to the success of the exciplex OLEDs is the effective harnessing of the triplet excitons by the exciplex through RISC. Any factor that facilitates the RISC directly affects the efficiency of the whole system. Therefore, the incorporation of inorganic complexes which are known to be good phosphors as one of the exciplex-forming components seems logical to enhance the efficiency of the exciplex OLEDs. Since the inorganic phosphors are excellent triplet exciton harvesters, their presence is expected to augment the RISC. The exciton decay routes in these unconventional exciplexes are modified by the presence of the inorganic phosphor. The idea is to suppress the non-radiative decay processes and extract as much light as possible. The strong spin-orbit coupling of the transition metal complex affects the ISC and RISC between the singlet and triplet excitons and also the phosphorescence decay channel from the triplet excitons. Based on this idea, Zhang *et al.* reported a red exciplex OLED using a PO-T2T:Ir(ppy)₃ blend exciplex system that showed a small ΔE_{ST} of 0.026 eV. The relevant device emits red emissions centered at 604 nm with an EQE of about 5 % [236]. Another

article by Cherpak *et al.* reported a yellow OLED based on a star-shaped tricarbazolyl triphenyl amine compound and Firpic. Emission from the relevant device was a combination of the blue phosphorescence from Firpic and a broad delayed fluorescence from the interfacial exciplex between them. The device showed a current efficiency of 15 cd A^{-1} , a brightness of 38000 cd m^{-2} , and an EQE of about 5 % [237]. Wang *et al.* reported exciplex OLEDs using two common phosphors, Ir(ppy)₂(acac) (Fig. 10) and PO-01 (Fig. 18), as donors and APDC-tPh (Fig. 7) as the acceptor. The photoluminescence emission peaks of the two phosphors are 515 and 580 nm respectively. On the contrary, 5 wt% blend films of Ir(ppy)₂(acac):APDC-tPh and PO-01:APDC-tPh systems exhibit luminescence at 717 and 727 nm respectively that are considerably red-shifted. This indicates exciplex formation between the phosphors and the acceptor. The subsequent OLEDs showed EQE of 0.19 % and 0.23 % respectively [238]. Unfortunately, the efficiency of these devices does not live up to the promises and significant improvements must be done to compete with the conventional exciplex systems.

7. Summary, conclusions, and prospects

On balance, exciplex OLEDs have come a long way since their debut because of their various exciting photonic properties. In this review, we attempted to summarize these properties and their promising outcome in light-emitting devices. The materials in OLEDs have evolved in the past two decades. Moreover, exciplexes are relatively new entrants as OLED material. The present OLED technology mainly uses organometallic phosphorescent emitters. However, some obvious limitations encourage the search for green alternatives, during which the TADF materials have emerged. Exciplexes are excellent TADF emitters that can be generated in simple donor-acceptor blends without paying much effort to tedious syntheses. The heteromolecular distribution of the FMOs renders a tiny singlet-triplet gap in the exciplexes, which is the foundation of the application of these virtual emitters in light-emitting devices. Although TADF materials have been heavily tested in OLEDs since their introduction, the exploration of the opportunities in exciplexes remains lacking. However, these materials have drawn appeal from the research community in the past couple of years because of their promising applications as emitters and hosts in OLEDs, and many milestones have been achieved since then. Nevertheless, exciplex emission has many intricacies. Several scopes for exciplex OLED performance improvement are discussed below.

7.1. Exciplex degradation

Exciplexes are excited-state entities that dissociate into the ground-state components as the excitation source is shut. Although the operational stability and device efficiency of the exciplex OLEDs have considerably improved through the decade, unwanted exciplex degradation remains a concern because this process can negatively affect the device performance. In a typical exciplex OLED, the exciton formation incorporates the LUMO of the donor and the HOMO of the acceptor, and the exciplex emission occurs at the type-II heterojunction of the organic molecules. Exciplex formation at the host interface in multiple-stacked OLEDs is where electrical stress effects on host materials influence EL. Therefore, a thorough understanding of exciplex degradation is important to discover high-performing devices. A related study by Na *et al.* undertook thermal stress-mediated exciplex degradation that reveals serious degradation issues when the thermal stress temperature is above the glass transition temperature of the emission layer [239]. The authors observed that the current level of the devices decreases with the increase of thermal stress time. Given that exciplex degradation in OLEDs seriously affects device performance, this process must be studied thoroughly to realize high-performance exciplex OLEDs and subsequent commercialization.

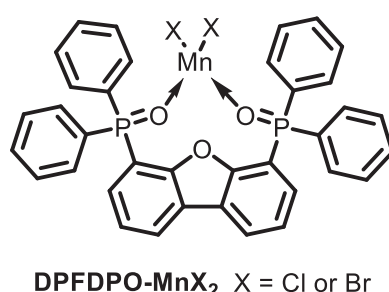


Fig. 29. Molecular structure of DPFDP-MnX₂.

7.2. Exciplex emission mechanism

As frequently mentioned throughout the article, the hype of exciplexes in OLEDs is due to their innately low singlet-triplet gap, leading to TADF emission with several advantages. Exciplexes are also established as excellent hosts in OLEDs because of their efficient energy transferability and ability to lower driving voltage. However, exciplex EL is intricate and needs further investigation. For instance, the ISC efficiency between ^1CT and ^3CT states in D-A molecules is less than that between ^1CT and ^3LE states of the same type of molecules because of the restricted spatial orbital angular momentum associated with the electronic transition in the former case [36]. This scenario indicates that the spin of the ^1CT state can only couple strongly to the ^3LE state. This second-order spin coupling process is mediated by vibronic coupling between the two states. Moreover, the exact orientation of the donor and acceptor molecules in exciplex blends is slightly crucial to SOC. At times, the TTA further complicates the scenario. Given that the charge separation distance plays an important role in the exciplex emission mechanism, proper modeling of through-space and through-bond charge transfer can yield valuable insights in this matter [240].

7.3. Operational stability

Exciplex-based OLEDs have the potential to be the next-generation metal-free display devices. However, the device lifetime of exciplex OLEDs is only occasionally reported perhaps because of the complexity of the measurement. The collected device data in the Tables in this article show that impressive EQEs have been achieved thus far, but only a few articles studied the operational stability of the relevant devices. The commercial application requires a high device lifetime, and the rarity of these data determines the necessity of this study, particularly for promising devices. The operational stability of OLEDs is mainly driven by the chemical degradation of the organic materials and the defect accumulation in the EML. As suggested by Wang et al., operational stability prediction and degradation mechanism analysis can be useful in this context [241].

7.4. Broad emission spectra

A common issue with the exciplex systems is their broad emission spectra which impedes color purity. The alignment of the various energy levels of the donor and acceptor counterparts affects the photophysical properties of the exciplexes between them. Therefore, the parameters such as emission spectral distribution, decay rates, photoluminescence quantum yield, and reverse intersystem crossing are modified based on the molecular properties of the donor and acceptor molecules. The conventional OLEDs with organic or organometallic materials usually have narrower electroluminescence spectra than those using exciplexes as the emitter. The fundamental difference between these two types of OLEDs is the nature of the emitter. The emitters in the conventional OLEDs are real materials that emit photons upon excitation. Researchers are quite familiar with the ground and excited electronic states of these emitters. In other words, the photophysical properties of such materials are easily tunable. On the contrary, exciplexes are virtual emitters that exist only in the excited states. The intermolecular interactions between the components are repulsive in the ground state and attractive in the excited state. The situation is further complicated in the solid state where molecular motions are restricted. Therefore, exciplexes between several energetically favorable conformations exist that emit photons over a broad energy region. Be that as it may, we believe in the potentiality of the exciplex systems and we also believe that the broad spectral issue raises new challenges which will be taken care of in the future with new material design strategy. Also, the broad spectral characteristics make exciplexes good hosts and amazing components for the wOLEDs.

7.5. Long-persistent luminescence

Exciplex systems exhibit long-persistent luminescence based on device thickness. This emission type is a combination of charge separation, charge accumulation, and charge recombination, which is quite different from that in phosphorescence. The long lifetime of phosphorescence is ascribed to the slow radiative decay of the triplet excitons due to the spin-forbidden nature of the concerning transition. On the contrary, slow charge recombination decelerates the dynamics of organic long-persistent luminescence. The observation of long-persistent luminescence from exciplex OLED using a thick emission layer and a low donor concentration has been recently reported in addition to exhibiting TADF, thereby making exciplexes an exciting class of materials in OLEDs [242]. At a high donor concentration, charge recombination is fast, and the associated luminescence usually has high brightness. By contrast, a thick emission layer and a low donor concentration delay the charge recombination and favor long-persistent luminescence. The typical exciplex OLEDs use a thin emission layer to increase conductivity and high donor concentration to increase PLQY. Thus, the chance of observing ultra-long-lived luminescence from such systems is low. However, concluding whether the long-persistent luminescence from exciplex OLEDs is a disadvantage or an advantage is too early. We believe that the luminescence lifetime of OLEDs should be in line with the response time of the relevant devices to produce a sharp picture.

7.6. Solution-processed exciplex OLEDs

Although OLED technology has now been commercialized, its cost is relatively higher than that of the existing LCDs because of the production cost of large display panels. The conventional OLED panels are manufactured via vacuum thermal evaporation, which is intricate, sophisticated, and costly when producing large display panels. Solution-processed manufacturing has the promise of producing large panels at a price considerably lower than those produced via the vacuum evaporation technique. However, the former has many limitations, such as obstacles with batch manufacturing and low operational lifetime. Nevertheless, the solution-processed OLEDs should be given substantial interest by the researchers because we believe that they will compete with the vacuum-processed OLEDs in the future. Exciplexes would further lower the manufacturing cost as they can be generated in a simple donor-acceptor blend.

7.7. Best of both worlds: exciplex-hosted TADF OLEDs

The discovery of TADF OLEDs is a breakthrough after the PhOLEDs as well as the exciplex OLED development. OLEDs consisting of TADF emitters and exciplex hosts can be the best alternative to PhOLEDs. In this case, both the emitters and the hosts have TADF properties that can almost quantitatively harvest the electrically generated excitons because of multiple RISC and effective energy transfer. However, this type of OLED has not been given much interest despite its outstanding promise. We believe that many scopes exist for OLED performance improvement where the exciplex-hosted TADF OLEDs can stand out.

CRediT authorship contribution statement

Monima Sarma: Writing – original draft, Funding acquisition. **Li-Ming Chen:** Visualization. **Yi-Sheng Chen:** Data collection. **Ken-Tsung Wong:** Writing – review & editing; Supervision, Funding acquisition.

Declaration of Competing Interest

The authors declare that they have no known competing financial interests or personal relationships that could have appeared to influence the work reported in this paper.

Acknowledgement

The author MS thanks Science and Engineering Research Board (SERB) [(Project No. SRG/2019/001365)], under Department of Science and Technology (DST), India , and KTW thanks the Ministry of Science and Technology (MOST), Taiwan (Project No. 110-2113-M-002-021) for the financial supports.

References

- [1] C.W. Tang, S.A. VanSlyke, Appl. Phys. Lett. 51 (1987) 913–915, <https://doi.org/10.1063/1.98799>.
- [2] (a) K. Müllen, U. Scherf. *Organ. Light Emit. Devices: Synth. Proper. Appli.*, Wiley-VCH, Weinheim, 2006;
- (b) I.G. Hill, A. Kahn, Z.G. Soos, R.A. Pascal Jr., Chem. Phys. Lett. 327 (2000) 181–188, [https://doi.org/10.1016/S0009-2614\(00\)00882-4](https://doi.org/10.1016/S0009-2614(00)00882-4).
- [3] D.J. Gaspar, E. Polikarpov. *OLED Fundament. Mater. Devices Process.Organ. Light-Emit. Diodes*, CRC Press, 2018.
- [4] M.A. Baldo, D.F. O'Brien, Y. You, A. Shoustikov, S. Sibley, M.E. Thompson, S. R. Forrest, Nature 395 (1998) 151–154, <https://doi.org/10.1038/25954>.
- [5] A. Endo, K. Sato, K. Yoshimura, T. Kai, A. Kawada, H. Miyazaki, C. Adachi, Appl. Phys. Lett. 98 (2011), 083302, <https://doi.org/10.1063/1.3558906>.
- [6] K.K. Rohotgi. *Fundamentals of Photochemistry*, third ed., New age international publishers, India, 2017.
- [7] T.A. Lin, T. Chatterjee, W.L. Tsai, W.K. Lee, M.J. Wu, M. Jiao, K.C. Pan, C.L. Yi, C. L. Chung, K.T. Wong, C.C. Wu, Adv. Mater. 28 (2016) 6976–6983, <https://doi.org/10.1002/adma.201601675>.
- [8] (a) M. Sarma, K.T. Wong, ACS Appl. Mater. Interfaces 10 (2018) 19279–19304, <https://doi.org/10.1021/acsm.7b18318>;
- (b) J.M. Teng, Y.F. Wang, C.F. Chen, J. Mater. Chem. C. 8 (2020) 11340–11353, <https://doi.org/10.1039/DOTC02682D>;
- (c) W.P. To, G. Cheng, G.S.M. Tong, D. Zhou, C.M. Che, Front. Chem. 8 (2020) 653, <https://doi.org/10.3389/fchem.2020.00653>.
- [9] B. Hu, Z. Yang, F.E. Karasz, J. Appl. Phys. 76 (1994) 2419–2422, <https://doi.org/10.1063/1.358458>.
- [10] (a) M. Cocchi, D. Virgili, G. Giro, V. Fattori, P. Di Marco, J. Kalinowski, Y. Shiroti, Appl. Phys. Lett. 80 (2002) 2401–2403, <https://doi.org/10.1063/1.1467614>;
- (b) L.H. Chan, R.H. Lee, C.F. Hsieh, H.C. Yeh, C.T. Chen, J. Am. Chem. Soc. 124 (2002) 6469–6479, <https://doi.org/10.1021/ja0255150>;
- (c) D. Kolosov, V. Adamovich, P. Djurovich, M.E. Thompson, C. Adachi, J. Am. Chem. Soc. 124 (2002) 9945–9954, <https://doi.org/10.1021/ja0263588>;
- (d) S.H. Liao, J.R. Shiu, S.W. Liu, S.J. Yeh, Y.H. Chen, C.T. Chen, T.J. Chow, C. Wu, J. Am. Chem. Soc. 131 (2009) 763–777, <https://doi.org/10.1021/ja807284e>.
- [11] (a) S.P. Singh, Y.N. Mohapatra, M. Qureshi, S.S. Manoharan, Appl. Phys. Lett. 86 (2005), 113505, <https://doi.org/10.1063/1.1884255>;
- (b) X.J. Xu, S.Y. Chen, G. Yu, C.A. Di, H. You, D.G. Ma, Y.Q. Liu, Adv. Mater. 19 (2007) 1281–1285, <https://doi.org/10.1002/adma.200601919>;
- (c) N. Matsumoto, M. Nishiyama, C. Adachi, J. Phys. Chem. C. 112 (2008) 7735–7741, <https://doi.org/10.1021/jp800443r>;
- (d) N. Matsumoto, C. Adachi, J. Phys. Chem. C. 114 (2010) 4652–4658, <https://doi.org/10.1021/jp9121062>;
- (e) M. Castellani, D. Berner, J. Appl. Phys. 102 (2007), 024509, <https://doi.org/10.1063/1.2757204>;
- (f) K. Kohary, J. Mater. Sci: Mater. Electron 20 (2009) 10–14, <https://doi.org/10.1007/s10854-007-9420-4>.
- [12] K. Goushi, K. Yoshida, K. Sato, C. Adachi, Nat. Photonics 6 (2012) 253–258, <https://doi.org/10.1038/nphoton.2012.31>.
- [13] K. Goushi, C. Adachi, Appl. Phys. Lett. 101 (2012), 023306, <https://doi.org/10.1063/1.4737006>.
- [14] Y.S. Park, K.H. Kim, J.J. Kim, Appl. Phys. Lett. 102 (2013), 153306, <https://doi.org/10.1063/1.4802716>.
- [15] M. Chapman, P. Pander, M. Vasylyieva, G. Wiosna-Salyga, J. Ulanski, F.B. Dias, P. Data, ACS Appl. Mater. Interfaces 11 (2019) 13460–13471, <https://doi.org/10.1021/acsm.8b18284>.
- [16] N.R. Al Amin, K.K. Kesavan, S. Biring, C.C. Lee, T.H. Yeh, T.Y. Ko, S.W. Liu, K. T. Wong, ACS Appl. Electron. Mater. 2 (2020) 1011–1019, <https://doi.org/10.1021/acsaem.0c00062>.
- [17] K. Shizu, Y. Sakai, H. Tanaka, S. Hirata, C. Adachi, H. Kaji, ITE Trans. Media Technol. Appl. 3 (2015) 108, <https://doi.org/10.1063/1.4935237>.
- [18] B. Valeur, M.N. Berberan-Santos. *Molecular Fluorescence: Principles and Applications*, second ed., Wiley–VCH., Weinheim, Germany, 2012.
- [19] D. Graves, V. Jankus, F.B. Dias, A. Monkman, Adv. Funct. Mater. 24 (2014) 2343–2351, <https://doi.org/10.1002/adfm.201303389>.
- [20] (a) X.K. Liu, Z. Chen, C.J. Zheng, C.L. Liu, C.S. Lee, F. Li, X.M. Ou, X.H. Zhang, Adv. Mater. 27 (2015) 2378–2383, <https://doi.org/10.1002/adma.201570095>;
- (b) M. Zhang, C.-J. Zheng, H. Lin, S.-L. Tao, Mater. Horiz. 8 (2021) 401–425, <https://doi.org/10.1039/dmh01245a>.
- [21] (a) H.B. Kim, D. Kim, J.J. Kim, in: H. Yersin (Ed.), *Exciplex: Its Nature and Application to OLEDs*, Wiley-VCH, Weinheim, 2019, pp. 331–376;
- (b) H.B. Kim, J.J. Kim, J. Inf. Disp. 20 (2019) 105–121, <https://doi.org/10.1080/15980316.2019.1650838>.
- [22] (a) P. Yuan, X. Qiao, D. Yan, D. Ma, J. Mater. Chem. C. 6 (2018) 5721–5726, <https://doi.org/10.1039/C8TC01260A>;
- (b) X. Zhao, X. Tang, R. Pan, J. Xu, F. Qua, Z. Xiong, J. Mater. Chem. C. 7 (2019) 10841–10850, <https://doi.org/10.1039/C9TC02896J>.
- [23] S.K. Cushing, W. Ding, G. Chen, C. Wang, F. Yang, F. Huang, N. Wu, Nanoscale 9 (2017) 2240–2245, <https://doi.org/10.1039/C6NR08286F>.
- [24] C.K. Moon, J.S. Huh, J.M. Kim, J.J. Kim, Chem. Mater. 30 (2018) 5648–5654, <https://doi.org/10.1021/acs.chemmater.8b02011>.
- [25] P.B. Deotare, W. Chang, E. Hontz, D.N. Congreve, L. Shi, P.D. Reusswig, B. Modtland, M.E. Bahlike, C.K. Lee, A.P. Willard, V. Bulović, T. Van Voorhis, M. A. Baldo, Nat. Mater. 14 (2015) 1130–1134, <https://doi.org/10.1038/nmat4424>.
- [26] (a) H. Nakatani, T. Furukawa, K. Morimoto, C. Adachi, Sci. Adv. 2 (2016), e1501470, <https://doi.org/10.1126/sciadv.1501470>;
- (b) B. Li, L. Gan, X. Cai, X.L. Li, Z. Wang, K. Gao, D. Chen, Y. Cao, S.J. Su, Adv. Mater. Interfaces 5 (2018) 1800025, <https://doi.org/10.1002/admi.201800025>;
- (c) H. Mu, Y. Jiang, H. Xie, Org. Electron. 66 (2019) 195–205, <https://doi.org/10.1016/j.orgel.2018.11.014>.
- [27] J. Jiang, X. Lin, H. Lei, J. Li, Z. Kou, Opt. Mater. 99 (2020), 109561, <https://doi.org/10.1016/j.optmat.2019.109561>.
- [28] (a) P.K. Nayak, N. Agarwala, N. Periasamy, M.P. Patankar, K.L. Narasimhan, Synth. Met. 160 (2010) 722–727, <https://doi.org/10.1016/j.synthmet.2010.01.010>;
- (b) L.C. Palilis, A.J. Mäkinen, M. Uchida, Z.H. Kafafi, Appl. Phys. Lett. 82 (2003) 2209–2211, <https://doi.org/10.1063/1.1563838>.
- [29] (a) Y. Liu, J. Guo, H. Zhang, Y. Wang, Angew. Chem. Int. Ed. 41 (2002) 182–184, [https://doi.org/10.1002/1521-3773\(20020104\)41:1<182::AID-ANIE182>3.0.CO;2-B](https://doi.org/10.1002/1521-3773(20020104)41:1<182::AID-ANIE182>3.0.CO;2-B);
- (b) M. Li, W. Li, L. Chen, Z. Kong, B. Chu, B. Li, Z. Hu, Z. Zhang, Appl. Phys. Lett. 88 (2006), 091108, <https://doi.org/10.1063/1.2181194>;
- (c) D.Y. Wang, W.L. Li, B. Chu, C.J. Liang, Z.R. Hong, M.T. Li, H.Z. Wei, Q. Xin, J. H. Niu, J.B. Xu, J. Appl. Phys. 100 (2006), 024506, <https://doi.org/10.1063/1.2214223>.
- [30] A.P. Kulkarni, S.A. Jenekhe, J. Phys. Chem. C. 112 (2008) 5174–5184, <https://doi.org/10.1021/jp076480z>.
- [31] (a) S.L. Lai, M.Y. Chan, Q.X. Tong, M.K. Fung, P.F. Wang, C.S. Lee, S.T. Lee, Appl. Phys. Lett. 93 (2008), 143301, <https://doi.org/10.1063/1.2993326>;
- (b) S.L. Lai, Q.X. Tong, M.Y. Chan, T.W. Ng, M.F. Lo, S.T. Lee, C.S. Lee, J. Mater. Chem. 21 (2011) 1206–1211, <https://doi.org/10.1039/C0JM02550J>;
- (c) Q.X. Tong, S.L. Lai, M.Y. Chan, J.X. Tang, H.L. Kwong, C.S. Lee, S.T. Lee, Appl. Phys. Lett. 91 (2007), 023503, <https://doi.org/10.1063/1.2756137>.
- [32] S.L. Lai, Q.X. Tong, M.Y. Chan, T.W. Ng, M.F. Lo, C.C. Ko, S.T. Lee, C.S. Lee, Org. Electron. 12 (2011) 541–546, <https://doi.org/10.1016/j.orgel.2010.12.026>.
- [33] T.W. Ng, M.F. Lo, S.T. Lee, C.S. Lee, Org. Electron. 13 (2012) 1641–1645, <https://doi.org/10.1016/j.orgel.2012.05.026>.
- [34] Q. Huang, S. Zhao, P. Wang, Z. Qin, Z. Xu, D. Song, B. Qiao, X. Xu, J. Lumin. 201 (2018) 38–43, <https://doi.org/10.1016/j.jlumin.2018.03.094>.
- [35] S. Jeong, Y. Lee, J.K. Kim, D.J. Jang, J.I. Hong, J. Mater. Chem. C. 6 (2018) 9049–9054, <https://doi.org/10.1039/C8TC02590H>.
- [36] P.L. Dos Santos, F.B. Dias, A.P. Monkman, J. Phys. Chem. C. 120 (2016) 18259–18267, <https://doi.org/10.1021/acs.jpcc.6b05198>.
- [37] N. Bunzmann, B. Krugmann, S. Weissenseel, L. Kudriashova, K. Ivaniuk, P. Stakhira, V. Cherpak, M. Chapran, G. Grybauskaite-Kaminskiene, J. V. Grazulevicius, V. Dyakovon, A. Sperlich, Adv. Electron. Mater. 7 (2021) 2000702, <https://doi.org/10.1021/aelm.202000702>.
- [38] X. Liu, H. Popli, O. Kwon, H. Malissa, X. Pan, B. Park, B. Choi, S. Kim, E. Ehrenfreund, C. Boehme, Z.V. Vardeny, Adv. Mater. (2020) 2004421, <https://doi.org/10.1002/adma.202004421>.
- [39] L. Niu, Y. Zhang, L. Chen, Q. Zhang, Y. Guan, Org. Electron. 87 (2020), 105971, <https://doi.org/10.1016/j.orgel.2020.105971>.
- [40] W.Y. Hung, G.C. Fang, S.W. Lin, S.H. Cheng, K.T. Wong, T.Y. Kuo, P.T. Chou, Sci. Rep. 4 (2014) 5161, <https://doi.org/10.1038/srep05161>.
- [41] W.Y. Hung, G.C. Fang, Y.C. Chang, T.Y. Kuo, P.T. Chou, S.W. Lin, K.T. Wong, ACS Appl. Mater. Interfaces 5 (2013) 6826–6831, <https://doi.org/10.1021/am402032z>.
- [42] X.K. Liu, Z. Chen, J. Qing, W.J. Zhang, B. Wu, H.L. Tam, F. Zhu, X.H. Zhang, C. S. Lee, Adv. Mater. 27 (2015) 7079–7085, <https://doi.org/10.1002/adma.201502897>.
- [43] W.Y. Hung, T.C. Wang, P.Y. Chiang, B.J. Peng, K.T. Wong, ACS Appl. Mater. Interfaces 9 (2017) 7355–7361, <https://doi.org/10.1021/acsami.6b16083>.
- [44] C.-H. Chen, J.-T. Cheng, W.-C. Ding, Z.-L. Lin, Y.-S. Chen, T.-L. Chiu, Y.-C. Lo, J.-H. Lee, K.-T. Wong, J. Chin. Chem. Soc. 68 (2021) 482–490, <https://doi.org/10.1002/jccs.202000456>.
- [45] T.C. Lin, M. Sarma, Y.T. Chen, S.H. Liu, K.T. Lin, P.Y. Chiang, W.T. Chuang, Y. C. Liu, H.F. Hsu, W.Y. Hung, W.C. Tang, K.T. Wong, P.T. Chou, Nat. Commun. 9 (2018) 3111, <https://doi.org/10.1038/s41467-018-05527-4>.
- [46] M. Zhang, W. Liu, C.J. Zheng, K. Wang, Y.Z. Shi, X. Li, H. Lin, S.L. Tao, X. H. Zhang, Adv. Sci. 6 (2019) 1801938, <https://doi.org/10.1002/advs.201801938>.
- [47] M. Guzauskas, D. Volyniuk, A. Tomkeviciene, A. Pidluzhna, A. Lazauskasc, J. V. Grazulevicius, J. Mater. Chem. C. 7 (2019) 25, <https://doi.org/10.1039/C8TC04708A>.
- [48] P. Yuan, X. Guo, X. Qiao, D. Yan, D. Ma, Adv. Opt. Mater. 7 (2019) 1801648, <https://doi.org/10.1002/adom.201801648>.
- [49] R. Keruckiene, M. Guzauskas, E. Narbutaitis, U. Tsiko, D. Volyniuk, Pei-Hsi Lee, Chia-Hsun Chen, Tien-Lung Chiu, Chi-Feng Lin, Jiun-Haw Lee, J.V. Grazulevicius, Org. Electron. 78 (2020), 105576, <https://doi.org/10.1016/j.orgel.2019.105576>.

- [50] B. Zhao, T. Zhang, B. Chu, W. Li, Z. Su, Y. Luo, R. Li, X. Yan, F. Jin, Y. Gao, H. Wu, *Org. Electron.* 17 (2015) 15–21, <https://doi.org/10.1016/j.orgel.2014.11.014>.
- [51] W.Y. Hung, P.Y. Chiang, S.W. Lin, W.C. Tang, Y.T. Chen, S.H. Liu, P.T. Chou, Y. T. Hung, K.T. Wong, *ACS Appl. Mater. Interfaces* 8 (2016) 4811–4818, <https://doi.org/10.1021/acsmami.5b11895>.
- [52] M. Wang, Y.H. Huang, K.S. Lin, T.H. Yeh, J. Duan, T.Y. Ko, S.W. Liu, K.T. Wong, B. Hu, *Adv. Mater.* 31 (2019) 1904114, <https://doi.org/10.1002/adma.201904114>.
- [53] (a) T.B. Nguyen, H. Nakanotani, T. Hatakeyama, C. Adachi, *Adv. Mater.* 32 (2020) 1906614, <https://doi.org/10.1002/adma.201906614>;
(b) T. Lin, T. Zhang, Q. Song, F. Jin, Z. Liu, Z. Su, Y. Luo, B. Chu, C.S. Lee, W. Li, *Org. Electron.* 38 (2016) 69–73, <https://doi.org/10.1016/j.orgel.2016.08.001>.
- [54] L. Zhang, C. Cai, K.F. Li, H.L. Tam, K.L. Chan, K.W. Cheah, *ACS Appl. Mater. Interfaces* 7 (2015) 24983, <https://doi.org/10.1021/acsmami.5b05597>.
- [55] M. Ichikawa, T. Kawaguchi, K. Kobayashi, T. Miki, K. Furukawa, T. Koyama, Y. Taniguchi, J. Mater. Chem. 16 (2006) 221–225, <https://doi.org/10.1039/B510720B>.
- [56] Y. Kawabe, J. Abe, *Appl. Phys. Lett.* 81 (2002) 493–495, <https://doi.org/10.1063/1.1494105>.
- [57] W.M. Su, W.L. Li, Q. Xie, Z.S. Su, B. Chu, D.F. Bi, H. He, J.H. Niu, *Appl. Phys. Lett.* 91 (2007) 043508, <https://doi.org/10.1063/1.2762298>.
- [58] L. Song, Y. Hu, Z. Liu, Y. Lv, X. Guo, X. Liu, *ACS Appl. Mater. Interfaces* 9 (2017) 2711–2719, <https://doi.org/10.1021/acsmami.6b13405>.
- [59] W. Yuan, H. Yang, M. Zhang, D. Hu, N. Sun, Y. Tao, *Front. Chem.* 7 (2019) 187, <https://doi.org/10.3389/fchem.2019.00187>.
- [60] (a) K. Suzuki, S. Kubo, K. Shizu, T. Fukushima, A. Wakamiya, Y. Murata, C. Adachi, H. Kaji, *Angew. Chem., Int. Ed.* 54 (2015) 15231–15235, <https://doi.org/10.1002/anie.201508270>;
(b) Y. Kitamoto, T. Namikawa, T. Suzuki, Y. Miyata, H. Kita, T. Sato, S. Oi, *Org. Electrochem.* 34 (2016) 208–217, <https://doi.org/10.1016/j.orgel.2016.04.030>;
(c) Y. Liu, G. Xie, K. Wu, Z. Luo, T. Zhou, X. Zeng, J. Yu, S. Gong, C. Yang, J. Mater. Chem. C. 4 (2016) 4402–4407, <https://doi.org/10.1039/C6TC01353H>.
- [61] D. Tanaka, T. Takeda, T. Chiba, S. Watanabe, J. Kido, *Chem. Lett.* 36 (2007) 262–263, <https://doi.org/10.1246/cl.2007.262>.
- [62] Q. Huang, S. Zhao, Z. Xu, X. Fan, C. Shen, Q. Yang, *Appl. Phys. Lett.* 104 (2014), 161112, <https://doi.org/10.1063/1.4870492>.
- [63] Y. Ling, Y. Lei, Q. Zhang, L. Chen, Q. Song, Z. Xiong, *Appl. Phys. Lett.* 107 (2015), 213301, <https://doi.org/10.1063/1.4936205>.
- [64] H.A. Al Attar, A.P. Monkman, *Adv. Mater.* 28 (2016) 8014–8020, <https://doi.org/10.1002/adma.201600965>.
- [65] T. Basel, D. Sun, S. Baniya, R. McLaughlin, H. Choi, O. Kwon, Z.V. Vardeny, *Adv. Electron. Mater.* 2 (2016) 1500248, <https://doi.org/10.1002/aelm.201500248>.
- [66] W. Zhang, J. Yu, K. Yuan, Y. Jiang, Q. Zhang, K. Cao, *Proc. Spie.* 76583V (2010), <https://doi.org/10.1117/12.867127>.
- [67] S.J. Su, T. Chiba, T. Takeda, J. Kido, *Adv. Mater.* 20 (2008) 2125–2130, <https://doi.org/10.1002/adma.200701730>.
- [68] D. Wang, W. Li, B. Chu, Z. Su, D. Bi, D. Zhang, J. Zhu, F. Yan, Y. Chen, T. Tsuoboi, *Appl. Phys. Lett.* 92 (2008), 053304, <https://doi.org/10.1063/1.2841060>.
- [69] T. Zhang, B. Chu, W. Li, Z. Su, Q.M. Peng, B. Zhao, Y. Luo, F. Jin, X. Yan, Y. Gao, H. Wu, F. Zhang, D. Fan, J. Wang, *ACS Appl. Mater. Interfaces* 6 (2014) 11907–11914, <https://doi.org/10.1021/am501164s>.
- [70] M. Cekaviciute, J. Simokaitiene, D. Volyniuk, G. Sini, J.V. Grazulevicius, *Dyes Pigments* 140 (2017) 187–202, <https://doi.org/10.1016/j.dyepig.2017.01.023>.
- [71] T. Deksnys, J. Simokaitiene, J. Keruckas, D. Volyniuk, O. Bezkonynyi, V. Cherpak, P. Stakhira, K. Ivaniuk, I. Helzhynskyy, G. Baryshnikov, B. Minaev, J. V. Grazulevicius, N. J. Chem. 41 (2017) 559–568, <https://doi.org/10.1039/C6NJ02865A>.
- [72] V. Jankus, C.J. Chiang, F. Dias, A.P. Monkman, *Adv. Mater.* 25 (2013) 1455–1459, <https://doi.org/10.1002/adma.201203615>.
- [73] X. Wang, R. Wang, D. Zhou, J. Yu, *Synth. Met.* 214 (2016) 50–55, <https://doi.org/10.1016/j.synthmet.2016.01.022>.
- [74] J. Li, H. Nomura, H. Miyazaki, C. Adachi, *Chem. Commun.* 50 (2014) 6174–6176, <https://doi.org/10.1039/C4CC01590H>.
- [75] C. Hippola, D. Danilovic, U. Bhattacharjee, C. Perez-Bolivar, K.A.N. Sachinthani, T.L. Nelson, P. Anzenbacher, J.W. Petrich, R. Shinari, J. Shinari, *Adv. Opt. Mater.* 8 (2020) 0191282, <https://doi.org/10.1002/adom.201901282>.
- [76] Y. Hu, Y.J. Yu, Y. Yuan, Z.Q. Jiang, L.S. Liao, *Adv. Opt. Mater.* 8 (2020) 1901917, <https://doi.org/10.1002/adom.201901917>.
- [77] V. Jankus, P. Data, D. Graves, C. McGuinness, J. Santos, M.R. Bryce, F.B. Dias, A. P. Monkman, *Adv. Funct. Mater.* 24 (2014) 6178–6186, <https://doi.org/10.1002/adfm.201400948>.
- [78] T. Zhang, B. Zhao, B. Chu, W. Li, Z. Su, X. Yan, C. Liu, H. Wu, F. Jin, Y. Gao, *Org. Electron.* 25 (2015) 6–11, <https://doi.org/10.1016/j.orgel.2015.06.017>.
- [79] D. Chen, Z. Wang, D. Wang, Y.C. Wu, C.C. Lo, A. Lien, Y. Cao, S.J. Su, *Org. Electron.* 25 (2015) 79–84, <https://doi.org/10.1016/j.orgel.2015.06.022>.
- [80] S.K. Jeon, K.S. Yook, J.Y. Lee, *Nanotechnology* 27 (2016), 224001, <https://doi.org/10.1088/0957-4484/27/22/224001>.
- [81] W. Liu, J.X. Chen, C.J. Zheng, K. Wang, D.Y. Chen, F. Li, Y.P. Dong, C.S. Lee, X. M. Ou, X.H. Zhang, *Adv. Funct. Mater.* 26 (2016) 2002–2008, <https://doi.org/10.1002/adfm.201505014>.
- [82] C.S. Oh, Y.J. Kang, S.K. Jeon, J.Y. Lee, *J. Phys. Chem. C.* 119 (2015) 22618–22624, <https://doi.org/10.1021/acsjpc.5b05292>.
- [83] E. Angioni, M. Chapran, K. Ivaniuk, N. Kostiv, V. Cherpak, P. Stakhira, A. Lazauskas, S. Tamulevičius, D. Volyniuk, N.J. Findlay, T. Tuttle, J. V. Grazulevicius, P.J. Skabar, J. Mater. Chem. C. 4 (2016) 3851, <https://doi.org/10.1039/C6TC00750C>.
- [84] T.L. Wu, S.Y. Liao, P.Y. Huang, Z.S. Hong, M.P. Huang, C.C. Lin, M.J. Cheng, C. H. Cheng, *ACS Appl. Mater. Interfaces* 11 (2019) 19294–19300, <https://doi.org/10.1021/acsmami.9b04365>.
- [85] T. Xiaofeng, D. Volyniuk, T. Matulaitis, J. Keruckas, K. Ivaniuk, I. Helzhynskyy, P. Stakhira, J.V. Grazulevicius, *Dyes Pigments* 117 (2020), 108259, <https://doi.org/10.1016/j.dyepig.2020.108259>.
- [86] S.K. Jeon, J.Y. Lee, *Org. Electron.* 76 (2020), 105477, <https://doi.org/10.1016/j.orgel.2019.105477>.
- [87] (a) Q.T. Siddiqui, A.A. Awasthi, P. Bhui, P. Parab, M. Munneer, S. Bose, N. Agarwal, *RSC Adv.* 9 (2019) 40248, <https://doi.org/10.1039/C9RA08227A>;
(b) Q.T. Siddiqui, A.A. Awasthi, P. Bhui, M. Munneer, K.R.S. Chandrakumar, S. Bose, N. Agarwal, *J. Phys. Chem. C.* 123 (2019) 1003–1014, <https://doi.org/10.1021/acsjpc.8b08357>.
- [88] J. Zhao, J. Ye, X. Du, C. Zheng, Z. He, H. Yang, M. Zhang, H. Lin, S. Tao, *Chem. Asian J.* 15 (2020) 4093–4097, <https://doi.org/10.1002/asia.202001091>.
- [89] H.T. Cao, J.W.B. Li, H. Zhang, L.H. Xie, C. Sun, Q.Y. Feng, W.J. Yu, W. Huang, *Dyes Pigments* 185 (2021), 108894, <https://doi.org/10.1016/j.dyepig.2020.108894>.
- [90] N. Zhang, C. Zheng, Z. Chen, J. Zhao, M. Zhang, H. Yang, Z. He, X. Du, S. Tao, *J. Mater. Chem. C.* 9 (2021) 600–608, <https://doi.org/10.1039/DOTC04315J>.
- [91] H.J. Jang, J.Y. Lee, *J. Phys. Chem. C.* 124 (2020) 15057–15065, <https://doi.org/10.1021/acs.jpc.0c04196>.
- [92] Y.T. Hung, D. Luo, L.-M. Chen, D.-C. Huang, J.-Z. Wu, Y.-S. Chen, C.-H. Chang, K.-T. Wong, J. Mater. Chem. C. 10 (2022) 4748–4756, <https://doi.org/10.1039/D1TC04700K>.
- [93] S. Uchida, Y. Nishikitani, *Adv. Funct. Mater.* (2019) 1907309, <https://doi.org/10.1002/adfm.201907309>.
- [94] (a) Z. Wang, C. Wang, H. Zhang, Z. Liu, B. Zhao, W. Li, *Org. Electron.* 66 (2019) 227–241, <https://doi.org/10.1016/j.orgel.2018.12.039>;
(b) B. Zhang, Z. Xie, *Front. Chem.* 7 (2019) 306, <https://doi.org/10.3389/fchem.2019.00306>;
(c) Q. Wang, Q. Tian, Y. Zhang, X. Tang, L. Liao, J. Mater. Chem. C. 7 (2019) 11329–11360, <https://doi.org/10.1039/C9TC03092A>.
- [95] M. Sarma, K.T. Wong, S.W. Liu, W.Y. Hung, *SID* 49 (2018) 328–331, <https://doi.org/10.1002/sdtp.12553>.
- [96] Y. Wang, J.H. Yun, L. Wang, J.Y. Lee, *Adv. Funct. Mater.* 31 (2020) 2008332, <https://doi.org/10.1002/adfm.202000832>.
- [97] T. Zhang, B. Zhao, B. Chu, W. Li, Z. Su, X. Yan, C. Liu, H. Wu, Y. Gao, F. Jin, F. Hou, *Sci. Rep.* 5 (2015) 10234, <https://doi.org/10.1038/srep10234>.
- [98] B. Zhao, T. Zhang, B. Chu, W. Li, Z. Su, H. Wu, X. Yan, F. Jin, Y. Gao, C. Liu, *Sci. Rep.* 5 (2015) 10697, <https://doi.org/10.1038/srep10697>.
- [99] K.H. Kim, C.K. Moon, J.W. Sun, B. Sim, J.J. Kim, *Adv. Opt. Mater.* 3 (2015) 895–899, <https://doi.org/10.1002/adom.201400644>.
- [100] H.G. Kim, K.H. Kim, C.K. Moon, J.J. Kim, *Adv. Opt. Mater.* 5 (2017) 1600749, <https://doi.org/10.1002/adom.201600749>.
- [101] X.K. Liu, Z. Chen, C.J. Zheng, M. Chen, W. Liu, X.H. Zhang, C.S. Lee, *Adv. Mater.* 27 (2015) 2025–2030, <https://doi.org/10.1002/adma.201500013>.
- [102] G. Sych, J. Simokaitiene, O. Bezkonynyi, U. Tsiko, D. Volyniuk, D. Gudeika, J. Vidas Grazulevicius, *J. Phys. Chem. C.* 122 (2018) 14827–14837, <https://doi.org/10.1021/acs.jpc.8b03895>.
- [103] C.J. Shih, C.C. Lee, T.H. Yeh, S. Biring, K.K. Kesavan, N.R. Al Amin, M.H. Chen, W.C. Tang, S.W. Liu, K.T. Wong, *ACS Appl. Mater. Interfaces* 10 (2018) 24090–24098, <https://doi.org/10.1021/acsmami.8b08281>.
- [104] (a) Y.C. Lo, T.H. Yeh, C.K. Wang, B.J. Peng, J.L. Hsieh, C.C. Lee, S.W. Liu, K. T. Wong, *ACS Appl. Mater. Interfaces* 11 (2019) 23417–23427, <https://doi.org/10.1021/acsmami.9b06612>;
(b) Y.C. Hu, Z.L. Lin, T.C. Huang, J.W. Lee, W.C. Wei, T.Y. Ko, C.Y. Lo, D. G. Chen, P.T. Chou, Y.W. Hung, K.T. Wong, *Mater. Chem. Front.* 4 (2020) 2029–2039, <https://doi.org/10.1039/D0QM00188K>;
(c) (n/a) Y.-C. Hu, L.-M. Chen, Z.-L. Lin, J.-W. Lee, W.-C. Wei, T.-Y. Ko, C.-Y. Lo, W.-Y. Hung, K.-T. Wong, *J. Chin. Chem. Soc.* (2022), <https://doi.org/10.1002/jccs.20220094>;
(d) L.-M. Chen, I.H. Lin, Y.-C. You, W.-C. Wei, M.-J. Tsai, W.-Y. Hung, K.-T. Wong, *Mater. Chem. Front.* 5 (2021) 5044–5054, <https://doi.org/10.1039/D1QM00425E>;
(e) Y.-S. Chen, D. Luo, W.-C. Wei, B.-L. Chen, T.-H. Yeh, S.-W. Liu, K.-T. Wong, *Adv. Opt. Mater.* 10 (2022) 2101952, <https://doi.org/10.1002/adom.202101952>.
- [105] X. Song, D. Zhang, H. Li, M. Cai, T. Huang, L. Duan, *ACS Appl. Mater. Interfaces* 11 (2019) 22595–22602, <https://doi.org/10.1021/acsmami.9b05963>.
- [106] H.J. Jang, J.Y. Lee, *J. Phys. Chem. C.* 123 (2019) 26856–26861, <https://doi.org/10.1021/acs.jpc.9b08261>.
- [107] P. Ledwon, R. Motyka, K. Ivaniuk, A. Pidluzhna, N. Martyniuk, P. Stakhira, G. Baryshnikov, B.F. Minaev, H. Ågren, *Dyes Pigments* 173 (2020), 108008, <https://doi.org/10.1016/j.dyepig.2019.108008>.
- [108] S. Baniya, Z. Pang, D. Sun, T. Basel, Y. Zhai, O. Kwon, H. Choi, Z.V. Vardeny, *Proc. SPIE* 9941 (2016) 99410H, <https://doi.org/10.1117/12.2249508>.
- [109] P. Data, A. Kurowska, S. Pluczyk, P. Zassowski, M. Lapkowski, R. Jedrysiak, M. Czwartosz, L. Otulakowski, J. Suwinski, M. Lapkowski, A.P. Monkman, *J. Phys. Chem. C.* 120 (2016) 2070–2078, <https://doi.org/10.1021/acs.jpc.5b11263>.
- [110] G. Xia, C. Qu, Y. Zhu, K. Ye, Z. Zhang, Y. Wang, J. Mater. Chem. C. 9 (2021) 6834–6840, <https://doi.org/10.1039/D1TC01537K>.
- [111] X. Wang, Y. Zhang, Z. Yu, Y. Wu, D. Wang, C. Wu, H. Ma, S. Ning, H. Dong, Z. Wu, *J. Mater. Chem. C.* 10 (2022) 1681–1689, <https://doi.org/10.1039/D1TC05700F>.

- [112] Y. Seino, H. Sasabe, Y.J. Pu, J. Kido, *Adv. Mater.* 26 (2014) 1612–1616, <https://doi.org/10.1002/adma.201304253>.
- [113] H. Shin, S. Lee, K.H. Kim, C.K. Moon, S.J. Yoo, J.H. Lee, J.J. Kim, *Adv. Mater.* 26 (2014) 4730–4734, <https://doi.org/10.1002/adma.201400955>.
- [114] J. Hu, C. Zhao, T. Zhang, X. Zhang, X. Cao, Q. Wu, Y. Chen, D. Zhang, Y. Tao, W. Huang, *Adv. Opt. Mater.* 5 (2017) 1700036, <https://doi.org/10.1002/adom.201700026>.
- [115] J.H. Lee, S.H. Cheng, S.J. Yoo, H. Shin, J.H. Chang, C.I. Wu, K.T. Wong, J.J. Kim, *Adv. Funct. Mater.* 25 (2015) 361–366, <https://doi.org/10.1002/adfm.201402707>.
- [116] Z. Wang, H. Wang, J. Zhu, P. Wu, B. Shen, D. Dou, B. Wei, *ACS Appl. Mater. Interfaces* 9 (2017) 21346–21354, <https://doi.org/10.1021/acsmami.7b04987>.
- [117] T. Zhang, J. Yao, S. Zhang, S. Xiao, W. Liu, Z. Wu, D. Ma, *J. Mater. Chem. C* 9 (2021) 6062–6067, <https://doi.org/10.1039/DOTC05842D>.
- [118] W. Song, H.L. Lee, J.Y. Lee, *J. Mater. Chem. C* 5 (2017) 5923–5929, <https://doi.org/10.1039/C7TC01552F>.
- [119] H. Lim, H. Shin, K.H. Kim, S.J. Yoo, J.S. Huh, J.J. Kim, *ACS Appl. Mater. Interfaces* 9 (2017) 37883–37887, <https://doi.org/10.1021/acsmami.7b10914>.
- [120] Y. Tao, Q. Wu, M. Wang, X. Cao, D. Zhang, N. Sun, S. Wan, *J. Mater. Chem. C* 6 (2018) 8784–8792, <https://doi.org/10.1039/C8TC02353K>.
- [121] Y. Seino, H. Sasabe, M. Kimura, S. Inomata, K. Nakao, J. Kido, *Chem. Lett.* 45 (2016) 283–285, <https://doi.org/10.1246/cl.151094>.
- [122] (a) Y.S. Kim, J. Lim, J.Y. Lee, Y. Lee, C. Choo, *Chem. Eng. J.* 429 (2022) 132584, <https://doi.org/10.1016/j.cej.2021.132584>;
(b) S.-G. Ihn, E.S. Kwon, Y. Jung, J.S. Kim, S. Nam, J. Kim, S. Kim, S.O. Jeon, Y. S. Chung, S. Park, D.H. Huh, H.J. Kim, H. Kang, N. Lee, H.J. Bae, H. Choi, *J. Mater. Chem. C* 9 (2021) 17412–17418, <https://doi.org/10.1039/D1TC04680B>.
- [123] Y.S. Park, W.I. Jeong, J.J. Kim, *J. Appl. Phys.* 110 (2011) 124519, <https://doi.org/10.1063/1.3672836>.
- [124] W. Song, J.Y. Lee, *Appl. Phys. Lett.* 106 (2015), 123306, <https://doi.org/10.1063/1.4916549>.
- [125] D.Y. Zhou, L.S. Cui, Y.J. Zhang, L.S. Liao, H. Aziz, *Appl. Phys. Lett.* 105 (2014), 153302, <https://doi.org/10.1063/1.4897994>.
- [126] S.Y. Kim, W.I. Jeong, C. Mayr, Y.S. Park, K.H. Kim, J.H. Lee, C.K. Moon, W. Brüttig, J.J. Kim, *Adv. Funct. Mater.* 23 (2013) 3896–3900, <https://doi.org/10.1002/adfm.201300104>.
- [127] Y.S. Park, S. Lee, K.H. Kim, S.Y. Kim, J.H. Lee, J.J. Kim, *Adv. Funct. Mater.* 23 (2013) 4914–4920, <https://doi.org/10.1002/adfm.201300547>.
- [128] J.H. Lee, S. Lee, S.J. Yoo, K.H. Kim, J.J. Kim, *Adv. Funct. Mater.* 24 (2014) 4681–4688, <https://doi.org/10.1002/adfm.201303453>.
- [129] J.B. Kim, J.H. Lee, C.K. Moon, K.H. Kim, J.J. Kim, *Org. Electron.* 15 (2014) 2715–2718, <https://doi.org/10.1364/OE.40.002715>.
- [130] T. Xu, J.G. Zhou, C.C. Huang, L. Zhang, M.K. Fung, I. Murtaza, H. Meng, L.S. Liao, *ACS Appl. Mater. Interfaces* 9 (2017) 10955–10962, <https://doi.org/10.1021/acsmami.6b16094>.
- [131] S.H. Li, S.F. Wu, Y.K. Wang, J.J. Liang, Q. Sun, C.C. Huang, J.C. Wu, L.S. Liao, M. K. Fung, *J. Mater. Chem. C* 6 (2018) 342–349, <https://doi.org/10.1039/C7TC04441K>.
- [132] T. Lu, W. Jiang, K. Sun, W. Tian, Y. Sun, *Dyes Pigments* 151 (2018) 35–44, <https://doi.org/10.1016/j.dyepig.2017.12.049>.
- [133] C.J. Shih, C.C. Lee, Y.H. Chen, S. Biring, G. Kumar, T.H. Yeh, S. Sen, S.W. Liu, K. T. Wong, *ACS Appl. Mater. Interfaces* 10 (2018) 2151–2157, <https://doi.org/10.1021/acsmami.7b15034>.
- [134] (a) C.-C. Lee, N.R.A. Amin, J.-J. Xu, B.-C. Wang, D. Luo, K. Sutanto, S. Biring, S.-W. Liu, C.-H. Chen, *J. Mater. Chem. C* 9 (2021) 9453–9464, <https://doi.org/10.1039/D1TC02290C>;
(b) C.-H. Chiu, N.R.A. Amin, J.-X. Xie, C.-C. Lee, D. Luo, S. Biring, K. Sutanto, S.-W. Liu, C.-H. Chen, *J. Mater. Chem. C* 10 (2022) 4955–4964, <https://doi.org/10.1039/D1TC04473G>.
- [135] J.H. Lee, H. Shin, J.M. Kim, K.H. Kim, J.J. Kim, *ACS Appl. Mater. Interfaces* 9 (2017) 3277–3281, <https://doi.org/10.1021/acsmami.6b14438>.
- [136] D.Y. Zhou, H.Z. Boni, Q. Wang, L.S. Liao, H. Aziz, *J. Phys. Chem. C* 118 (2014) 24006–24012, <https://doi.org/10.1021/jp508228Z>.
- [137] T. Ito, H. Sasabe, Y. Nagai, Y. Watanabe, N. Onuma, J. Kido, *Chem. Eur. J.* 25 (2019) 7308–7314, <https://doi.org/10.1002/chem.201805907>.
- [138] S. Lee, D. Limbach, K.H. Kim, S.J. Yoo, Y.S. Park, J.J. Kim, *Org. Electron.* 14 (2013) 1856–1860, <https://doi.org/10.1016/j.jorgel.2013.04.020>.
- [139] S. Lee, K.H. Kim, D. Limbach, Y.S. Park, J.J. Kim, *Adv. Funct. Mater.* 23 (2013) 4105–4110, <https://doi.org/10.1002/adfm.201300187>.
- [140] Z. Xia, B. Zhaoa, L. Chenaa, W. Lid, H. Wangaa, X. Liua, B. Xua, *Org. Electron.* 57 (2018) 21–27, <https://doi.org/10.1016/j.jorgel.2018.07.030>.
- [141] M. Wu, Z. Wang, Y. Liu, Y. Qi, J. Yu, *Dyes Pigments* 164 (2019) 119–125, <https://doi.org/10.1016/j.dyepig.2019.01.020>.
- [142] H.L. Lee, K.H. Lee, J.Y. Lee, *J. Mater. Chem. C* 7 (2019) 5988–5994, <https://doi.org/10.1039/C9TC00701F>.
- [143] T. Xu, Y.X. Zhang, B. Wang, C.C. Huang, I. Murtaza, H. Meng, L.S. Liao, *ACS Appl. Mater. Interfaces* 9 (2017) 2701–2710, <https://doi.org/10.1021/acsmami.6b13077>.
- [144] D. Saito, H. Sasabe, T. Kikuchi, T. Ito, H. Tsuneyama, J. Kido, *J. Mater. Chem. C* 9 (2021) 1215, <https://doi.org/10.1039/D0TC05234E>.
- [145] W. Li, A. Wu, T. Fu, X. Gao, Y. Wang, D. Xu, C. Zhang, Z. Sun, Y. Lu, D.J. Young, H. Li, X.-C. Hang, *J. Phys. Chem. Lett.* 13 (2022) 1494–1499, <https://doi.org/10.1021/acsclett.1c03748>.
- [146] H. Tsuneyama, H. Sasabe, Y. Saito, T. Noda, D. Saito, J. Kido, *J. Mater. Chem. C* 10 (2022) 2073–2079, <https://doi.org/10.1039/D1TC05417A>.
- [147] Z.-L. Zhu, J.-H. Tan, W.-C. Chen, Y. Yuan, L.-W. Fu, C. Cao, C.-J. You, S.-F. Ni, Y. Chi, C.-S. Lee, *Adv. Funct. Mater.* 31 (2021) 2102787, <https://doi.org/10.1002/adfm.202102787>.
- [148] L. Jia, L. Jin, K. Yuan, L. Chen, J. Yuan, S. Xu, W. Lv, R. Chen, *ACS Sustain. Chem. Eng.* 6 (2018) 8809–8815, <https://doi.org/10.1021/acssuschemeng.8b01155>.
- [149] D. Dou, P. Wu, Z. Liao, J. Hao, J. Zhang, Z. Wang, *RSC Adv.* 9 (2019) 23810, <https://doi.org/10.1039/C9RA02875G>.
- [150] J. Zhao, X. Du, S. Yuan, C. Zheng, H. Lin, S. Tao, *Org. Electron.* 43 (2017) 136–141, <https://doi.org/10.1016/j.orgel.2017.01.020>.
- [151] V.V. Patil, J. Lim, J.Y. Lee, *Dyes Pigments* 189 (2021), 109247, <https://doi.org/10.1016/j.dyepig.2021.109247>.
- [152] X. Guo, P. Yuan, X. Qiao, D. Yang, Y. Dai, Q. Sun, D. Ma, *Adv. Opt. Mater.* 8 (2020) 2000991, <https://doi.org/10.1002/adom.202000991>.
- [153] J. Grüne, N. Bunzmann, M. Meinecke, V. Dyakonov, A. Sperlich, *J. Phys. Chem. C* 124 (2020) 25667–25674, <https://doi.org/10.1021/acs.jpcc.0c06528>.
- [154] J.W. Sun, J.H. Lee, C.K. Moon, K.H. Kim, H. Shin, J.J. Kim, *Adv. Mater.* 26 (2014) 5684–5688, <https://doi.org/10.1002/adma.201401407>.
- [155] Y. Seino, S. Inomata, H. Sasabe, Y.J. Pu, J. Kido, *Adv. Mater.* 28 (2016) 2638–2664, <https://doi.org/10.1002/adma.201503782>.
- [156] B.S. Kim, J.Y. Lee, *Adv. Funct. Mater.* 24 (2014) 3970–3977, <https://doi.org/10.1002/adfm.201303730>.
- [157] D. Chen, K. Liu, L. Gan, M. Liu, K. Gao, G. Xie, Y. Ma, Y. Cao, S.J. Su, *Adv. Mater.* 28 (2016) 6758–6765, <https://doi.org/10.1002/adma.201600612>.
- [158] Y.T. Hung, Z.Y. Chen, W.Y. Hung, D.G. Chen, K.T. Wong, *ACS Appl. Mater. Interfaces* 10 (2018) 34435–34442, <https://doi.org/10.1021/acsmami.8b14070>.
- [159] H. Sasabe, R. Sato, K. Suzuki, Y. Watanabe, C. Adachi, H. Kaji, J. Kido, *Adv. Opt. Mater.* 6 (2018) 1800376, <https://doi.org/10.1002/adom.201800376>.
- [160] L.Y. Zhang, Q. Ran, Q. Wang, Y. Liu, C. Han, X. Zhang, C. Fan, H. Xu, *Adv. Mater.* 31 (2019) 1902368, <https://doi.org/10.1002/adma.201902368>.
- [161] K. Traskovskis, A. Sebris, I. Novosjolova, M. Turks, M. Guzauskas, D. Volyniuk, O. Bezzivkonyi, J.V. Grazulevicius, A. Mishnev, R. Grzibovskis, A. Vembrisd, J. Mater. Chem. C 9 (2021) 4532, <https://doi.org/10.1039/DOTC05099G>.
- [162] C. Duan, C. Han, J. Zhang, X. Zhang, C. Fan, H. Xu, *Adv. Funct. Mater.* 31 (2021) 2102739, <https://doi.org/10.1002/adfm.202102739>.
- [163] J.-X. Chen, H. Wang, K. Wang, X. Zhang, L. Zhou, Y.-Z. Shi, J. Yu, X.-H. Zhang, *Mater. Today Energy* 21 (2021), 100818, <https://doi.org/10.1016/j.mtener.2021.100818>.
- [164] M. Vasiliopoulos, A.R. b Mohd Yusoff, M. Daboczi, J. Conforto, A.E.X. Gavim, W. J. da Silva, A.G. Macedo, A. Soutlati, G. Pistolis, F.K. Schneider, Y. Dong, P. Jacquot, G. Rotas, J. Jang, G.C. Vougioukalakis, C.L. Chochos, J.-S. Kim, N. Gasparini, *Nat. Commun.* 12 (2021) 4868, <https://doi.org/10.1038/s41467-021-25135-z>.
- [165] Y.-Y. Wang, K.-N. Tong, K. Zhang, C.-H. Lu, X. Chen, J.-X. Liang, C.-K. Wang, C.-C. Wu, M.-K. Fung, J. Fan, *Mater. Horiz.* 8 (2021) 1297–1303, <https://doi.org/10.1039/D1MH0028D>.
- [166] M. Regnat, P. Pernstich, K.H. Kim, J.J. Kim, F. Nüesch, B. Ruhstaller, *Adv. Electron. Mater.* 22 (2019) 1900804, <https://doi.org/10.1002/adem.201900897>.
- [167] T.C. Yeh, J.D. Lee, L.Y. Chen, T. Chatterjee, W.Y. Hung, K.T. Wong, *Org. Electron.* 70 (2019) 55–62, <https://doi.org/10.1016/j.orgel.2019.04.003>.
- [168] (a) J. Kido, K. Hongawa, K. Okuyama, K. Nagai, *Appl. Phys. Lett.* 64 (1994) 815–817, <https://doi.org/10.1063/1.111023>;
(b) J. Kido, M. Kimura, K. Nagai, *Science* 267 (1995) 1332–1334, <https://doi.org/10.1126/science.267.5202.1332>;
(c) P. Xiao, J. Huang, Y. Yu, J. Yuan, D. Luo, B. Liu, D. Liang, *Appl. Sci.* 8 (2018), <https://doi.org/10.3390/app8091449>;
(d) P. Xiao, T. Dong, J. Xie, D. Luo, J. Yuan, B. Liu, 299 and references therein, *Appl. Sci.* 8 (2018), <https://doi.org/10.3390/app8020299>.
- [169] (a) M. Kim, Y.W. Park, J.H. Choi, B.K. Ju, J.H. Jung, J.K. Kim, *Appl. Phys. Lett.* 90 (2007), 033506, <https://doi.org/10.1063/1.2431773>;
(b) Q.X. Tong, S.L. Lai, M.Y. Chan, J.X. Tang, H.L. Kwong, C.S. Lee, S.T. Lee, *Appl. Phys. Lett.* 91 (2007), 023503, <https://doi.org/10.1063/1.2756137>;
(c) Y.W. Park, Y.M. Kim, J.H. Choi, T.H. Park, H.J. Choi, H.J. Yu, M.J. Cho, D. H. Choi, S.H. Kim, B.K. Ju, J. Nanosci. Nanotechnol. 11 (2011) 1381–1384, <https://doi.org/10.1166/jnn.2011.3376>;
(d) K.S. Lee, D.C. Choo, T.W. Kim, *Thin Solid Films* 519 (2011) 5257–5259, <https://doi.org/10.1016/j.tsf.2011.01.171>;
(e) 2012 H.J. Ji, J.G. Jang, Mol. Cryst. Liq. Cryst. 563 (2012) 223–229, <https://doi.org/10.1080/15421406.2012.689721>.
- [170] G. Zucchi, T. Jeon, D. Tondelier, D. Aldakov, P. Thuéry, M. Ephritikhine, B. Geffroy, *J. Mater. Chem.* 20 (2010) 2114–2120, <https://doi.org/10.1039/B921740A>.
- [171] Y. Zhao, L. Duan, X. Zhang, D. Zhang, J. Qiao, G. Dong, L. Wang, Y. Qiu, *RSC Adv.* 3 (2013) 21453–21460, <https://doi.org/10.1039/C3RA43017K>.
- [172] J. Zhu, W. Li, L. Han, B. Chu, G. Zhang, D. Yang, Y. Chen, Z. Su, J. Wang, S. Wu, T. Tsuboi, *Opt. Lett.* 34 (2009) 2946–2948, <https://doi.org/10.1364/OL.34.002946>.
- [173] G. Grybauskaitė-Kaminskiene, K. Ivaniuk, G. Bagdzūnas, P. Turyk, P. Stakhira, G. Baryshnikov, D. Volyniuk, V. Cherpak, B. Minaev, Z. Hotra, H. Ågren, J. V. Grazulevicius, J. Mater. Chem. C 6 (2018) 1543–1550, <https://doi.org/10.1039/C7TC05392D>.
- [174] T. Xu, J.G. Zhou, M.K. Fung, H. Meng, *Org. Electron.* 63 (2018) 369–375, <https://doi.org/10.1016/j.jorgel.2018.09.026>.
- [175] H. Baek, S.E. Lee, H.W. Lee, G.J. Yun, J. Park, W.Y. Kim, Y.K. Kim, *Phys. Status Solidi A* 215 (2017) 1700530, <https://doi.org/10.1002/pssa.201700530>.
- [176] G. Sych, D. Volyniuk, O. Bezzivkonyi, R. Lytvyn, J.V. Grazulevicius, *J. Phys. Chem. C* 123 (2019) 2386–2397, <https://doi.org/10.1021/acs.jpcc.8b09908>.

- [177] H. Wang, D. Dong, L. Lian, F. Zhu, D. Xu, S. Wu, G. He, Phys. Status Solidi A 216 (2019) 1900034, <https://doi.org/10.1002/pssa.201900034>.
- [178] D. Luo, C.T. Hsieh, Y.P. Wang, T.C. Chuang, H.H. Chang, C.H. Chang, RSC Adv. 8 (2018) 30582, <https://doi.org/10.1039/C8RA04986F>.
- [179] Z. Li, J. Yu, X. Liao, L. Li, Org. Electron. 91 (2021), 106076, <https://doi.org/10.1016/j.orgel.2021.106076>.
- [180] C.K. Vipin, A. Shukla, K. Rajeev, M. Hasan, S.-C. Lo, E.B. Namdas, A. Ajayaghosh, K.N.N. Unni, J. Phys. Chem. C. 125 (2021) 22809–22816, <https://doi.org/10.1021/acs.jpcc.1c06323>.
- [181] D. Yang, Y. Duan, Y. Yang, N. Hu, X. Wang, F. Sun, Y. Duan, J. Lumin. 166 (2015) 77–81, <https://doi.org/10.1016/j.jlumin.2015.05.009>.
- [182] Y. Duan, F. Sun, D. Yang, Y. Yang, P. Chen, Y. Duan, Appl. Phys. Express 7 (2014), 052102, <https://doi.org/10.7567/APEX.7.052102>.
- [183] C.H. Chang, S.W. Wu, C.W. Huang, C.T. Hsieh, S.E. Lin, N.P. Chen, H.H. Chang, Jpn. J. Appl. Phys. 55 (2016) 03CD02, <https://doi.org/10.7567/JJAP.56.129209>.
- [184] J. Wang, J. Chen, X. Qiao, S.M. Alshehri, T. Ahamad, D. Ma, ACS Appl. Mater. Interfaces 8 (2016) 10093–10097, <https://doi.org/10.1021/acsm.6b00861>.
- [185] T. Xu, J.G. Zhou, M.K. Fung, H. Meng, Org. Electron. 63 (2018) 369–375, <https://doi.org/10.1016/j.orgel.2018.09.026>.
- [186] Y. Chen, Y. Wu, C. Lin, Y. Dai, S. Yang, X. Qiao, D. Ma, J. Mater. Chem. C. 8 (2020) 12450–12456, <https://doi.org/10.1039/D0TC03053H>.
- [187] T. Zhang, C. Shi, N. Sun, Z. Wu, D. Ma, Org. Electron. 92 (2021), 106123, <https://doi.org/10.1016/j.orgel.2021.106123>.
- [188] X. Tang, X.Y. Liu, Y. Yuan, Y. Wang, H.C. Li, Z.Q. Jiang, L.S. Liao, ACS Appl. Mater. Interfaces 10 (2018) 29840–29847, <https://doi.org/10.1021/acsm.8b09418>.
- [189] X. Tang, X.Y. Liu, Z.Q. Jiang, L.S. Liao, Adv. Funct. Mater. 29 (2019) 1807541, <https://doi.org/10.1002/adfm.201807541>.
- [190] J. Zhao, S. Yuan, X. Du, W. Li, C. Zheng, S. Tao, X. Zhang, Adv. Opt. Mater. 6 (2018) 1800825, <https://doi.org/10.1002/adom.201800825>.
- [191] Y.L. Zhang, Q. Ran, Q. Wang, J. Fan, L.S. Liao, J. Mater. Chem. C. 7 (2019) 7267, <https://doi.org/10.1002/adma.201902368>.
- [192] S. Ying, P. Pang, S. Zhang, Q. Sun, Y. Dai, X. Qiao, D. Yang, J. Chen, D. Ma, ACS Appl. Mater. Interfaces 11 (2019) 31078–31086, <https://doi.org/10.1021/acsm.9b09429>.
- [193] R. Sheng, A. Li, F. Zhang, J. Song, Y. Duan, P. Chen, Adv. Opt. Mater. 8 (2019) 1901247, <https://doi.org/10.1002/adom.201901247>.
- [194] Z. Chen, X.K. Liu, C.J. Zheng, J. Ye, C.L. Liu, F. Li, X.M. Ou, C.S. Lee, X.H. Zhang, Chem. Mater. 27 (2015) 5206–5211, <https://doi.org/10.1021/acs.chemmater.5b01188>.
- [195] (a) Y. Tang, G. Xie, X. Yin, Y. Gao, J. Ding, C. Yang, J. Phys. Chem. Lett. 11 (2020) 5255–5262, <https://doi.org/10.1021/acs.jpcllett.0c01482>;
 (b) H. Shahroosvand, L. Heydari, B.N. Bidehab, B. Pasheaei, RSC Adv. 10 (2020) 14099–14106, <https://doi.org/10.1039/C9RA10761D>;
 (c) M. Wei, G. Gui, Y.H. Chung, L. Xiao, B. Qu, Z. Chen, Phys. Status Solidi B: Basic Solid State Phys. 252 (2015) 1711–1716, <https://doi.org/10.1002/pssb.201552098>.
- [196] (a) W. Song, J.Y. Lee, Y.J. Cho, H. Yu, H. Aziz, K.M. Lee, Adv. Sci. 5 (2018) 1700608, <https://doi.org/10.1002/advs.201700608>;
 (b) X. Zhan, Z. Wu, Y. Gong, J. Tu, Y. Xie, Q. Peng, D. Ma, Q. Li, Z. Li, Research 2020 (2020) 8649102, <https://doi.org/10.34133/2020/8649102>;
 (c) M. Jung, K.H. Lee, J.Y. Lee, T. Kim, Mater. Horiz. 7 (2020) 559–565, <https://doi.org/10.1039/C9MH01268K>.
- [197] D. Luo, X.L. Li, Y. Zhao, Y. Gao, B. Liu, ACS Photonics 4 (2017) 1566–1575, <https://doi.org/10.1021/acsphotonics.7b00364>.
- [198] D. Luo, Y. Xiao, M. Hao, Y. Zhao, Y. Yang, Y. Gao, B. Liu, Appl. Phys. Lett. 110 (2017), 061105, <https://doi.org/10.1063/1.4975480>.
- [199] S. Zhang, J. Yao, Y. Dai, Q. Sun, D. Yang, X. Qiao, J. Chen, D. Ma, Org. Electron. 85 (2020), 105821, <https://doi.org/10.1016/j.orgel.2020.105821>.
- [200] Z. Liu, B. Zhao, Y. Gao, H. Chen, B. Dong, Y. Xu, H. Wang, B. Xu, W. Li, RSC Adv. 10 (2020) 33461, <https://doi.org/10.1039/dra06658c>.
- [201] L. Wang, Z. Kou, B. Wang, J. Zhou, Z. Lu, L. Li, Opt. Mater. 115 (2021), 111059, <https://doi.org/10.1016/j.optmat.2021.111059>.
- [202] M. Chapran, E. Angioni, N.J. Findlay, B. Breig, V. Cherpak, P. Stakhira, T. Tuttle, D. Volyniuk, J.V. Grazulevicius, Y.A. Nastishin, O.D. Lavrentovich, P.J. Skabara, ACS Appl. Mater. Interfaces 9 (2017) 4750–4757, <https://doi.org/10.1021/acsm.6b13689>.
- [203] J. Song, F. Zhang, L. Yang, K. Chen, A. Li, R. Sheng, Y. Duan, P. Chen, Mater. Adv. 2 (2021) 3677–3684, <https://doi.org/10.1039/DQMA01005G>.
- [204] S.-Q. Sun, H. Liu, D.-D. Feng, C.-C. Huang, T.-T. Wang, W. He, Y.-J. Zhang, W. Luo, Q. Sun, M.-K. Fung, J. Mater. Chem. C. 9 (2021) 14327–14333, <https://doi.org/10.1039/D1TC02934G>.
- [205] G. Wang, M. Yin, Y. Miao, Y. Guo, H. Zhou, Q. Lu, J. Huang, H. Wang, J. Mater. Chem. C. 10 (2022) 6654–6664, <https://doi.org/10.1039/D2TC00711H>.
- [206] T. Chiba, Y.J. Pu, J. Kido, in: S. Ogawa (Ed.), *Organic Electronics Materials and Devices*, Springer, Japan, 2015, pp. 195–219.
- [207] S. Wang, H. Zhang, B. Zhang, Z. Xie, W.Y. Wong, Mater. Sci. Eng. R. 140 (2020), 100547, <https://doi.org/10.1016/j.mser.2020.100547>.
- [208] X. Ban, F. Chen, J. Pan, Y. Liu, A. Zhu, W. Jiang, Y. Sun, Chem. Eur. J. 9 (2020) 3090–3102, <https://doi.org/10.1002/chem.201904415>.
- [209] M. Colella, P. Pander, A.P. Monkman, Org. Electron. 62 (2018) 168, <https://doi.org/10.1016/j.orgel.2018.07.020>.
- [210] P.H. Pander, S. Gogoc, M. Colella, P. Data, F.B. Dias (DOI), ACS Appl. Mater. Interfaces 10 (2018) 28796–28802, <https://doi.org/10.1021/acsm.8b07554>.
- [211] Y. Zhou, C. Li, J. Ye, X. Du, M. Zhang, H. Lin, S. tao, X. Zhang, Mater. Horiz. 6 (2019) 1425–1432, <https://doi.org/10.1039/C9MH00373H>.
- [212] P.L. Zhong, C.J. Zheng, M. Zhang, J.W. Zhao, H.Y. Yang, Z.Y. He, H. Lina, S. L. Tao, X.H. Zhang, Org. Electron. 76 (2020), 105449, <https://doi.org/10.1016/j.orgel.2019.105449>.
- [213] X. Ban, T. Zhou, K. Zhang, Q. Cao, F. Ge, D. Zhang, P. Zhu, Z. Liu, Z. Li, W. Jiang, Chem. Eng. J. 441 (2022), 135898, <https://doi.org/10.1016/j.cej.2022.135898>.
- [214] J. Saghaei, T. Leitner, V.T.N. Mai, C.S.K. Ranasinghe, P.L. Burn, I.R. Gentle, A. Pivrikas, P.E. Shaw, ACS Appl. Electron. Mater. 3 (2021) 4757–4767, <https://doi.org/10.1021/acsealm.1c00630>.
- [215] X. Zhang, Q. Yang, Y. Fu, Y. Zhang, ACS Macro Lett. 10 (2021) 1236–1242, <https://doi.org/10.1021/acsmacrolett.1c00501>.
- [216] Y.X. Zhang, B. Wang, Y. Yuan, Y. Hu, Z.Q. Jiang, L.S. Liao, Adv. Opt. Mater. 5 (2017) 1700012, <https://doi.org/10.1002/adom.201700012>.
- [217] X. Ban, K. Sun, Y. Sun, B. Huang, S. Ye, M. Yang, W. Jiang, ACS Appl. Mater. Interfaces 7 (2015) 25129–25138, <https://doi.org/10.1021/acsm.5b06424>.
- [218] X. Ban, K. Sun, Y. Sun, B. Huang, W. Jiang, ACS Appl. Mater. Interfaces 8 (2016) 2010–2016, <https://doi.org/10.1021/acsm.5b10335>.
- [219] J. Peng, X. Xu, X.J. Feng, L. Li, J. Lumin. 198 (2018) 19–23, <https://doi.org/10.1016/j.jlumin.2018.02.010>.
- [220] Y. Feng, T. Lu, D. Liu, W. Jiang, Y. Sun, Org. Electron. 67 (2019) 136–140, <https://doi.org/10.1016/j.orgel.2019.01.022>.
- [221] H.Y. Yang, C.J. Zheng, M. Zhang, J.W. Zhao, P.L. Zhong, H. Lin, S.L. Tao, X. H. Zhang, Org. Electron. 73 (2019) 36–42, <https://doi.org/10.1016/j.orgel.2019.06.001>.
- [222] L. Chen, J. Lv, S. Wang, S. Shao, L. Wang, Adv. Opt. Mater. 9 (2021) 2100752, <https://doi.org/10.1002/adom.202100752>.
- [223] S. Cho, N.Y. Kwon, C.W. Kim, H. Lee, J.M. Ha, H.J. Kim, H.Y. Woo, S. Park, M. J. Cho, D.H. Choi, Polym. Chem. 13 (2022) 1824–1830, <https://doi.org/10.1039/D1PY01700D>.
- [224] K. Kishore Kesavan, J. Jayakumar, M. Lee, C. Hexin, S. Sudheendran Swamyaprabha, D. Kumar Dubey, F.-C. Tung, C.-W. Wang, J.-H. Jou, Chem. Eng. J. 435 (2022), 134879, <https://doi.org/10.1016/j.cej.2022.134879>.
- [225] S. Wang, X. Wang, B. Yao, B. Zhang, J. Ding, Z. Xie, L. Wang, Sci. Rep. 5 (2015) 12487, <https://doi.org/10.1038/srep12487>.
- [226] X. Liu, B. Yao, Z. Zhang, X. Zhao, B. Zhang, W.Y. Wong, Y. Cheng, Z. Xie, J. Mater. Chem. C. 4 (2016) 5787–5794, <https://doi.org/10.1039/C6TC01270A>.
- [227] Y. Zhang, C. Liu, X.C. Hang, Q. Xie, G. Xie, C. Zhang, T. Qin, Z. Sun, Z.K. Chen, W. Huang, J. Mater. Chem. C. 6 (2018) 8035–8041, <https://doi.org/10.1039/C8TC02757A>.
- [228] A. Shahalizad, D.H. Kim, S.R. Bobbara, Y. Tsuchiya, A. D'Aléo, C. Andraud, J. C. Ribierre, J.M. Nunzi, C. Adachi, Appl. Phys. Lett. 114 (2019), 033301, <https://doi.org/10.1063/1.5054721>.
- [229] M.Z. Shafikov, P. Pander, A.V. Zaytsev, R. Daniels, R. Martinscroft, F.B. Dias, J.A. G. Williams, V.N. Kozhevnikov, J. Mater. Chem. C. 9 (2021) 127–135, <https://doi.org/10.1039/D0TC04881J>.
- [230] X. Ban, K. Sun, Y. Sun, B. Huang, W. Jiang, Org. Electron. 33 (2016) 9–14, <https://doi.org/10.1016/j.orgel.2016.02.041>.
- [231] Z. Fan, N. Li, Y. Quan, Q. Chen, S. Ye, Q. Fan, W. Huang, H. Xu, J. Mater. Chem. C. 2 (2014) 9754–9759, <https://doi.org/10.1039/C4TC01870B>.
- [232] Z. He, C. Wang, J. Zhao, X. Du, H. Yang, P. Zhong, C. Zheng, H. Lin, S. Tao, X. Zhang, J. Mater. Chem. C. 7 (2019) 11806–11812, <https://doi.org/10.1039/C9TC03468D>.
- [233] X. Ban, Y. Liu, J. Pan, F. Chen, A. Zhu, W. Jiang, Y. Sun, Y. Dong, ACS Appl. Mater. Interfaces 12 (2020) 1190–1200, <https://doi.org/10.1021/acsm.9b20903>.
- [234] C.C.A. Voll, G. Markopoulos, T.C. Wu, M. Welborn, J.U. Engelhart, S. Rochat, G.G. D. Han, G.T. Sazama, T.A. Lin, T.V. Voorhis, M.A. Baldo, T.M. Swager, Org. Mater. 2 (2020) 1–10, <https://doi.org/10.1055/s-0039-3402059>.
- [235] Y. Qin, P. Tao, L. Gao, P. She, S. Liu, X. Li, F. Li, H. Wang, Q. Zhao, Y. Miao, W. Huang, Adv. Opt. Mater. 7 (2019) 1801160, <https://doi.org/10.1002/adom.201801160>.
- [236] M. Zhang, K. Wang, C.J. Zheng, D.Q. Wang, Y.Z. Shi, H. Lin, S.L. Tao, X. Li, X. H. Zhang, Front. Chem. 7 (2019) 16, <https://doi.org/10.3389/fchem.2019.00016>.
- [237] V. Cherpak, P. Stakhira, B. Minaev, G. Baryshnikov, E. Stromylo, I. Helzhynsky, M. Chapran, D. Volyniuk, Z. Hotra, A. Dabuliene, A. Tomkeviciene, L. Voznyak, J. V. Grazulevicius, ACS Appl. Mater. Interfaces 7 (2015) 1219–1225, <https://doi.org/10.1021/am507050g>.
- [238] X.Q. Wang, Y. Hu, Y.J. Yu, Q.S. Tian, W.S. Shen, W.Y. Yang, Z.Q. Jiang, L.S. Liao, J. Phys. Chem. Lett. 12 (2021) 6034, <https://doi.org/10.1021/acs.jpclett.1c01609>.
- [239] I. Na, K.J. Kim, G.T. Kim, Y. Seo, Y. Kim, Y.K. Kim, M.K. Joo, Appl. Phys. Lett. 117 (2020), 063303, <https://doi.org/10.1063/5.0016096>.
- [240] H. Miranda-Salinas, Y.T. Hung, Y.S. Chen, D. Luo, H.C. Kao, C.H. Chang, K. T. Wong, A. Monkman, J. Mater. Chem. C. 9 (2021) 8819–8833, <https://doi.org/10.1039/D1TC02316K>.
- [241] Z. Wang, M. Li, L. Gan, X. Cai, B. Li, D. Chen, S.J. Su, Adv. Sci. 6 (2019) 1802246, <https://doi.org/10.1002/advs.201802246>.
- [242] S. Tan, K. Jinnai, R. Kabe, C. Adachi, Adv. Mater. 33 (2021) 2008844, <https://doi.org/10.1002/adma.202008844>.



Dr. Monima Sarma obtained her Ph.D. degree from the University of Hyderabad, India in 2013. She was a postdoctoral research scientist at National Taiwan University, Taiwan before joining as an Assistant Professor in KL Deemed to be University (KLEF), Andhra Pradesh, India in 2019. Her research is mainly focused on the design and development of novel luminescent π -conjugated organic and organometallic materials for photonic applications such as light-emitting devices, bioimaging, and nonlinear optical materials (NLO) for biological applications.



Yi-Sheng Chen obtained his Master of Science degree from National Kaohsiung Normal University (NKNU) in 2014. He joined Dr. Ken-Tsung Wong's group for his Ph.D. degree in 2016. He conducted organic syntheses and characterizations of novel molecules mainly focused on hole-transporting materials (HTMs) for organic light-emitting diodes (OLEDs).



Li-Ming Chen obtained his Bachelor of Science degree from National Taiwan University (NTU) in 2020. He joined Dr. Ken-Tsung Wong's group in his junior year in 2018, with an interest in organic synthesis and applications. He conducted organic synthesis of novel materials for organic light-emitting diodes as the undergraduate research project. Currently working as a research assistant after graduation, he mainly focuses on the organic synthesis of novel near-infrared fluorescent probes for *in vivo* bioimaging applications.



Dr. Ken-Tsung Wong obtained his Ph.D. degree from National Taiwan University (NTU) in 1993, conducted postdoctoral researches at University of Illinois at Urbana-Champaign in 1995–1996 and Université Louis Pasteur Strasbourg in 1996–1998. He joined the Department of Chemistry NTU as an assistant professor and promoted to an associate professor in 2002 and professor in 2006. His research mainly focuses on the molecular design and organic synthesis of novel π -conjugated materials for optoelectronic applications such as organic light-emitting diode, electrogenerated chemiluminescence, solid-state light-emitting electrochemical cells, organic transistors, and photovoltaic devices.